Title
The Assessment of Glioblastoma Tumorspheres Reveals Molecular Determinants of Proliferation and Therapeutic Response

Author
Laks, Dan RIchard

Publication Date
2015

Peer reviewed|Thesis/dissertation

UNIVERSITY OF CALIFORNIA

Los Angeles

The Assessment of Glioblastoma Tumorspheres Reveals Molecular Determinants of Proliferation and Therapeutic Response

A dissertation submitted in partial satisfaction of the requirements for the degree Doctor of Philosophy in Biological Chemistry

By

Dan Richard Laks

2015

ABSTRACT OF THE DISSERTATION

The Assessment of Glioblastoma Tumorspheres Reveals Molecular Determinants of Proliferation and Therapeutic Response

By

Dan Richard Laks

Doctor of Philosophy in Biological Chemistry

University of California, Los Angeles, 2015

Professor Kathrin Plath, Co-Chair

Professor Harley Kornblum, Co-Chair

Glioblastoma (GBM) is one of the most lethal cancers and new therapies are urgently needed. One key limitation in the development of therapeutics is the availability of appropriate in vitro models in which key molecular pathways can be identified and potential novel therapies can be tested. One model of GBM is through the growth of "tumorspheres", patient derived GBM cultures grown in neurosphere conditions that generally grow as non-adherent spheres of cells. We assessed gene expression profiling, in vitro phenotypes, and patient survival from a large cohort of high-grade glioma tumorsphere cultures. Through interrogation of the tumorsphere model system, we discovered molecular determinants of proliferation (PTGR1, EFEMP2, LGALS8), effective combinatorial treatment targeting ERK and mTOR, and a mechanism of resistance to chronic mTOR inhibition through GSK3B and MAP1B.

The dissertation of Dan Richard Laks is approved.

John Colicelli

Judith Gasson

Kathrin Plath, Committee Co-Chair

Harley Kornblum, Committee Co-Chair

University of California, Los Angeles

2015

Dedication

This work is dedicated to my wife, Pam Cash, for her inspiring brilliance and loving support, and to my parents, Batya Casper and Hillel Laks, for their exemplary inimitability.

Table of Contents

Figures and Tables

Chapter 2

Chapter 3

Figures and Tables

Chapter 3 (continued)

Chapter 4

Figures and Tables

Chapter 4 (Continued)

Acknowledgements

This work was constructed upon the guidance, support, scientific acumen, and creative intervention of Dr. Harley Kornblum. It was a great privilege to have him as a mentor and to collaborate on this work with him.

I would like to acknowledge the insights and training provided by my thesis committee members: Dr. Kathrin Plath, Dr. John Colicelli, and Dr. Judith Gasson. I am indebted to their wisdom, teaching, and gracious participation in shepherding this thesis to fruition.

Finally, I would like to thank those scientists who have paved the way and those who continue to sustain the light of empirical, tested, scientific knowledge and understanding into the future.

Chapter 1 to this dissertation contains an updated and adapted version of the published work: Brain Tumor Stem Cells as Therapeutic Targets in Models of Glioma. Dan R. Laks, Koppany Visnyei, and Harley I. Kornblum(Laks et al., 2010).

Chapter 2 is a version of a work in preparation for publication:
Large-scale assessment of the tumorsphere model system for glioblastoma. Dan R Laks, Thomas J Crisman, Michelle Shih, Jack Mottahedeh, Fuying Gao, Matthew Garrett, William Yong, Timothy Cloughesy, Linda M Liau, Albert Lai, Giovanni Coppola, Harley I Kornblum.

Chapter 3 is a version of a work in preparation for publication:
Interrogation of a Broad Spectrum of Glioblastoma Tumorspheres Informs Targeting of the PI3Kinase Pathway. Dan R Laks, Thomas J Crisman, Michelle Shih, Serli Nazarian,

Anjelica Cardenas, Jonathan Nakashima, Kelvin Zhang, Jack Mottahedeh, Fuying Gao, Matthew Garrett, Giovanni Coppola, Harley I Kornblum.

Chapter 4 is a version of a work in preparation for publication: Phosphorylation Dependent Attenuation of GSK3B is an Adaptive Mechanism that Confers Resistance to Chronic mTOR Inhibition through MAP1B. Dan R Laks, Juan Oses, Alma L Burlingame, Daniel Azzam, Robert Damoiseaux, Bryan France, Lisa Ta, Nicholas Orozco, Koppany Visnyei, Jonathan Nakashima, Harley I Kornblum

I would like to acknowledge the contribution of these collaborators:

Daniel Azzam: Cell assays and western blots for the mTOR resistance project.

Giovanni Coppola: Data analysis for tumorsphere expression profiling.

Thomas J Crisman: Data analysis for tumorsphere expression profiling.

Michelle Shih: Cell assays for PI3Kinase Inhibitor project.

Jack Mottahedeh: Cell doubling time assays fro tumorsphere project.

Fuying Gao: Data analysis of microarrays.

Matthew Garrett: IDH1 work on the tumorsphere project.

Anjelica Cardenas: Cell assays for PI3K study.

Serli Nazarian: Cell assays for PI3K study.

Lisa Ta: Collaborated on transplants for the mTOR inhibition study.

Jonathan Nakashima: Subcutaneous transplants, blinded drug treatment, and optical imaging of mice for PI3K and mTOR study.

Juan A Oses-Prieto: Phosphoproteomics for mTOR Inhibition study.

Shreya Chand: Assisted in phosphoproteomics for mTOR inhibition study.

Alma L Burlingame: Phosphoproteomics for mTOR Inhibition study

Robert Damoiseaux: Supervised targeted shRNA screen.

Bryan France: Assisted in targeted shRNA screen for mTOR Inhibition study.

Nicholas Orozco: Preliminary studies on mTOR inhibition.

Koppany Visnyei: Collaborated on in vivo transplants of Rapamcyin resistant cells.

Andre Gregorian: Westerns of *EGFR*vIII and *PTEN*.

William Yong: Pathology on tumors.

Albert Lai: *IDH1* mutation status qRT-PCR.

Linda M Liau: Surgical resection of tumors.

Timothy Cloughesy: Survival data on patients.

Harley I Kornblum: Guidance, insight, and supervision of all studies.

This work was partially funded by the Whitcome Fellowship.

Biographical Sketch

Dan Richard Laks

Education

2010-2015 U.C. Los Angeles, Los Angeles, CA

PhD Candidate, Department of Biological Chemistry

2004-2007 U.C. Berkeley, Berkeley, CA

Master of Science (M.S.), Environmental Health Science

1993 University of Pennsylvania, Philadelphia, PA

M.D./PhD Program: One semester completed with Honors.

1988-1992 U.C. Berkeley, Berkeley, CA

Double Major: B.A. Neuroscience/ English Literature

Academic and Professional Honors

Whitcome Fellowship, Molecular Biology Institute, UCLA 2014-15

Phi Beta Kappa 1989-1992

Graduated with Honors, UC Berkeley, 1992

Selected 1st Author Publications

Laks, D.R. (2014). Mercury rising: response to the EPA assessment of mercury exposure. Biometals : an international journal on the role of metal ions in biology, biochemistry, and medicine *27*, 1-4.

Laks, Dan R.. Visnyei, Koppany, Kornblum, Harley I. Brain Tumor Stem Cells as Therapeutic Targets in Models of Glioma. Yonsei Medical Journal, 2010, Sept.; 51(5):633-40.

Laks, Dan R.. Assessment of chronic mercury exposure within the U.S. population, National Health and Nutrition Examination Survey, 1999-2006. Biometals, 2009, Aug; 22(6), 1103-1114.

Laks, Dan R.. Luteinizing hormone provides a causal mechanism for mercury associated disease. Medical Hypotheses, 2009, Apr; 74(4), 698-701.

Laks, Dan R, Masterman-Smith, M., Visnyei, K., Angenieux, B., Orozco, N. M., Foran, I., Yong, W. H., Vinters, H. V., Liau, L. M., Lazareff, J. A., Mischel, P. S., Cloughesy, T. F., Horvath, S., Kornblum, H. I.. Neurosphere formation is an independent predictor of clinical outcome in malignant glioma. Stem Cells, 2009, Apr; 27(4), 980-987.

Laks, Dan R., Beckwith, Leilah & Cohen, Sarale E.. Mother's Use of Personal Pronouns When Talking to Toddlers. Genetic Psychology, 1990, Mar; 151(2), 25-32.

Chapter 1

Introduction

Glioblastoma

Glioma describes any tumor that arises from the supportive material of the brain. As they arise from, reside in, and infiltrate the brain, glioma cases are considered intrinsic brain tumors. Originally thought to arise from glial cells (astrocytes, oligodendrocytes, and ependymal cells), the term glioma may be considered nominal as certain studies identify neural stem cells as the etiology of glioblastoma, the most severe type of glioma (Alcantara Llaguno et al., 2009; Chen et al., 2012; Zhu et al., 2014). Glioma are classified based on histopathological criteria into 4 grades that represents a "malignancy scale" and reflect the degree of undifferentiation, anaplasia (cellular loss of structure, orientation and differentiation), and aggressiveness (Louis et al., 2007). These classes are generally referred to as low grade (grades 1 and 2) and high grade (grades 3 and 4). High grade are considered malignant glioma. Glioma account for 29% of all primary brain and central nervous system (CNS) tumors (Dolecek et al., 2012). Glioblastoma (GBM), the most aggressive malignant primary brain tumor, accounts for 54% of all glioma (Dolecek et al., 2012).

Histologically, glioblastoma are marked by increased cellularity and mitotic activity, necrosis, and vascular proliferation(Omuro and DeAngelis, 2013). These neoplasms are highly invasive and infiltrate brain parenchyma (functional tissue) that makes them difficult to resect surgically. Due to their heterogeneous cellular constituency, with cells bearing pleomorphic features (varying in size and shape),

glioblastoma was termed glioblastoma multiforme (GBM), but this term, multiforme, is no longer in use although, anachronistically, GBM remains the abbreviation for glioblastoma.

Incidence

The incidence of GBM is almost three fold higher in men than in women and the overall risk for glioma rises with age (Dolecek et al., 2012). The incidence of malignant brain tumors rose steadily over the last quarter of a century in both adults and children(Deltour et al., 2009; Deorah et al., 2006; Hess et al., 2004; Jukich et al., 2001; Pirouzmand and Sadanand, 2007; Smith et al., 1998). A proportion of this trend may be due to improved neuro-imaging techniques and access to medical care(Schwartzbaum et al., 2006). Familial gene mutations, immune disease, and high dose ionizing irradiation are known risk factors of brain tumors but are likely responsible for a minority of cases. Epidemiological studies and geographic variability in case numbers suggest that the etiology of brain tumors may be associated with environmental factors and exposure to carcinogens(Fisher et al., 2007; Schwartzbaum et al., 2006; Wrensch et al., 2002). Association between brain tumors and cell phone use has yielded no consistent evidence for a link, although there is some evidence for an association between cell phone use and acoustic neuroma(Benson et al., 2013; Omuro and DeAngelis, 2013). Due to the dramatic use of cell phones in recent history, careful monitoring may be cautioned as the long term effects of constant cell phone exposure (over 20 years) has yet to be assessed.

While brain tumors in the United States constitute a minority of cancer cases, with an incidence of 14.8 brain tumors per 100,000 person years, and roughly half diagnosed

as benign, the malignant forms of brain tumor present a devastating prospect of morbidity and mortality(Buckner et al., 2007). GBM have a median overall survival of approximately 1 year(Daumas-Duport et al., 1988).

Treatment

Currently the standard treatment for GBM is surgical resection followed by a combination of radiotherapy and chemotherapy(Stupp et al., 2005). Most commonly, temozolomide (TMZ), a DNA alkylating agent, is the chemotherapy employed. DNA alkylating agents are most effective when the MGMT gene, a DNA repair enzyme, is silenced by methylation(Wick et al., 2014). In MGMT active patients, TMZ is not effective and radiotherapy alone may be the best course of treatment(Hegi et al., 2005). In MGMT depleted patients (methylated MGMT) TMZ plus radiation improves survival to 21.7 months as compared to 15.3 months for radiation alone(Hegi et al., 2005). At this time, MGMT testing for gene silencing is not a standard of care. With standard TMZ plus radiation, median survival for all GBM patients only improves from 12 months (radiation alone) to 15 months(Stupp et al., 2005). In every scenario, TMZ does not provide a cure for GBM and only marginally extends life. Therefore, new treatment strategies for GBM are in dire need.

BTSC

One novel strategy for treating GBM is to focus on brain tumor stem cells as the main therapeutic target. Divergent perspectives on the fundamental nature of brain tumor biology fuel a debate that revolves around the theory of brain tumor stem cells (BTSC) as a model of glioma(Laks et al., 2010). The cancer stem cell (CSC) theory posits that only a specific, minority of tumor cells possess the ability to produce a tumor (Jordan et al., 2006; Pardal et al., 2003; Reya et al., 2001). The brain tumor stem cell theory holds that BTSC produce all the cells of a tumor and therefore represent the essential, specific targets of effective treatment necessary to prevent recurrence(Nakano and Kornblum, 2006). To identity a brain tumor stem cell requires distinguishing the ability of a tumor cell to form a tumor upon orthotopic xenotransplantation that recapitulates the cellular heterogeneity of the parent tumor(Lathia et al., 2015).

Although not an essential element of the CSC hypothesis, cancer stem cells may arise from mutations in normal stem or progenitor cells. The notion that glioma tumors are caused by transformed neural stem cells was originally fueled by the discovery that brain tumors expressed nestin, an intermediate filament that can be expressed by neural stem cells(Dahlstrand et al., 1992; Tohyama et al., 1992), although it is also expressed by more limited progenitors as well as by other cells within the body(Wiese et al., 2004). In this BTSC model, brain tumor stem cells arise from oncogenic mutations in neural stem cells. This hypothesis was supported by several observations: gliomas can arise near the lateral ventricles, a site housing neural stem cells that reside in the subventricular proliferative zone; neural stem cells proliferate enough to make them susceptible to transformation; and neural stem cells and BTSC share essential mechanisms for

proliferation and survival(Hadjipanayis and Van Meir, 2009; Sanai et al., 2005). Numerous transcription factors essential to neural stem cells have been shown to distinguish BTSC (Lathia et al., 2015).

Evidence for the BTSC model of glioma first came from several laboratories (Ignatova et al., 2002),(Hemmati et al., 2003),(Singh et al., 2003). These studies demonstrated biological similarities between brain tumor initiating cells and neural stem cells through the use of neurosphere cultures. Reynolds and Weiss et al. originally isolated and enriched neural stem cells from the adult brain through the use of neurosphere cultures (Reynolds et al., 1992; Reynolds and Weiss, 1992). Neural stem cells distinguished themselves from other cells in the brain by their ability to grow as neurospheres (floating spheres of cells) in relatively simple, serum free media with the addition of epidermal growth factor (EGF), basic fibroblast growth factor (bFGF), or both. Neurospheres could subsequently differentiate into the multiple lineages of brain cells upon removal of growth factors. In like manner, cells derived from brain tumors form serially passaged clonal neurosphere cultures in serum free media, and, upon removal of growth factors, differentiate into multiple lineages to recapitulate tumor morphologies. In other words, in vitro, BTSC behave in a similar fashion to neural progenitor cells; they respond to the same mitogens, and they express similar markers.

The theory of BTSC was further substantiated when Galli et al. demonstrated that GBM derived neurosphere cultures were tumorigenic upon xenotransplantation into immunodeficient mice(Galli et al., 2004) and Singh et al.(Singh et al., 2004a) demonstrated that tumor cells expressing CD133 (a putative marker of human neural stem cells), when sorted from patient samples, formed tumors in immunodeficient mice

while the CD133 negative fraction did not. The theory of BTSC gained acceptance and the model developed that BTSC may originate from transformed neural stem or progenitor cells, and furthermore, are unique amongst other tumor cells in that BTSC possess the capacities to extensively self renew, initiate tumors upon orthotopic transplantation, and give rise to a heterogeneous population of cells such as those found in their parent tumors. More recent studies demonstrated that the ability of glioma tumors to form neurosphere cultures is an independent predictor of clinical outcome(Laks et al., 2009; Pallini et al., 2008). These data provide further evidence that BTSC play a central role in tumor progression and aggressiveness. However, BTSC remains a hypothesis and both the definition and terminology are still debated. Some scientists prefer the less declarative terms “brain tumor initiating cells” or “brain tumor stem like cells”.

Recently, compelling evidence has emerged that BTSC do exist in GBM and they are responsible for chemoresistance and tumor formation(Alcantara Llaguno et al., 2009; Chen et al., 2012; Zhu et al., 2014; Zong et al., 2015). Both Dr. Parada’s group (Allcantara Llaguno et al., and Chen et al) and Zhu et al. found that BTSC likely arise from neural stem cells (NSC), are responsible for tumor formation, are slow dividing in vivo and relatively quiescent, and can self renew or give rise in a hierarchical manner to non-BTSC. If these discoveries from mouse models hold true for human GBM, then BTSC may provide the optimal target for therapeutic intervention. Instead of treating the tumor bulk and all its cells as equivalent targets of therapy, effective treatment may rely on specific targeting of BTSC to prevent tumor recurrence. However, targeting BTSC necessitates identifying them, providing a model system in which to study them, and finding suitable therapeutics to target them.

Modeling Glioma

Many models exist to explain the etiology and function of the heterogeneous cell populations that form glioma tumors(Hadjipanayis and Van Meir, 2009). The hierarchical model of BTSC contrasts with the more established stochastic model of cancer in which variegated cell populations possess equivalent capabilities to form tumors. In the stochastic model of tumors, different populations undergo clonal evolution in competition with each other in a process driven by mutation to form the tumor bulk(Nowell, 1976). It is thought that multiple mutations are required to transform a normal cell into a malignant, cancer cell(Miller, 1980). Possibly, a mutator phenotype is a requirement to produce malignant cells(Loeb, 2001). In this model, a primary mutation causes genetic instability that drives further mutations; this mutator phenotype eventually produces cancerous cells. In this clonal evolution model of tumors, the diversity of cells within a tumor is not caused by a single BTSC but by a heterogeneous population of genetically distinct cancer cells

Evidence is accruing that tumors are in a state of genetic flux. Analysis of lymphoblastic leukemia patients revealed that cancer recurrences differed in DNA copy number from their original, primary cancers(Mullighan et al., 2008). Similarly, recurrences of breast cancer tumors were shown to have different mutational profiles than their original, primary tumors(Shah et al., 2009). This evidence suggests that tumors possess a heterogeneous population of genetically distinct cells that undergo clonal evolution. The ongoing debate between the cancer stem cell model and the clonal evolution model has been reviewed by Shakleton et al.(Shackleton et al., 2009). Glioma seem to fit well within the cancer stem cell model because tumorigenic capacity is a

relatively rare trait among glioma tumor cells and not a uniform trait as would be predicted by the clonal evolution model. Indeed, glioma BTSC have been shown to demonstrate a hierarchical model(Galli et al., 2004), capable of generating a diversity of cells.

It has been demonstrated that there is considerable genetic variability within populations of neural stem cells in the brain(Rehen et al., 2001; Westra et al., 2008). In fact, it can even be assumed that some genetic variation and instability found in neurosphere cultures represents the genetic variation and instability within the brain(Sareen et al., 2009). A systems based approach may syncretize the disparate models of glioma in order to address the manifest complexity of these tumors. In contrast to clonal evolution, a complex system model considers the features of adaptive and resistant behavior exhibited by malignant brain tumors to be the emergent properties of a complex adaptive system consisting of multiple brain tumor stem cells. In this model, both genetic and potentially reversible epigenetic changes may explain not only the cellular diversity, but also the increased plasticity these tumors exhibit upon therapeutic intervention.

BTSC as a Complex Adaptive System

Cancer has been characterized as a robust, complex system(Kitano, 2004, 2007; Schwab and Pienta, 1996) and tumors have been described as a cooperative system of interacting cells(Axelrod et al., 2006; Heppner, 1984). Therefore it is worthwhile to assess cancer as a complex adaptive system(Grizzi and Chiriva-Internati, 2005, 2006). A complex adaptive system is characterized by emergent, global properties that are produced by a requisite diversity of local interactions(Ashby, 1958). These emergent

properties are only ascribed to the complex system itself and cannot be reduced to the properties of the individual components of the system(Ashby, 1958; Grizzi and Chiriva-Internati, 2006; Schwab and Pienta, 1996). Emergent properties confer the hallmarks of a complex adaptive system: organization, adaptability, and survival.

Gliomas fit the essential criteria for a complex adaptive system, they are heterogeneous, self adaptive and self organized. Evidence exists for interactions between BTSC and local environmental cues that play a role in BTSC survival and proliferation(Gilbertson and Rich, 2007). Autocrine and paracrine factors are secreted by brain tumor stem cells to enhance infiltration and migration into surrounding brain tissue(Hoelzinger et al., 2007). Diffusible factors and adherence cues emitted from surrounding vasculature exert an influence on BTSC proliferation and survival(Calabrese et al., 2007). With all these factors involved in BTSC proliferation, survival, and infiltration it is conceivable that a diversity of brain tumor stem cells may arise as a complex adaptive system that interacts through diffusible factors and adherence cues. Recently it has been shown in a Drosophila model that diverse, adjacent tumor cells can cooperate to produce emergent properties of tumorigenesis and infiltration(Wu et al.). To what extent this occurs in human glioma has yet to be determined.

In order to model the tumorigenic process of glioma, it is necessary to ascertain which processes are involved. Besides the brain tumor stem cell model and the clonal evolution model are more complex systems whose roles in glioma are in the realm of possibility. In order to prioritize therapeutic targets of glioma, it is important to have the most informative model of glioma tumorigenesis.

A study by Shapiro et al. in 1981 performed karyotypic analysis of different glioma tumors and the cultures derived from them and discovered 3-21 genetically distinct subpopulations within the average glioma tumor(Shapiro et al., 1981) with varying chemosensitivities(Yung et al., 1982). As this study was done in an age before neurosphere cultures, one cannot determine from this experiment how many genetically distinct, tumorigenic cultures were derived from each tumor. Recently, Piccirillo et al. (Piccirillo et al., 2006) isolated two genetically distinct populations of cells from distinct regions of a GBM tumor. However, only one population was tumorigenic, so one cannot assume that multiple populations of cancer stem cells existed in that particular tumor. However, this data does suggest the possibility that genotypically distinct BTSC may coexist within the same tumor. Recently, the existence of multiple genetically and phenotypically distinct BTSC within the same GBM culture has been demonstrated(Meyer et al., 2015b; Patel et al., 2014). Furthermore, this clonal heterogeneity was shown to confer chemoresistance(Meyer et al., 2015b). The existence of multiple BTSC within a single GBM tumor is evidence that supports the complex adaptive system model of GBM (Laks et al., 2010). In support of this complex adaptive model system is evidence that the degree of heterogeneity in tumors is correlated to poor clinical outcome of patients(Patel et al., 2014).

Personalized Medicine

A promising approach to the treatment of GBM is personalized medicine(Ene and Holland, 2015). This therapeutic strategy relies upon the characterization of each

individual tumor in order to provide effective tumor specific targets for a tailored treatment regimen. Characterization may rely upon genetic driver mutations, mRNA expression profiles, or even protein levels that signify activity of molecular signaling pathways. Yet, for this approach to be efficacious, the crucial parameters of the tumor must be identified. One approach to address personalized medicine is to test tumor derived tumorsphere cultures for response to treatment.

Molecular targeting

If one embraces the BTSC model of GBM, then the crucial molecular mechanisms that drive BTSC must be identified and targeted in order to treat GBM effectively with personalized medicine. Many cellular processes involved in regulating neural stem cells are also essential in glioma brain tumor stem cells. For example, certain cell cycle regulators and transcription factors involved in the regulation of neural progenitors, such as c-MYC, OCT-4, BMI-1, Olig-2, and MELK, also regulate brain tumor and putative BTSC proliferation and survival(Horvath et al., 2006; Ivanova et al., 2002; Li et al., 2009; Nakano and Kornblum, 2006; Nakano et al., 2007; Nakano et al., 2005; Taipale and Beachy, 2001; Wechsler-Reya and Scott, 2001). Similarly, multiple secreted growth factors involved in neural stem cell proliferation, such as EGF (epidermal growth factor), and IGF (insulin like growth factor), bind with receptor tyrosine kinases to activate downstream proliferation and survival pathways in brain tumor initiating cells(Li et al., 2009).

Noteworthy is the PI3 kinase/AKT pathway, a key regulator of signaling via different pathways, including those regulated by EGF and IGF receptors. The

PI3kinase/AKT pathway has received a lot of attention as a target for cancer treatment(Choe et al., 2003; Vivanco and Sawyers, 2002). Recently, expression of AKT and PI3 kinase activity has been shown to be associated with glioma tumor grade(Wang et al., 2010a). There are many agents available to researchers that specifically target this pathway, and this area of research promises to change therapeutic strategies utilized in glioma treatment(Maira et al., 2009). Rapamycin is a microbial derived therapeutic that acts specifically on mTOR(Bjornsti and Houghton, 2004; Brown et al., 1994; Chiu et al., 1994; Sabatini et al., 1994). mTOR is one downstream effector of the AKT pathway that can also act via a feedback loop to influence AKT signaling(O'Reilly et al., 2006). Recently, Rapamycin has made its way to clinical trials for the treatment of glioma(Cloughesy et al., 2008). However, Rapamycin treatment in clinical trials as well as in laboratory trials produces cellular resistance (Cloughesy et al., 2008; Hosoi et al., 1998). Further research is necessary to determine whether this resistance is due to the many feedback loops inherent in the pathway(Carracedo et al., 2008; Efeyan and Sabatini, 2009) or to some other biological process. A recent study has suggested that improved inhibitors of mTOR may decrease resistance(Thoreen et al., 2009; Thoreen and Sabatini, 2009).

Another critical signaling pathway involved in both neural progenitor and glioma proliferation and survival is the Notch pathway(Androutsellis-Theotokis et al., 2006; Gaiano and Fishell, 2002; Purow et al., 2005; Solecki et al., 2001). Notch is a family of transmembrane receptors that interact with adjacent cells. Upon ligand binding to Notch, gamma secretase cleaves the intracellular portion of the Notch receptor (NICD), thereby releasing NICD to translocate to the nucleus where it acts as a transcription factor

promoting proliferation and inhibiting differentiation. Evidence is accumulating that the Notch pathway plays a crucial role in the formation and growth of glioma tumors(Pierfelice et al., 2008) and drugs that inhibit gamma secretase are gaining interest as therapeutic agents in the treatment of glioma. Indeed, it has been demonstrated that Notch inhibition targets cancer stem cells in embryonal brain tumors(Fan et al., 2006).

Studies have demonstrated that Ephrin signaling, through modulation of the ERK pathway, is a therapeutic target involved in tumorigenesis and self-renewal of BTSC(Binda et al., 2012; Day et al., 2013). Other pathways implicated in glioma proliferation and malignancy are the Hedgehog, Wnt, and Bone Morphogenic Protein (BMP) pathways(Ng and Curran, 2011; Paul et al., 2013; Piccirillo et al., 2006). In addition, STAT3 signaling has been linked to GBM progression, while Integrin signaling has been linked to GBM migration and proliferation(Luwor et al., 2013; Uhm et al., 1999). The post-transcriptional modification of miRNAs has also been shown to regulate glioma(Hadjipanayis and Van Meir, 2009; Hambardzumyan et al., 2008; Li et al., 2009). In addition, alterations in INK4A, CDK4, RB, and TP53, which may disrupt cell cycle and apoptosis, have also been described in human astrocytic glioma (Furnari et al., 2007).

To address the multiplicity of oncogenic pathways, future treatment for glioma patients may include molecular expression characterization of tumor biopsies followed by a tailored regimen of combinatorial, targeted therapy. Another aim of research is to determine molecular and genetic diagnostic criteria for tumor biopsies that are predictive of which oncogenic pathways are the essential targets for tailored therapy.

Resistance

A central concern with utilizing specific drug targets is whether the redundancy of multiple oncogenic pathways confers resistance to single-pathway-targeted therapy(Mischel and Cloughesy, 2003; Stommel et al., 2007). For example, the Notch pathway and AKT pathway have been shown to interact in multiple ways(Chan et al., 2007; Ma et al., 2010; Mungamuri et al., 2006; Perumalsamy et al., 2009; Wang et al., 2010b) and this interaction may confer chemoresistance(Mungamuri et al., 2006). Hence, many investigators purport that combinatorial therapy provides a more robust therapeutic strategy(Kitano, 2007). By targeting both the driving molecular signaling pathway of the tumors, and its molecular mechanism of adaptive resistance, such combinatorial targeting efforts in pharmacology research hope to provide synergistic combinations of target specific drugs.

Chemoresistance represents a known challenge to glioma therapy. In addition to mechanisms of resistance that are dependent on specific signaling pathways, brain tumors possess other mechanisms of chemo-resistance. Chemoresistance to a broad spectrum of cytotoxic agents, termed multi drug resistance (MDR), is a characteristic of glioma and represents a major obstacle in effective treatment(Lu and Shervington, 2008). MDR may be the result of genetic evolution, an adaptation through mutations that occurs during chemotherapy, or it may be an a priori property of certain tumor cells. In both cases increased expression of drug transporters, such as the ATP binding cassette super-family (ABC transporters), act to pump cytotoxic agents out of the cell(Dean et al., 2005). Evidence that a distinct “side population” exists within tumors with enhanced drug efflux capacity suggests that MDR may be the intrinsic property of a minority of distinct tumor

cells with enhanced drug transporting capacity(Hirschmann-Jax et al., 2004). This multi drug resistant "side population" is believed to be enriched for brain tumor stem cells. It is unknown whether MDR is due to an intrinsic property of BTSC, or to ongoing mutational evolution, or is the result of a systemic response to treatment.

Resistance to therapy may include diverse mechanisms of adaptation including regulation of transcription, post-translational modifications of signaling pathways, genetic alterations, and copy number alterations. An alternative mechanism of resistance is one of selection, wherein resistant subtypes of cells are selected for by drug treatment. Selection may be of particular concern given that there is heterogeneity of BTSC within GBM tumors that reflects differential chemosensitivities (Meyer et al., 2015b; Piccirillo et al., 2015).

Tumors/TCGA

While gliomas are classified on the basis of histopathological criteria into four grades, molecular expression profiling has also been effective at distinguishing subclasses of glioma(Rickman et al., 2001). Molecular expression profiles provide an advantage by offering valuable insights into the specific oncogenic pathways that drive tumor proliferation and, thereby, produce a more specific characterization of each tumor. Classification of high grade glioma based on molecular expression profiles have classified 3-5 distinct types of malignant tumors that resemble different stages in neurogenesis, predict patient prognosis, and indicate that activation of the AKT and Notch canonical oncogenic pathways reflect the aggressiveness of these

neoplasms(Gunther et al., 2008; Phillips et al., 2006; Tso et al., 2006). Efforts by Verhaak et al. studying data from The Cancer Genome Atlas (TCGA) produced a defining classification of GBM tumors into 4 subtypes: Classical, Mesenchymal, Proneural and Neural (Verhaak et al., 2010). For the purposes of this paper, we will refer to the Verhaak et al. classification system as TCGA. This classification system was based on differential expression of 1740 highly variable genes in 200 GBM samples and 2 normal brain samples. This system was refined to 840 predictive genes across a large catalog of 173 core GBM tumor samples. This TCGA classification system has become the standard for distinguishing molecular subtypes of GBM tumors. These TCGA subtypes were also correlated to copy number variation data. The Classical subtype is characterized by Notch and Sonic hedgehog pathway activation, chromosome 7 amplification and chromosome 10 loss, consistent (97%) *EGFR* amplification, a lack of *TP53* mutation, and *CDKN2A* deletion. The Mesenchymal subtype was characterized by loss of activation of the NF-kB pathway, loss of *NF1*, and expression of mesenchymal genes. The Proneural subtype had activation of PDGFRA, OLIG2, and point mutations of *IDH1*. The Neural subtype had expression of neuron specific markers. The Proneural subtype alone did not show a significant response to intensive therapy. The TCGA classification system provides a method by which to distinguish GBM tumors based on molecular and genomic differences. Is this a major advance in personalized medicine? The answer to this question depends on whether a differential response to treatment is based on TCGA classification.

It is interesting to note, that when Verhaak et al. extended this classification to xenografts (cells derived from tumors and passaged in in vivo mouse models) they only

distinguished 3 classifications: Classical, Mesenchymal, and Proneural. The Neural class was no longer evident. In addition, the two normal brain samples included in the classifications of the original tumor samples were both categorized as Neural. This raises the possibility that the Neural classification is due to the remnants of normal brain tissue and not a description of the tumor cells. This possibility is further substantiated by a study that removed normal brain tissue from tumors, performed single cell RNA-seq, classified cells by TCGA methods, and found no Neural subgroup, only Classical, Mesenchymal, and Proneural (Patel et al., 2014).

Another important addendum to the TCGA classification is that it was originally performed on bulk tumor samples. When tumors were studied by single-cell RNA-seq, there was heterogeneity of TCGA classifications within a single tumor sample(Patel et al., 2014). This observation of heterogeneous TCGA classification within one sample was reiterated in tumor derived tumorsphere cultures(Meyer et al., 2015b).

To date, no large-scale assessment of tumor derived tumorsphere cultures has been performed in order to determine the relevance of TCGA classification in this model system.

Tumorspheres

The landmark TCGA classification system for GBM may provide a method for distinguishing different treatment regimens of targeted therapy for each subtype. However, as tumors are a static body of tissue, therapies cannot be directly tested on them to see how they respond. In order to study therapeutic response one requires a

dynamic system with living, proliferating cells. One in vitro system for this is the tumorsphere model.

One key limitation in the development of therapeutics is the availability of appropriate in vitro models in which key molecular pathways can be identified and potential novel therapies can be tested. Cell culture models utilized in the past include, amongst others, cultures derived from GBM patients that are continuously passaged in the presence of serum (Hecht et al., 1995). While these cultures have advanced our understanding of GBM biology, they have significant drawbacks, including their failure to produce tumors that are similar to GBM when implanted into animal models (Lee et al., 2006). Over the past decade, a novel, serum-free culture system has become widely used and accepted. GBMs and other brain tumors contain cells that have neural stem cell-like properties (Reynolds and Weiss, 1992) in that they grow as spheroid cultures in the presence of epidermal growth factor (EGF) and basic fibroblast growth factor and that are capable of producing the varied cell types found within the parent tumor (Hemmati et al., 2003; Ignatova et al., 2002; Singh et al., 2003). In fact, these sphere cultures are thought to be enriched for a set of cells capable of initiating tumors when implanted at very low numbers—so-called glioma stem or tumor initiating cells (Galli et al., 2004; Jordan et al., 2006; Laks et al., 2010; Nakano and Kornblum, 2006; Pardal et al., 2003; Reya et al., 2001; Singh et al., 2004b). Here, we will refer to the growth of primary GBM cultures in neurosphere conditions as tumorspheres as they generally grow as non-adherent spheres of cells.

The utility of tumorsphere cultures as a model has been supported by their ability to retain the major mutations found within the parent tumor and to produce tumors that

bear striking resemblances to human GBM following xenotransplantation (Galli et al., 2004; Lee et al., 2006; Singh et al., 2003). In contrast to mouse models of GBM, tumorsphere models retain a clonal heterogeneity of the GBM tumor(Meyer et al., 2015b). Therefore, the tumorsphere system may be a more suitable model for the complex adaptive system of the GBM tumor than mutant mouse models that generate endogenous, clonal, tumors.

Given that there is a diversity of GBM in terms of mutation and molecular expression, our approach was to assess a broad spectrum of GBM in order to determine which molecular signaling pathways are associated with sphere formation, proliferation, and therapeutic response.

Aims and Hypothesis

This dissertation has 3 aims.

- 1. To perform a comprehensive assessment of the GBM tumorsphere model system.
- 2. To test the hypothesis that interrogation of the tumorsphere system is informative for the study of targeted therapy.
- 3. To determine the molecular mechanism of resistance to chronic mTOR inhibition.

Chapter 2

Large-scale assessment of the tumorsphere model system for glioblastoma

Aim 1. To perform a comprehensive assessment of the GBM tumorsphere model system.

Abstract

Tumorsphere cultures are widely utilized, but not well validated for the study of glioblastoma (GBM) biology and therapy. Using the gene expression-based TCGA classification, we observed that tumorsphere cultures retained their classification over many passages, but do not always harbor the same classification as their parent tumor. Unsupervised clustering of tumorspheres distinguished two general expression categories while multi-dimensional scaling (MDS) distinguished three main groups and a fourth minor group. Important molecular pathways, including PI3Kinase, Protein Kinase A, mTOR, ERK, Integrin, and Beta Catenin were associated with in vitro measures of proliferation and clonal sphere formation. In addition, we correlated gene expression with tumorsphere phenotypes and patient outcome and identified genes not previously associated with GBM: *PTGR1*, that suppresses proliferation, and *EFEMP2* and *LGALS8*, that promote cell proliferation. This comprehensive assessment provides support and outlines limitations for the utility of the tumorsphere system to model GBM biology.

Background

Glioblastoma (GBM) is one of the most lethal cancers and new therapies are urgently needed (Daumas-Duport et al., 1988; Miller and Perry, 2007). One key limitation in the development of therapeutics is the availability of appropriate in vitro models in which key molecular pathways can be identified and potential novel therapies can be tested. Cell culture models utilized in the past include, amongst others, cultures derived from GBM patients that are continuously passaged in the presence of serum (Hecht et al., 1995). While these cultures have advanced our understanding of GBM biology, they have significant drawbacks, including their failure to produce tumors that are similar to GBM when implanted into animal models (Lee et al., 2006). Over the past decade, a novel, serum-free culture system has become widely used and accepted. GBMs and other brain tumors contain cells that have neural stem cell-like properties (Reynolds and Weiss, 1992) in that they grow as spheroid cultures in the presence of epidermal growth factor (EGF) and basic fibroblast growth factor and that are capable of producing the varied cell types found within the parent tumor (Hemmati et al., 2003; Ignatova et al., 2002; Singh et al., 2003). In fact, these sphere cultures are considered enriched for a set of cells capable of initiating tumors when implanted at very low numbers—so-called glioma stem or tumor initiating cells (Galli et al., 2004; Jordan et al., 2006; Laks et al., 2010; Nakano and Kornblum, 2006; Pardal et al., 2003; Reya et al., 2001; Singh et al., 2004b). Here, we will refer to the growth of primary GBM cultures in neurosphere conditions as tumorspheres as they generally grow as non-adherent spheres of cells. The utility of tumorsphere cultures as a model has been supported by their ability to retain the major mutations found within the parent tumor and to produce tumors that bear striking

resemblances to human GBM following xenotransplantation (Galli et al., 2004; Lee et al., 2006; Singh et al., 2003). However, a comprehensive assessment of tumorsphere mRNA expression profiles in relationship to in vitro phenotypes and patient survival has not yet been performed.

GBM subtypes are often defined by histopathological criteria, however several studies have demonstrated that high-grade gliomas, including GBM, can be further classified through gene expression into clinically relevant subgroups (Phillips et al., 2006; TCGA, 2008; Verhaak et al., 2010). The Cancer Genome Atlas (TCGA) produced a classification of GBM tumors into 4 subtypes: Proneural, Neural, Classical, and Mesenchymal. This classification system was based on differential gene expression across a catalog of tumor samples and correlates with genetic mutation and other phenotypes, such as hypermethylation (Noushmehr et al., 2010). Whether this TCGA classification system is optimal for tumorspheres, or is predictive of in vitro phenotypes has not been well characterized.

Despite the many advantages of the tumorsphere culture system, much remains unknown about how closely the biology of spheres represents that of human GBM in situ. Previously, we found a strong direct relationship between our ability to obtain tumorsphere cultures and the clinical aggressiveness of the tumor (Laks et al., 2009). However, it is unclear how tumorspheres reflect the molecular heterogeneity of GBM as described by the TCGA and other classifications and whether the study of tumorsphere cultures can reveal important molecular and phenotypic aspects that cannot be gleaned from direct examination of the parent tumor.

We have established a large bank of tumorspheres and have assayed their phenotypic and genomic characteristics in relationship to the parent tumor and patient outcome. Analysis of tumorspheres using the TCGA classification indicates that tumorspheres do not necessarily reflect the TCGA subgrouping of the parent tumor. Unsupervised clustering based on transcriptional profiling reveals two main categories of tumorspheres, a "Mesenchymal" and "non-Mesenchymal" group, similar to prior reports (Bhat et al., 2013). Weighted gene coexpression network analysis (WCGNA) reveals an association between sphere formation and Protein Kinase A, mTOR, and Integrin signaling pathways. By selecting genes based on in vitro outcome and patient survival, we discovered that *EFEMP1* and *LGALS8* act as determinants of proliferation and clonal sphere formation, while *PTGR1* suppresses clonal sphere formation.

Taken together, our data provide further evidence that tumorspheres reflect certain aspects of GBM biology. Yet, we also identify some limitations of this tumorsphere system as a model for GBM. Employing both in vitro phenotypic analysis and survival data, we demonstrate that the dynamic tumorsphere model can be utilized in a manner that distinguishes it from an assessment of the original, static tumor sample. The tractable tumorsphere system offers a unique platform for the discovery of novel genes involved in proliferation and tumor biology.

Results

Description of Tumorsphere Dataset:

We studied 71 tumorsphere cultures (Supp. Table 1) from 67 individuals derived from surgical resection of high-grade glioma patients who were predominately diagnosed with Grade IV glioma: GBM (69/71). One sample, (NS039) was originally resected elsewhere and cultured at UCLA after passaging in animals(Sarkaria et al., 2007). Four pairs of tumors were derived from the same four patients at two separate resections. Microarray-based gene expression profiling was performed on all samples using the Affymetrix U133 plus 2.0 platform. The average age of the patients who contributed the 70 tumorsphere cultures resected at our institution was 55.7 years ± 16.4 years (range=20-86, Figure 1A) and 67.1 were male (Table 1, Figure 1A,B). Clinical and pathological reports were available for the 69 grade 4 gliomas; 39.1% (27/69) of the tumorspheres were derived from primary tumors, 43.5% (30/69) from recurrent tumors, and 17.4% (12/69) were from secondary tumors (Table 1, Figure 1C). 19.7% (12/61) had *EGFR*vIII rearrangement, while fifty percent (23/46) were found to have EGF receptor (*EGFR*) amplification at cytogenetic analysis (Table 1, Figure 1D,E). We validated the tumorsphere cultures for *EGFR*vIII by western blot. All of the tumors that were positive for *EGFR*vIII in pathology were also positive for *EGFR*vIII in the tumorspheres (Table 1). Only HK361 was *EGFR*vIII positive in tumorsphere culture but negative in the tumor pathology report. Six patients were found to have the R132H mutation in *IDH1*, and retention of the mutation was confirmed by direct sequencing of the tumorsphere cultures. Of the 71 high-grade tumorsphere cultures, one was given the pathological

diagnosis of Grade III Anaplastic Oligodendroglioma, and seven out of the 69 GBM were sub-classified as Gliosarcoma (Table 1).

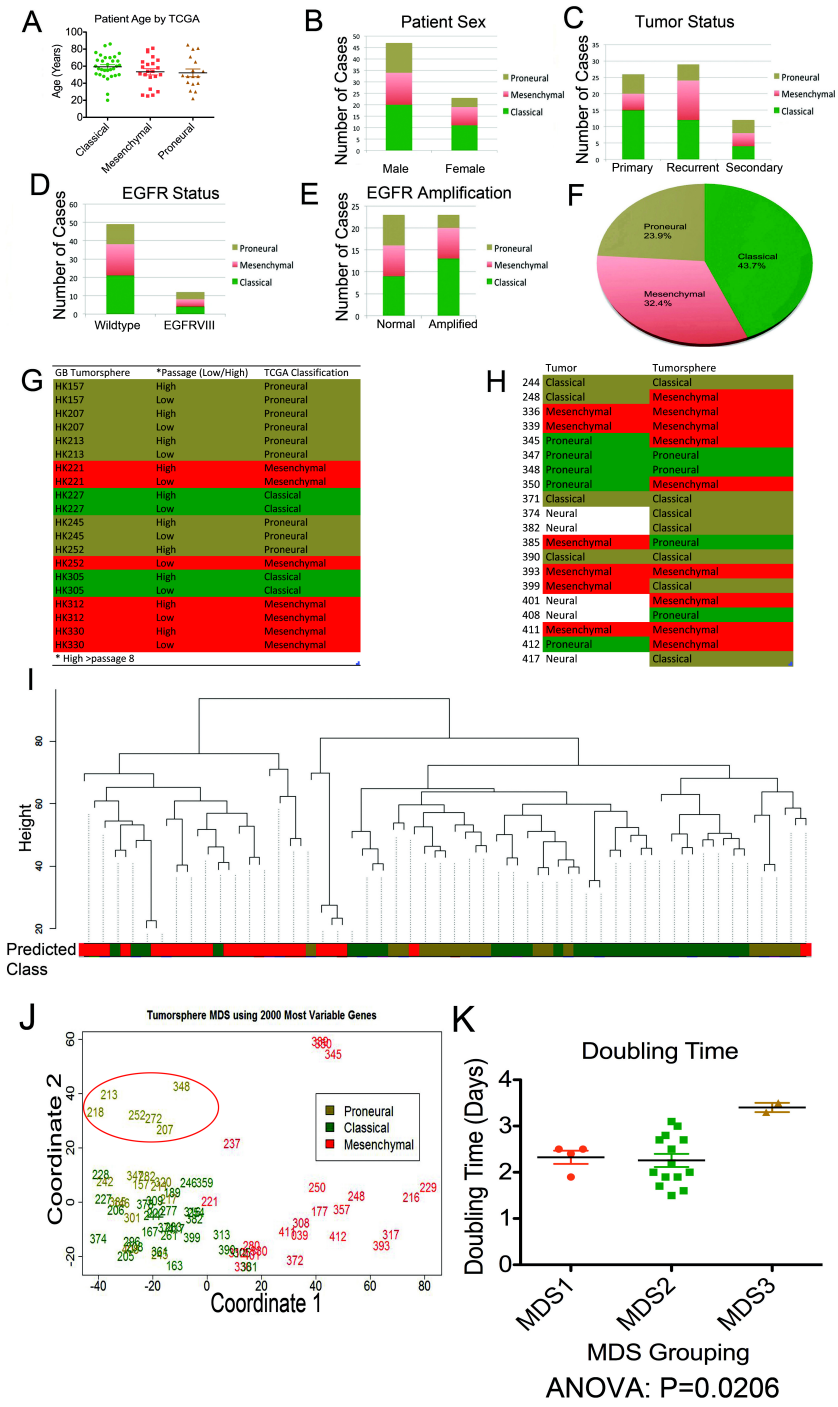
A
Patient Age by TCGA
Age (Years)
Classical
Mesenchymal
Proneural
B
Patient Sex
Number of Cases
Male
Female
Proneural
Mesenchymal
Classical
C
Tumor Status
Number of Cases
Primary
Recurrent
Secondary
D
EGFR Status
Number of Cases
Wildtype
EGFRVIII
E
EGFR Amplification
Number of Cases
Normal
Amplified
F
Proneural 23.9%
Classical 43.7%
Mesenchymal 32.4%
G
GB Tumorsphere | *Passage (Low/High) | TCGA Classification
HK157 | High | Proneural
HK157 | Low | Proneural
HK207 | High | Proneural
HK207 | Low | Proneural
HK213 | High | Proneural
HK213 | Low | Proneural
HK221 | High | Mesenchymal
HK221 | Low | Mesenchymal
HK227 | High | Classical
HK227 | Low | Classical
HK245 | High | Proneural
HK245 | Low | Proneural
HK252 | High | Proneural
HK252 | Low | Mesenchymal
HK305 | High | Classical
HK305 | Low | Classical
HK312 | High | Mesenchymal
HK312 | Low | Mesenchymal
HK330 | High | Mesenchymal
HK330 | Low | Mesenchymal
* High >passage 8
H
Tumor | Tumorsphere
244 Classical | Classical
248 Classical | Mesenchymal
336 Mesenchymal | Mesenchymal
339 Mesenchymal | Mesenchymal
345 Proneural | Mesenchymal
347 Proneural | Proneural
348 Proneural | Proneural
350 Proneural | Mesenchymal
371 Classical | Classical
374 Neural | Classical
382 Neural | Classical
385 Mesenchymal | Proneural
390 Classical | Classical
393 Mesenchymal | Mesenchymal
399 Mesenchymal | Classical
401 Neural | Mesenchymal
408 Neural | Proneural
411 Mesenchymal | Mesenchymal
412 Proneural | Mesenchymal
417 Neural | Classical
I
Height
Predicted Class
J
Tumorsphere MDS using 2000 Most Variable Genes
Coordinate 1
Coordinate 2
Proneural
Classical
Mesenchymal
K
Doubling Time
Doubling Time (Days)
MDS1
MDS2
MDS3
MDS Grouping
ANOVA: P=0.0206

Figure 1

Figure 1. Summary statistics on 71 tumorsphere samples. A-E. Distribution, according to TCGA classification of patients' age in years (A), sex (B), type of parent tumor (primary, recurrent, or secondary) (C), *EGFR* mutation status, wildtype or *EGFR*V3 mutant, (D), and *EGFR* amplified status (E). F. Tumorsphere distribution for each of 3 TCGA classifications. G. TCGA classification of tumorspheres across high and low passages (high>8 passages). H. TCGA classification of parent tumors and their derived tumorsphere cultures. I. Hierarchical clustering of 71 tumorsphere cultures based on gene expression profiles of the top 2000 most variable genes identifies two main clusters. One of them (Mesenchymal) comprises most of the samples with TCGA Mesencymal classification. Color codes: Classical=Green, Mesenchymal= Red, Proneural=Gold. J. Multidimensional scaling (MDS) of 71 tumorphere cultures based on the top 2,000 most variable genes distinguishes 2 groups on the first principal component (PC1=coordinate 1), and 3 groups when incorporating the second principal component (PC2= coordinate 2) with a minor 4^{th} group. The red oval distinguishes the 3^{rd} subgroup of Proneural tumorspheres delineated by MDS. 3-digit numbers represent the GBM tumorsphere identification numbers. K. Cell doubling time (inverse of proliferation rate) is plotted for the 3 MDS groups from MDS plot Figure 1J. MDS3 (MDS group 3) has a slower doubling time than the other groups (ANOVA: P=0.021). Group 1= Right side of plot (all Mesenchymal) Group 2=Lower left side of plot (mostly Classical with some Proneural and Mesenchymal), Group3=Upper left side of plot, delineated by red oval (all Proneural). MDS groupings for each tumorsphere sample are reported in Supplementary Table 1. Mean +/- standard error of the mean is depicted as bars. In all figures Classical=Green, Mesenchymal= Red, Proneural=Gold.

Sumary Table of Tumorspheres and Characteristics, Mutations, Phenotype, and Patient Treatment

ID	*EGFR*vIII Pathology Report	*EGFR*vIII-Tumorsphere	EGFR Amp	IDHR132H*	Diagnosis	Age	Sex	tumor Category	TCGA Class	Cluster**	3 MDS groups***	Doubling Time (Days)	Sphere Formation(%)	Sphere Total Volume(uM^3)
NS_039		Yes							Mesenchymal	group1	1		10.3	1.16E+08
HK_146	Yes	Yes			GBM	55	Male	Recurrent	Proneural	group2	2		23.2	4.61E+07
HK_157	No	No			GBM	54	Female	Primary	Proneural	group2	2	1.9	43.73333	2.23E+08
HK_163		ND (not determined)			GBM	67	Female	Primary	Classical	group2	2			
HK_167		ND			GBM	75	Male	Primary	Classical	group2	2			
HK_177	Yes	Yes	Yes		GBM	47	Male	Primary	Mesenchymal	group1	1			
HK_189	No	No	No		GBM	48	Male	Recurrent	Classical	group2	2			
HK_205		ND			GBM	84	Male	Primary	Classical	group2	2			
HK_206	No	No	No		GBM	48	Male	Recurrent	Classical	group2	2	2.7	3.92	
HK_207	No	No	No	Yes	GBM	31	Male	Recurrent	Proneural	group2	3	3.3	4	963602
HK_208		ND			GBM	60	Female	Primary	Classical	group2	2	2		
HK_211	Yes	Yes	No	Yes	GBM	41	Female	Secondary	Proneural	group2	2			
HK_213	No	No	No	Yes	recurrent HGG	39	Male	Secondary	Proneural	group2	3	3.5	2.9	799487
HK_216	No	ND	No		GBM/Gliosarcoma	50	Male	Recurrent	Mesenchymal	group1	1	3.4		
HK_217	No	No	No		GBM	81	Male	Primary	Proneural	group2	2	1.7		
HK_218	No	No	No	Yes	Grade III A.O.****	49	Female		Proneural	group2	3			
HK_221		ND			GBM	62	Male	Primary	Mesenchymal	group2	2			
HK_222	No	No	Yes		GBM	70	Male	Secondary	Classical	group2	2	2.6		
HK_227	No	No	Yes		GBM	62	Male	Recurrent	Classical	group2	2		12.15	3.65E+07
HK_228	No	No	No		GBM	57	Male	Primary	Classical	group2	2			
HK_229	No	No	No		GBM/Gliosarcoma	54	Male	Recurrent	Mesenchymal	group1	1	1.9		
HK_233	No	No	No		GBM	86	Male	Primary	Classical	group2	2	2.5		
HK_237	No	No			GBM	25	Female	Secondary	Mesenchymal	group2	2			
HK_242		No			GBM	80	Male	Recurrent	Proneural	group2	2	2.9		
HK_244	No	No			GBM	66	Female	Primary	Classical	group2	2	3.5	10.1	2.09E+07
HK_245		Yes	Yes		GBM	48	Male	Recurrent	Proneural	group2	2			
HK_246		Yes			GBM	49	Male	Recurrent	Classical	group2	2			
HK_248	No	No			GBM	77	Male	Recurrent	Mesenchymal	group1	1	2.5	39.8	2.99E+08
HK_250	No	No	No		GBM	30	Female	Recurrent	Mesenchymal	group1	1	2.5		
HK_252	No	No	Yes	Yes	GBM	40	Male	Secondary	Proneural	group2	3	3.2	3.5	1167633
HK_254	No	No			GBM	51	Female	Recurrent	Classical	group2	2	2.5		
HK_261	Yes	ND			GBM	50	Male	Secondary	Classical	group2	2	3.7		
HK_272		ND	No		GBM	22	Male	Primary	Proneural	group2	3			
HK_277	No	No			GBM	20	Female	Secondary	Classical	group2	2		5.7	1630512
HK_280	No	No	Yes		GBM	79	Male	Primary	Mesenchymal	group1	2			
HK_282	No	No			GBM	85	Male	Primary	Proneural	group2	2	2.1		
HK_296	Yes	Yes	Yes		GBM	76	Male	Recurrent	Classical	group2	2	3.1	45.4	2.04E+07
HK_301	Yes	Yes	Yes		GBM	65	Male	Primary	Proneural	group2	2		15.33333	1.47E+08
HK_305	No	No	Yes		GBM	60	Female	Secondary	Classical	group1	2			
HK_308	Yes	Yes			GBM	50	Female	Recurrent	Mesenchymal	group1	2	2.2	21.8	7.67E+07
HK_309	No	No	No		GBM	55	Male	Recurrent	Classical	group2	2	2.7	10.6	2.79E+07
HK_312	No	No	Yes		GBM	63	Male	Secondary	Mesenchymal	group1	2			
HK_313	No	No	Yes		GBM	66	Female	Primary	Classical	group1	2			
HK_316	No	No	Yes		GBM	56	Female	Recurrent	Classical	group2	2			
HK_317	No	No			GBM	67	Male	Primary	Mesenchymal	group1	2			
HK_320	No	No		Yes	GBM	30	Female	Secondary	Proneural	group2	2			
HK_330	No	No	Yes		GBM	51	Female	Secondary	Mesenchymal	group1	2			
HK_336	No	No	No		GBM	65	Male	Recurrent	Mesenchymal	group1	2	1.9		
HK_339	No	No	No		GBM/Gliosarcoma	26	Female	Recurrent	Mesenchymal	group2	1			
HK_345		Yes			GBM/Gliosarcoma	26	Female	Recurrent	Mesenchymal	group2	1			
HK_347	No	No	No		GBM	48	Male	Recurrent	Proneural	group2	2	2.8		
HK_348	No	No			GBM/Gliosarcoma	71	Male	Primary	Proneural	group2	3			
HK_350	Yes	Yes	Yes		GBM	81	Female	Recurrent	Mesenchymal	group2	1	2.4		
HK_357	No	No			GBM	58	Male	Recurrent	Mesenchymal	group1	2			
HK_359	Yes	Yes	Yes		GBM	27	Male	Recurrent	Classical	group2	2	2.8		
HK_361	No	Yes	Yes		GBM	50	Male	Recurrent	Classical	group2	2	2.3		
HK_371	No	No	Yes		GBM	56	Female	Recurrent	Classical	group2	2			
HK_372	No	No	Yes		GBM	33	Male	Primary	Mesenchymal	group1	2			
HK_374	Yes	Yes	Yes		GBM	45	Male	Primary	Classical	group2	2	1.5		
HK_378	No	No	Yes		GBM	61	Male	Recurrent	Classical	group2	2	2	18.1	5.16E+08
HK_381	No	No	Yes		GBM	57	Female	Primary	Classical	group1	2	3	27.5	3.04E+07
HK_382	No	No	No		GBM	66	Male	Primary	Classical	group2	2	2.7		
HK_385	Yes	Yes			GBM	48	Male	Primary	Proneural	group2	2			
HK_390	No	No	No		GBM	73	Male	Primary	Classical	group1	2	2	14.4	7.39E+07
HK_393	No	ND	No		GBM/Gliosarcoma	54	Male	Secondary	Mesenchymal	group1	2	1.6		
HK_399	No	No	No		GBM	70	Male	Primary	Classical	group2	2			
HK_401	No	No	No		GBM/Gliosarcoma	48	Male	Recurrent	Mesenchymal	group1	2			
HK_408		ND	Yes		GBM	55	Female	Primary	Classical	group2	2			
HK_411	No	No			GBM	71	Male	Recurrent	Mesenchymal	group1	2			
HK_412	Yes	Yes	Yes		GBM	59	Female	Primary	Mesenchymal	group1	2			
HK_417	No	ND	No		GBM	71	Male	Primary	Classical	group2	2			

* IDH1 mutation detemined by sequencing
**Cluster (1="Mesenchymal", 2="Non-Mesenchymal")
*** MDS group1= Right Side of Coordinate 1, MDS group2= Bottom left side of MDS plot, MDS group3=Top left side of MDS plot.
**** AO=Anaplastic Oligodendroglioma

Table 1

Table 1. Summary Table of Tumorsphere and Patient Characteristics.

*EGFR*vIII-tumorsphere was obtained from western blots of tumorsphere cultures. Data on *EGFR*vIII, *EGFR* Amplification, Diagnosis, Age, and Tumor Category are gleaned from the medical record and the official pathology report. The IDH mutation status was obtained first from the pathology report and then verified in tumorspheres.

Four sets of two samples each were derived from the same patients following re-resections. All patients with recurrent tumors had been treated with Temozolomide (TMZ) and radiation prior to collection of tissue. Other therapies were also used in some of the patients. Following initial resection, all primary GBM patients were also treated with TMZ and radiation amongst other therapies.

Molecular Classification of Tumorspheres:

We used microarray analysis to determine the molecular classification of tumorsphere samples. We assigned each tumorsphere culture a TCGA classification of Classical, Mesenchymal, or Proneural based on the TCGA panel, using 789 genes out of the original 840 TCGA genes that were present in our array platform. Initially, we used all four classifications including Neural, as well as Classical, Mesenchymal, and Proneural. However, only two of the 71 tumorspheres were classified as Neural. As very few samples classified as Neural, we followed the strategies of others (Meyer et al., 2015a) and eliminated the Neural classification because this classification may be more representative of normal brain rather than tumor (Verhaak et al., 2010). Indeed, when normal brain cells were excluded from single-cell RNA-seq of GBM tumor cells, the Neural group did not appear upon TCGA classification(Patel et al., 2014). Of the 71 tumorsphere cultures, 31 (43.7%) were categorized as Classical, 23 (32.4%) were Mesenchymal, and 17 (23.9%) were Proneural (Figure 1F, Table 1).

In order to determine whether tumorsphere cultures maintained their expression profiles over time and passaging, we classified a subset of tumorsphere cultures at early

(<8) and later (>8) passages. Nine of ten tumorsphere cultures maintained their TCGA classification from low to high passage number (P<0.003, chi-square test)(Figure 1G). These data suggest that the TCGA classification of tumorsphere cultures is robust to repeated passaging. In three out of four cases tumorspheres derived from different resections from the same patient retained their TCGA classification. In one case the classification changed from Classical to Mesenchymal.

Prior reports indicate that some of the common oncogenic mutations are associated with particular TCGA subtypes (Brennan et al., 2013). For example *EGFR*vIII has been associated with the Classical phenotype and *IDH1* mutations are associated with the Proneural phenotype. From the tumor pathology report, *EGFR* amplification (ANOVA, P=0.328), or *EGFR*vIII rearrangement (ANOVA, P=0.721), were not significantly associated with any one of the three TCGA classifications. *EGFR*vIII in tumorspheres was also not correlated with TCGA classification (ANOVA, P=0.664). However, *IDH1* mutations were uniformly (6/6 cases) associated with the Proneural classification (Table 1). TCGA classification of tumorspheres was not associated with whether the source tumor was primary, recurrent, or secondary (ANOVA, P=0.477). Of the seven tumorspheres derived from gliosarcomas, six were classified as Mesenchymal subtype. This data supports the hypothesis that tumorsphere cultures retain important hallmarks of the parent tumor such as *IDH1* mutations preferentially classified as Proneural(Verhaak et al., 2010), and gliosarcoma tumors, which was previously reported to exhibit a mesenchymal molecular signature (deCarvalho et al., 2010), are predominately classified as Mesenchymal subtype.

Next, we used unbiased methods to analyze gene expression in the tumorspheres. First, we performed unsupervised clustering of the tumorsphere cultures based on the top 2000 most variable genes (Figure 1I). This revealed two general subgroups, one containing most of the Mesenchymal sphere cultures and another largely consisting of Proneural and Classical tumorspheres (Figure 1I). This phenomenon wherein the Mesenchymal subtype is tightly clustered has been reported previously (Bhat et al., 2013). Multi-dimensional scaling (MDS) of the tumorspheres generally supports the concept of two groups when viewed along the first principal component (PC1), which accounts for 48.28% of the variance. However, when considering the second principal component (PC2), which accounts for 9.63% of the variance, a subset of six Proneural tumorspheres appears to segregate separately (red oval in Figure 1J) as does a minor group of 3 Mesenchymal samples (top right quadrant, Figure 1J). Interestingly, within this subset of 3 very closely related Mesenchymal samples are a couple of tumorspheres that were derived from the same patient diagnosed with a secondary GBM, in surgeries separated by only 49 days. The third Mesenchymal sample from that subgroup was also derived from a secondary GBM.

Tumors and Tumorspheres:

To determine whether tumors and tumorspheres from the same samples were molecularly similar, we split 20 tumor samples in half, directly isolating RNA from one half and generating tumorsphere cultures from the other (Figure 1H). Sixty percent of the samples (excluding 5 tumors that fell into the Neural subclass) yielded the same TCGA classification in tumor and spheres, but this overlap was not statistically different from

chance (P=0.102, Chi-squared Test), possibly because of our small sample size. For those samples with differing subclassifications, there were no trends in the manner in which they switched categories. That is, tumors in one subtype did not tend to yield spheres in another particular subtype. Tumorspheres derived from tumor samples that classified into the Neural group did not classify into any one particular classification. In addition, when we analyzed the two cluster groups ("Mesenchymal" vs. "Non-Mesenchymal") identified by unsupervised clustering, only 50% of the tumorspheres retained the same grouping as their parent tumor (P=0.658, Chi-squared Test).

We next sought to determine gene expression differences between tumors and tumorsphere samples as a whole. We performed pairwise comparisons of gene expression from each tumor and its derived tumorsphere and identified 188 differentially expressed genes using a nominal p-value of 0.001 as our statistical threshold. Ingenuity analysis revealed the molecular and cellular functions associated with these changes, including cellular development (Range of $P=6.57*10^{-4}$-$4.02*10^{-2}$), cell growth and proliferation (Range of $P=6.57*10^{-4}$-$4.04*10^{-2}$), cell cycle (Range of $P=9.81*10^{-4}$-$4.82*10^{-2}$), cell signaling (Range of P=0.00171-0.0313), post-translational modification (Range of P=0.00171-0.0244) and Clathrin-mediated endocytosis signaling (P=0.0182) (Table 2). We then used a more conservative threshold (false discovery rate adjusted p-values of $P<0.05$) and identified a subset of 13 differentially expressed genes between tumor and tumorspheres (Table 2). Our data indicate that, while there are certain changes in expression from tumors to tumorspheres related to cell proliferation, the vast majority of genes do not undergo consistent changes across tumorsphere cultures.

Molecular Expression Changes from Tumor to Tumorsphere

Significant Molecular and Cellular Functions (Ingenuity Analysis)

Name	P-Value	# Molecules
Cellular Development	0.000657-0.0403	16
Cellular Growth and Proliferation	0.000657-0.0404	14
Cell Cycle	0.000981-0.0482	13
Cell Signaling	0.00171-0.0313	15
Post Translational Modification	0.00171-0.0244	21

Significant Canonical Pathways (Ingenuity Analysis)

Ingenuity Canonical Pathways	P Value	Ratio	Molecules
Fcγ Receptor-mediated Phagocytosis in Macrophages and Monocytes	0.00724	4.3E-02	ACTR2,ARF6,CBL,FYB
Clathrin-mediated Endocytosis Signaling	0.0182	2.7E-02	ACTR2,ARF6,CBL,USP9X,APOC1

Gene Changes (FDR P<0.05)

Gene	FDR P Value	Mean of differences T-N
ZW10	0.0162	-0.392
CLN6	0.00371	-0.451
SYNJ2BP	0.0245	-0.713
SCIN	<0.001	0.483
C1QB	0.000543	0.935
FCER1G	0.0433	0.726
TAF6L	0.0289	-0.324
ANKRD37	0.00867	0.363
MS4A7	0.0433	0.796
RGS1	0.0433	0.865
PTPRC	0.0245	0.683
GIMAP6	0.0268	0.681
ZNF492	0.00197	0.463

Table 2. Molecular Expression Changes from Tumor to Tumorsphere. Ingenuity analysis of gene list comparing significant genes (P<0.001) differing between 20 tumors and their derived tumorspheres. The ratio is the number of genes in our list divided by the number of genes in the pathway. Canonical pathways are shown if they are significant (P<0.05) and contain >2 genes in the list. Gene changes depicts the list of genes significantly changed between tumors and their derived tumorspheres with a false discovery rate (FDR) P<0.05. Mean of differences T-N depicts the difference of the tumor minus the tumorsphere mean gene expression levels. Therefore, a negative number represents enrichment of gene expression in the tumorsphere culture as compared to the tumor, while a positive number represents depletion of gene expression in the tumorsphere culture as compared to the tumor.

Association of Tumorsphere Gene Expression with Phenotype:

To both assess the utility of different analytic schemes and to determine factors associated with the characteristics of tumorspheres we examined 3 properties of the tumorsphere formation: clonal sphere formation, sphere total volume, and proliferation rate (the inverse of doubling time). As anticipated, doubling time was inversely associated with sphere total volume (Linear Regression, P=0.0182) (Figure 2). However, doubling time was not significantly associated with clonal sphere formation (P=0.16), suggesting that clonal sphere formation is not merely a reflection of overall proliferation. None of the three tumorsphere characteristics was associated with TCGA classification, *EGFR* mutational status, or with one of the two clusters (Mesenchymal and non-Mesenchymal), identified by unsupervised clustering. However, if we categorize the tumorspheres based on the three main MDS groups observed (Figure 1J), then group 3 (the Proneural subgroup in the red oval) has the slowest proliferation (largest doubling time) (Anova: P=0.0206)(Figure 1K). This suggests that unsupervised classification using MDS may identify 3 biologically distinct subgroups.

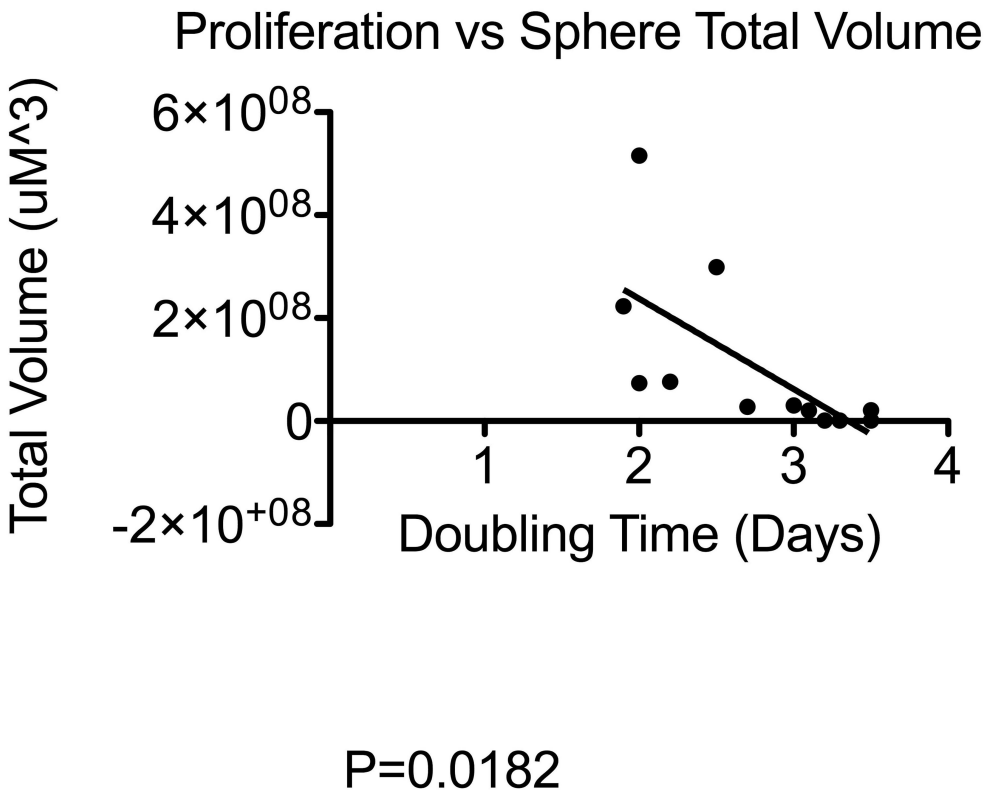

Figure 2. Linear regression analysis shows an inverse correlation between tumorsphere doubling time in bulk cultures with sphere total volume at clonal density (P=0.0182).

To further investigate molecular predictors of tumorsphere characteristics, we correlated gene expression levels with the three tumorsphere phenotypes. We chose to study genes whose expression correlated with the three phenotypes at $p<0.001$. For example, *KLHL9* expression was inversely correlated (Pearson's $r=-0.758$, $P<0.0001$) with sphere formation. Utilizing TFacts (www.TFacts.org), a tool that predicts activation or inhibition of transcription factors through gene expression changes, we identified a significant association between genes correlated to sphere formation and three activated transcription factors: HIF1A, TCF7, and CTNNB1 (Beta Catenin) (Table 3). These results were supported by an Ingenuity analysis (www.ingenuity.com) that generated a list of canonical pathways associated with sphere formation including HIF1A, ($P<0.001$), Wnt/Beta Catenin ($P=0.000447$), and other pathways associated with tumor initiation such as PI3K ($P<0.001$), EGF ($P<0.001$), mTOR ($P=0.0417$), and ERK ($P=0.000813$). PI3Kinase, mTOR, Beta Catenin, and the ERK pathways were significantly ($P<0.05$) associated with both sphere formation and sphere total volume, a measure of clonal proliferation.

Transcription Factors Associated* with Genes Whose Expression Correlates with Phenotypic Outcome of GBM Tumorspheres

Outcome	Factor	Activated	P value	E value	Q value	FDR control (B-H)	Intersection	Target genes
% Sphere formation	HIF1A	Activated	<0.001	<0.001	<0.001	0.000455	14	22
% Sphere formation	TCF7	Activated	0.00015	0.0165	0.00825	0.000909	9	17
% Sphere formation	CTNNB1	Activated	0.00042	0.0462	0.0154	0.00136	62	300
Proliferation Rate	TP53	Activated	<0.001	0.0108	0.0108	<0.001	11	97

*Tfacts Signed Analysis(www.Tfact.org, de Duve Institute)

Table 3. Transcription Factors Associated with Genes Whose Expression Correlates with Phenotypic Outcome of GBM Tumorspheres. TFacts signed analysis of our list of significant genes ($P<0.001$) associated with the in vitro phenotypic outcomes listed. The E-value takes into account the significance of repeated comparisons and the likelihood of the observed value being different than the expected value. The Q value is the

measurement of the false discovery rate. We chose transcription factors as significant if the E value <0.05. The intersection depicts how many genes from our list coincide with the known target genes of the transcription factor. “Target genes” denotes the number of genes that are known targets of the indicated transcription factor.

Ingenuity analysis determined overrepresented pathways from genes associated with proliferation rate (inverse of doubling time) ($P<0.001$) that included several proliferation associated pathways such as HIF1A ($P=0.0162$), and p70S6K ($P=0.0468$). Interestingly, TFacts analysis indicates that activated TP53 is associated with proliferation rate (inverse of doubling time) (Table 3).

Another method of analyzing gene expression is via weighted gene correlation network analysis (WGCNA) that identifies modules of tightly coexpressed genes. We performed a signed WGCNA analysis of the gene expression for the tumorsphere cultures to determine co-regulated modules of genes that were associated with phenotype (Figure3A). Sphere formation was most highly correlated to the “Orange Red” module (Correlation=0.5, $P<0.0001$) (Figure 3A). Several pathways, as revealed by Ingenuity analysis, were overrepresented within this group of genes, including Protein Kinase A (PRKACA) ($P=0.00280$), mTOR ($P=0.0339$), and Integrin signaling ($P=0.0389$) (Figure3B).

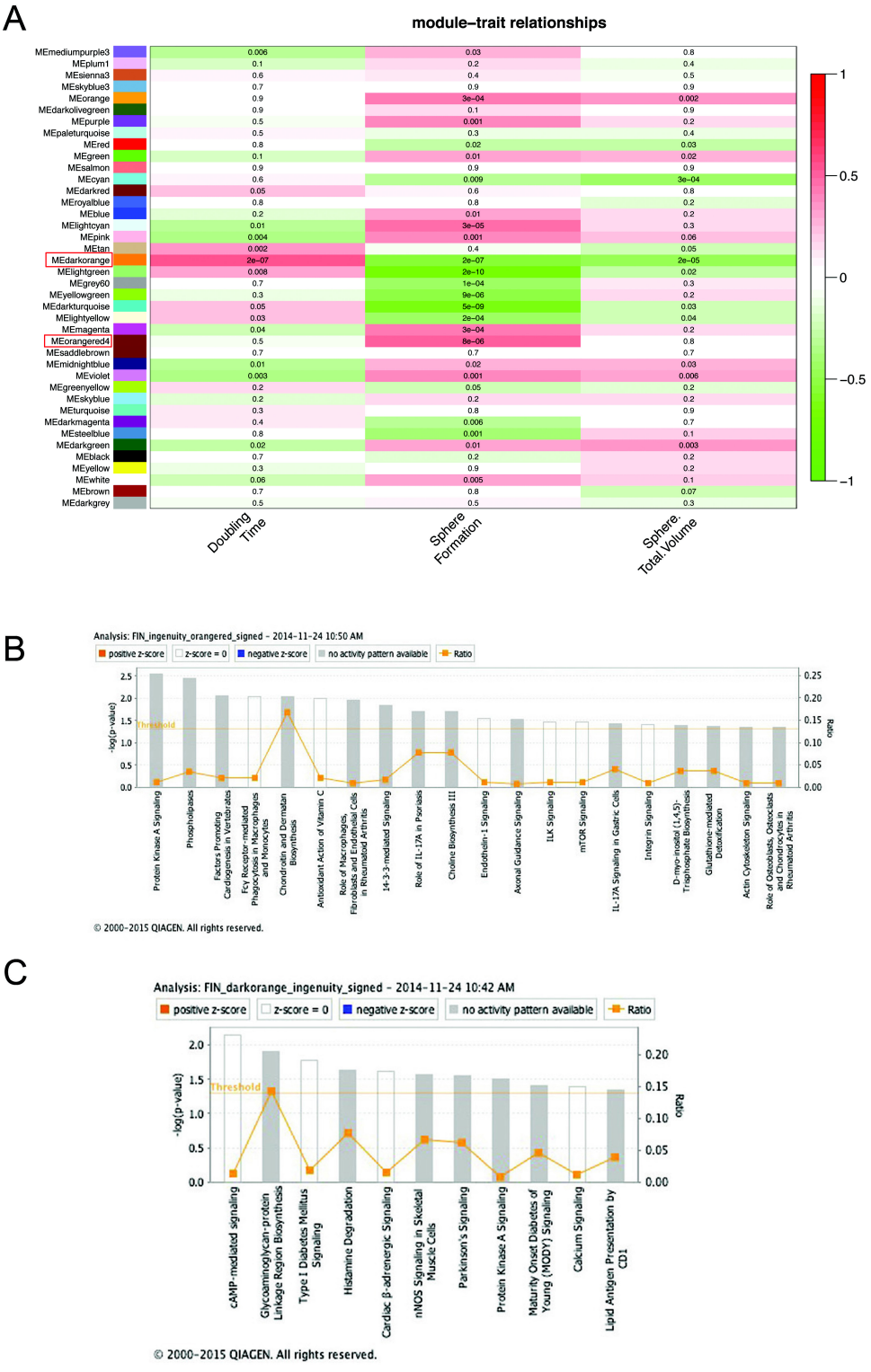
A
module–trait relationships
MEmediumpurple3 0.006 0.03 0.8
MEplum1 0.1 0.2 0.4
MEsienna3 0.6 0.4 0.5
MEskyblue3 0.7 0.9 0.9
MEorange 0.9 3e−04 0.002
MEdarkolivegreen 0.9 0.1 0.9
MEpurple 0.5 0.001 0.2
MEpaleturquoise 0.5 0.3 0.4
MEred 0.8 0.02 0.03
MEgreen 0.1 0.01 0.02
MEsalmon 0.9 0.9 0.9
MEcyan 0.6 0.009 3e−04
MEdarkred 0.05 0.6 0.8
MEroyalblue 0.8 0.8 0.2
MEblue 0.2 0.01 0.2
MElightcyan 0.01 3e−05 0.3
MEpink 0.004 0.001 0.06
MEtan 0.002 0.4 0.05
MEdarkorange 2e−07 2e−07 2e−05
MElightgreen 0.008 2e−10 0.02
MEgrey60 0.7 1e−04 0.3
MEyellowgreen 0.3 9e−06 0.2
MEdarkturquoise 0.05 5e−09 0.03
MElightyellow 0.03 2e−04 0.04
MEmagenta 0.04 3e−04 0.2
MEorangered4 0.5 8e−06 0.8
MEsaddlebrown 0.7 0.7 0.7
MEmidnightblue 0.01 0.02 0.03
MEviolet 0.003 0.001 0.006
MEgreenyellow 0.2 0.05 0.2
MEskyblue 0.2 0.2 0.2
MEturquoise 0.3 0.8 0.9
MEdarkmagenta 0.4 0.006 0.7
MEsteelblue 0.8 0.001 0.1
MEdarkgreen 0.02 0.01 0.003
MEblack 0.7 0.2 0.2
MEyellow 0.3 0.9 0.2
MEwhite 0.06 0.005 0.1
MEbrown 0.7 0.8 0.07
MEdarkgrey 0.5 0.5 0.3
1
0.5
0
−0.5
−1
Doubling Time
Sphere Formation
Sphere Total Volume
B
Analysis: FIN_ingenuity_orangered_signed - 2014-11-24 10:50 AM
positive z-score
z-score = 0
negative z-score
no activity pattern available
Ratio
-log(p-value)
Threshold
Ratio
Protein Kinase A Signaling
Phospholipases
Factors Promoting Cardiogenesis in Vertebrates
Fcγ Receptor-mediated Phagocytosis in Macrophages and Monocytes
Chondroitin and Dermatan Biosynthesis
Antioxidant Action of Vitamin C
Role of Macrophages, Fibroblasts and Endothelial Cells in Rheumatoid Arthritis
14-3-3-mediated Signaling
Role of IL-17A in Psoriasis
Choline Biosynthesis III
Endothelin-1 Signaling
Axonal Guidance Signaling
ILK Signaling
mTOR Signaling
IL-17A Signaling in Gastric Cells
Integrin Signaling
D-myo-inositol (1,4,5)-Trisphosphate Biosynthesis
Glutathione-mediated Detoxification
Actin Cytoskeleton Signaling
Role of Osteoblasts, Osteoclasts and Chondrocytes in Rheumatoid Arthritis
© 2000-2015 QIAGEN. All rights reserved.
C
Analysis: FIN_darkorange_ingenuity_signed - 2014-11-24 10:42 AM
positive z-score
z-score = 0
negative z-score
no activity pattern available
Ratio
-log(p-value)
Threshold
Ratio
cAMP-mediated signaling
Glycosaminoglycan-protein Linkage Region Biosynthesis
Type I Diabetes Mellitus Signaling
Histamine Degradation
Cardiac β-adrenergic Signaling
nNOS Signaling in Skeletal Muscle Cells
Parkinson's Signaling
Protein Kinase A Signaling
Maturity Onset Diabetes of Young (MODY) Signaling
Calcium Signaling
Lipid Antigen Presentation by CD1
© 2000-2015 QIAGEN. All rights reserved.

Figure 3

Figure 3. WGCNA analysis of in vitro phenotypes. A. WGCNA analysis of 71 GBM tumorsphere cultures identified 40 modules of coexpressed genes. The module eigengene, representing the expression changes of all the genes in the module, was correlated with phenotypic characteristics. The "Orange Red" module, outlined in red, is associated with Sphere Formation ($P<0.0001$). The "Dark Orange" module, outlined in red, is associated with both Sphere Formation and Doubling time ($P<0.0001$ for both). The heat-map depicts the Pearson correlation between module eigengens and trait, according to the scale on the side. P-values for each association are in each cell. B. Significant ($P<0.05$) canonical pathways associated with the "Orange Red" module, which is associated with sphere formation. The bars represent the –log(P-Value) from a Fischer's exact test. Yellow line: 0.05 p-value threshold. The orange graphing line with the orange box points represents the ratio of the number of genes in the pathway from our list divided by the total number of genes in the pathway. Grey bars represent no activity pattern available for the pathway and white bars indicate the Z-score=0, no activation or inactivation of the pathway. C. Significant ($P<0.05$) canonical pathways associated with the "Dark Orange" module that is associated with both proliferation (sphere doubling time) and sphere total volume.

Both Total Sphere Volume (an assessment of clonal proliferation rate) and Doubling Time (the inverse of proliferation rate) were most highly correlated with the "Dark Orange" module (Correlations =-0.49, P<0.0001 and Correlation P=0.57, P<0.0001, respectively) (Figure 3A). Thus, the "Dark Orange" module is inversely correlated to both outcomes of proliferation and may be assumed to be associated with lack of proliferation. Ingenuity analysis of the "Dark Orange" module revealed associated canonical pathways including cAMP signaling (P=0.00724), and Protein Kinase A (P=0.0316) (Figure 3C). Although the ingenuity analysis of the modules did not signify whether the Protein Kinase A pathway was activated or inactivated, Protein Kinase A (PRKACA) was directly associated with Sphere Total Volume in the gene-by-gene analysis (P=0.000816, Correlation=0.388). This suggests that the Protein Kinase A pathway activation is associated with proliferation (Sphere Total Volume).

Aggressive In Vitro Phenotype and Survival Outcome in TCGA

We compiled a list of 111 probes for 89 genes that were significantly associated with aggressive phenotype (proliferation) in all 3 in vitro outcomes: sphere formation, sphere total volume, and sphere doubling time. We tested whether this list of genes associated with in vitro aggressiveness enriched for genes that were also associated with tumor malignancy, defined as poor patient survival. To this end, we performed survival analysis in the TCGA database of glioblastoma on this list of 89 genes and found that 37 genes were associated with survival outcome in TCGA (P<0.05). When we used a false discovery rate (FDR) of P<0.05, 5 genes were associated with survival outcome in TCGA: *MDK, PLAT, HEATR2, LGALS8, EFEMP2*. These 5 genes were all significantly

associated with malignancy (poor survival in the TCGA database) (Figure 4, 5). Since the entire list of 12,042 genes in TCGA only harbored 12 genes significantly associated with patient outcome with a FDR, $P<0.05$, our determination of these 5 genes correlated to survival in our database was highly significant (Fisher's Exact T-Test, $P=1.43 \times 10^{-7}$). These data indicate that our list of genes that are consistently associated with all aggressive in vitro phenotypes is enriched for genes associated with poor survival.

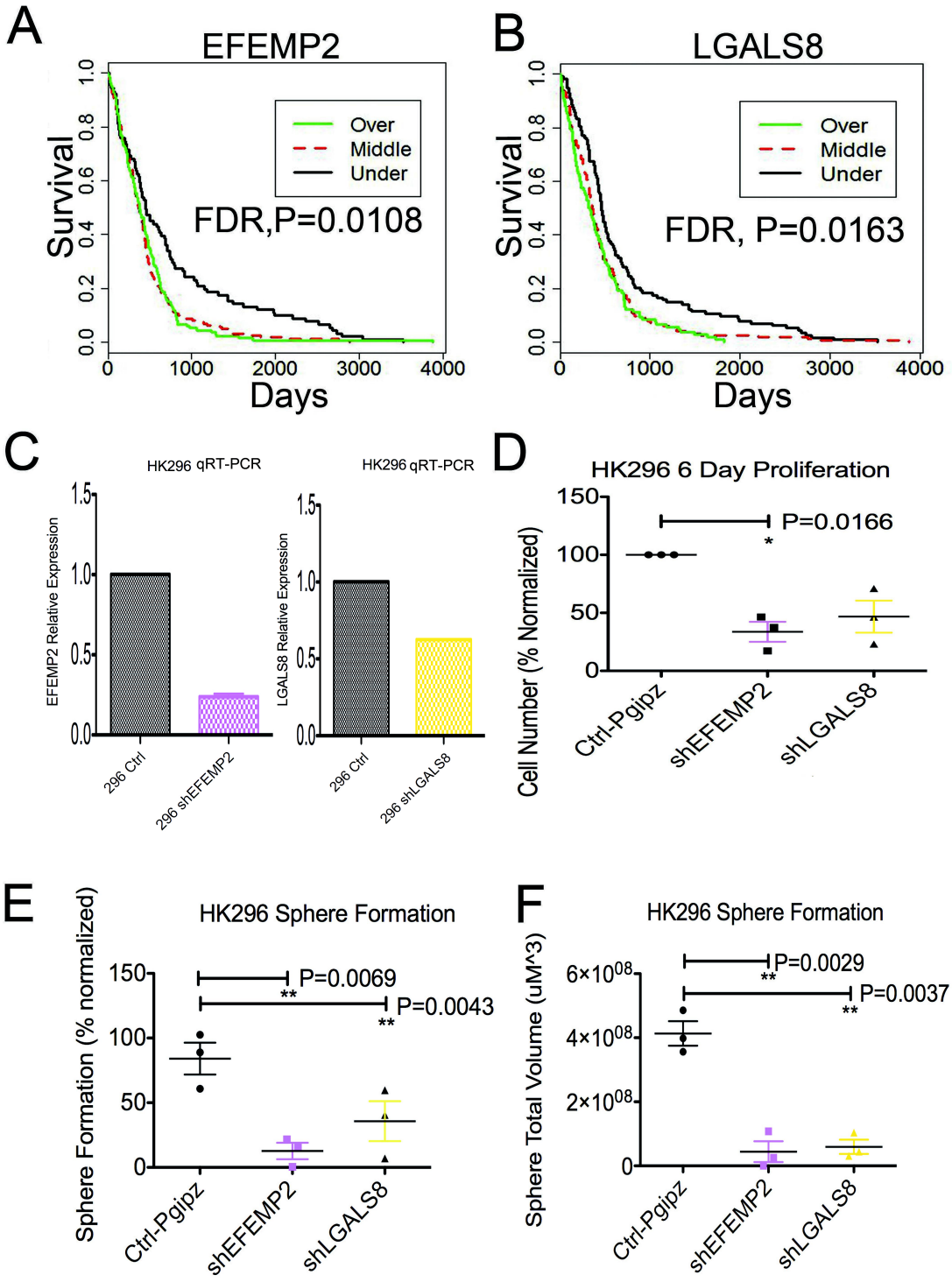
A
EFEMP2
Survival
Days
Over
Middle
Under
FDR,P=0.0108
B
LGALS8
Survival
Days
Over
Middle
Under
FDR, P=0.0163
C
HK296 qRT-PCR
EFEMP2 Relative Expression
296 Ctrl
296 shEFEMP2
HK296 qRT-PCR
LGALS8 Relative Expression
296 Ctrl
296 shLGALS8
D
HK296 6 Day Proliferation
Cell Number (% Normalized)
P=0.0166
*
Ctrl-Pgipz
shEFEMP2
shLGALS8
E
HK296 Sphere Formation
Sphere Formation (% normalized)
P=0.0069
**
P=0.0043
**
Ctrl-Pgipz
shEFEMP2
shLGALS8
F
HK296 Sphere Formation
Sphere Total Volume (uM^3)
P=0.0029
**
P=0.0037
**
Ctrl-Pgipz
shEFEMP2
shLGALS8

Figure 4

Figure 4. *EFEMP2* and *LGALS8* play functional roles in promoting GBM proliferation and are associated with poor survival in TCGA. A. *EFEMP2* expression is associated with poor survival in TCGA. TCGA Kaplan Meier curve for *EFEMP2* with FDR P-Value listed (P=0.0108). B. *LGALS8* expression is associated with poor survival in TCGA. TCGA Kaplan Meier curve for *LGALS8* with FDR P-Value listed (P=0.0163). C. Confirmation of knockdown of *EFEMP2* and *LGALS8* by qRT-PCR in HK296 GBM cells. Relative expression of *EFEMP2* and *LGALS8* as indicated on Y-axis are each normalized to *GAPDH*. shEFEMP2 depicts standard error bars for 2 biological replicates (Mean=0.238, +/- 0.0276 Std. Dev.). shLGALS8 depicts results for one biological replicate (Mean=0.653). D. shEFEMP2 inhibits cell proliferation. Graph of HK296 GBM cell cultures after 6 days of proliferation with control cells, or shRNA mediated knockdown of *EFEMP2* or *LGALS8*. Mean values, normalized to Ctrl are depicted +/- standard error of the mean. Each of the three biological replicates represents 16 technical replicates. shEFEMP2 (Mean=33.7+/-15.0) is significantly lower by 66% than Control (Paired T-Test, P=0.0166, N=3). shLGALS8 (Mean=46.8+/-23.9) is not significantly lower than Control (Paired T-Test, P=0.0611 N=3) but there is a trend towards a reduction in proliferation as indicated by the 53% reduction in the mean cell number. E. shEFEMP2 and shLGALS8 inhibit clonal sphere formation. Estimation of cell numbers of HK296 GBM cell cultures after 15 days of clonal sphere formation with control cells, or knockdown of *EFEMP2* or *LGALS8*. Mean values of % sphere formation are depicted +/- standard error of the mean. Each of the three biological replicates represents the mean of 20 technical replicates. Sphere formation for shEFEMP2 (Mean=12.7 +/- 11) is significantly lower by 85% than Control (Mean=84.1 +/- 21.3, Paired T-Test, P=0.00690,

N=3). shLGALS8 (Mean=35.7 +/- 26.7) is significantly lower by 58% than Control (Paired T-Test, P=0.00430, N=3). F. shEFEMP2 and shLGALS8 inhibit clonal sphere total volume. Graph of HK296 GBM cell cultures after 15 days of clonal sphere formation with control cells, or knockdown of *EFEMP2* or *LGALS8*. Mean values of clonal sphere total volume in uM^3 are depicted +/- standard error of the mean. shEFEMP2 (Mean=$4.44*10^7$ +/- $5.62*10^7$) is significantly lower by 89% than Control (Mean=$4.13*10^8$ +/- $6.63*10^7$, Paired T-Test, P=0.00290, N=3). shLGALS8 (Mean=$5.95*10^8$ +/- $3.87*10^7$) is significantly lower by 86% than Control (Paired T-Test, P=0.00370, N=3).

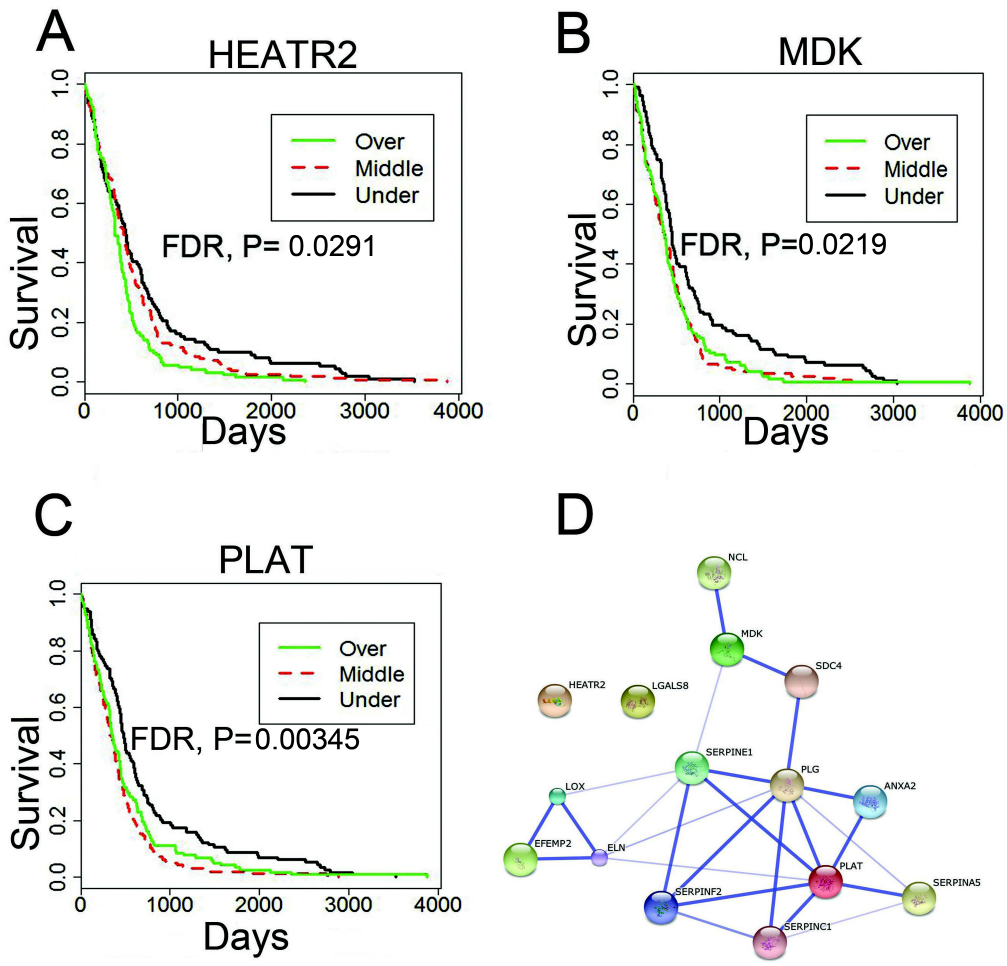
A
HEATR2
Survival
Days
Over
Middle
Under
FDR, P= 0.0291
B
MDK
FDR, P=0.0219
C
PLAT
FDR, P=0.00345
D
NCL
MDK
SDC4
HEATR2
LGALS8
SERPINE1
PLG
ANXA2
LOX
EFEMP2
ELN
PLAT
SERPINA5
SERPINF2
SERPINC1

Figure 5

Figure 5: Kaplan Meier survival curves of TCGA demonstrate that *HEATR2, MDK*, and *PLAT* are associated with poor survival. A *HEATR2* expression is associated with poor survival in TCGA. TCGA Kaplan Meier curve for *HEATR2* with FDR P-Value listed (P=0.0291). B. *MDK* expression is associated with poor survival in TCGA. TCGA Kaplan Meier curve for *MDK* with FDR P-Value listed (P=0.0219). E. *PLAT* expression is associated with poor survival in TCGA. TCGA Kaplan Meier curve for *PLAT* with FDR P-Value listed (P=0.00345). F. STRING diagram of these 5 genes associated with malignancy in association with each other reveals that 3/5 of these genes (*MDK, PLAT*, and *EFEMP2*) are correlated with each other through molecular intermediates (www.STRING.com).

Two of the 5 genes associated with both aggressive in vitro phenotype and tumor malignancy have already been shown to regulate GBM proliferation: MDK and PLAT(Luo et al., 2015; Yamashita et al., 2015). (Luo et al., 2015; Yamashita et al., 2015). This provides strong support for the use of a tumorsphere model in the identification of candidate targets. The remaining three genes (*HEATR2*, *EFEMP2*, *LGALS8*) are novel candidates of potential interest. *EFEMP2* is particularly interesting as it is correlated with both *MDK* and *PLAT* in an association matrix (STRING.com), indicating that these 3 genes may interact to regulate tumor cell proliferation (Figure 5D).

We chose to further study *EFEMP2* and *LGALS8*. We used lentiviral-mediated shRNA knockdown for each gene and confirmed the resulting *EFEMP2* and *LGALS8* mRNA depletion via qRT-PCR (Figure 4C). *EFEMP2* depletion resulted in a 66% decrease in cell number after 6 days in culture (P=0.0166, Figure 4D). Depletion of *LGALS8* reduced cell proliferation by a 53.2% decrease that did not reach statistical significance over this brief period (P=0.0611). Next, we performed a sphere formation assay under clonal conditions for 15 days; depletion of *EFEMP2* and *LGALS8* in HK296 GBM cells resulted in an 85% (P=0.00690) and 58% (P=0.00430) reduction, respectively, in clonal sphere formation (Figure 4E). There was no significant change in mean sphere diameter, indicating that those rare cells which do form spheres either escape knockdown or utilize other mechanisms to compensate for the depletion of the gene and proliferate normally. The change in sphere formation resulted in an 89% decrease in sphere total volume after *EFEMP2* knockdown (P=0.00290) and an 86% decrease after *LGALS8* knockdown (P=0.00370) (Figure 4F). These results demonstrate that *EFEMP2* and *LGALS8* play functional roles to promote GBM tumor cell

proliferation and clonal sphere formation. Similar results were obtained in the HK308 GBM cell line (Figure 6).

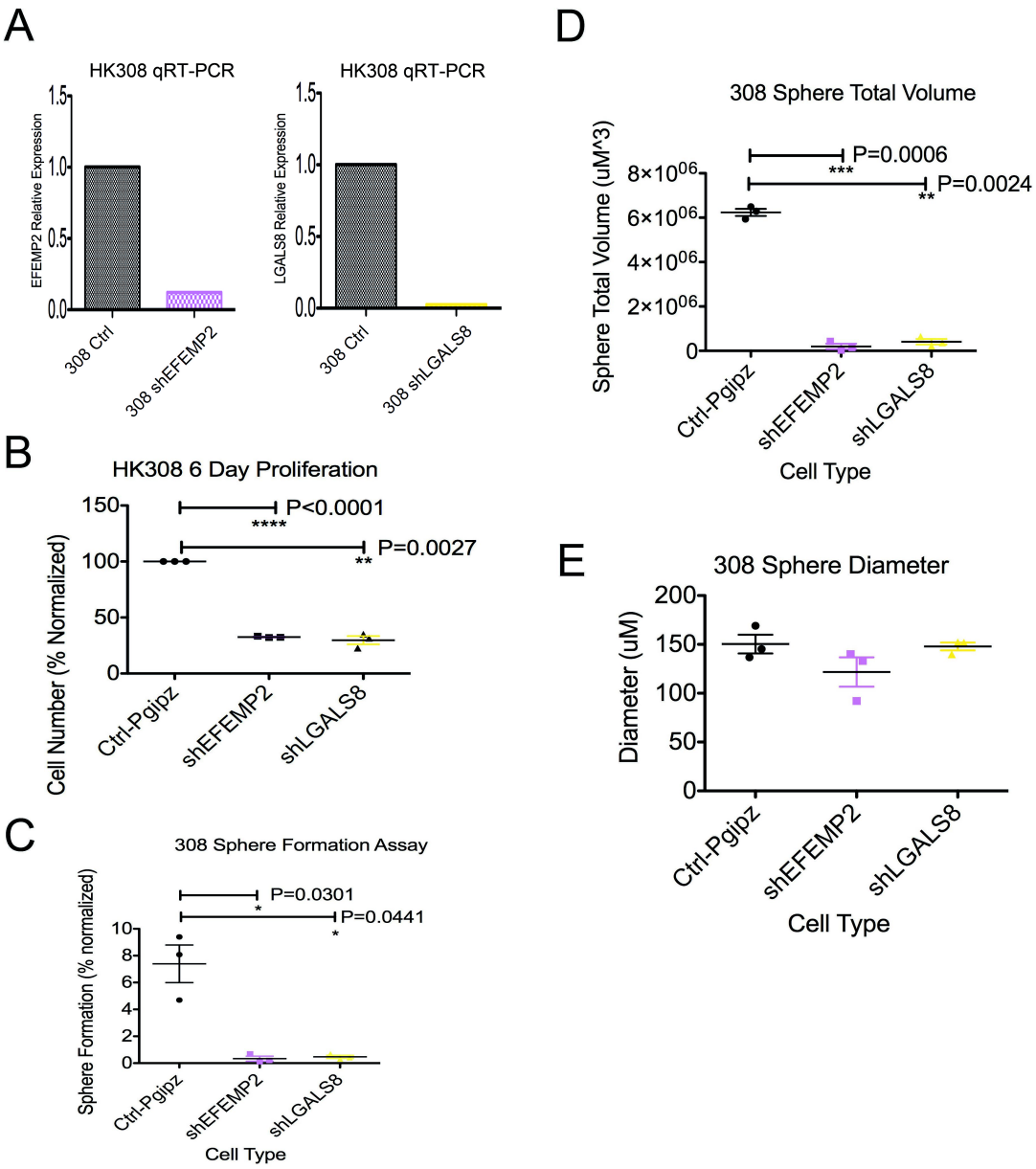
A
HK308 qRT-PCR
EFEMP2 Relative Expression
1.5
1.0
0.5
0.0
308 Ctrl
308 shEFEMP2
HK308 qRT-PCR
LGALS8 Relative Expression
1.5
1.0
0.5
0.0
308 Ctrl
308 shLGALS8
B
HK308 6 Day Proliferation
Cell Number (% Normalized)
150
100
50
0
P<0.0001
****
P=0.0027
**
Ctrl-Pgipz
shEFEMP2
shLGALS8
C
308 Sphere Formation Assay
Sphere Formation (% normalized)
10
8
6
4
2
0
P=0.0301
*
P=0.0441
*
Ctrl-Pgipz
shEFEMP2
shLGALS8
Cell Type
D
308 Sphere Total Volume
Sphere Total Volume (uM^3)
8×10^06
6×10^06
4×10^06
2×10^06
0
P=0.0006
***
P=0.0024
**
Ctrl-Pgipz
shEFEMP2
shLGALS8
Cell Type
E
308 Sphere Diameter
Diameter (uM)
200
150
100
50
0
Ctrl-Pgipz
shEFEMP2
shLGALS8
Cell Type

Figure 6

Figure 6. *EFEMP2* and *LGALS8* play functional roles in promoting GBM proliferation in HK308 GBM cell culture. A. Knockdowns of *EFEMP2* and *LGALS8* were efficient in HK308 as confirmed by qRT-PCR. Relative expression of *EFEMP2* and *LGALS8* as indicated on Y-axis are each normalized to *GAPDH*. shEFEMP2 depicts standard error bars for two technical replicates (Mean=0.121). shLGALS8 depicts results for two technical replicates (Mean=0.0251). B. shEFEMP2 and shLGALS8 inhibit cell proliferation. Graph of HK308 GBM cell cultures after 6 days of proliferation with control cells, or knockdown of *EFEMP2* or *LGALS8*. Mean values are depicted +/- standard error of the mean. Each of the three biological replicates represents the mean of 16 technical replicates. shEFEMP2 (Mean=32.6) is significantly lower by 77% than Control (Paired T-Test, P<0.0001, N=3). shLGALS8 (Mean=29.7) is significantly lower by 70% than Control (Paired T-Test, P=0.00270, N=3). C. shEFEMP2 and shLGALS8 inhibit clonal sphere formation. Graph of HK308 GBM cell cultures after 18 days of clonal sphere formation with control cells, or knockdown of *EFEMP2* or *LGALS8*. Mean values of % sphere formation are depicted +/- standard error of the mean. Each of the three biological replicate represents the mean of 20 technical replicates. shEFEMP2 (Mean=0.333) is significantly lower by 95% than Control (Mean=7.39, Paired T-Test, P0.0301, N=3). shLGALS8 (Mean=0.467) is significantly lower by 87% than Control (Paired T-Test, P=0.0441, N=3). D. shEFEMP2 and shLGALS8 inhibit clonal sphere total volume. Graph of HK308 GBM cell cultures after 15 days of clonal sphere formation with control cells, or knockdown of *EFEMP2* or *LGALS8*. Mean values of clonal sphere total volume in uM^3 are depicted +/- standard error of the mean. Each of the three biological replicate represents the mean of 20 technical replicates. shEFEMP2

(Mean=1.98*10^5) is significantly lower by 97% than Control (Mean=6.24*10^6, Paired T-Test, P=0.0006, N=3). shLGALS8 (Mean=4.08*10^5) is significantly lower by 93% than Control (Paired T-Test, P=0.00240, N=3). E. shEFEMP2 and shLGALS8 do not affect clonal sphere diameter. Graph of HK308 GBM cell cultures after 15 days of clonal sphere formation with control cells, or knockdown of *EFEMP2* or *LGALS8*. Mean values of sphere diameter in uM are depicted +/- standard error of the mean. Each of the three biological replicate represents the mean of 20 technical replicates. shEFEMP2 (Mean=122 uM) is not significantly lower than Control (Mean=150 uM, Paired T-Test, P=0.358, N=3). shLGALS8 (Mean=148) is not significantly lower than Control (Paired T-Test, P=0.816, N=3).

Tumorsphere Genes Associated with Patient Survival:

The above analysis studied genes of interest and their associations with survival in publically available databases. Next, we focused our analysis on factors associated with the survival of patients included in our own dataset. Neither the tumorsphere TCGA classification nor the Mesenchymal vs. Non-Mesenchymal unsupervised clustering classification was significantly associated with patient survival although we observed a non-significant trend for poorer survival in the Mesenchymal cluster (P=0.109) (Figure 7B) (Table 4). *EGFR* or *PTEN* mutation status, as indicated by the pathology report, was also not significantly associated with patient outcome in our cohort (Table 4). Patients with recurrent tumors had poorer survival as compared to primary tumors (P=0.007)(Figure 8A). Additionally, male patients had poorer survival as compared to female patients (P=0.004) (Figure 8B) and age was related to poorer survival (Hazard Ratio=1.025, CI: 1.01-1.04, P=0.01) (Table 4).

Phenotypic Correlation with Survival

Outcome	Explanatory Variable	Analysis	P-Value	Hazard Ratio	95% Confidence Interval
Survival	*EGFR*V3	Cox Regression	0.976	1.01	0.573-1.77
Survival	*EGFR*V3 or Amplification	Cox Regression	0.651	1.12	0.682-1.85
Survival	*PTEN* Deletion	Cox Regression	0.168	0.714	0.442-1.15
Survival	TCGA Tumorsphere	Cox Regression	0.587	0.918	0.674-1.25
Survival	Age of Patient	Cox Regression	0.01	1.025	1.01-1.04
Survival	Recurrence vs Primary	Cox Regression	0.007	2.36	1.26-4.40
Survival	Gender (Male vs Female)	Cox Regression	0.004	3.07	1.44-6.52
Survival	Gender adjusted for age	Cox Regression	0.009	2.74	1.28-5.86
	Age	Cox Regression	0.038	1.02	1.00-1.04
Survival	Gender adjusted for age and Recurrence	Cox Regression	0.137	1.81	0.828-3.95
	Age	Cox Regression	0.002	4.06	1.68-9.84
	Recurrence	Cox Regression	0.002	1.04	1.01-1.06

Table 4. Phenotypic Correlation with Survival. Results from cox regression analysis for survival in our patient dataset of tumorspheres.

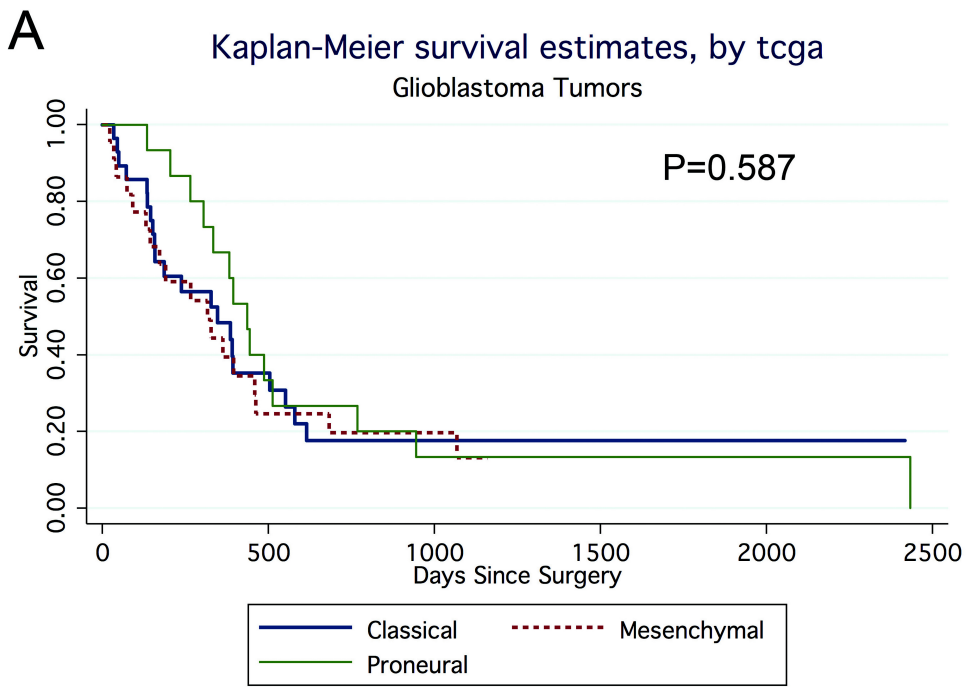
A
Kaplan-Meier survival estimates, by tcga
Glioblastoma Tumors
P=0.587
Survival
0.00
0.20
0.40
0.60
0.80
1.00
0
500
1000
1500
2000
2500
Days Since Surgery
Classical
Mesenchymal
Proneural

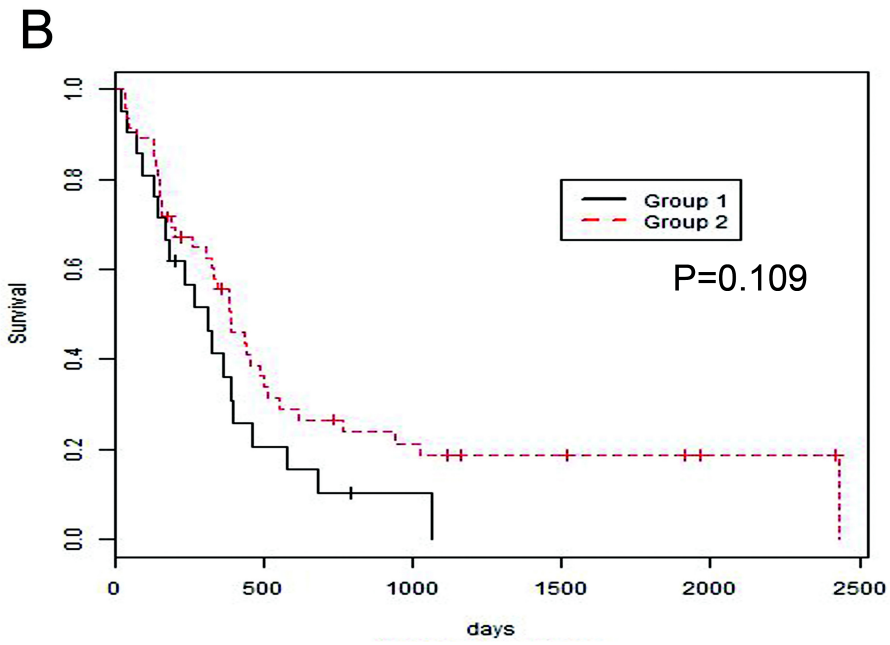
B
Survival
0.0
0.2
0.4
0.6
0.8
1.0
Group 1
Group 2
P=0.109
0
500
1000
1500
2000
2500
days

Figure 7

Figure 7. Kaplan Meier curves demonstrate no significant correlation between survival and either TCGA classification or unsupervised clustering into 2 groups. A. Kaplan Meier curve of TCGA classification in tumorspheres and survival of the patient. P-Value=0.587. B. Kaplan Meier curve of unsupervised clustering of tumorspheres into 2 groups: Group1= “Mesenchymal”, Group2=”Non-Mesenchymal”. P-Value=0.109.

A

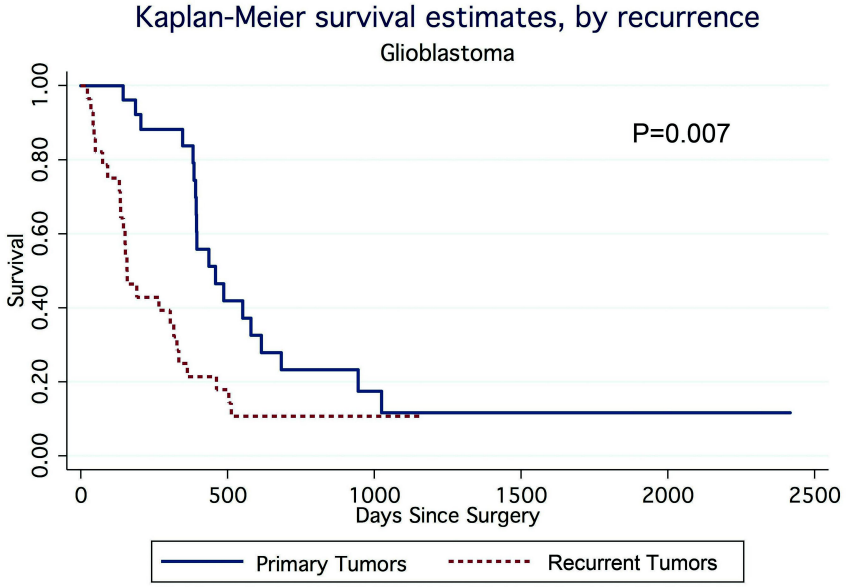
Kaplan-Meier survival estimates, by recurrence
Glioblastoma
P=0.007
Survival
0.00
0.20
0.40
0.60
0.80
1.00
0
500
1000
1500
2000
2500
Days Since Surgery
Primary Tumors
Recurrent Tumors

B

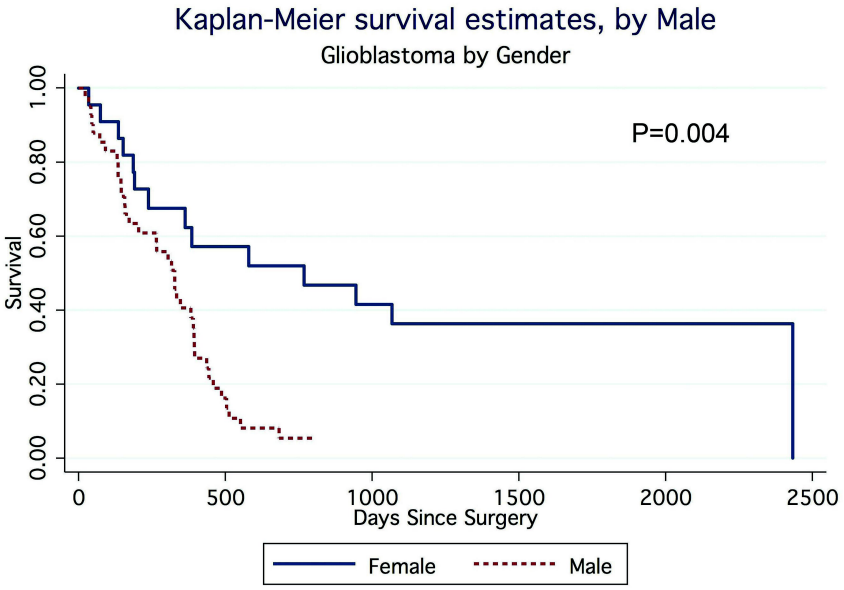
Kaplan-Meier survival estimates, by Male
Glioblastoma by Gender
P=0.004
Survival
0.00
0.20
0.40
0.60
0.80
1.00
0
500
1000
1500
2000
2500
Days Since Surgery
Female
Male

Figure 8

Figure 8. Kaplan Meier curves demonstrate both recurrence and Male gender are associated with poorer patient survival. A. Kaplan Meier curve of recurrent tumor derived tumorspheres vs. non-recurrent derived tumorspheres displays a significant disadvantage for recurrent tumors in terms of patient survival (P=0.007). B. Kaplan Meier curve of gender (Male vs. Female derived tumorspheres) displays a significant disadvantage for Male patients in terms of survival (P=0.004).

The tumorsphere culture system offers a unique model with which to determine tumor specific genes associated with survival in a robust manner. While there are many potential artifacts of any culture system, we hypothesized that tumorsphere genes associated with patient survival would be of high value, as the cultures are enriched for true tumor cells rather than other elements in the microenvironment. We analyzed various outcomes for associations with patient survival using Cox Regression analysis and Kaplan Meier graphs.

We found 22 annotated genes that were significantly associated with patient outcome (FDR $P<0.05$) (Table 5). These genes seem to be unrelated, except for *BRE* and *E2F3* that are both involved in the BRCA1 DNA damage response.

Tumorsphere Gene Expression Significantly Associated with Patient Survival

Gene	Tumorsphere Database	FDR, P-Value	Rembrandt Glioma	Rembrandt GBM
LOC100128071	Death	0.00941	-	-
SYT6	Survival	0.0186	Survival	No
MMRN1	Survival	0.0228	Death	No
LOC494150	Death	0.0263	Survival	No
RAB3B	Death	0.0324	No	No
C19orf6	Death	0.0324	No	No
ZNF346	Survival	0.0324	No	No
ARPC5	Survival	0.0381	No	No
E2F3	Survival	0.0381	No	No
YPEL2	Death	0.0392	Survival	No
MAP2K5	Death	0.0392	Death	Death
BRE	Death	0.0392	No	No
NAP1L1	Survival	0.0392	Survival	Survival
NAP1L1	Survival	0.0449	Survival	Survival
PBX2	Survival	0.0449	No	Death
NPL	Survival	0.0469	No	No
GPATCH2	Survival	0.0477	No	No
PDE9A	Survival	0.0493	Survival	No
LCORL	Death	0.0493	No	No
TTPAL	Survival	0.0493	Death	No
PTGR1	Death	0.0496	Death	Death
VTI1A	Survival	0.0496	Survival	Survival
TAF1	Death	0.0497	No	No

No= Not significantly associated with survival. - = Data unknown.

Table 5. Tumorsphere Gene Expression Significantly Associated with Patient Survival. Genes associated with survival (FDR, P<0.05) in our tumorsphere dataset. Additional information is provided to signify whether those genes are also significantly associated with survival in the Rembrandt dataset of Glioma (P<0.05) or GBM (P<0.05).

In order to validate these findings, we searched the Rembrandt dataset. Ten of the 22 genes identified in our study were also significantly associated ($P<0.05$) with patient outcome in glioma cases in the Rembrandt database of tumor gene expression. However, only seven of these ten genes had consistent (sign sensitive) associations in both databases (the other 3 had inconsistent associations; for example, better survival in one database and poorer survival in the other or vice versa) (Table 5). Of the genes with consistent associations, 57% (4/7) were also significantly ($P<0.05$) associated with outcome in the Rembrandt database of tumor expression within the restricted subpopulation of glioblastoma (Table 5). Thus, we have distinguished 4 genes that are significantly associated with patient outcome in a robust manner, both in GBM-derived tumorspheres (Figure 9 A-D) and in GBM tumors themselves (Figure 10).

Our data indicate that one must be cautious in interpreting the meaning of a gene's relationship with tumorsphere phenotype or survival. A gene's association with patient outcome was not necessarily reflected in its association with in vitro tumorsphere phenotype. For example, higher expression of *MAP2K5* is associated with shorter survival, but *MAP2K5* levels are associated with a slower proliferation rate of the tumorsphere cultures ($P=0.0203$). *VTI1A*, whose expression is associated with better patient survival, is also significantly associated with a faster proliferation rate of the tumorsphere cultures ($P=0.0428$). Thus, a complex system exists wherein gene expression associated with patient outcome is not strictly related to tumorsphere proliferation in a simple, predictive manner. *PTGR1* has a complex phenotypic characterization as both high expression and under expression of *PTGR1* are associated with poor survival as compared to the mean in our tumorsphere dataset (Figure 9B).

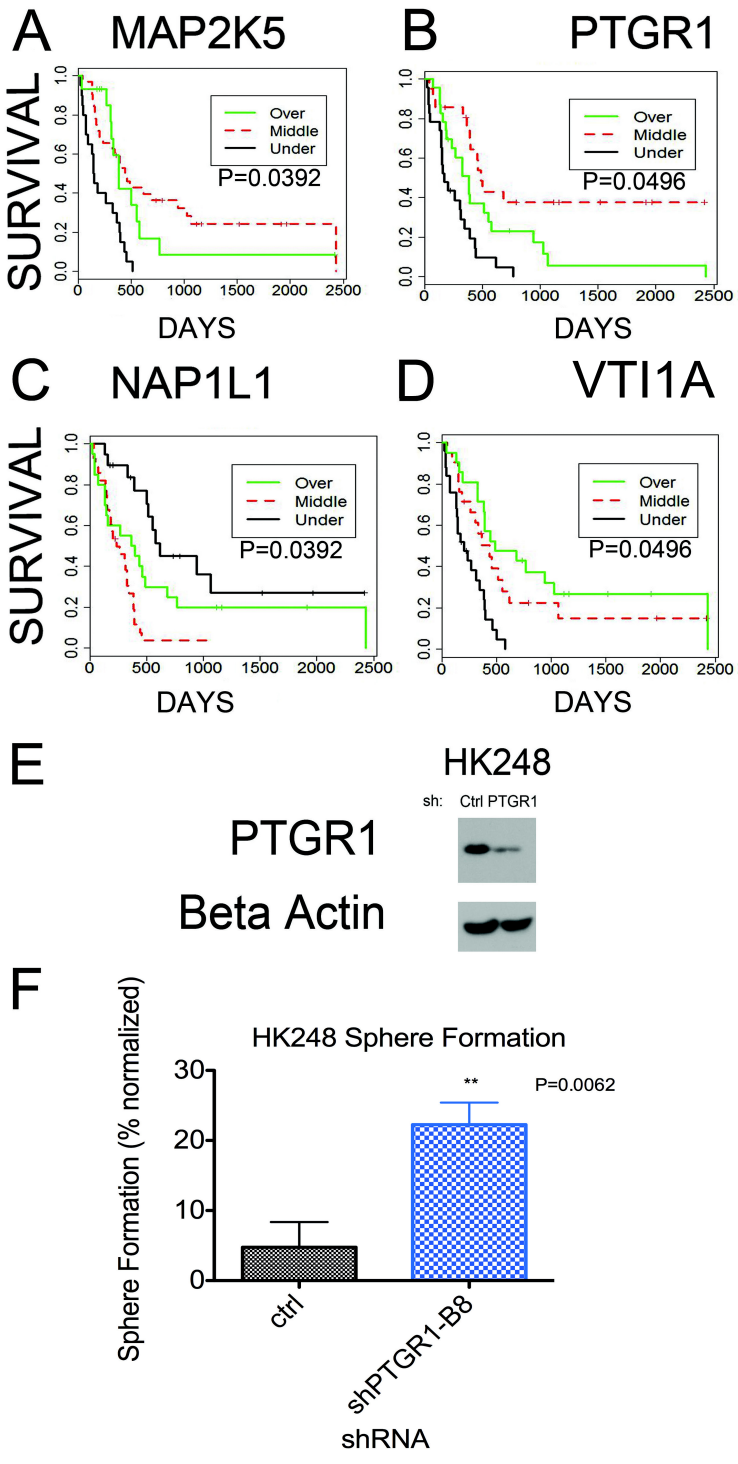
A
MAP2K5
SURVIVAL
Over
Middle
Under
P=0.0392
DAYS
B
PTGR1
Over
Middle
Under
P=0.0496
DAYS
C
NAP1L1
SURVIVAL
Over
Middle
Under
P=0.0392
DAYS
D
VTI1A
Over
Middle
Under
P=0.0496
DAYS
E
HK248
sh: Ctrl PTGR1
PTGR1
Beta Actin
F
HK248 Sphere Formation
Sphere Formation (% normalized)
**
P=0.0062
ctrl
shPTGR1-B8
shRNA

Figure 9

Figure 9. PTGR1 plays a functional role in impairing GBM proliferation. A-D. Kaplan Meier survival curves from our tumorsphere dataset of gene expression in tumorsphere cultures and patient survival for 4 genes associated with survival in both our tumorsphere dataset and in the Rembrandt dataset for glioblastoma. E. Western blot depicts depletion of PTGR1 in HK248 cells upon shRNA knockdown of PTGR1. Beta actin serves as the loading control. F. Normalized sphere formation percentage displays a significant 272% increase in sphere formation upon knockdown of PTGR1 in HK248 GBM cell culture (Paired T-Test, P=0.00620, N=4). The mean for Ctrl was 4.76%, and for shPTGR1, 22.3%. Cells were grown at clonal density (50 cells/well) for 21 days.

A

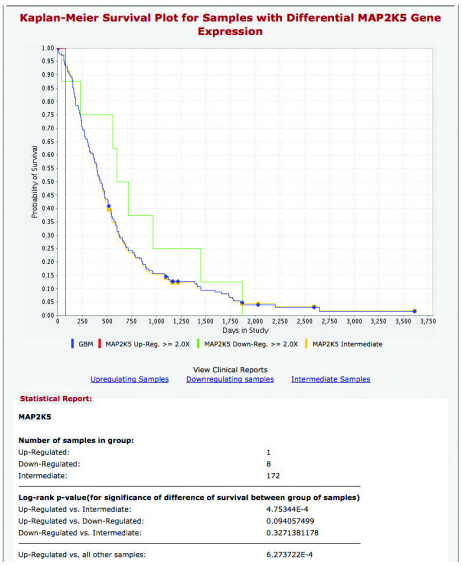

C

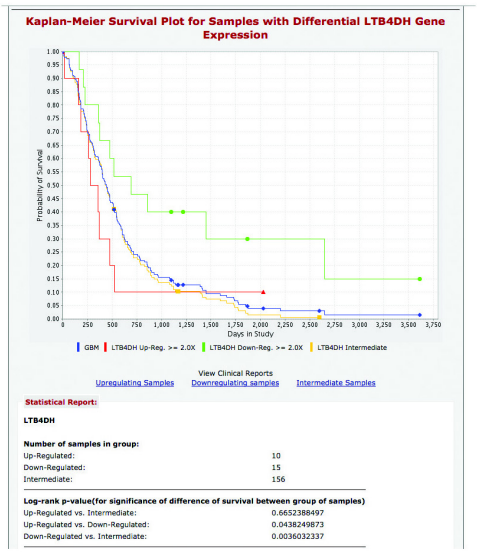

B

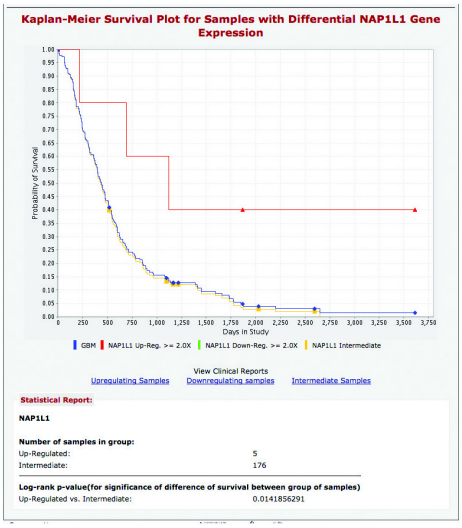

D

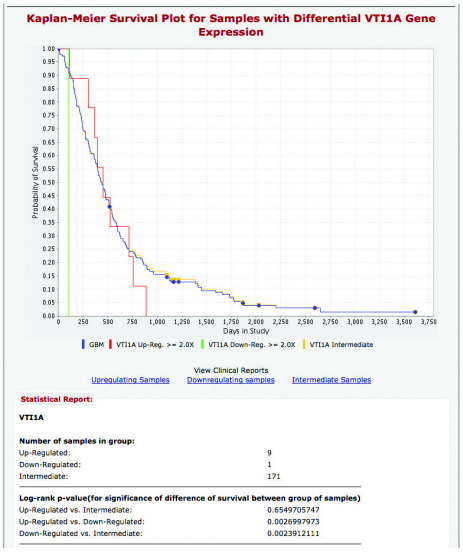

Figure 10

Figure 10. Kaplan Meier curves of the Rembrandt database for glioblastoma tumor gene expression and survival. The red line is overexpression of the gene; the green line is under-expression of the gene. The genes are indicated, as are the P-values.

PTGR1 expression in tumorspheres is consistently related to the aggressive phenotype: a faster rate of proliferation (P=0.000507), greater sphere total volume (Correlation=0.638, P<0.001), and increased sphere formation (Correlation=0.453, P=7.34E-05). From our assessment of tumorsphere phenotypes, we chose *PTGR1* as a candidate gene for further study.

Using lentiviral mediated shRNA transfection, we knocked down *PTGR1* in GBM cell culture HK248. Depletion of PTGR1 was demonstrated via western blot (Figure 9E). We performed a sphere formation assay under clonal conditions and after 21 days of growth, PTGR1 depletion resulted in a 4.8 fold increase in mean percentage sphere formation (Ctrl=4.76%, shPTGR1=22.3%), with no change in mean sphere diameter (Figure 9F). These significant results (P=0.0062) demonstrate that *PTGR1* plays a functional role in impeding GBM tumor cell proliferation and sphere formation. Thus, *PTGR1* is a potential tumor suppressor. This is a good example of the caution one must employ in assessing correlations between expression and phenotype. Although *PTGR1* expression was correlated with a more aggressive in vitro phenotype, it behaved functionally as a tumor suppressor. Yet, the anti proliferative function of *PTGR1* is consistent with the observed correlation in our tumorsphere dataset between poor survival and *PTGR1* under expression (Figure 9B).

Discussion

Our large-scale study of the comparison of tumorsphere expression shows both phenotypic variance and expression differences between our diverse tumorsphere samples. Additionally, we compared and contrasted expression changes between these tumorspheres and their parent tumors using microarray data in an attempt to determine the strengths and weaknesses of this model system. One key discovery was that TCGA classification in our tumorspheres was not universally predictive of phenotype, nor universally consistent with original tumor classification. One possible explanation for this discrepancy is a process of enrichment within some tumorsphere samples for an important subset of cells amongst the tumor heterogeneity. Single-cell RNA-seq has demonstrated that clonal heterogeneity exists within a tumor(Patel et al., 2014). Therefore, it is feasible that tumorspheres may select for a certain subtype of BTSC from the tumor. However, a recent report has observed that variegated clones, phenotypically and genetically distinct, persist within tumorsphere cultures(Meyer et al., 2015a). This implies that tumorsphere heterogeneity may reflect the biology of the tumor and model the complex phenotypic features of clonal selection and drug response. This tumorsphere heterogeneity implies that these bulk tumorsphere cultures may be more biologically relevant than single cell derived, clonal cultures or cell lines or genetically modified mouse models. However, this heterogeneous model system does not rule out differential BTSC selection or bias in the tumorsphere cultures that could account for the discrepancy between classification of certain tumors and their derived tumorspheres.

The discrepancy in classification between tumors and their derived tumorspheres lies in contrast to the small number of genes (13) that were consistently altered from

tumors to tumorspheres. These data suggest that tumorsphere cultures may not be enriching for expression of a consistent set of canonical brain tumor stem cell genes. On the other hand, these data also indicate that tumorspheres do not create consistent artifacts of culture, that they are not a disparate model system from their parent tumors, at least in terms of changes that can be detected by gene expression.

Interestingly, TCGA classification of tumorspheres did preserve the previously reported associations of *IDH1* mutation with Proneural (Verhaak et al., 2010) classification and largely supports the classification of gliosarcoma tumors with Mesenchymal. However, offering a non-biased alternative to TCGA classification, unsupervised clustering of the most variable genes supports the classification of tumorspheres into 2 general categories, Mesenchymal and non-Mesenchymal sub-groups. In contrast to a previous report (Bhat et al., 2013), we find both Proneural and Classical were clustered against the Mesenchymal sub-group, whereas the previous study defined the two contrasting sub-groups as entirely Proneural vs. Mesenchymal. However, multidimensional scaling, utilizing principal component analysis, did provide support for separating at least some Proneural samples from the "Classical/Proneural" subset. In fact, this MDS grouping of a Proneural subgroup had a significantly slower proliferation rate than the other MDS groups, suggesting that unbiased MDS classification may distinguish biologically relevant subgroups which the other classification systems (TCGA and Clustering) missed. These results are consistent with a recent study of 20 tumorsphere cultures that distinguished two clusters including a predominately Proneural subtype, the "stem like" group, associated with slower sphere formation rates and longer survival upon xenograft transplantation(Cusulin et al., 2015).

Our results present a complex picture of the tumorsphere system, where some elements of TCGA classification are effective at describing tumorspheres (i.e. Proneural and *IDH1* mutations, gliosarcoma and Mesenchymal) and other elements of tumorspheres may be better assessed with different methods of examination (i.e. non-biased assessment of gene expression and phenotype). However, the TCGA classification is robust in that tumorspheres generally retained their TCGA classification from low to high passages in culture. These data indicate a stability of tumorspheres over time, at least in regard to relative expression levels.

One key aim carried out in this paper was an analysis of the phenotypes of the tumosphere cultures and their relationship with gene expression. First, we assessed the correlation between gene expression levels and phenotypes; second, we identified modules of co-expressed genes using WGCNA, and correlated their module eigengenes with the phenotypic traits. While there are advantages and disadvantages to each method, they can support and supplement each other. In terms of tumorsphere phenotype, we distinguished associations between sphere formation or proliferation with the Beta Catenin, PI3Kinase, ERK, Protein Kinase A, Integrin and mTOR pathways. These associations bind in vitro phenotypes with established pathways that play essential roles in tumor biology and malignancy. The data, from both WGCNA and gene-by-gene correlation supports the hypothesis that Protein Kinase A signaling is directly associated with proliferation. This association between Protein Kinase A and glioma proliferation has been shown in a previous study wherein protein kinase A mediated the *EGFR*vIII stimulus to proliferate (Feng et al., 2014). A validation of our methodology was *KLHL9*. *KLHL9* expression was inversely correlated (Pearson's r=-0.758, P<0.0001) with sphere

formation, consistent with a previous study reporting that *KLHL9* expression reduced tumor viability in glioblastoma (Chen et al., 2014). This demonstrates that upon examination of tumorsphere gene expression and dynamic phenotypic outcomes provided by the tumorsphere model, one can distinguish crucial pathways involved in malignancy and tumor biology. This validation of the tumorsphere system as a model of tumor biology supports the strategy to interrogate the tumorsphere model for novel genes with important roles in tumor biology.

An important question is whether tumorsphere cultures provide additional information that cannot be gleaned from data on the whole tumor. Besides offering a dynamic model for study, an additional advantage to the tumorsphere model is its tumor cell-specific composition. Tumors may contain a variety of extraneous non-tumor cells within the sample while tumorspheres serve as a more rarified environment that can be considered tumor specific. Here, when comparing malignant-like phenotypes to survival, we discovered 5 genes that were associated with aggressiveness in all 3 outcomes for in vitro phenotype and with malignancy in terms of poor patient survival in the TCGA database of glioblastoma. These genes include 2 known oncogenes, *PLAT* and *MDK* and 3 genes with no known role in glioblastoma biology: *EFEMP2, HEATR2*, and *LGALS8*. We chose to study *EFEMP2* and *LGALS8* for a functional role in GBM proliferation by using lentiviral mediated shRNA knockdown of each gene. Using this reasoned analysis to identify genes correlated with malignant-like traits, we discovered that both *EFEMP2* and *LGALS8* facilitate proliferation and clonal sphere formation of GBM tumorspheres. Our data is consistent with a previous report that *EFEMP2* (also known as *MBP1*) promotes proliferation and transformation in rat embryonic fibroblasts (Gallagher et al.,

1999). Further study is necessary to determine if *EFEMP2* serves as an oncogene in GBM. Interestingly, both EFEMP2 and LGALS8 are secreted proteins and therefore, they may serve as suitable biomarkers for GBM tumor proliferation and also may be amenable to pharmacologic intervention.

Expression in tumorspheres may harbor unique and meaningful correlations with patient survival as gene expression in tumorspheres is tumor cell specific and not due to brain parenchyma in the tumor sample. We found 22 genes whose expression in tumorspheres was significantly associated with patient survival. Of these candidates, we found four genes robustly associated with survival in both GBM tumorspheres and in the Rembrandt database of GBM tumors: *MAP2K5, NAP1L1, PTGR1 (LTB4DH), VTI1A*. These genes were not only robust predictors of survival, with associations that persisted from the tumor to tumorsphere conditions, but their correlation with survival in our tumorsphere dataset indicates that these associations are specific to tumor biology and not due to an artifact of contaminating non-tumor tissue. *PTGR1* is unique in that its expression associated with poor prognosis in our tumor database as well as with all 3 outcomes of aggressive in vitro phenotype. However, *PTGR1* under-expression was also correlated with poor survival in our tumorsphere dataset. Our experimental data indicate that *PTGR1* has a functional role in suppressing GBM sphere formation. Thus, in vitro *PTGR1* expression may serve as a biomarker of proliferation, perhaps a transcriptional reaction to the aggressive in vitro phenotype, and not a driver of that phenotype. These results support the unique relevance of the tumorsphere dataset survival outcome where we detected that under expression of *PTGR1* was associated with poor survival. This inverse association of expression with malignancy is consistent with a role for *PTGR1* as

an inhibitor of proliferation. Our data support the need for more study of *PTGR1* and indicate that correlations between genes and in vitro phenotypes do not always predict their functional role.

In summary, our data distinguishes the tumorsphere system as a suitable model of fundamental molecular pathways involved in GBM biology. Tumorspheres demonstrate in vitro phenotypes that are correlated with canonical pathways involved in GBM tumor biology. The tumorsphere model provides a unique platform for the discovery of novel genes involved in proliferation and may be utilized to elucidate the molecular determinants of malignancy.

Methods

Clinical Data and Tumor Collection: High grade human glioma tumors from 70 surgical resections were collected under institutional review board-approved protocols and graded by the neuropathologists as previously described(Laks et al., 2009). One tumor sample was obtained from Duke University after it had been resected and placed as a xenograft. This sample was utilized because it has been widely published (Nathanson et al., 2014; Sarkaria et al., 2007). There were 67 distinct patients as four pairs of tumorspheres were derived from the same patients at different resections.

Tumorsphere Culturing: Tumorspheres were cultured from GBM tumor samples as previously described(Hemmati et al., 2003; Laks et al., 2009). Cells were grown in Dulbeco's modified Eagle's medium (DMEM)/F12 supplemented with B27 (Life Technologies), 20 ng/ml basic fibroblast growth factor (bFGF, Peprotech), 50ng/ml epidermal growth factor (EGF, Life Technologies), penicillin/streptomycin (Invitrogen), Glutamax (Invitrogen), and 5ug/ml heparin (Sigma-Aldrich). Tumorspheres were passaged every 7-10 days following enzymatic dissociation with TrypLE (Life Technologies).

The Cancer Genome Atlas Glioblastoma Classification: The Cancer Genome Atlas (TCGA) unified gene expression dataset for the 173 core tumor samples from the glioblastoma TCGA classification paper (Verhaak et al., 2010) was used to create our models. The unified gene expression dataset is the combined expression data from all three platforms, Affymetrix HuEx array, Affymetrix U133A array and Agilent 244K

array into a single expression pattern that was used for the original classification into four categories by TCGA (Verhaak et al., 2010). The unified gene expression data was combined with our Tumor and Tumorsphere data which was obtained on the Affymetrix U133 plus 2.0 array and normalized with the using the R package limma (Smyth, 2005). Batch effects were then adjusted using ComBat (Johnson et al., 2007) on the normalized data. ClaNC, the LDA based centroid classification algorithm used by Verhaak et al. to create the classifications was then applied to determine a 3-class centroid-based classifier using only the data from Mesenchymal, Proneural or Classical TCGA samples (Dabney, 2006). 56 Mesenchymal samples, 53 Proneural and 38 Classical samples consisting of 147 total samples excluding the 26 Neural samples were used in building the classifier. This classifier was then used to assign a TCGA category (Mesenchymal, Proneural or Classical) to each sample within the Tumor and Tumorsphere sets. Because of the lack of gene name overlap from the Affymetrix U133A array used by TCGA and the Affymetrix U133 plus 2.0 microarray used for our classifications, only 789 of the original 840 genes were used to classify the samples.

Survival Curves: Kaplan-Meier survival curves were created for all 54,675 probes using the R 'survival' package (Therneau, 2014). Statistical significance was assessed using the Mantel-Haenszel test as implemented in the G-rho family of tests by Harrington and Fleming (Harrington, 1982). False Discovery Rate adjustment was carried out on all 54,675 p-values and only values with an FDR adjusted p-value of less than 0.05 were kept as significant and reported. FDR adjustment was carried out using the Benjamini and Hochberg approach (Benjamini, 1995).

Determining genes associated with survival in our cohort: First, we performed a gene by gene correlation to survival by evaluating the significant differences between high and low expression in each gene's Kaplan-Meier curve. Groups of high and low expression were defined as being one half of one standard deviation higher or lower than the average expression for a given gene. Kaplan-Meier curves were then created using these three groups, those that were over-expressed, under-expressed and those that were neither for a given gene. We then ranked these Kaplan-Meier curves using p-values calculated using the log-rank (Mantel-Haenszel) test. Significant results were defined as having an FDR adjusted p-value of less than 0.05.

Paired Student's T-test of Tumorspheres and Their Parent Tumors:

Means were compared between tumorspheres and their parent tumors using a paired Student's *t* test as implemented in the R core package (Team, 2013). Transcripts with a false discovery rate (FDR) <0.05 were reported as significant.

In vitro Assays: We studied the percentage of sphere formation for cultures at clonal density (plating 50 cells/100uL/well of a 96 well plate). This feature may reflect the % of tumor initiating cells within the population. We measured the total volume of spheres formed through the formula: sphere total volume = Mean # spheres formed * mean sphere volume ($4/3\ \pi * r^3$, where r is the mean measured radius of the spheres counted). As sphere total volume takes into account both % sphere formation and diameter, it is an accurate assessment of proliferation at clonal density. We assessed proliferation rate by measuring doubling time of 39 tumorspheres cultures. Doubling time is therefore the inverse of relative proliferation rate. Doubling time was assessed by counting cells every

day after plating at 5000 cells/100uL/well of a 96 well plate well using alamar blue as a readout.

Cell Proliferation Assays: Cells were plated at 5000 cells/100uL/well of a 96 well plate and grown for 5-7 days. Cell number was assessed using Dojindo Cell Counting Kit-8 (Dojindo Molecular Technologies Inc.).

Ingenuity Analysis: Ingenuity analysis of gene expression lists was performed at www.ingenuity.com. Canonical pathways were considered to be significantly associated with gene lists at $P<0.05$.

TFacts analysis: Sign sensitive analysis of transcription factor associations with our gene lists of interest was performed at http://www.tfacts.org/TFactS-new/TFactS-v2/index1.html. Transcription factors were considered to be significantly associated with gene lists if $E<0.05$.

shRNA: Lentiviral mediated shRNA knockdowns of *EFEMP2, LGALS8*, and *PTGR1* were performed using constructs from the Dharmacon-Harmon library (General Electric: http://dharmacon.gelifesciences.com/shrna/gipz-lentiviral-shrna/?Parent=12884902157). *EFEMP2* (full hairpin sequence: TGCTGTTGACAGTGAGCGCGCAGTGATAT TGATGAGTGTATAGTGAAGCCACAGATGTATACACTCATCAATATCACTGCA TGCCTACTGCCTCGGA. *LGALS8* (Full hairpin sequence:TGCTGTTGACAGT

GAGCGAGGCATTTATGGCAAAGTGAATTAGTGAAGCCACAGATGTAATTCAC TTTGCCATAAATGCCCTGCCTACTGCCTCGGA). *PTGR1* (Full hairpin sequence: TGCTGTTGACAGTGAGCGATGGAGCCATCTCTACATATAATAGTGAAGCCAC AGATGTATTATATGTAGAGATGGCTCCACTGCCTACTGCCTCGGA).

qRT-PCR: qRT-PCR was performed with the following primers: *GAPDH*: Fwd-AGCCACATCGCTCAGACAC, Rev-CGCCCAATACGACCAAATC. *EFEMP2*: Fwd-CTTCAACTCCTATGGGACCTTC, Rev-AGCGGTACTGACAGAGGTAG. *LGALS8*: Fwd- CCAGCTTAGCCTGCCATTC, Rev- CCTGCTAGTAGGTCAACATTAAAGC.

Gene trait correlations: Gene-trait correlations and p-values were obtained using the standard Pearson correlation coefficient *r* using the cor() function in R. A $p<0.001$ threshold was used to select the most interesting candidates.

Clustering: Hierarchical clustering was obtained using the hclust function in R using standard parameters.

Microarray methods: Concentration and quality of RNA samples was examined using the NanoDrop ND-1000 spectrophotometer (NanoDrop Technologies) and the Agilent 2100 Bioanalyzer (Agilent Technologies, Inc). RNA samples were reverse transcribed and labeled according to manufacturer's instructions and hybridized to Affymetrix high-density oligonucleotide HG-U133A Plus 2.0 Human Arrays. Microarray data analysis was performed as previously described (Coppola, 2011). Briefly, array preprocessing was completed in the R computing environment (http://www.r-project.org) using

Bioconductor (http://www.bioconductor.org). Raw data was normalized using the robust multi-array (RMA) method (Irizarry et al., 2003). To eliminate batch effects, additional normalization was performed using the R package "ComBat" (http://statistics.byu.edu/johnson/ComBat/) (Johnson et al., 2007) with default parameters. Contrast analysis of differential expression was performed using the LIMMA package (Smyth, 2005). After linear model fitting, a Bayesian estimate of differential expression was calculated using a modified t-test. The threshold for statistical significance was set at $p<0.005$ for differential expression analysis and $p<0.01$ for explorative analyses (gene ontology and pathway analysis). Gene Ontology and Pathway analysis were carried out using the Database for Annotation, Visualization and Integrated Discovery (DAVID) and Ingenuity Pathway Analysis (www.ingenuity.com).

Weighted Gene Co-expression Network Analysis (WGCNA) was conducted using the R package as previously described (Langfelder et al., 2008; Zhang and Horvath, 2005). Briefly, correlation coefficients were constructed between expression levels of genes, and a connectivity measure (topological overlap, TO) was calculated for each gene by summing the connection strength with other genes. Genes were then clustered based on their TO, and groups of co-expressed genes (modules) were identified. Each module was assigned a color, and the first principal component (eigengene) of a module was computed and considered to be representative of the gene expression profiles in a module. We then correlated eigengenes for each module with phenotypic traits of interest.

Survival Outcome: Time to survival (TTS) for patients in our database was determined by the duration of life from the date of surgery using death certificates and the social security death index.

RNA samples preparation: RNA was isolated from tumorspheres and tumors samples using the Qiagen RNA isolation kit (RNeasy Kit, Qiagen).

Western Blots: We performed western blots for PTGR1(ABCAM#107005), EFEMP2(ABCAM #125073), LGALS8(Sigma#) and utilized Beta Actin as a loading control (ABCAM #8277). Samples of protein for Western blots were prepared by collecting equal amounts of cells, counted using the Countess Automated Cell Counter (Life Technologies), and then boiled in Laemmli Sample Buffer (Bio-Rad #161-0737) with 5% beta mercaptoethanol for five minutes. An equal numbers of cells (125,000 cells/lane) were loaded on to 10% Mini-Protean Pre-cast gels (Bio-Rad #456-1036) and the western blots were performed according to standard procedure.

Pathology Reporting: The readout of clinical diagnosis, the presence of *EGFR*vIII rearrangement and cytogenetic analysis were obtained from the official pathology report.

*EGFR*vIII in tumorspheres: *EGFR*vIII mutation in tumorsphere cultures was ascertained by western blots using an EGFR antibody (Millipore #06-847).

Sequencing of *IDH1and IDH2*

Genomic DNA was isolated from the cultured glioma-sphere cells by using DNeasy Blood and Tissue Kit (Qiagen). The *IDH1* and *IDH2* genotypes were determined by Sanger sequencing as follows: (1) IDH1 fragment with R132 codon and IDH2 fragment with R140 and R172 codons were amplified from the genomic DNAs by PCR. The PCR primers for *IDH1* fragment are forward 5'-GCGTCAAATGTG CCACTATC-3' and reverse 5'-GCAAAATCACATTATTGCCAA C-3'. The PCR primers for IDH2 fragment are forward 5'- AATTTTAGGACCCCCGTCTG -3' and reverse 5'-TGTGGCCTTGTACTGCAGAG -3'; (2) then, the PCR products were sequenced by using the BigDye Terminator v3.1 (Applied Biosystems) and analyzed on a 3730 sequencer (Applied Biosystems). The sequencing primers are the same as the PCR forward primers.

Statistics: For comparison of small groups we used a cutoff of $P<0.05$ to distinguish significant differences. For analysis of gene correlations to survival, we used a false discovery rate (FDR) $P<0.05$ for greater stringency. Statistics for comparing cell proliferation, sphere formation, sphere diameter, and sphere total volume between groups of control cells and shRNA mediated knockdowns were done in GraphPad Prism software (http://www.graphpad.com/scientific-software/prism/) utilizing the paired T-test. Prism was also used for ANOVA comparison of TCGA classification and EGFR mutational status, EGFR amplification, and tumor status (primary, recurrent, secondary). Other analysis utilized CHI(2) tests using STATA 8.0 software (StataCorp, http://www.stata.com/) to compare TCGA classifications of high vs. low passages for tumorspheres and to compare TCGA classification or unbiased expression clustering

group of tumors vs. tumorspheres. STATA software was also utilized to perform linear regression of doubling time vs. sphere total volume or sphere formation.

Chapter 3

Interrogation of a Broad Spectrum of Glioblastoma Tumorspheres Informs Targeting of the PI3Kinase Pathway

Aim2. To test the hypothesis that interrogation of the tumorsphere system is informative for the study of targeted therapy.

Abstract

We interrogated a broad spectrum of glioblastoma (GBM) tumorsphere cultures with a panel of differential PI3Kinase (PI3K) pathway inhibitors. Responses to these drugs were unrelated to each other, and unrelated to the molecular classification of tumorspheres. Clathrin signaling was the sole signaling pathway associated with response to all PI3K pathway inhibitors tested. Across a variety of analytical approaches to the molecular expression of our tumorsphere library, ERK pathway activation was associated with response to mTOR inhibition. We observed that approximately 83% of GBM cultures were sensitized to MEK/ERK inhibition by mTOR inhibition, from either Rapamycin or BEZ235. We demonstrated in vivo that combinatorial treatment with Selumetinib (MEK/ERK inhibition) and Rapamycin (mTOR inhibition) produced a treatment response greater than response to treatment of either drug alone. Our data supports the idea that molecular analysis of the GBM tumorsphere model system can inform therapeutic treatment strategies.

Background

The Cancer Genome Atlas (TCGA) classified GBM tumors into 4 subtypes based on differential gene expression profiling(Verhaak et al., 2010). This classification system may apprise personalized medicine if each subtype requires its own tailored therapy. The hypothesis that the TCGA classification of GBM may inform therapy can be tested in a suitable in vitro system. Here, we test the hypothesis that PI3Kinase targeting will have differential response based on TCGA classification by utilizing the tumorsphere model system of GBM.

Targeting the phosphatidylinositol-3 kinase (PI3K) pathway is a promising approach for the treatment of cancer(Choe et al., 2003; Vivanco and Sawyers, 2002). This therapeutic strategy may be particularly suitable for GBM where the PI3K pathway is frequently activated through mutation. One study observed that 86% of GBM harbor mutation in the PI3K pathway(TCGA, 2008). A later study found that 89.6% of GBM had at least one alteration in the PI3K pathway, while 39% had two or more(Brennan et al., 2013). In 15-40% of primary GBM there are genetic alterations in phosphatase and tensin homolog (*PTEN*)(Ohgaki and Kleihues, 2009). Mutation of upstream pathway molecules such as phosphatidylinositol 3-kinase (*PI3KCA*) and *PTEN* may result in activation of downstream effectors, such as protein kinase B (AKT) and mammalian target of Rapamycin (mTOR), that control cell growth and proliferation(Dibble and Manning, 2013). Both PI3K activity and expression of *AKT* are directly associated with glioma tumor grade and therefore malignancy (Wang et al., 2010a). Moreover, inhibition of the AKT pathway has been shown to target glioblastoma brain tumor stem cells

(BTSC), the cells purported to be responsible for tumor formation and recurrence (Gallia et al., 2009).

Presently, therapeutic targeting of the PI3K pathway consists of numerous drugs that impair different nodes of the molecular signaling cascade (Maira et al., 2009). Inhibitors of EGFR, PI3K, mTOR, and AKT have all been developed(Wen et al., 2012). One aim of devising such targeted therapy is to personalize medicine through tailored therapy for each individual patient or tumor type(Olar and Aldape, 2014). Another aim of targeted therapy is to overcome resistance. The PI3K pathway has multiple feedback loops that may override inhibition at a single node(Sami and Karsy, 2013). In part to overcome resistance, single chemotherapeutic agents have been developed that target multiple nodes in the PI3K pathway. An example is NVP-BEZ235 that targets PI3KCA, mTORc1, and mTORc2. Certain PI3K pathway therapeutics are in, or are advancing to, clinical trials.

In the fight against cancer, some success has been forged by combinatorial therapy including combinatorial treatments for childhood ALL, Hodgkin's lymphoma, colon cancer, and breast cancer(Chabner and Roberts, 2005). However, if a single agent targets too broad a range of molecules, it may become less useful for tailored therapy. In addition, dual inhibitors may contravene one method of resistance but trigger yet another due to the complex interconnection of molecular signaling pathways. For these reasons, finding the optimal molecular targets for inhibition in GBM remains a challenge.

To identify the optimal therapeutic strategy for a complex, intractable disease such as GBM requires a suitable biological model system. In this study, we interrogated the GBM tumorsphere model system and appraised its capacity to inform an effective

course of treatment. This study tested a broad spectrum of primary GBM cultures in response to a panel of PI3K inhibitors and utilized several methods to analyze relationships with molecular expression data. We utilized Erlotinib to target EGFR, Rapamycin to target mTORc1, and NVP-BEZ235 to target mTORc1/mTORc2/PI3KCA (Figure 11). In addition, we used Selumetinib to target the extracellular signal regulated kinase (ERK) pathway that is also downstream of EGFR (Figure 1).

We found no evidence that TCGA classification was associated with response to PI3K pathway inhibitors. However, we did find that the tumorsphere model is suitable for developing therapeutic strategies. Results from this study indicate that the ERK pathway is consistently correlated with tumorsphere response to inhibition of mTOR. This study demonstrates that inhibition of the mTOR pathway sensitizes GBM to inhibition of ERK in a vast majority of patient derived GBM tumorsphere cultures. In an in vivo model, the efficacy of combinatorial ERK/mTOR inhibition was ingeminated. This study supports the hypothesis that interrogation of the tumorsphere model system may inform therapeutic strategies for the treatment of GBM.

Results

Description of dataset: We tested 17 GBM tumorsphere cultures for in vitro dose response to the mTORc1 inhibitor, Rapamycin. 27 GBM tumorsphere cultures were tested for in vitro dose response to the mTORc1,c2 /PI3K inhibitor, NVP-BEZ235. 25 tumorsphere cultures were tested for in vitro dose response to the MEK inhibitor, Selumetinib. MEK inhibition effectively inhibits the downstream effector kinase ERK and, for the purpose of this paper, will be termed MEK/ERK inhibition. 26 tumorsphere cultures were tested for in vitro dose response to the EGFR inhibitor, Erlotinib (Table 6). All samples underwent microarray-based gene expression profiling utilizing the Affymetrix U133 plus 2.0 platform. Molecular classification of tumorsphere cultures was performed as previously described (Chapter 2).

Each tumorsphere culture was treated for one week with a panel of different inhibitors and their effect on cell number was assessed. IC50 values were determined for each inhibitor in each tumorsphere culture. For Rapamycin, only a % survival at 1uM was used as many of the cell cultures did not pass below the 50% cell number after treatment in our titration and therefore IC50 values could not be calculated. In Figure 11 and Table 6 the results from these titrations are exhibited. Figure 11E displays the nodes of the PI3Kinase pathway that each inhibitor targets. Rapamycin is an mTORc1 inhibitor, NVP-BEZ235 is an mTORc1, mTORc2, and PI3Kinase inhibitor, Selumetinib is a MEK (ERK) inhibitor, and Erlotinib is an EGFR inhibitor (Figure 11E).

Summary of Tumorsphere Cultures and Response to PI3Kinase Inhibitors

Inhibitor Targets:	mTOR		mTORc1,c2/ PI3K		MEK/ERK		EGFR	
Outcome:	**Rapamycin Survival at 1 uM**		**NVP-BEZ235 IC50 (nM)**		**Selumetinib IC50 (uM)**		**Erlotinib IC50 (nM)**	
Tumorsphere ID #	Mean	Std. Deviation	Mean	Std. Deviation	Mean	Std. Deviation	Mean	Std. Deviation
39			22.3	3.65			3.31	2.12
157	19.9	1.92	7.77	3.63	0.104	0.0282	0.743	0.315
206			8.14	0.0945	0.271	0.132	13.6	11.5
207	41.2	7.78						
213	49.8	0.283	1.64	1.42	0.0101	0.0143	0.983	0.14
217	24.1	8.35	6.11	0.811	0.0483	0.0536	17.3	3.59
229			4.21	1.35	0.731	0.379	1.32	0.235
248	57.9	0.96	3.02	0.023	0.156	0.0965	1.16	0.469
250	25	0.563	7.55	1.33	0.282	0.168	0.241	0.0942
254	41.3	0.141	10.9	0.63	0.00997	0.0133	1.7	1.49
277	49.9	8.36						
296	38.8	6.87	6.98	2.76	1.14	0.812	1.34	1.22
301	29.2	6.01	6.46	0.102	0.801	0.323	0.298	0.115
308	41.6	0.283	7.87	0.331	1.37	0.777	0.635	0.463
322	53.6	11.8						
336	30.5	4.38	8.45	2	0.246	0.221	1.49	1.14
345			0.892	0.734	0.677	0	0.842	0.487
347			6.43	1.14	0.192	0.114	1.01	0.388
348			14	2.13				
350	23.3	0.0253	0.709	0.345	0.119	0.0532	1.76	0.942
371	39.1	5.59						
374			7.94	3.05	1.35	0.881	6.19	4
378	40.9	1.07	7.37	1.94	0.476	0.147	0.00716	0.00418
381			2.85	0.0745	3.31	0.458	0.362	0.111
382			4.96	0.803	0.085	0.00209	2.15	0.913
390	21.3	4.85	4.54	0.837	0.56	0.118	0.239	0.106
393			2.08	0.813	0.00909	0.00491	5.81	0
401			3.05	0.471	0.0172	0.0183	3.04	0.634
412			1.72	0.24	0.149	0.0699	0.0995	0.0325
413			3.12	0.169	1.93	0.529	2.54	0.0933
423			8.62	4.16	0.103	0.0582	0.221	0.000354

Table 6. Summary of tumorsphere cultures and response to PI3K inhibitors. List of tumorsphere cultures and their responses to PI3K pathway inhibitors: Rapamycin (mTORc1), BEZ235 (mTORc1, c2, PI3K), Selumetinib (ERK), and Erlotinib (EGFR). IC50 values are indicated except for Rapamycin response which is % survival at 1uM dose, as most cultures did not pass the IC50 value in our titration and therefore IC50 values could not be estimated.

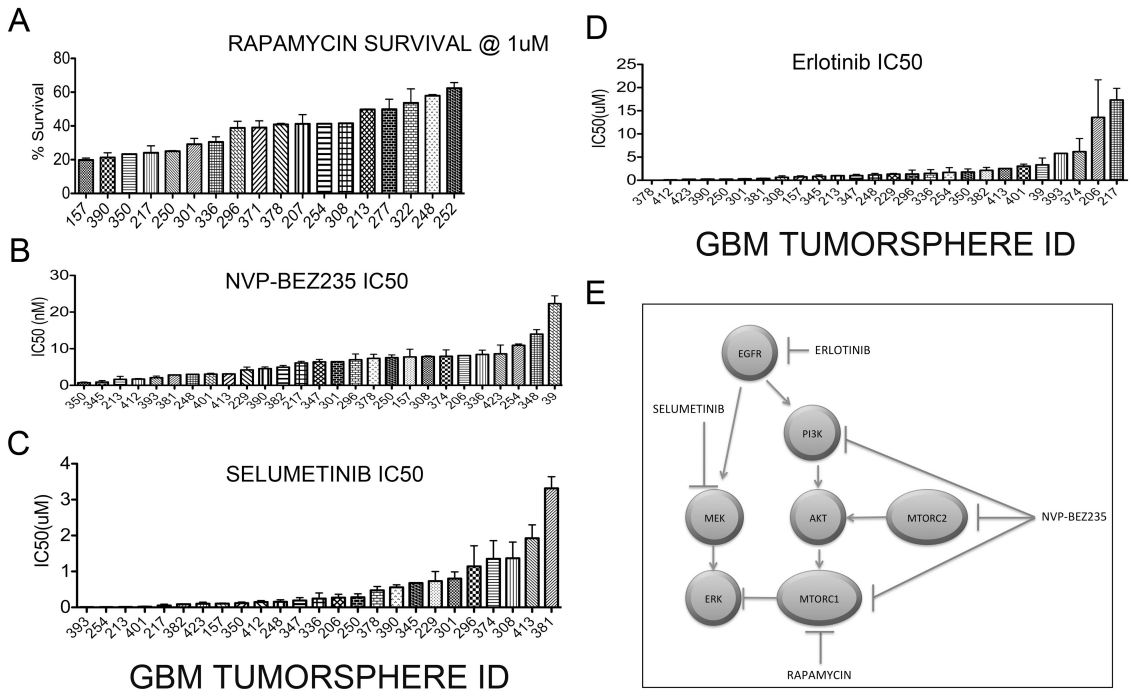

Figure 11. Differential response of GBM tumorspheres to a panel of inhibitors targeting different nodes of the PI3Kinase pathway. A. % survival after 7 days of treatment with 1uM of Rapamycin. Bars indicate means +/- std. error of the mean. N=2 biological replicates. B. Calculated IC50s (nM) after 1 one week of treatment with a titration of NVP-BEZ235. Bars indicate means +/- std. error of the mean. N=2 biological replicates. C. Calculated IC50s (uM) after 1 one week of treatment with a titration of Selumetinib. Bars indicate means +/- std. error of the mean. N=2 biological replicates. D. Calculated IC50s (uM) after 1 one week of treatment with a titration of Erlotinib. Bars indicate means +/- std. error of the mean. N=2 biological replicates. E. Schematic of the PI3Kinase pathway and the targets of inhibition for each therapeutic used.

From Figure 11, it is apparent that there is a differential response to each inhibitor across our panel of GBM cell cultures. We asked whether this differential response was related to TCGA classification. None of the four inhibitors had a response that was associated with TCGA classification (Figure 12) or unsupervised clustering (Figure 13). Next we analyzed whether recurrent tumors were differentially sensitive or resistant as compared to primary non-recurrent tumors. Rapamycin was the only inhibitor with differential response related to recurrence status; specifically tumorsphere cultures derived from recurrent tumors were more resistant to Rapamycin treatment than non – recurrent primary tumor derived tumorspheres (P=0.049, Mann-Whitney)(Figure 14a).

Surprisingly, response to any one inhibitor was not significantly associated with response to any other inhibitor across our panel of tumorsphere cultures (Figure 15,16). Our data suggests that each different PI3Kinase pathway inhibitor may have a different group of tumorspheres that would be optimal therapeutic responders. As neither TCGA classification nor unsupervised clustering predicts response to PI3K pathway inhibition, other biomarkers may be needed to determine the optimal target population of each inhibitor.

We analyzed the correlation between a particular drug response and mutational status for *EGFRV3*, *EGFR* Amplification, *EGFR*V3 or Amplification, and *PTEN* deletion (Table 7). Cultures with *EGFR*V3 (in tumors or tumorspheres) or *EGFR* amplification (in tumors) were more resistant to Rapamycin (P=0.0303, Figure 16A, Table 7). *EGFR* amplification (in tumors) trended with Selumetinib resistance (P=0.0523, Mann-Whitney test, Figure 16B, Table 7). (Figure 16, Table 7). *EGFR*vIII was associated with higher resistance to Selumetinib (P=0.0484, Figure 16C, Table7). And *EGFR*V3 or *EGFR*

amplified cell cultures were associated with resistance to Selumetinib (P=0.0133, Figure 16D, Table 7).

Next we asked what sets of genes are associated with response to our panel of PI3K pathway inhibitors. We did gene-by-gene correlation analysis to the IC50 values of each drug across our panel of tumorsphere cultures. For Rapamycin we used the % survival values at 1uM Rapamycin treatment since our titration didn't produce many IC50 values as most tumorsphere cultures reached a floor in their response above the 50% cell number value. We analyzed our list of genes significantly associated (P<0.001) to response for each drug and analyzed these lists in Ingenuity. We analyzed the list of significant genes (P<0.001) in TFacts, an online tool that predicts transcription factor activation or repression based on sign sensitive associations (direct vs. inverse associations). For Rapamycin, TFacts assessed that 4 transcription factors were activated in association with Rapamycin resistance: SP1 (E<0.001), CTNNB1 (Beta Catenin) (E<0.001), JUN (E=0.0327), CEBPA (E=0.03597) (Table 8). Ingenuity analysis indicates that Wnt/Beta-catenin signaling is the second most significant canonical pathway associated with Rapamycin response (P<0.001). In addition, the ERK pathway is also significantly associated with Rapamycin response (P=0.037).

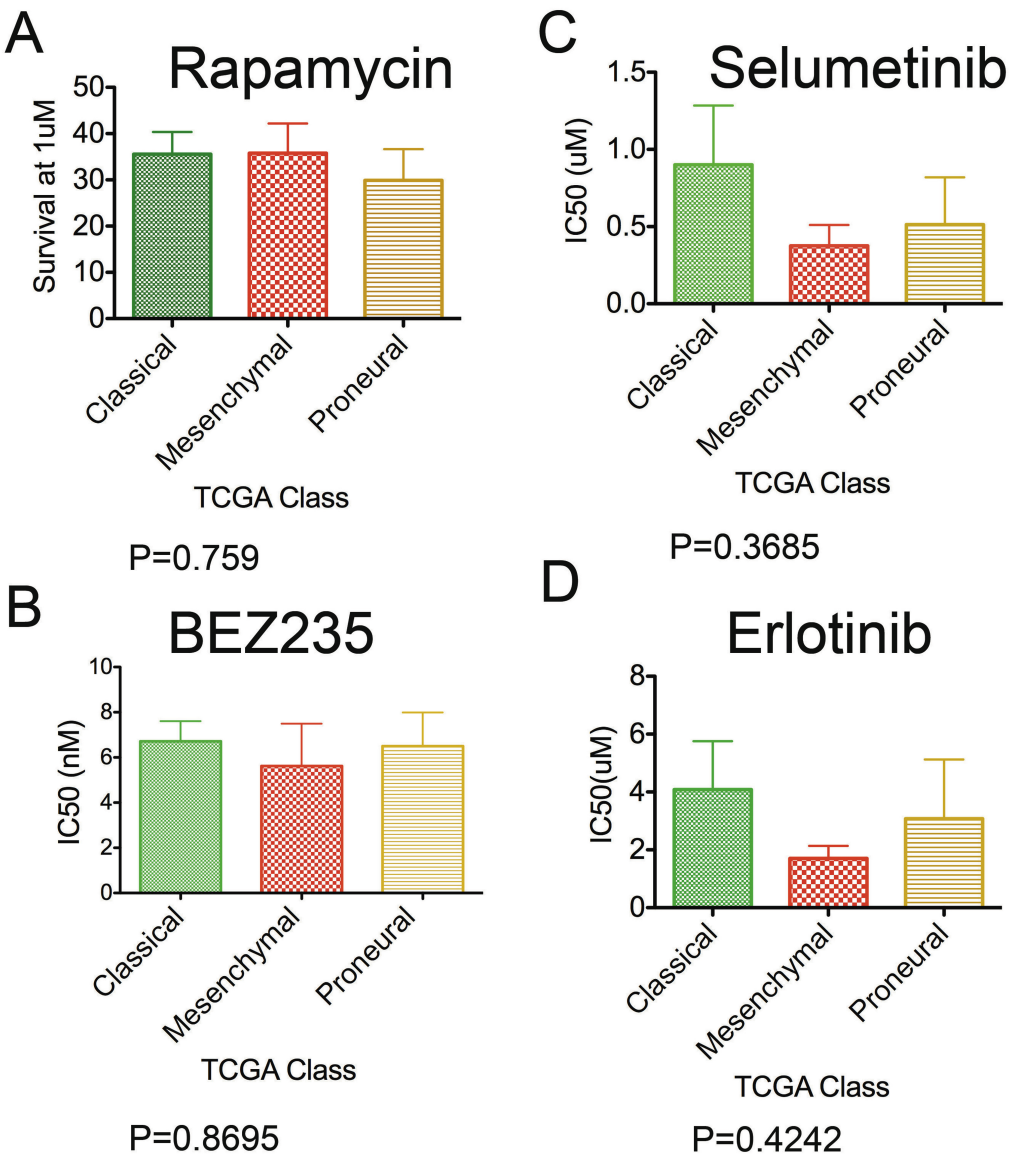
A
Rapamycin
Survival at 1uM
50
40
30
20
10
0
Classical
Mesenchymal
Proneural
TCGA Class
P=0.759
C
Selumetinib
IC50 (uM)
1.5
1.0
0.5
0.0
Classical
Mesenchymal
Proneural
TCGA Class
P=0.3685
B
BEZ235
IC50 (nM)
10
8
6
4
2
0
Classical
Mesenchymal
Proneural
TCGA Class
P=0.8695
D
Erlotinib
IC50(uM)
8
6
4
2
0
Classical
Mesenchymal
Proneural
TCGA Class
P=0.4242

Figure 12

Figure 12. No TCGA classification demonstrates differential sensitivity to PI3K pathway inhibition. A. % Survival after one week of treatment with 1uM Rapamycin is categorized by TCGA classification of tumorspheres. Bars indicate mean values +/- std. error of the mean. ANOVA P-value is displayed (P=0.759). B. BEZ235 IC50 and TCGA classification (P=0.8695, ANOVA). Calculated IC50's (nM) after one week of treatment with a titration of NVP-BEZ235 is categorized by TCGA classification of tumorspheres. ANOVA P-value is displayed. C. Calculated IC50's (uM) after one week of treatment with a titration of Selumetinib is categorized by TCGA classification of tumorspheres. ANOVA P-value is displayed (P=0.3685). D. Calculated IC50's (uM) after one week of treatment with a titration of Erlotinib is categorized by TCGA classification of tumorspheres. ANOVA P-value is displayed (P=0.4242).

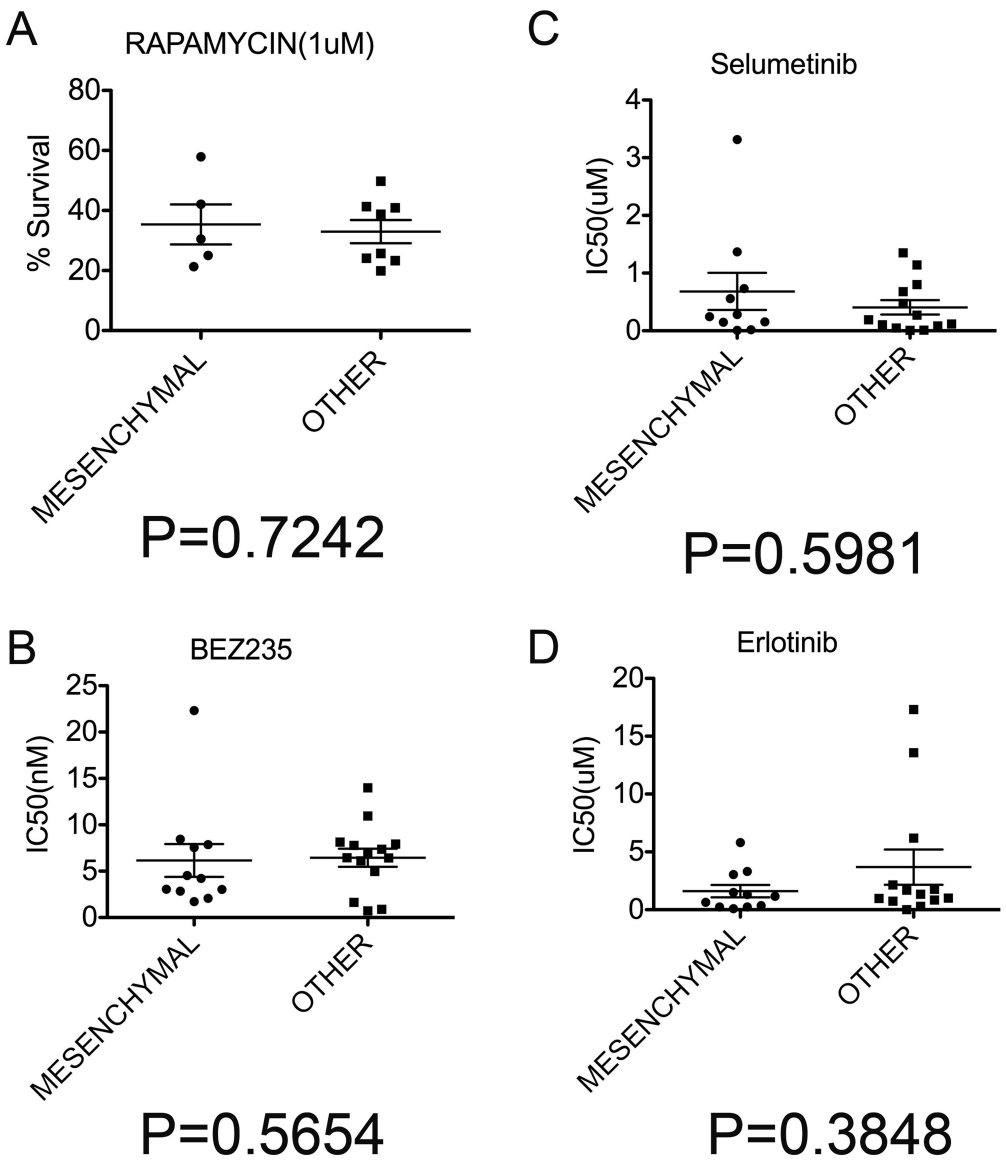
A
RAPAMYCIN(1uM)
% Survival
80
60
40
20
0
MESENCHYMAL
OTHER
P=0.7242
C
Selumetinib
IC50(uM)
4
3
2
1
0
MESENCHYMAL
OTHER
P=0.5981
B
BEZ235
IC50(nM)
25
20
15
10
5
0
MESENCHYMAL
OTHER
P=0.5654
D
Erlotinib
IC50(uM)
20
15
10
5
0
MESENCHYMAL
OTHER
P=0.3848

Figure 13

Figure 13. No unbiased clustering group is associated with differential sensitivity to PI3K pathway inhibition. Unbiased clustering of the top 2000 most variable genes distinguished 2 groups, primarily “Mesenchymal” and non-Mesenchymal or “Other”. A. % Survival after one week of treatment with 1uM Rapamycin is categorized by clustering groups of tumorspheres. Bars indicate mean values +/- std. error of the mean. T-test P-value is displayed (P=0.7242). B. BEZ235 IC50 is categorized by clustering groups of tumorspheres. Bars indicate mean values +/- std. error of the mean. T-test P-value is displayed (P=0.5654). C. Calculated IC50’s (uM) after one week of treatment with a titration of Selumetinib is categorized by clustering groups of tumorspheres. Bars indicate mean values +/- std. error of the mean. T-test P-value is displayed (P=0.5981). D. Calculated IC50’s (uM) after one week of treatment with a titration of Erlotinib is categorized by clustering groups of tumorspheres. Bars indicate mean values +/- std. error of the mean. T-test P-value is displayed (P=0.3848).

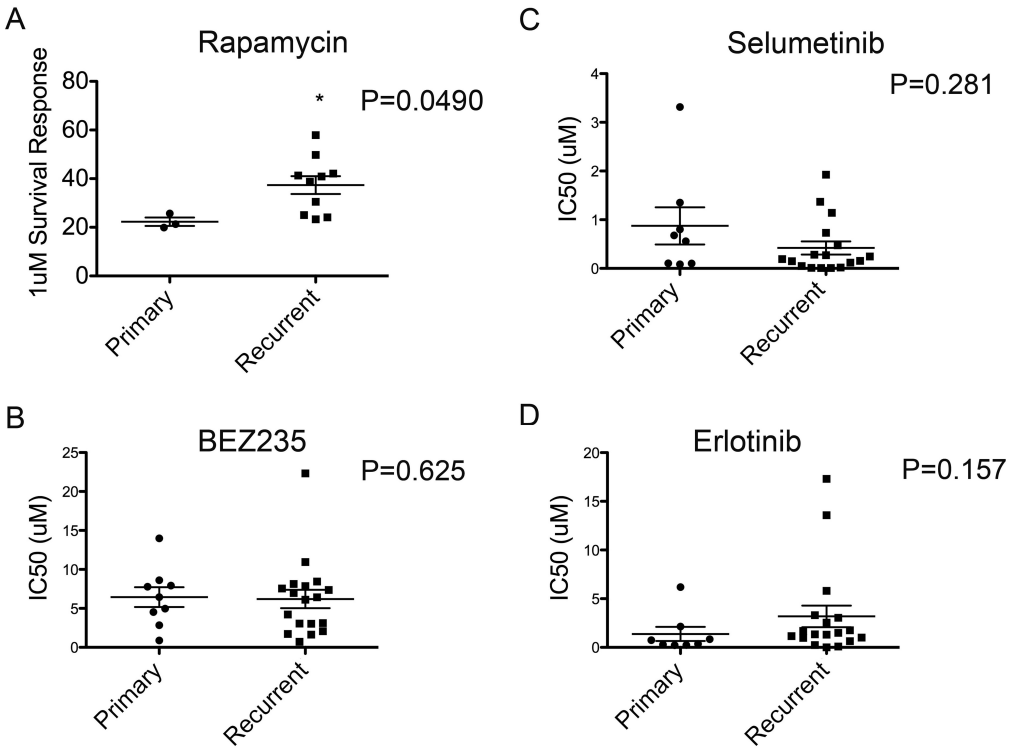

Mann-Whitney U test - non parametric

Figure 14

Figure 14. Recurrent tumors are more resistant to Rapamycin. A. % Survival after one week of treatment with 1uM Rapamycin is categorized by recurrent tumor or non-recurrent tumor. The non-parametric Mann-Whitney test, P-value is displayed (P=0.0490). Bars indicate mean values +/- std. error of the mean. B. Calculated IC50's (nM) after one week of treatment with a titration of NVP-BEZ235 is categorized by recurrent tumor or non-recurrent tumor. The non-parametric Mann-Whitney test, P-value is displayed (P=0.625). Bars indicate mean values +/- std. error of the mean. C. Calculated IC50's (uM) after one week of treatment with a titration of Selumetinib is categorized by recurrent tumor or non-recurrent tumor. The non-parametric Mann-Whitney test, P-value is displayed (P=0.281). Bars indicate mean values +/- std. error of the mean. D. Calculated IC50's (uM) after one week of treatment with a titration of Erlotinib is categorized recurrent tumor or non-recurrent tumor. The non-parametric Mann-Whitney test, P-value is displayed (P=0.157). Bars indicate mean values +/- std. error of the mean.

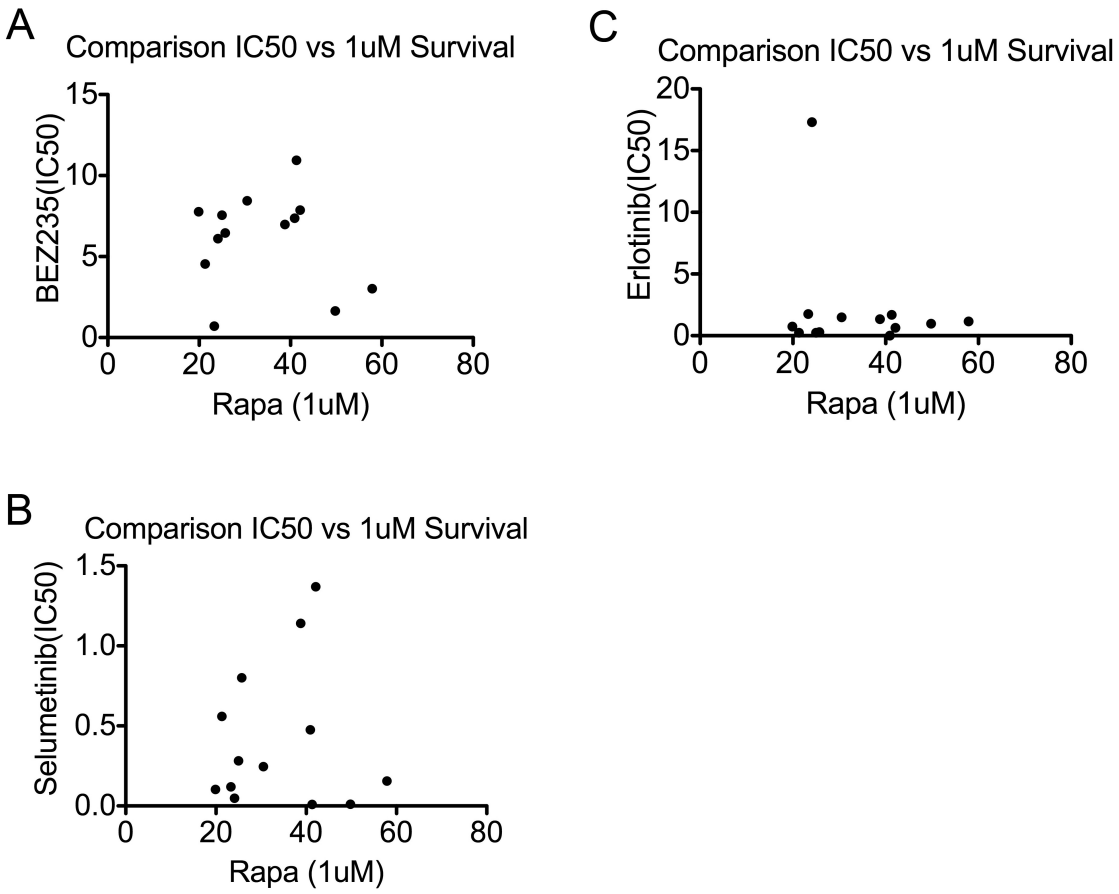

Figure 15. Plot of response to 1uM Rapamycin (% survival) vs. IC50 values for PI3K pathway inhibitors depicts no correlation between GBM tumorsphere response to different PI3K pathway inhibitors.

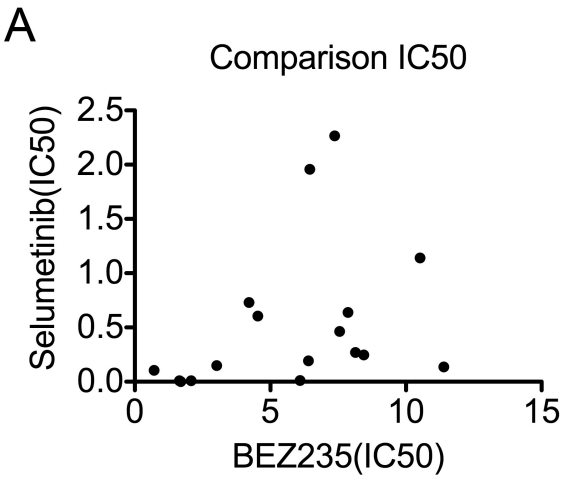
A
Comparison IC50
Selumetinib(IC50)
2.5
2.0
1.5
1.0
0.5
0.0
0
5
10
15
BEZ235(IC50)

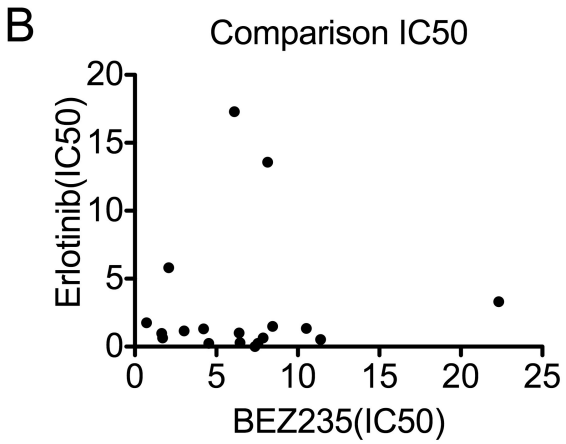
B
Comparison IC50
Erlotinib(IC50)
20
15
10
5
0
0
5
10
15
20
25
BEZ235(IC50)

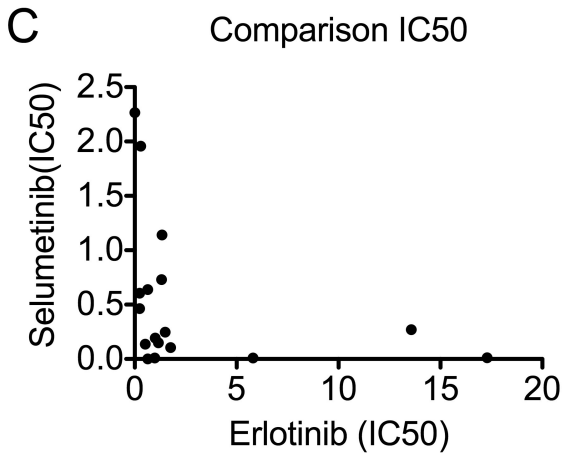
C
Comparison IC50
Selumetinib(IC50)
2.5
2.0
1.5
1.0
0.5
0.0
0
5
10
15
20
Erlotinib (IC50)

Figure 16

Figure 16. Plot of IC50 values for PI3K pathway inhibitors depicts no correlation between GBM tumorsphere response to different PI3K pathway inhibitors.

Response to PI3Kinase inhibitors and Tumorsphere Mutation Status

Outcome	Explanatory Variable	Test	P-Value	Difference
Rapamycin 1uM	*EGFR*V3	Mann-Whitney	1	
	EGFR Amplification	Mann-Whitney	0.1111	
	EGFR V3 or Amplification	Mann-Whitney	0.0303	V3/ Amp are more resistant
	PTEN deletion	Mann-Whitney	0.2168	
BEZ235 IC50	*EGFR*V3	Mann-Whitney	0.4036	
	EGFR Amplification	Mann-Whitney	0.8365	
	EGFR V3 or Amplification	Mann-Whitney	0.7612	
	PTEN deletion	Mann-Whitney	0.9711	
Selumetinib IC50	*EGFR*V3	Mann-Whitney	0.0484	V3 are more resistant
	EGFR Amplification	Mann-Whitney	0.0523	Amp trend more resistant
	EGFR V3 or Amplification	Mann-Whitney	0.0133	V3/ Amp are more resistant
	PTEN deletion	Mann-Whitney	0.6345	
Erlotinib IC50	*EGFR*V3	Mann-Whitney	0.6723	
	EGFR Amplification	Mann-Whitney	0.1074	
	EGFR V3 or Amplification	Mann-Whitney	0.1564	
	PTEN deletion	Mann-Whitney	0.9368	

Note: *EGFR*V3 status was determined in tumorsphere cultures by western.
EGFR amplifiaction was determing in tumors by pathology.
PTEN was determined in tumorspheres by western.

Table 7: Response to PI3K inhibitors and Tumorsphere Mutation Status. Correlation between response to Rapamycin and *EGFR* status. *EGFR*VIII status is from westerns of the tumorsphere cultures. *EGFR* amplification status is from the pathology report of the parent tumor. Mutations in *PTEN* are from western blots of the tumorsphere cultures. P-values for the Mann-Whitney, non-parametric comparison are indicated.

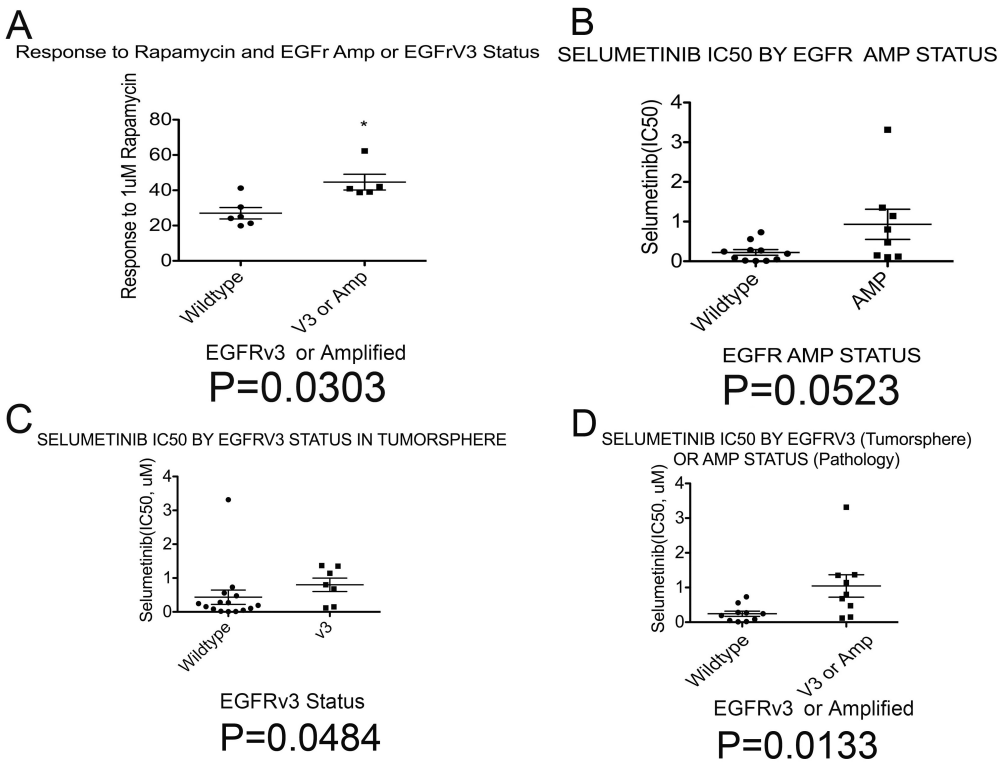
A
Response to Rapamycin and EGFr Amp or EGFrV3 Status
Response to 1uM Rapamycin
80
60
40
20
0
*
Wildtype
V3 or Amp
EGFRv3 or Amplified
P=0.0303
B
SELUMETINIB IC50 BY EGFR AMP STATUS
Selumetinib(IC50)
4
3
2
1
0
Wildtype
AMP
EGFR AMP STATUS
P=0.0523
C
SELUMETINIB IC50 BY EGFRV3 STATUS IN TUMORSPHERE
Selumetinib(IC50, uM)
4
3
2
1
0
Wildtype
v3
EGFRv3 Status
P=0.0484
D
SELUMETINIB IC50 BY EGFRV3 (Tumorsphere)
OR AMP STATUS (Pathology)
Selumetinib(IC50, uM)
4
3
2
1
0
Wildtype
V3 or Amp
EGFRv3 or Amplified
P=0.0133

Figure 17

Figure 17. EGFR activation is associated with enhanced resistance to Rapamycin and enhanced resistance to Selumetinib. A. *EGFR* activation (*EGFR*V3 in tumorspheres or tumor) or amplification (in tumor) is associated with enhanced resistance to Rapamycin. Mean (wide horizontal bar) +/- std. error of the mean (short horizontal bars) for % survival at 1uM Rapamycin treatment for a week, categorized by *EGFR* wildtype or activating mutation (V3 or amplification). Mann-Whitney test P value is indicated (P=0.0303). B. *EGFR* activation (*EGFR* amplification) is trending towards an association with enhanced resistance to Selumetinib. Mean (wide horizontal bar) +/- std. error of the mean (short horizontal bars) for IC50 values for Selumetinib treatment for a week, categorized by *EGFR* wildtype or EGFR amplification. Mann-Whitney test P value is indicated (P=0.0523). C. *EGFR* activation (*EGFR*V3 in tumorspheres) is associated with enhanced resistance to Selumetinib. Mean (wide horizontal bar) +/- std. error of the mean (short horizontal bars) for IC50 values for Selumetinib treatment for a week, categorized by *EGFR* wildtype or *EGFRVIII*. Mann-Whitney test P value is indicated (P=0.0484). D. *EGFR* activation (*EGFR*V3 in tumorspheres or amplification in tumor) is associated with enhanced resistance to Selumetinib. Mean (wide horizontal bar) +/- std. error of the mean (short horizontal bars) for IC50 values for Selumetinib treatment for a week, categorized by *EGFR* wildtype vs. *EGFR VIII* or amplification. Mann-Whitney test P value is indicated (P=0.0133).

Transcription factors associated with genes that correlate with PI3Kinas inhibitor response

Associated Treatment	Transcription Factor	Activated/Repressed	P Value	E Value	FDR
Rapamycin	SP1	A	<0.001	<0.001	0.000459
Rapamycin	CTNNB1	A	<0.001	<0.001	0.000917
Rapamycin	JUN	A	0.0003	0.0327	0.00138
Rapamycin	CEBPA	A	0.00033	0.036	0.00184
NVP-BEZ235	SMAD7	A	<0.001	0.00073	0.000685
NVP-BEZ236	LEF1	A	0.00042	0.0307	0.00137

*TFacts Analysis

Table 8. Transcription factors associated with genes that correlate with PI3K inhibitor response. TFacts sign-sensitive analysis of genes significantly associated (P=0.001) with response to each indicated PI3K inhibitor distinguishes transcription factors associated with response.

For NVP-BEZ235, TFacts assessed that 2 transcription factors were activated in association with BEZ235 resistance: SMAD7 (E<0.001), LEF1 (E=0.00042) (Table 8). LEF1 is a co-activator of transcription along with CTNNB1 (Beta catenin). Ingenuity analysis confirmed that Wnt/Beta-catenin signaling is the third most significant canonical pathway associated with BEZ235 response (P=0.00151). In addition, ERK5 pathway is also significantly associated with BEZ235 response (P=0.0051).

Next, we looked at canonical pathways for cell signaling associated with mTOR inhibition by both acute Rapamcyin and BEZ235 (Table 9). Ingenuity analysis of canonical pathways indicates that 12 signaling pathways are consistently associated with mTOR inhibition by both Rapamycin and BEZ235 (Table 9). Ephrin signaling, the canonical signaling pathway with the second strongest association to mTOR inhibition (Average P=0.0259, Table 9), has been demonstrated to regulate ERK signaling in GBM, the pathway with the 4th strongest association to mTOR inhibition (Average P=0.0265, Table 9) (Day et al., 2013). In addition, Integrin signaling, the canonical signaling pathway with the 3rd strongest association to mTOR inhibition (Average P=0.0262, Table 9), is also associated with ERK signaling in glioma stem cells(Nakada et al., 2013). Thus, we inferred that the ERK signaling pathway is the predominant signaling pathway consistently associated with response to mTOR inhibition as it is involved in 3 of the top 4 correlated canonical signaling pathways.

Signaling associated with mTOR inhibitors

	Acute Rapamycin		BEZ235			
Signaling Pathway	P-Value	Ratio	P-Value	Ratio	Avg. P-Value	Avg. Ratio
Wnt/B-catenin	0.0479	5.30E-01	0.00151	2.50E-01	0.0247	0.39
Ephrin	0.0479	5.42E-01	0.00389	2.38E-01	0.0259	0.39
Integrin	0.0479	4.50E-01	0.00447	2.32E-01	0.0262	0.341
MAPK/ERK	0.0479	4.79E-01	0.00513	2.95E-01	0.0265	0.387
PTEN	0.0479	4.49E-01	0.0251	2.31E-01	0.0365	0.34
eNOS	0.0479	4.33E-01	0.0282	2.24E-01	0.0380	0.329
Aldosterone	0.0479	4.34E-01	0.0282	2.20E-01	0.0380	0.327
B Cell receptor	0.0479	4.94E-01	0.0302	2.16E-01	0.0390	0.355
ILK	0.0479	4.84E-01	0.0380	2.10E-01	0.0429	0.347
Clathrin	0.0479	4.81E-01	0.0479	2.07E-01	0.0479	0.344
HER-2	0.0479	5.26E-01	0.0479	2.37E-01	0.0479	0.382
iCOS-iCOSL	0.0479	5.00E-01	0.0479	2.27E-01	0.0479	0.364

Signaling associated with PI3K pathway inhibitors in this study

	Acute Rapamycin		BEZ235		Selumetinib		Erlotinib			
Signaling Pathway	P-Value	Ratio	P-Value	Ratio	P-Value	Ratio	P-Value	Ratio	Avg. P-Value	Avg. Ratio
Clathrin	0.0479	0.481	0.0479	0.207	0.0110	1.68E-01	0.0380	1.08E-01	0.0362	0.241

Table 9. Signaling associated with mTOR inhibitors and with PI3K pathway inhibitors. The top section of the table depicts canonical signaling pathways associated with response to both mTOR inhibitors as determined by Ingenuity analysis. The bottom section of the table depicts canonical signaling of Clathrin as the only signaling pathway associated with all PI3K pathway inhibitors studied, as determined by Ingenuity analysis. For each, Ingenuity analyzed a list of genes significantly ($P<0.001$) associated with response to each drug. The canonical signaling pathways listed were significantly associated ($P<0.05$) with response.

For Selumetinib, TFacts did not identify any transcription factors as significantly (E<0.05) associated with response. Ingenuity analysis indicates that Wnt/Beta-catenin signaling is a canonical pathway significantly associated with response to Selumetinib (P<0.00257). In addition, mTOR signaling (P=0.0011) and ERK5 signaling (P=0.0177) are associated with Selumetinib response.

For Erlotinib, TFacts did not identify any transcription factors as significantly (E<0.05) associated with response. Ingenuity analysis indicates that FGF signaling is associated with response (P=0.000851) and EGF signaling is associated with response (P=0.0427). Erlotinib acts upstream of the other PI3K pathway inhibitors we studied, and it seems to have a distinct set of canonical pathways associated with response. Interestingly, the gene *MDM2* was associated with resistance to Erlotinib (Pearson=0.682, P<0.0001). *MDM2* is extra-chromosomally amplified in response to Erlotinib treatment (Nathanson et al., 2014) and our data suggests that it may play a role in resistance to Erlotinib. Clathrin signaling is the only canonical signaling pathway associated with response to all of our PI3K inhibitors (Table 9).

We performed a chronic Rapamycin assay on a panel of our tumorsphere cultures. To this end, we measured the % sphere formation after 20 days of growth at clonal density. Again we generated a list of genes correlated to response (P<0.001). For Chronic Rapamycin, TFacts did not identify any transcription factor as significantly (E<0.05) associated with response. Ingenuity analysis indicates that p70S6K signaling is significantly associated with response (P=0.000145), as is ERK signaling (P=0.000501), PTEN signaling (P=0.000562), Wnt/Beta Catenin Signaling (P=0.00457), PI3K signaling (P=0.00933), PI3K/AKT signaling (P=0.0257), and mTOR signaling (P=0,0447). These

results indicate that the PI3Kinase pathway is associated with chronic Rapamycin response as would be expected. In addition, this analysis recapitulates that Wnt/Beta Catenin and ERK are both consistently implicated in response to PI3Kinase pathway specific inhibition.

WGCNA- Sign Sensitive

We performed a signed, weighted gene correlation network analysis (WGCNA) to assess correlations between modules of co-expressed genes and PI3K pathway drug response (Figure 18). Rapamycin demonstrated a consistent correlation to module "DarkRed" across different concentrations of Rapamaycin that is most pronounced in the 1uM Rapamycin treatment column (0.62 correlation, $P<0.001$). When we analyzed the list of genes in the "DarkRed" module through TFacts in a sign insensitive manner (since the module is a signed analysis to begin with), TFacts produced a list of 6 transcription factors associated with the "DarkRed" module (Table 10). CREB1 forms a transcriptionally active complex with CTNNB1(Hecht et al., 2000; Takemaru and Moon, 2000). FOS interaction with JUN enables DNA binding (Sassone-Corsi et al., 1988). FOS is regulated by ERK (Monje et al., 2005). When we run the gene list associated with the "DarkRed" module through ingenuity, ERK1/2 is the top upstream regulator predicted to be associated with this gene list ($P<0.001$).

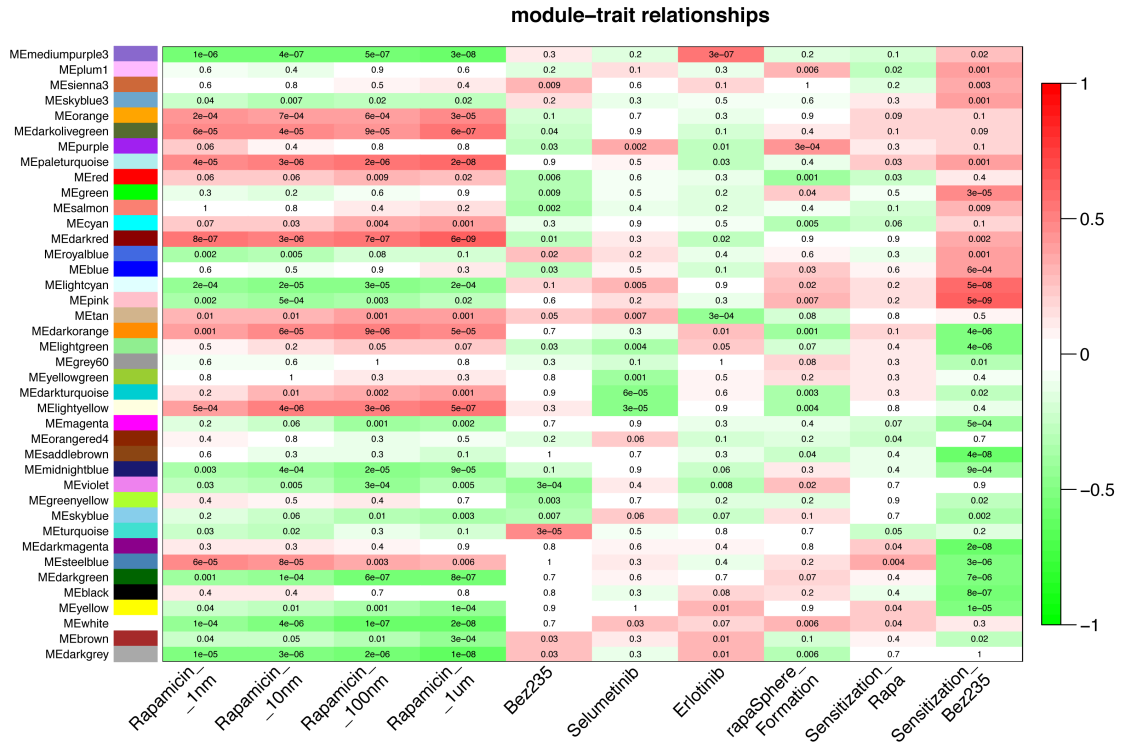

Figure 18. Signed WGCNA analysis of GBM tumorsphere cultures displays modules of genes and their correlation with drug response. The P-values are depicted in each cell for each module and its correlation to outcome, while the colors represent the Pearson correlation according to the heat map scale on the side. The Dark red module is highly associated with Response to Rapamycin across the range of doses utilized ($P<0.001$). The "RapaSphereFormation" group refers to the clonal formation of spheres under chronic Rapamycin. The other groups are 7 day treatments.

Transcription Factors Associated* with the "Dark Red" module which is correlated with Response to Rapamcyin

Outcome Variable	Module	Transcription Factor	P Value	E Value	FDR
Rapamycin Treatment (1uM)	DarkRed	USF2	<0.001	<0.001	0.001
Rapamycin Treatment (1uM)	DarkRed	USF1	<0.001	0.001	0.002
Rapamycin Treatment (1uM)	DarkRed	CREB1	0.00005	0.0025	0.003
Rapamycin Treatment (1uM)	DarkRed	JUN	0.00006	0.003	0.004
Rapamycin Treatment (1uM)	DarkRed	PPARG	0.00033	0.0165	0.005
Rapamycin Treatment (1uM)	DarkRed	FOS	0.00052	0.026	0.006

*Tfacts Analysis of modules associated with outcome

Table 10. Transcription factors associated with "Dark Red" module that is correlated to genes associated with Rapamycin response at 1uM.

BEZ235 resistance was most correlated with the "Turquoise" WGCNA module (Pearson=0.48, $P=3*10^{-5}$) (Figure18). When we analyze the "Turquoise" module in Ingenuity, we find many canonical pathways associated with genes in this module, including PI3K/AKT signaling (P=0.0479), p70s6K signaling (0.0174), ERK/MAPK signaling (P=0.00955), integrin signaling (P=0.000166), and mTOR signaling (P=0.000263). ERK/MAPK signaling is considered activated in this gene set.

Erlotinib resistance is most correlated with the "MediumPurple3" module (Pearson=0.57, $P=3*10^{-7}$) (Figure 18). This module only consisted of 11 genes and so was not amenable to effective analysis by Ingenuity. Of these genes, *MDM2* is the most significant gene (Pearson=0.900, P<0.001).

More than other signaling pathways, ERK/MAPK signaling was distinguished by consistent correlations with response to mTOR inhibition from both Rapamycin and NVP-BEZ235. Specifically, activated ERK signaling is associated with resistance to mTOR inhibition. In addition, mTOR signaling is associated with response to MEK/ERK inhibition by Selumetinib. If we assume biological significance to these correlations, our results support the hypothesis that combinatorial treatment of Selumetinib with Rapamycin or BEZ235 may be efficacious.

Sensitization:

Next we looked at dual inhibition of mTOR and ERK. We performed combinatorial treatment of a panel of tumorsphere cultures with both a titration of Selumetinib in the presence of Rapamycin (100nM) or a titration of Selumetinib in the presence of BEZ-235 (10nM). We produced titration dose response curves, calculated IC50 values and

determined if Rapamcyin or BEZ235 conferred sensitivity to Selumetinib treatment. If the relative IC50 value of the combinatorial treatment fell below 50% of the relative IC50 of Selumetinib alone, we considered that a sensitization effect (Figure 19A). We also did a statistical analysis to compare IC50 values that generated P-values to distinguish statistically significant differences in IC50 values (Table 11). We observed that 52.2% of our tumorspheres displayed sensitization to Selumetinib by Rapamycin treatment while 68.4% of our tumorspheres displayed sensitization to Selumetinib by BEZ-235. 83.3% were sensitized to Selumetinib by either Rapamycin or BEZ235, and 44.4% were sensitized by both Rapamycin and BEZ235 (Table 11). HK374 is a good example of profound sensitization to MEK/ERK inhibition conferred by both Rapamycin and BEZ235 (Figure 19B). These data indicate that a majority of GBM tumorsphere cultures are sensitized to MEK/ERK inhibition by mTOR inhibition. These results provide support for the hypothesis that such combinatorial therapy may be an effective therapeutic strategy in the treatment of a majority of glioblastoma cases.

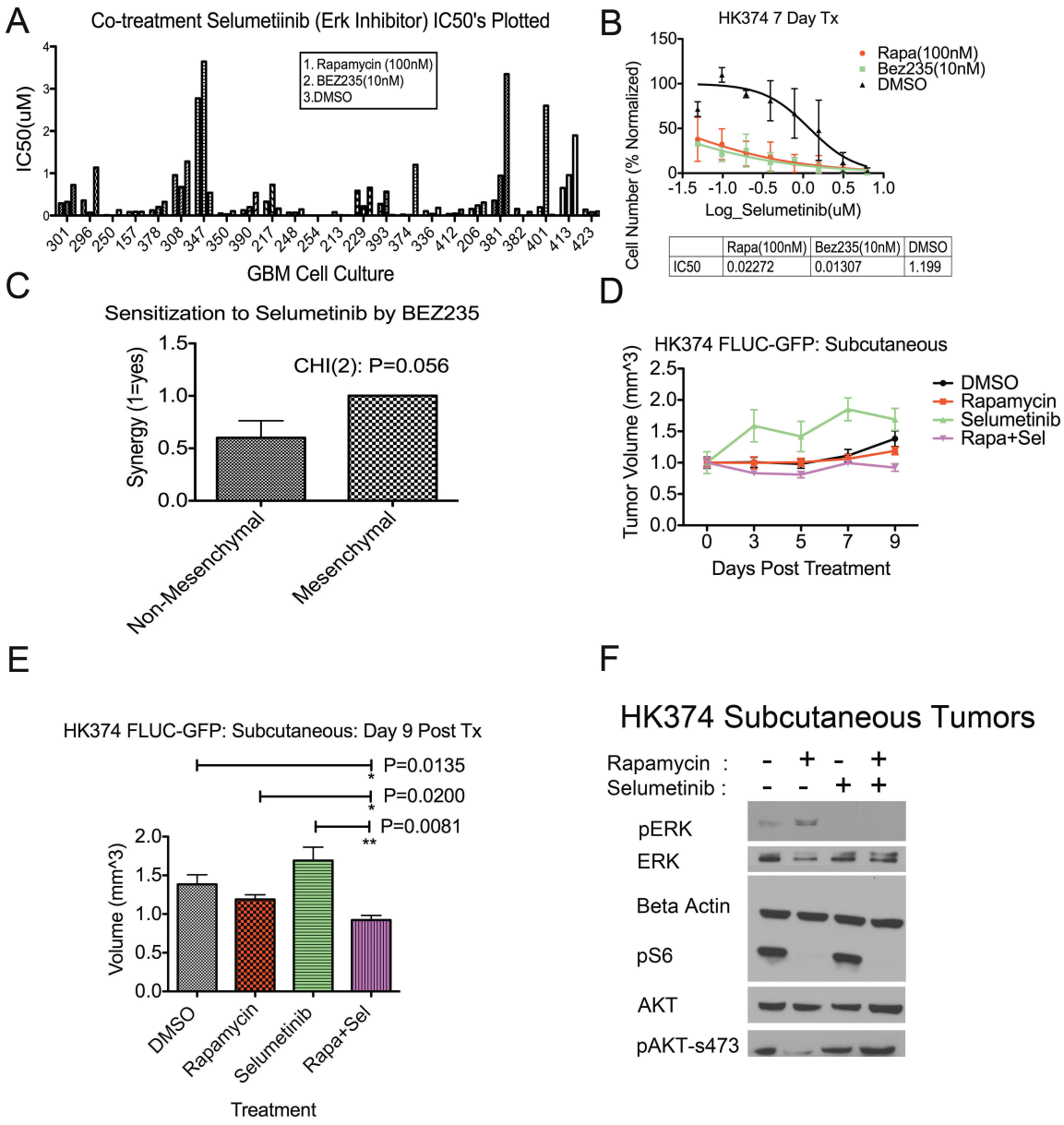
A
Co-treatment Selumetiinib (Erk Inhibitor) IC50's Plotted
1. Rapamycin (100nM)
2. BEZ235(10nM)
3.DMSO
IC50(uM)
301 296 250 157 378 308 347 350 390 217 248 254 213 229 393 374 336 412 206 381 382 401 413 423
GBM Cell Culture
B
HK374 7 Day Tx
Rapa(100nM)
Bez235(10nM)
DMSO
Cell Number (% Normalized)
Log_Selumetinib(uM)
Rapa(100nM) Bez235(10nM) DMSO
IC50 0.02272 0.01307 1.199
C
Sensitization to Selumetinib by BEZ235
CHI(2): P=0.056
Synergy (1=yes)
Non-Mesenchymal
Mesenchymal
D
HK374 FLUC-GFP: Subcutaneous
DMSO
Rapamycin
Selumetinib
Rapa+Sel
Tumor Volume (mm^3)
Days Post Treatment
E
HK374 FLUC-GFP: Subcutaneous: Day 9 Post Tx
P=0.0135
P=0.0200
P=0.0081
Volume (mm^3)
DMSO
Rapamycin
Selumetinib
Rapa+Sel
Treatment
F
HK374 Subcutaneous Tumors
Rapamycin : - + - +
Selumetinib : - - + +
pERK
ERK
Beta Actin
pS6
AKT
pAKT-s473

Figure 19

Figure 19. Combinatorial treatment with Selumetinib and either Rapamycin of BEZ235 produces a sensitization effect in a majority of GBM cultures. A. IC50s(uM) of Selumetinib calculated after one week treatment with either DMSO, Rapamycin (100nM), or BEZ235 (10nM). For each GBM tumorsphere culture listed, the results are graphed in the order: 1.DMSO 2.Rapamycin 3. BEZ235. B. Representative sample of sensitization effect on HK374. Log scale of a titration of doses of Selumetinib (uM) in the presence of DMSO (black line), 100nM Rapamycin (red line) or 10nM BEZ235 (green line). The relative cell number was estimated using Acumen plated reader and total fluorescence of Hoechst nuclear staining (see Methods). The calculated IC50 values are displayed for each combinatorial treatment (Selumetinib + second inhibitor listed). C. Sensitization to Selumetinib by BEZ235 is trending towards an association with the Mesenchymal clustering group. Mean +/- standard error of the mean is graphed as a bar graph for each clustering group. The Y-axis displays the fraction with sensitization (synergy) with 1=Yes sensitization ("Synergy") and 0=No sensitization. Sensitization was assessed using a statistical comparison of the calculated IC50 values ($P<0.05$ = significant). The Chi2 test results are displayed below with P-value ($P=0.056$). D. In vivo, combinatorial therapy targeting mTOR (Rapamycin, 5mg/Kg) + ERK (Selumetinib, 35mg/Kg) improves treatment response. Subcutaneous xenografts of human HK374 tumors into the flanks of mice were measured using calipers over 9 days of treatment that initiated 12 days after tumors were implanted and allowed to develop. Tumor volume is indicated on the Y-axis and treatment groups are color coded. E. Combinatorial treatment of Selumetinib + Rapamycin improves treatment response beyond single therapies. Quantification of in vivo tumor formation at Day 7. Treatment groups (mean +/- std. error

of the mean) are compared to the DMSO treated control. P-values for the Mann-Whitney statistical comparison test are indicated for each comparison. ANOVA comparing all groups had P=0.0010. F. Western blot depicts effective targeting of Rapamycin and Selumetinib after 9 days of treatment. Western blot of pooled xenograft tumors depicts down regulated pS6, downstream of mTORc1, after Rapamycin treatment (inhibition of mTORc1), and down regulated pERK1/2, downstream of MEK, after Selumetinib treatment (inhibition of MEK). Beta Actin serves as a loading control.

Summary Table of Sensitization Effect for Rapamycin or BEZ235 on Selumetinib Response

	Selumetinib IC50 in the Presence of:						
Tumorsphere ID	Rapamycin(100nM)	BEZ235(10nM)	DMSO	Sensitization with Rapa	P Value	Sensitization with BEZ235	P Value
157	0.0797	0.0860	0.0842	No	0.866	No	0.960
206	0.155	0.238	0.307	Yes	0.0499	No	0.329
213	0.0774	0.00970	0.00440	?	?	No	0.625
217	0.329	0.729	0.165	No	0.752	Yes	0.0273
229	0.585	0.217	0.657	No	0.637	Yes	0.0019
248	0.0697	0.0697	0.146	Yes	0.025	Yes	0.0451
250	0.00727	0.00284	0.125	Yes	<0.0001	?	?
254	0.00000197		0.000595	No	0.479	Yes	0.0003
296	0.356	0.0689	1.136	Yes	0.0002	Yes	0.0134
301	0.287	0.321	0.721	No	0.158	Yes	0.0009
308	0.954	0.675	1.28	No	0.155	Yes	0.0151
336	0.103	0.0375	0.181	Yes	0.001	Yes	0.0009
347	2.771	3.642	0.5397	Yes	0.0017	Yes	0.0002
350	0.0443	0.0248	0.0998	No	0.593	?	?
374	0.0227	0.0131	1.20	Yes	<0.0001	Yes	<0.0001
378	0.121	0.200	0.322	Yes	0.0033	No	0.139
381	0.352	0.941	3.345	Yes	<0.0001	Yes	0.0064
382	0.154		0.085	No	0.194	?	?
390	0.124	0.197	0.536	Yes	<0.0001	Yes	<0.0001
393	0.272	0.562	0.00863	Yes	<0.0001	?	?
401	0.194	2.60	0.0155	No	0.152	?	?
412	0.0360	0.0448	0.138	Yes	<0.0001	Yes	<0.0001
413	0.650	0.955	1.89	No	0.119	No	0.273
423	0.138	0.0789	0.0954	No	0.325	No	0.489

?= Calculated line did not cross IC50 or fitted line could not be calculated

Table 11. Tumorsphere cultures and their sensitization to MEK/ERK inhibitor, Selumetinib, by mTOR inhibitors Rapamycin or BEZ235. P-values are for the F-test comparison of the calculated IC50 values of each condition. $P<0.05$ was considered significant sensitization.

The list of genes associated with sensitization of Selumetinib by Rapamyin was too short (12 annotated genes) to perform a network analysis. *MAGEH1* (P=0.00021), *NR4A3* (P=0.00069), *IFIH1* (P=0.00077), and *TTF2* (P=0.00077) were the only categorized genes on this list.

WGCNA indicates that the "Pink" module is the most highly correlated module to sensitization of Selumetinib by BEZ235 (P<0.0001) (Figure 18). Ingenuity analysis of the genes in the "Pink" module reveals a list of canonical pathways associated with Bez235 induced sensitization to Selumetinib that includes activated NF-kB signaling, as well as 44 other canonical pathways.

The Mesenchymal cluster from unsupervised clustering trended more likely to respond with sensitization for Selumetinib by BEZ235 than the other, "Non-Mesenchymal", cluster (CHI2: P=0.056, Figure 19C).

In Vivo Combinatorial Therapy

In vivo GBM tumors exhibit enhanced response to combinatorial treatment. We chose to do combinatorial therapy of Selumetinib (35mg/Kg)+ Rapamycin (5mg/Kg) on in vivo subcutaneous xenografts of HK374 GBM cells expressing luciferase and GFP (HK374 GFP-FLUC). Subcutaneous xenografts were allowed to grow for 12 days and form tumors before treatment began. Figure 19E displays the caliper measurements of tumor size (mm^3) over days of treatment and depicts the enhanced response of tumors to combinatorial treatment. Figure 19F displays the quantification of tumors sizes (mm^3) at Day7 with mean values +/- standard error of the mean and P-values depicting a significant reduction in tumor size between combinatorial treated mice and single agent

treated mice or controls. Optical imaging of tumors at day 9 revealed a trend of lowest total intensity in the combinatorial treatment group (data not shown), however the variance was large between mice and the comparison was non significant ($P>0.05$). Bioluminescent imaging may not be optimal for discriminating small differences in subcutaneous tumor size because hypoxic conditions within the tumor mass may reduce bioluminescence imaging signal intensity (Khalil et al., 2013). Western blots of protein recovered from the tumors demonstrate that administered therapeutic treatments effectively inhibited their molecular targets. Rapamycin inhibited pS6 levels, downstream of mTORc1, the target of Rapamycin. Selumetinib inhibited pERK levels, downstream of MEK, the target of Selumetinib. Importantly, the western blot also depicts activation of pERK in the chronic Rapamycin group. Surprisingly, pAKT is downregulated in the chronic Rapamycin group and this suggests that chronic Rapamycin in HK301 cells inhibits mTORc2 as well as mTORc1. We performed the in vivo combinatorial treatment in a separate trial with a higher dose of Selumetinib (75mg/Kg) (Figure 20). With this higher dose of Selumetinib, we observed a greater effect on tumor response to combinatorial treatment, however several of the combinatorial treated mice expired at the 7^{th} day of treatment and therefore no optical imaging could be performed.

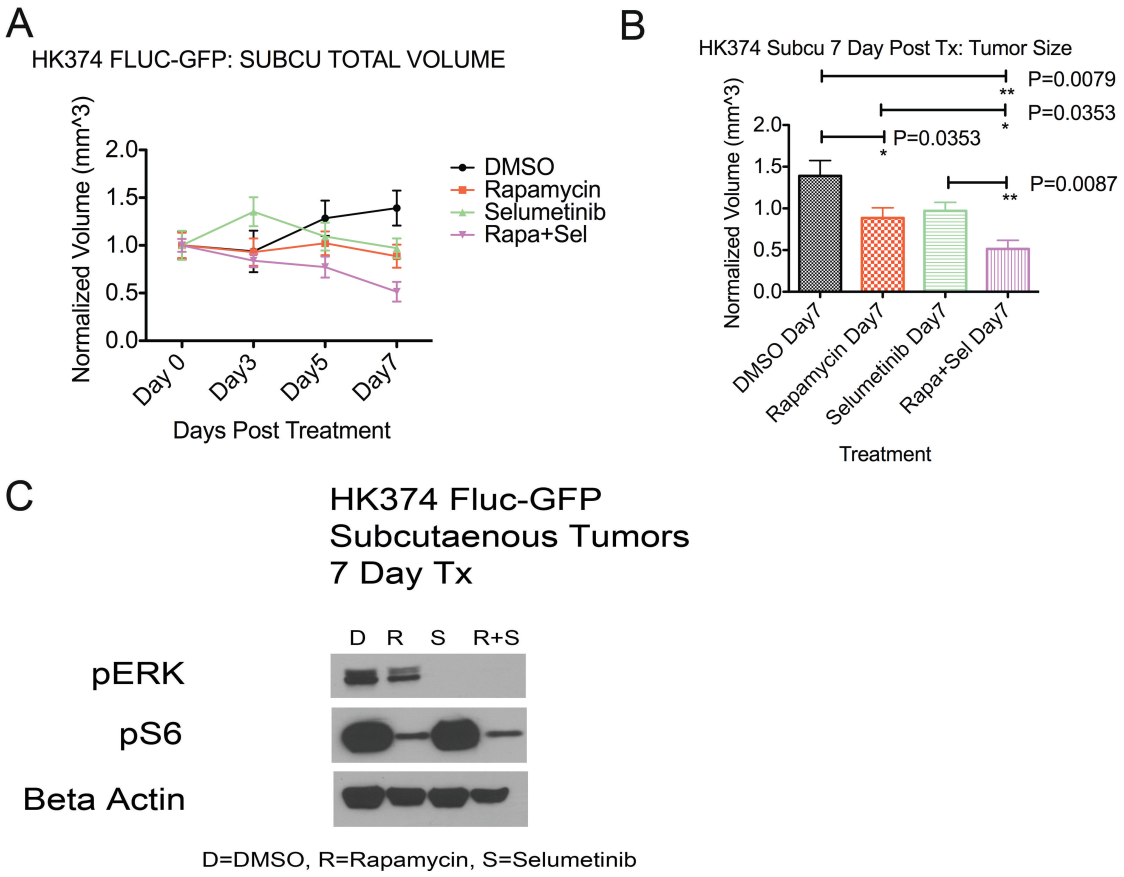
A
HK374 FLUC-GFP: SUBCU TOTAL VOLUME
Normalized Volume (mm^3)
2.0
1.5
1.0
0.5
0.0
Day 0
Day3
Day5
Day7
Days Post Treatment
DMSO
Rapamycin
Selumetinib
Rapa+Sel
B
HK374 Subcu 7 Day Post Tx: Tumor Size
P=0.0079
P=0.0353
P=0.0353
P=0.0087
Normalized Volume (mm^3)
DMSO Day7
Rapamycin Day7
Selumetinib Day7
Rapa+Sel Day7
Treatment
C
HK374 Fluc-GFP
Subcutaenous Tumors
7 Day Tx
D R S R+S
pERK
pS6
Beta Actin
D=DMSO, R=Rapamycin, S=Selumetinib

Figure 20

Figure 20. A. In vivo, combinatorial therapy targeting mTOR (Rapamycin, 5mg/Kg) + ERK (Selumetinib, 75 mg/Kg) improves treatment response. Subcutaneous xenografts of human HK374 tumors into the flanks of mice were measured using calipers over 7 days of treatment that initiated 14 days after tumors were implanted and allowed to develop. Tumor volume is indicated on the Y-axis and treatment groups are color coded. B. Combinatorial treatment of Selumetinib + Rapamycin improves treatment response beyond single therapies. Quantification of in vivo tumor formation at Day 7. Treatment groups (mean +/- std. error of the mean) are compared to the DMSO treated control. P-values for the Mann-Whitney statistical comparison test are indicated for each comparison. The comparison between Selumetinib treatment and DMSO was not significant (P=0.0673). C. Western blot depicts effective targeting of Rapamycin and Selumetinib after 10 days of treatment. Western blot of pooled xenograft tumors depicts down regulated pS6, downstream of mTORc1, after Rapamycin treatment (inhibition of mTORc1), and down regulated pERK1/2, downstream of MEK, after Selumetinib treatment (inhibition of MEK). Beta Actin served as a loading control.

Discussion

Our data was surprising in that each single therapeutic, targeting a unique node or nodes in the PI3Kinase pathway, had a specific pattern of differential responses across our panel of tumorsphere cultures. These results may be due to specific modes of resistance, or perhaps to the specific modes of inhibition.

One aim of this study was to assess GBM tumorspheres as a model for therapeutic testing. Classification of the tumorspheres into conventional TCGA groups or into 2 clusters by unsupervised clustering did not predict response to any of the tested PI3K pathway inhibitors. However, the Mesenchymal unsupervised cluster did trend to be most prone to sensitization of response to Selumetinib (ERKi) by BEZ235 (mTORi). This is interesting as both pERK and pS6K (downstream of mTOR) are activated in the Mesenchymal subgroup of TCGA classified tumors(Brennan et al., 2013).

We observed that Clathrin was the only molecular signaling pathway correlated to response for all PI3K pathway inhibitors. This may be due to the role of Clathrin pathway signaling in receptor endocytosis or, alternatively, to some other role of Clathrin. Further studies on Clathrin and drug response are warranted.

We determined that ERK signaling was the signaling pathway with the most profound and consistent association to mTOR inhibition. In addition, mTOR signaling was associated with response to MEK/ERK inhibition. This informed a course of combinatorial treatment that was effective in a majority of GBM tumorspheres.

ERK and mTORc1 have been shown to interact in GBM (Sunayama et al., 2010). Studies have demonstrated that combinatorial inhibition of mTOR and ERK results in impaired glioma cell proliferation that is more profound than inhibition of either target

alone(Paternot and Roger, 2009; Sunayama et al., 2010). However, it was previously unknown how pervasive this phenomena was among different patient derived GBM cultures. We discovered that sensitization to MEK/ERK inhibition by mTOR inhibition occurs in a majority of patient derived GBM tumorspheres. This indicates that this combinatorial treatment may be an effective treatment for most GBM.

Our in vivo study of combinatorial therapy with both Rapamycin and Selumetinib demonstrates that tumor size is reduced by combinatorial therapy significantly more so than by single agents alone. In vivo experiments utilizing either a higher dose (75mg/Kg) or a lower dose (35mg/Kg) of Selumetinib informs our conclusion that this combinatorial treatment requires a minimized dosage of Selumetinib which prevents toxicity yet still impairs its molecular target (MEK). To date, no published study on GBM has utilized in vivo administration of this combinatorial treatment. Previously, the only in vivo study of combinatorial ERK/mTOR inhibition performed on GBM had utilized pre-treated cells(Sunayama et al., 2010) and there are limitations to the inferences that can be drawn from in vivo studies utilizing pre-treated cells. Specifically, our method of administering treatment to the growing tumor is more clinically relevant than tests done on pre-treated cells that are then used to form tumors.

Data from western blots performed on the treated tumors support the hypothesis that activated ERK (pERK) is an adaptive mechanism of resistance to chronic mTOR inhibition. mTOR inhibition has previously been demonstrated in vitro to induce activated ERK signaling through phosphorylation of ERK (Albert et al., 2009). However, to date, this is the first published in vivo evidence that GBM xenograft tumors exhibit activated ERK signaling in response to chronic mTOR inhibition. These results provide a

biochemical rational for the effectiveness of our combinatorial treatment. As pAKT is downregulated in the chronic Rapamycin group, this suggests that mTORc2 is inhibited and that activated AKT is not a primary mechanism of resistance to chronic mTOR inhibition in this model. Chronic Rapamycin has been shown to target mTORc2 in certain cell cultures(Sarbassov et al., 2006).

In conclusion, our results support the tumorsphere culture system as a model for therapeutic testing. Our interrogation of the tumorsphere model system informed the hypothesis that combinatorial targeting of mTOR and ERK is a therapeutic strategy that may be effective for a majority population of GBM patients.

Methods

Tumor collection: As previously described in Chapter 2.

RNA samples preparation: As previously described in Chapter 2.

TCGA classification: As previously described in Chapter 2.

WGCNA: As previously described in Chapter 2.

Outcomes:

Chronic Rapamycin Sphere Formation: Cells were plated at 50 cells/well of a 96 well plate in 100uL media. Cells were treated with 100nM Rapamycin or DMSO every week and allowed to grow and proliferate. After 21 days, spheres were counted under 4x microscopy. Sphere number was normalized to DMSO controls.

BEZ235: 5000 cells were plated in each well of a 96 well plate and treated with either DMSO or a serial dilution of BEZ235. 7 days later, cell number was assessed by relative fluorescence of Hoechst labeled cells as detected by the Acumen 3 plate reader (TTPLabtech). Relative IC50 values were generated using Prism software (GraphPad).

Erlotinib: 5000 cells were plated in each well of a 96 well plate and treated with either DMSO or a serial dilution of Erlotinib. 7 days later, cell number was assessed by relative fluorescence of Hoechst labeled cells as detected by the Acumen 3 plate reader (TTPLabtech). Relative IC50 values were generated using Prism software (GraphPad).

Selumetinib: 5000 cells were plated in each well of a 96 well plate and treated with either DMSO or a serial dilution of Selumetinib. 7 days later, cell number was assessed by relative fluorescence of Hoechst labeled cells as detected by the Acumen 3 plate reader (TTPLabtech). Relative IC50 values were generated using Prism software (GraphPad).

Sensitization Selumetinib+Rapamycin or BEZ235: 5000 cells were plated in each well of a 96 well plate and treated with a serial dilution of Selumetinib with either DMSO, 100nM Rapamycin, or 10nM BEZ235. After 7 days cell number was assessed by relative fluorescence of Hoechst labeled cells as detected by the Acumen 3 plate reader (TTPLabtech). Relative IC50 values were generated using Prism software (GraphPad).

Acute Rapamycin: 5000 cells were plated in each well of a 96 well plate and treated with either 1nM, 10nM, 100nM or 1uM Rapamycin or DMSO. After 7 days cell number was assessed by relative fluorescence of cyto-9 labeled cells (which labels DNA and RNA) as detected by the Acumen 3 plate reader (TTPLabtech). Relative survival at each dose of Rapamycin treatment was calculated.

FLUC-GFP: Fluc=Firefely luciferase, GFP=green fluorescent protein from Auquorea (jellyfish). Fluc-GFP (backbone= pRRL-sinCMV-iresGFP) was produced by UCLA Vectorcore and supported by Molecular Technologies Core (IMTC) CURE/P30 DK41301-26.

Optical Imaging:

Optical imaging was performed at the Crump Institute for Molecular Imaging at UCLA. Mice were anesthetized by inhalation of isoflurane. Intraperitoneal injection of 100uL of d-luciferin (30mg/ml) was followed by 10 minutes of live uptake to interact with the luciferase expressing HK374 FLUC-GFP cells and produce bioluminescence. The IVIS Lumina 2 imaging system (Caliper life sciences) was utilized for in vivo bioluminescent imaging. A photograph of the mice is overlaid with a color scale of a region of interest representing total flux (photon/second) and quantified with the LivingImage software package (Xenogen Corporation, Alameda, Calif.).

In Vivo Subcutaneous Xenotransplantation: $1X10^6$ of HK374 FLUC-GFP GBM cells (constitutively expressing a construct of luciferase (FLUC) and green fluorescence protein (GFP)) were injected into both flanks of 24, male, 2 month old, nod scid, gamma null mice. After 12days, mice underwent optical imaging to assess tumor size. Daily intraperitoneal injection treatment in one of 4 groups was initiated after 14 days of tumor proliferation: Group1: DMSO, Group2: 5mg/Kg Rapamycin, Group3: 35mg/Kg Selumetinib, Group4: Rapamycin (5mg/Kg) + Selumetinib (35mg/Kg). Each treatment was delivered in DMSO as a vehicle + 12.5% carbowax (PEG 400)(Fisher Scientific) in a final volume of 100uL. Rapamycin was from LC Laboratories (#R-5000). Selumetinib was from Selleckchem (#S1008). Tumors were measured with calipers every 2 days. Bioluminescent imaging of the tumors was carried out after 9 days of treatment. Tumors were collected, weighed, and then lysed in Ripa buffer with phosphatase and protease

inhibitors, and homogenized with a mechanical tissue homogenizer (Brinkman Polytron PT3000 (Kinematica AG)). This in vivo study was performed in the same manner in a separate trial but with 75mg/Kg Selumetinib, and treatment was initiated after 14 days of tumor growth.

Tumor Volume Measurements: The tumor volume was calculated for the volume of a sphere with the formula Volume=4/3*3.1415*(Diameter/2)^3. The mean diameter of the tumors for each mouse was utilized.

Western blots: Protein from subcutaneous tumors was collected and pooled by treatment category. Protein concentration was determined by Bradford assay. Protein was boiled in an equal volume of Laemmli Sample Buffer (Bio-Rad #161-0737) with 5% beta mercaptoethanol for five minutes. Western blots were carried out to validate inhibition of therapeutic targets with Beta Actin(ABCAM #8277) as a loading control, pS6 (Cell Signaling # 5364S) as a downstream target of mTOR inhibition (Rapamycin), and pERK1/2 (Cell Signaling #9101S) as a downstream target of MEK inhibition (Selumetinib).

Gene trait correlations: As previously described in Chapter 2.

Clustering: As previously described in Chapter 2.

Microarray methods: As previously described in Chapter 2.

*EGFR*V3 determination: As previously described in Chapter 2.

PTEN deletion: *PTEN* deletion was determined by western blot of tumorsphere samples using antibody #9559S, Cell Signaling.

Statistics: For comparison of small groups we used a cutoff of $P<0.05$ to distinguish significant differences. For gene by gene correlations to drug response we used a cutoff for significance of $P<0.001$ to account for multiple comparisons. Statistics were done in GraphPad Prism software (http://www.graphpad.com/scientific-software/prism/). For comparisons of TCGA class and drug response we performed an ANOVA test. For comparisons of drug response and recurrence and for drug response and mutations (Figure 14, 17) we used the non-parametric Mann-Whitney test. To detect correlations between different drug responses, we performed linear regression analysis using STATA 8.0 software (Statcorp). To compare IC50 values (Figure 19b, table 11) we used GraphPad Prism software to perform an F-test comparison of calculated IC50 values, with $P<0.05$ considered significant. For comparison of binomial variables we used CHI(2) test using STATA (Figure 19 C, D).

Chapter 4

Phosphorylation Dependent Attenuation of GSK3B is an Adaptive Mechanism that Confers Resistance to Chronic mTOR Inhibition through MAP1B

Aim 3: To determine the molecular mechanism of resistance to chronic mTOR inhibition.

Abstract

Glioblastoma multiforme (GBM) is the highest grade, most lethal, and most common form of Glioma. Novel therapies are needed for the effective treatment of this malignancy. The mammalian target of Rapamycin (mTOR) pathway is a major regulator of cell proliferation that is frequently upregulated in GBM and as such has garnered considerable attention as a therapeutic target. mTOR pathway specific inhibition via Rapamycin or NVP-BEZ235 has potential as a therapeutic approach for the treatment of GBM, but like many cancer therapies, resistance to chronic treatment is an issue. We sought to determine the molecular mode of resistance that results from chronic mTOR pathway specific inhibition in order to understand the cellular mechanism of adaptation. In order to decipher the mechanism of cellular resistance to chronic mTOR inhibition, we employed a serial screening approach that combined a phosphoproteomics screen

followed by a targeted shRNA screen. First, we performed a phosphoproteomics analysis using iTRAQ of chronic Rapamycin treated primary GBM cell cultures. We analyzed the list of significantly altered phosphopeptides with Kinase Enrichment Analysis (KEA) and discovered that GSK3B was significantly associated with observed changes in phosphorylation due to chronic Rapamycin treatment. Utilizing western blots and in vitro cell growth assays, we discovered that, in response to chronic mTOR pathway specific inhibition, GSK3B undergoes inhibitory phosphorylation that confers resistance to both Rapamycin and NVP-BEZ235 in a variety of GBM primary cultures. Using shRNA, we depleted GSK3B and demonstrated that this confers resistance to mTOR pathway specific inhibition. We also used a pharmacological inhibitor of GSK3b and observed the same effect. Next, we performed a targeted shRNA screen on 50/52 candidates with altered phosphorylation in chronic Rapamycin that were associated with GSK3B. From this approach and further validation, we discovered that MAP1B mediates resistance to chronic mTOR inhibition. We depleted MAP1B using shRNA and discovered that this sensitized glioblastoma cells to chronic mTOR inhibition. Targeting this mechanism of molecular adaptation presents a novel therapeutic approach for the effective treatment of GBM.

Background

Representing 40% of all primary, malignant central nervous system tumors, glioblastoma multiforme (GBM) are the most common type of glioma, which is the most common type of malignant brain tumor (Miller and Perry, 2007). The current standard of treatment for GBM is surgical resection followed by a combination of radiotherapy and chemotherapy(Stupp et al., 2005). GBM have a median overall survival of approximately 1 year(Daumas-Duport et al., 1988) with a 5 year survival rate of less than 3%(Ohgaki and Kleihues, 2005). The poor prognosis of GBM necessitates continued efforts to discover and develop effective new treatment.

Rapamycin (rapa) is a mammalian target of Rapamycin (mTOR) pathway specific inhibitor(Bjornsti and Houghton, 2004; Brown et al., 1994; Chiu et al., 1994; Sabatini et al., 1994). mTOR is one downstream effector of the AKT pathway that, in a complex termed mTORC1, activates protein translation through phosphorylation of p70S6 (pS6) and 4EBP. mTORc1 also promotes transcription through Stat3(Yokogami et al., 2000) and inhibits autophagy through ATG13(Hosokawa et al., 2009). In mammals, there are two distinct TOR complexes, each with a TOR, several regulatory subunits, and a unique accessory protein that distinguishes and defines each complex: RAPTOR is specific to mTORc1 and RICTOR is specific to mTORc2(Shaw and Cantley, 2006; Zoncu et al., 2011). The targeting and effects of Rapamycin are primarily directed at mTORc1, however, mTORc2 assembly has been found, in certain cell cultures, to be impaired by chronic Rapamycin treatment (Sarbassov et al., 2006).

Rapamycin has been used in clinical trials for the treatment of glioma(Cloughesy et al., 2008). Half of the glioma patients treated with Rapamycin responded with reduced tumor cell proliferation that correlated with mTOR inhibition. However, many of the patients did not respond to treatment, did not show evidence of mTOR inhibition, and in fact, had elevated mortality associated with increased AKT activation. There are many feedback loops involved in mTOR signaling which makes it a complex therapeutic target(Carracedo et al., 2008; Efeyan and Sabatini, 2009). The increased AKT activation was possibly due to the feedback loop of S6Kinase (pS6K), a downstream target of mTOR, as inhibition of pS6K leads to upregulation of PI3K signaling that activates AKT. For a review of mTOR, see (Wullschleger et al., 2006; Zoncu et al., 2011).

Hosoi et al. reports that cancer cell resistance to Rapamycin varies between cell lines, is not dependent on the levels of mTOR inhibition, and correlates with Rapamycin's ability to induce c-MYC(Hosoi et al., 1998). Yet, other reports indicate that Rapamycin does not completely inhibit mTOR and this lack of complete mTOR inhibition may confer resistance(Thoreen et al., 2009; Thoreen and Sabatini, 2009). Recently, Wang et al. provide evidence that Rapamycin's inability to inhibit 4EBP1 and mTORc2 leads to resistance through insufficient gene regulation(Wang et al., 2011). Indeed, Rapamycin primarily prevents S6K activation and does not effectively inhibit 4EBP1 activation(Feldman et al., 2009), yet 4EBP1 activation and its regulation of cap dependent translation have been shown to be the primary oncogenic pathway in mTOR signaling(Hsieh et al., 2010). Another recent study has shown that Rapamycin induced activation of pERK and pAKT leads to BAD phosphorylation, degradation, and resistance(Liu et al., 2011). In fact, ERK activation is linked to resistance in yet another

report by Hoang et al.(Hoang et al., 2012). In addition, the gene *SKP2* has been linked to Rapamycin resistance(Totary-Jain et al., 2012). Another recent report indicates that histone de-acetylation is responsible for resistance in renal cell carcinoma cells(Juengel et al., 2012). Reports from the clinical trial of Rapamycin in glioma argue that resistance is not cell intrinsic but perhaps due to bioavailability of the agent(Akhavan et al., 2010; Cloughesy et al., 2008). While there are divergent views on the different possible modes of Rapamycin resistance, there has yet to be a comprehensive characterization of the mechanisms that modulate Rapamycin resistance within GBM cells.

We hypothesized that phosphorylation changes associated with a chronic Rapamycin resistant population would reveal candidate proteins involved in resistance. This reasoning was based on the knowledge that phosphorylation changes are key modulators of cell signaling pathways essential to cell proliferation and survival. Here we utilize an unbiased approach to detect genes involved in resistance to mTOR pathway specific inhibition. Utilizing iTRAQ and a phosphoproteomics analysis of specific post-translational modifications associated with chronic Rapamycin treatment in primary GBM cultures we generated a list of proteins that undergo changes in phosphorylation state after chronic Rapamycin treatment. This list was analyzed by Kinase Enrichment Analysis (KEA) to generate a list of kinases significantly associated with our phosphorylated protein list. GSK3B was second among the top kinases from this analysis. Further testing demonstrated that GSK3B inhibition is an adaptive mechanism of resistance to chronic mTOR inhibition. After a targeted shRNA screen against proteins that underwent phosphorylation changes and were associated with GSK3B, we discovered that MAP1B mediates this resistance.

Results

Chronic Rapamycin Treatment produces an enhanced malignant phenotype in certain glioblastoma cultures. We performed removal assays where glioblastoma cultures were chronically pre-treated in Rapamycin for at least 10 days and then cells were removed from treatment and grown in vitro at clonal density under regular tumorsphere conditions or else they are grown in vivo after intracranial xenotransplantation into mice. These removal experiments demonstrate that chronic Rapamycin treatment results in larger diameter spheres (Figure 1A, Rapa-DMSO) as well a higher percentage of sphere formation (Figure 1B). These chronically treated cells form larger spheres after returning from Rapamycin into further Rapamycin ($P<0.001$), thus displaying Rapamycin resistance (Figure 1A). Moreover, the Rapamycin resistant cells form tumors that are approximately twice as large as the tumors formed by control, DMSO treated cells (Figure 1C,D). These data indicate chronic Rapamycin treatment results in resistance to Rapamycin and an enhanced malignant phenotype. Furthermore, these results suggest that further study of chronic Rapamycin treatment may lead to fundamental insights into the molecular signaling of brain tumor stem cells as they are the cells responsible for tumor formation.

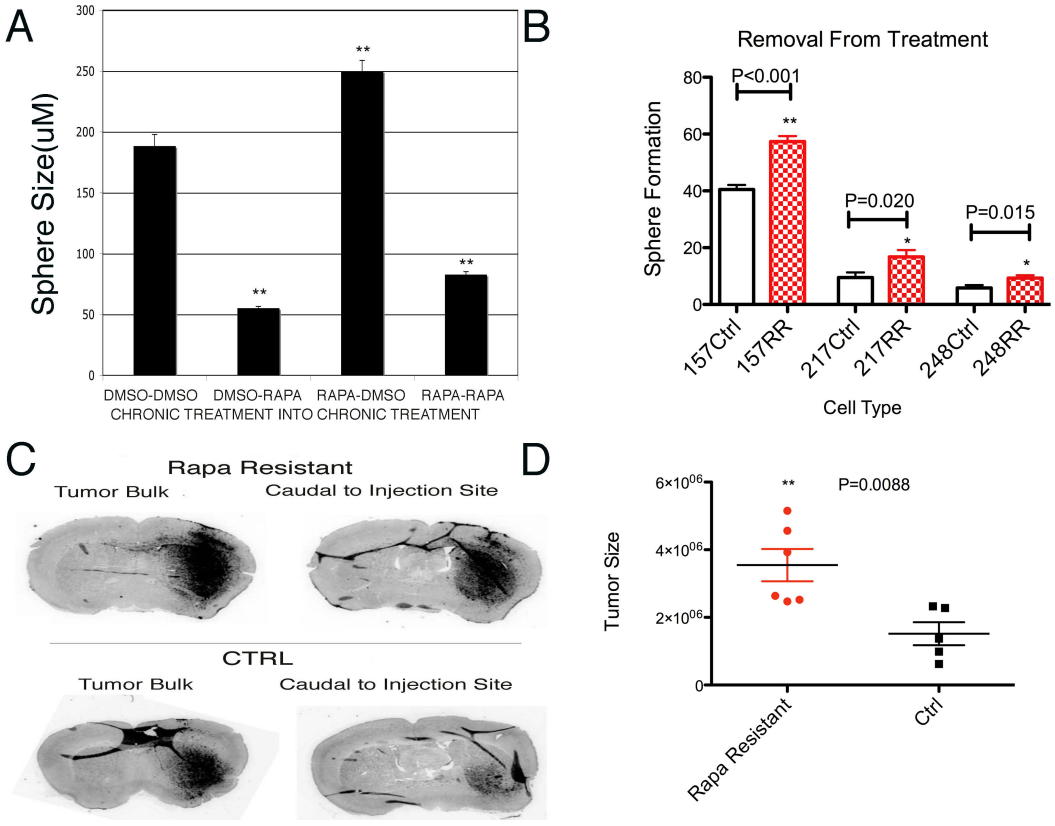
A
Sphere Size(uM)
300
250
200
150
100
50
0
**
**
**
DMSO-DMSO
DMSO-RAPA
RAPA-DMSO
RAPA-RAPA
CHRONIC TREATMENT INTO CHRONIC TREATMENT
B
Removal From Treatment
Sphere Formation
80
60
40
20
0
P<0.001
P=0.020
P=0.015
157Ctrl
157RR
217Ctrl
217RR
248Ctrl
248RR
Cell Type
C
Rapa Resistant
Tumor Bulk
Caudal to Injection Site
CTRL
Tumor Bulk
Caudal to Injection Site
D
Tumor Size
6×10^06
4×10^06
2×10^06
0
**
P=0.0088
Rapa Resistant
Ctrl

Figure 21

Figure 21: Removal assay of Chronic Rapamycin treatment. A. Sphere diameter (uM) +/- standard error of spheres grown in clonal density (less than 50 cells/100uL/well). The first drug listed in the legend is pre-treatment and the second drug listed is the removal condition. DMSO-DMSO is the control, DMSO condition removed into a control, DMSO condition; DMSO-Rapa is the DMSO (untreated) placed into 100nM Rapamycin; Rapa-DMSO is pre-treated for 10-14 days in Rapamycin then removed into DMSO/untreated conditions; Rapa-Rapa is pre-treatment with 100nM Rapamycin and then placed again into 100nM Rapamycin. There is enhanced sphere size indicating a rebound effect after pre-treatment with Rapamycin into removal DMSO conditions (Rapa-DMSO) as compared to the control (DMSO-DMSO) ($P<0.001$). There is also enhanced sphere size indicating resistance to Rapamycin after pretreatment with Rapamycin and placed into further Rapamycin (Rapa-Rapa) as compared to the DMSO-Rapa which is pre-treated with DMSO and then placed in Rapamycin($P<0.001$). B. 3 different glioblastoma cell cultures display enhanced sphere formation capacity in removal conditions. Sphere forming capacity +/- standard error is represented. "RR" indicates pre-treatment of cells with 100nM Rapamycin for 10-14 days. Cells are then seeded at clonal density (50 cells/100uL/well) and grown in the absence of Rapamycin. All 3 cell cultures demonstrate a rebound effect wherein there is enhanced sphere formation capacity after pre-treatment with Rapamycin. C. Sections of mouse brain demonstrate enhanced malignancy of Rapamycin resistant cell cultures in vivo. 100 thousand cells were xenotransplanted intracranially into mouse striatum. Cells were pre-treated for approximately 30 days with either Rapamycin (100nM) or DMSO and then equal numbers of live cells were counted on a hematocytometer using trypan blue

exclusion. D. Quantification of tumor size demonstrates an approximate two-fold increase in tumor size for Rapamycin resistant cells (cells pre-treated with Rapamycin) as compared to untreated controls. Quantification was done using Typhoon imaging of GFP labeled glioblastoma cells and Image-quant software.

iTRAQ Phosphoprotemics array of acute (4 hour) and chronic (42 Day) Rapamycin treated glioblastoma cultures as compared to DMSO treated controls reveals distinct phosphorylation events in chronic Rapamycin conditions as compared to acute Rapamycin treatment. We performed an iTRAQ phsophoproteomics array on HK296 glioblastoma cell culture. We quantified 4408 unique phosphopeptides from 1732 proteins. There were 578 peptides in Acute and 798 peptides in Chronic conditions that had a greater than 2 fold change in phosphorylation. Our heat map displays that there are certain proteins that were phosphorylated in both Acute and Chronic Rapamycin but other proteins that had inverse changes in Acute as compared to Chronic Rapamycin (Figure 22A). We applied stringent criteria to determine which phosphorylation events were to be considered promising candidates. These stringent criteria included several spectra for each phosphopeptide, no discrepancies between overlapping phosphopeptides, and a small standard deviation. We distinguished 425 proteins that adhered to our stringent criteria and were determined to have significant phosphorylation changes after chronic Rapamycin treatment. We validated two of these phosphorylation changes via western blot: 4EBP1-t37,46 that decreased twofold in phosphorylation after chronic Rapamycin and pRB1-s249 that increased twofold in phosphorylation (Figure 22B). These data indicate that chronic Rapamycin treated glioblastoma cells undergo certain phosphorylation changes that are distinct from the acute response to Rapamycin treatment. This supports the idea that phosphorylation changes under chronic Rapamycin treatment may signify key proteins that modulate resistance and play a fundamental role in brain tumor stem cells.

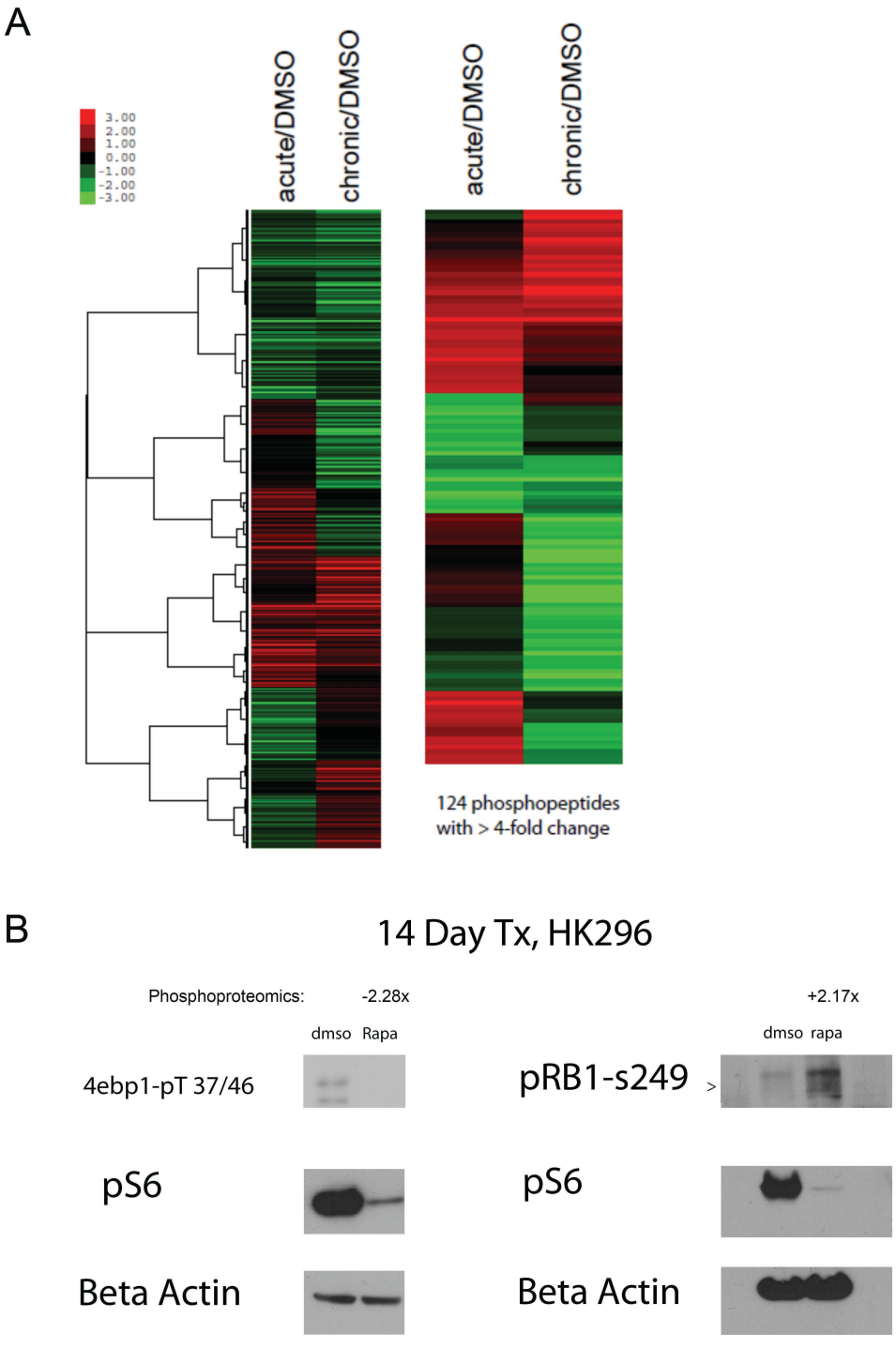
A
3.00
2.00
1.00
0.00
-1.00
-2.00
-3.00
acute/DMSO
chronic/DMSO
acute/DMSO
chronic/DMSO
124 phosphopeptides
with > 4-fold change
B
14 Day Tx, HK296
Phosphoproteomics:
-2.28x
+2.17x
dmso Rapa
dmso rapa
4ebp1-pT 37/46
pRB1-s249
pS6
pS6
Beta Actin
Beta Actin

Figure 22

Figure 22: Phosphoproteomics results and validation. A. Chronic Rapamycin treatment conditions (42 days, 100nM Rapamycin) harbor unique phosphorylation changes as compared to acute Rapamcyin treatment conditions (4 Hours, 100nM Rapamycin) in HK296 GBM cells. Heat map of the phosphoproteomics results comparing chronic Rapamcyin treatment or acute Rapamcyin treatment to DMSO treated controls. Relative levels of phosphopeptides, expressed as log2 of the ratios relatives to control (DMSO). B. Western blot validates 2/2 phosphoproteomics candidates tested. Phosphoproteomics line displays fold change in phosphorylation from the phosphoproteomics data; below the western blot shows validation of these changes after 14 days of chronic Rapamycin treatment (100nM). Western blot shows knockdown of mTOR by Rapamycin through its downstream target pS6. Beta Actin is the loading control.

Kinase Enrichment Analysis (KEA) of proteins that underwent significant phosphorylation changes in chronic Rapamycin conditions reveals that GSK3B is significantly associated with 52/425 of these phosphorylated proteins (P<0.001) (Table 12). GSK3B is second on the list of kinases significantly associated with our phosphoproteomics catalog of 425 proteins that underwent phosphorylation changes in chronic Rapamycin conditions. The first kinase on the list is CDC2 (P<0.0001). We targeted CDC2 with Roscovitine, a pharmacological inhibitor of CDC2 (kinase CDK1) but found no evidence for an alteration of response in the presence of 100nM Rapamycin (Figure 23). As GSK3B had a higher number of substrates than CDC2 and as it was next on our list of kinases associated with phosphorylation changes, therefore we decided to determine if GSK3B plays a role in resistance to Rapamycin.

List of kinases associated with phosphorylation changes under chronic rapamycin

Kinase	Substrates/Input	Substrates/Database	Fraction/Input	Fraction/Database	Difference	p-Value
CDC2	48	421	0.306	0.106	0.200	2.56E-11
GSK3B	52	501	0.331	0.126	0.205	7.40E-11
CDK2	44	398	0.280	0.100	0.180	5.86E-10
PRKCB1	33	254	0.210	0.0639	0.146	3.82E-09
RPS6KA3	36	330	0.229	0.0831	0.146	4.57E-08
MAPK14	38	377	0.242	0.0949	0.147	1.23E-07
PRKDC	20	200	0.127	0.0503	0.0770	0.000202
PRKACA	18	180	0.115	0.0453	0.0693	0.000428
PRKG1	12	93	0.0764	0.0234	0.0530	0.000544
AKT1	17	176	0.108	0.0443	0.0640	0.000895

Table 12. KEA analysis generated a list of kinases significantly (P<0.001) associated with the input list of genes that underwent significant phosphorylation changes under chronic Rapamycin conditions.

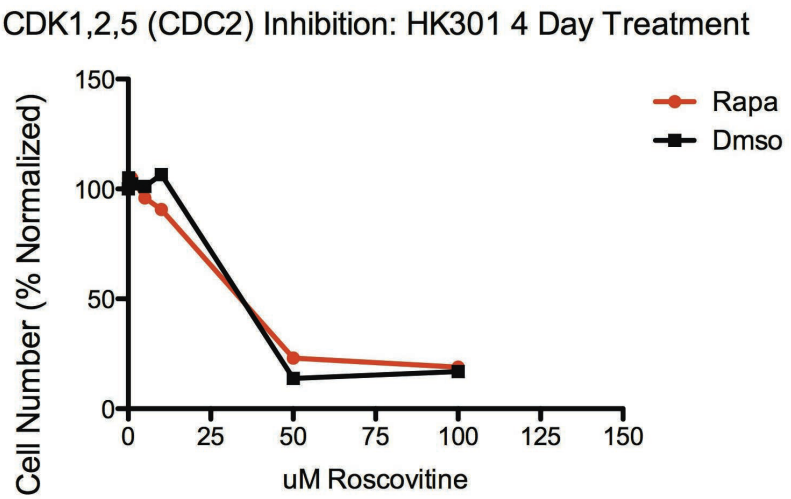

Figure 23: No evidence for role of CDC2 in mediating resistance to Rapamycin.

Normalized cell number estimated by Dojindo Kit8 for a titration of Roscovitine in the presence of 100nM Rapamycin or DMSO in HK301 glioblastoma cell culture (N=1).

GSK3B inhibition confers resistance to mTOR pathway specific inhibition. Combinatorial treatment of glioblastoma cultures with a titration of CHIR99021, a GSK3B inhibitor, and either Rapamycin or the mTORc1/mTORc2/PI3K inhibitor, NVP-BEZ235, confers resistance to GSK3B inhibition (Figure 24A, B). This was true in a variety of cell cultures tested (Figure 25). Combinatorial treatment of glioblastoma cultures with a titration of Rapamycin or NVP-BEZ235 in the presence of 1uM CHIR99021 confers resistance to Rapamycin (Figure 24C) and to NVP-BEZ235 (Figure 24D). This was true in a variety of cell cultures tested (Figure 26,27). A western blot of glioblastoma cultures after treatment with the inhibitor CHIR99021 displays that GSK3B is inhibited as its downstream target p4EBP1-t46 is diminished (upper band, Figure 24E).

GSK3B depletion via shRNA knockdown confers resistance to mTOR pathway specific inhibition. (Figure 28) Western blot displays that shRNA knockdown of GSK3B results in depletion of GSK3B (Figure 28). Depletion of GSK3B results in a dramatic increase in resistance to Rapamycin (Figure 28B) and to NVP-BEZ235 (Figure 28C). This was true in a variety of cell cultures tests (Figure 29). This data demonstrates that GSK3B modulates resistance to mTOR pathway specific inhibition.

Inhibitory phosphorylation of GSK3B is a cellular adaptive response associated with resistance to mTOR pathway specific inhibition. Western blots of GSK3B after a time course of Rapamycin treatment demonstrate that GSK3B becomes phosphorylated after chronic treatment (48 Hours) (Figure 30A). In addition, this inhibitory phosphorylation of GSK3B is persistent even after 14 days of Rapamycin treatment or NVP-BEZ235 treatment (Figure 30A).

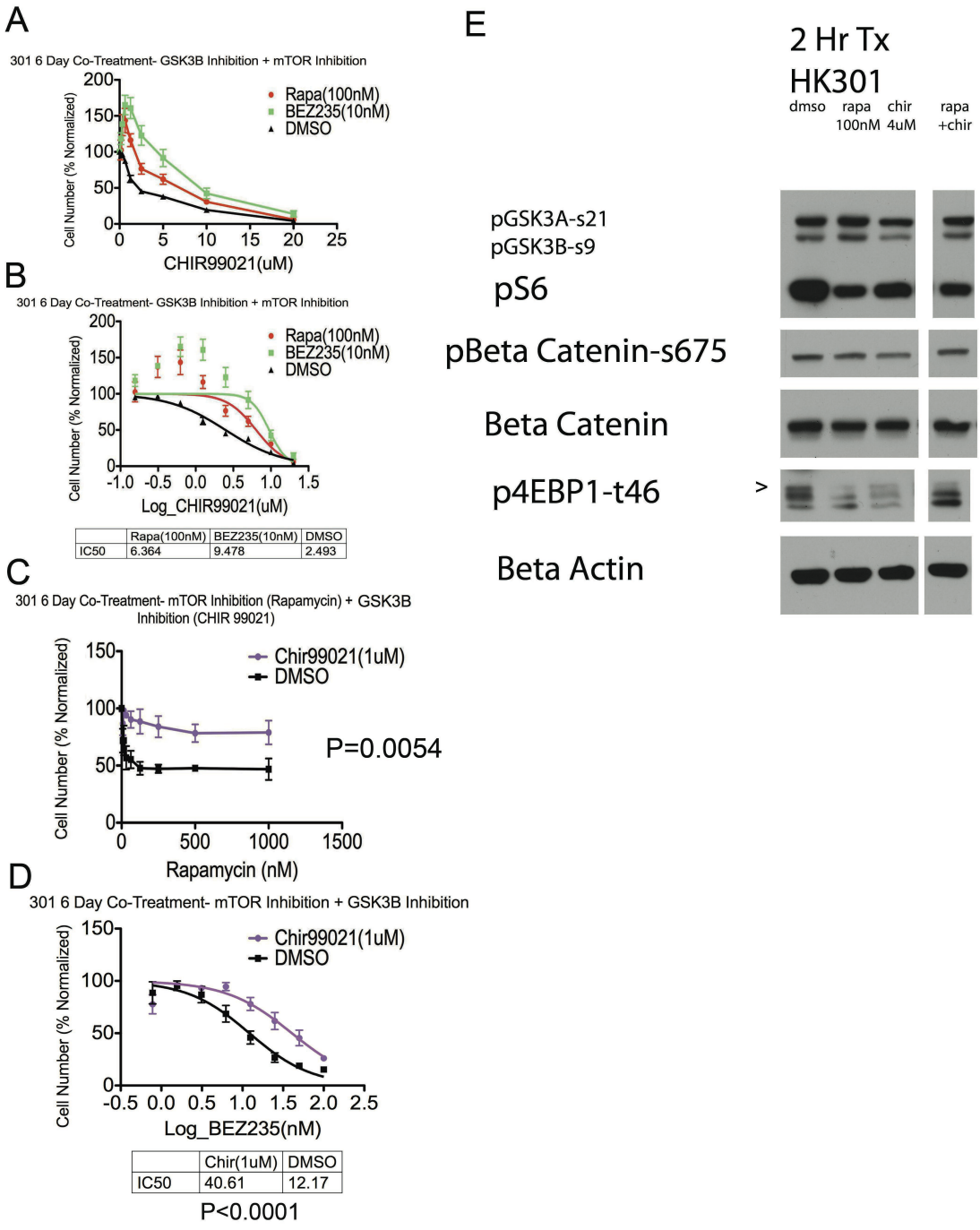
A
301 6 Day Co-Treatment- GSK3B Inhibition + mTOR Inhibition
Cell Number (% Normalized)
CHIR99021(uM)
Rapa(100nM)
BEZ235(10nM)
DMSO
B
301 6 Day Co-Treatment- GSK3B Inhibition + mTOR Inhibition
Cell Number (% Normalized)
Log_CHIR99021(uM)
Rapa(100nM)
BEZ235(10nM)
DMSO
Rapa(100nM) BEZ235(10nM) DMSO
IC50 6.364 9.478 2.493
C
301 6 Day Co-Treatment- mTOR Inhibition (Rapamycin) + GSK3B Inhibition (CHIR 99021)
Cell Number (% Normalized)
Rapamycin (nM)
Chir99021(1uM)
DMSO
P=0.0054
D
301 6 Day Co-Treatment- mTOR Inhibition + GSK3B Inhibition
Cell Number (% Normalized)
Log_BEZ235(nM)
Chir99021(1uM)
DMSO
Chir(1uM) DMSO
IC50 40.61 12.17
P<0.0001
E
2 Hr Tx
HK301
dmso rapa 100nM chir 4uM rapa +chir
pGSK3A-s21
pGSK3B-s9
pS6
pBeta Catenin-s675
Beta Catenin
p4EBP1-t46
Beta Actin

Figure 24

Figure 24. GSK3B inhibition confers resistance to mTOR pathway inhibition. A. Rapamycin or BEZ235 treated GBM cells undergo a growth advantage with co-treatment with the GSK3B inhibitor, CHIR99021. Dose response curve of HK301 GBM cell cultures to the GSK3B inhibitor CHIR99021 with co-treatment of Rapamycin (100nM), BEZ235 (10nM), or DMSO-Ctrl display an increase in proliferation with co-treatment above baseline (N=5), mean values and standard error bars. Live cell number was determined by Dojindo Kit 8, hydrogenase activity detection. Cell number is normalized to control wells and each condition control is set at 100%. B. Same as A except a fitted curve and estimated IC50's demonstrating an increase in resistance to mTOR inhibition under GSK3B inhibition. C. GSK3B inhibition confers resistance to Rapamycin. Dose response to a titration of Rapamycin with co-treatment of the GSK3B inhibitor CHIR99021 (1uM) (N=3). CHIR99021 treated sample fitted line does not converge and therefore IC50 values and comparison of lines cannot be carried out. However, a non-parametric Mann-Whitney test signifies that the conditions are significantly different (P=0.0054). D. Fitted line of log transformed values and calculated IC50's demonstrate that GSK3B inhibition confers resistance to BEZ235 (N=3). Dose response to a titration of BEZ235 with co-treatment of the GSK3B inhibitor CHIR99021 (1uM). P-value<0.0001 is depicted that compares IC50 values. E. Western blot demonstrates that GSK3B inhibitor CHIR99021 hits its target at 2hours of treatment. Western blot of HK301 cells after 2 hours treatment with DMSO, Rapamycin (100nM), CHIR99021 (4uM), or Rapamycin (100nM)+CHIR99021 (4uM). The top band of three bands in the p4EBP1 is the threonine-46 phosphorylation and it is reduced after 2 hours of treatment.

A

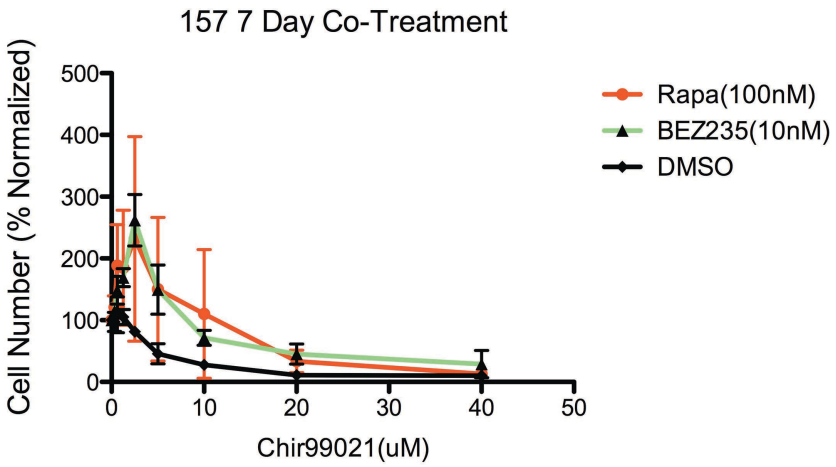
157 7 Day Co-Treatment
Cell Number (% Normalized)
500
400
300
200
100
0
0
10
20
30
40
50
Chir99021(uM)
Rapa(100nM)
BEZ235(10nM)
DMSO

B

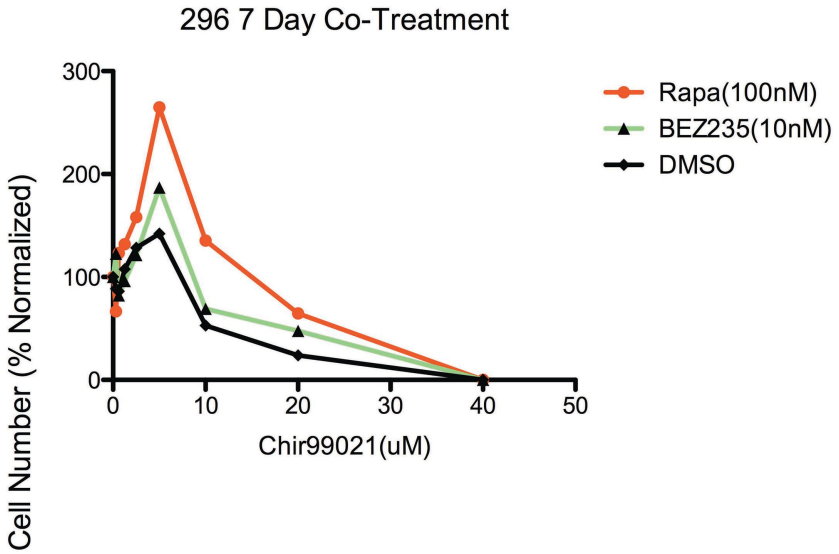
296 7 Day Co-Treatment
Cell Number (% Normalized)
300
200
100
0
0
10
20
30
40
50
Chir99021(uM)
Rapa(100nM)
BEZ235(10nM)
DMSO

Figure 25

Figure 25. Rapamycin or BEZ235 treatment increases resistance to GSK3B inhibition. A. Relative cell number with mean and standard error bars estimated by Dojindo Kit8 for a titration of CHIR99021, a GSK3B inhibitor, in HK157 glioblastoma cell culture (N=3). B. Relative cell number with mean and standard error bars estimated by Dojindo Kit8 for a titration of CHIR99021, a GSK3B inhibitor, in HK296 glioblastoma cell culture (N=1).

A

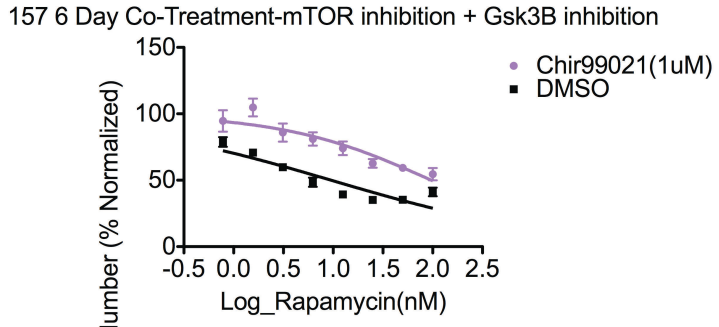

	Chir99021(1uM)	DMSO
IC50	96.92	9.538

P<0.0001

B

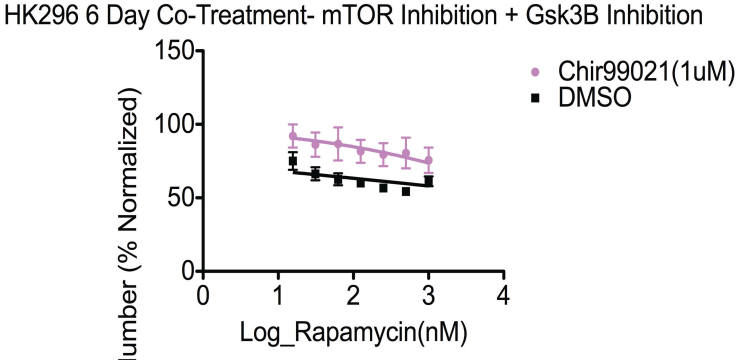

	Chir99021(1uM)	DMSO
IC50	95740	3469

P=0.3499

C

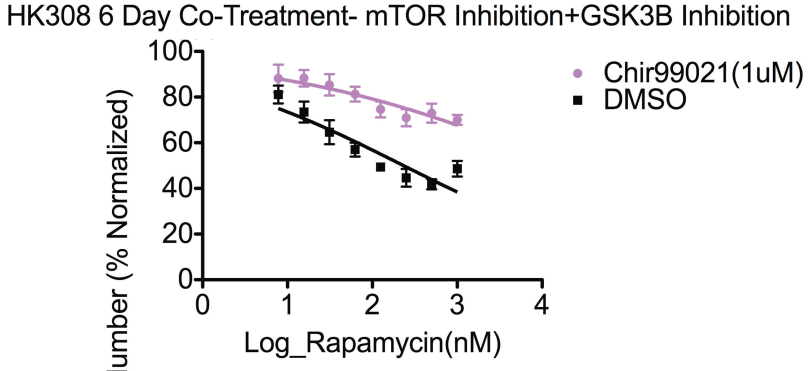

	Chir99021(1uM)	DMSO
IC50	17401	233.2

P<0.0001

Figure 26

Figure 26. Pharmacological inhibition of GSK3B confers resistance to Rapamycin treatment. Results in 3 different GBM cultures from 6 day co-treatment with a titration of the mTOR inhibitor Rapamycin and with GSK3B inhibitor, Chir99021 or DMSO-control. A. GSK3B inhibition confers resistance to Rapamycin in HK157. Dose response to a titration of Rapamycin in HK157 with co-treatment of the GSK3B inhibitor CHIR99021 (1uM), fitted line for non-linear regression, and standard error bars (N=3), log scale. Calculated IC50 values are displayed. P-value<0.0001 is depicted that compares the IC50 values. B. GSK3B inhibition does not confer resistance to Rapamycin in HK296 after 6 days. Dose response to a titration of Rapamycin in HK296 with co-treatment of the GSK3B inhibitor CHIR99021 (1uM), fitted line, mean values and standard error bars (N=3), log scale. P-value=0.3499 is depicted that compares IC50 values. C. GSK3B inhibition confers resistance to Rapamycin in HK308 cells. Dose response to a titration of Rapamycin in HK308 with co-treatment of the GSK3B inhibitor CHIR99021 (1uM), fitted line, mean values and standard error bars (N=3), log scale. P-value<0.0001 is depicted that compares IC50 values.

A

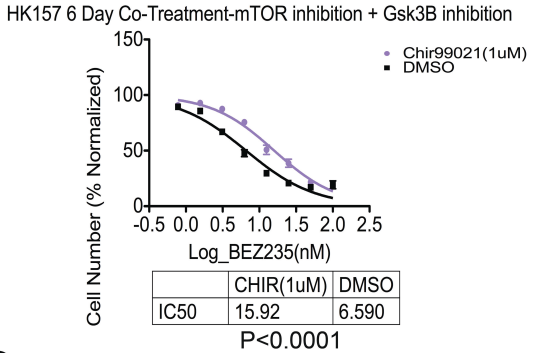

	CHIR(1uM)	DMSO
IC50	15.92	6.590

P<0.0001

B

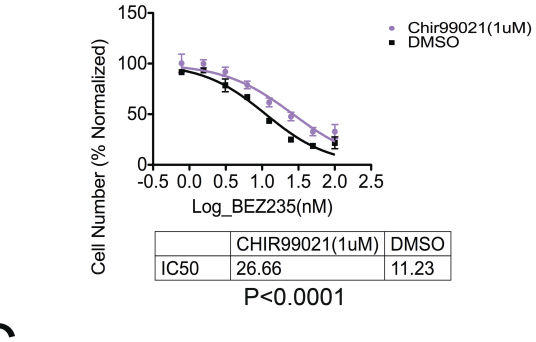

	CHIR99021(1uM)	DMSO
IC50	26.66	11.23

P<0.0001

C

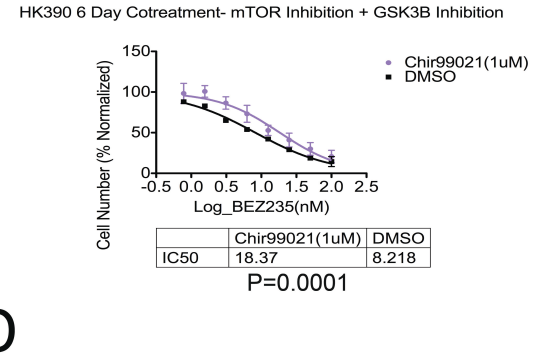

	Chir99021(1uM)	DMSO
IC50	18.37	8.218

P=0.0001

D

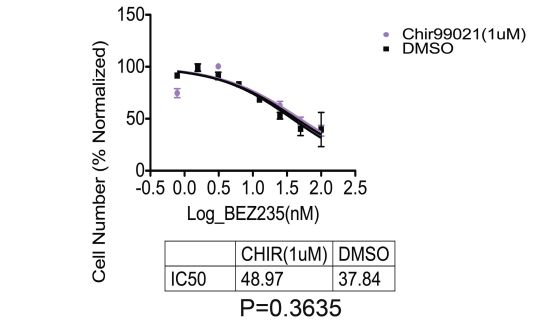

	CHIR(1uM)	DMSO
IC50	48.97	37.84

P=0.3635

Figure 27

Figure 27. Pharmacological inhibition of GSK3B confers resistance to NVP-BEZ235 treatment in multiple GBM cell cultures. A. GSK3B inhibition confers resistance to NVP-BEZ235. Dose response to a titration of BEZ235 in HK157 with co-treatment of the GSK3B inhibitor CHIR99021 (1uM), fitted line for non-linear regression, and standard error bars (N=3), log scale. Calculated IC50 values are displayed. P-value<0.0001 is depicted that compares IC50 values. B. GSK3B inhibition confers resistance to NVP-BEZ235. Dose response to a titration of BEZ235 in HK308 with co-treatment of the GSK3B inhibitor CHIR99021 (1uM), fitted line for non-linear regression, and standard error bars (N=3), log scale. Calculated IC50 values are displayed. P-value<0.0001 is depicted that compares IC50 values. C. GSK3B inhibition confers resistance to NVP-BEZ235. Dose response to a titration of BEZ235 in HK390 with co-treatment of the GSK3B inhibitor CHIR99021 (1uM), fitted line for non-linear regression, and standard error bars (N=3), log scale. Calculated IC50 values are displayed. P-value=0.0001 is depicted that compares IC50 values. D. GSK3B inhibition does not confer resistance to NVP-BEZ235 in HK296 cells after 6 days. Dose response to a titration of BEZ235 in HK296 with co-treatment of the GSK3B inhibitor CHIR99021 (1uM), fitted line for non-linear regression, and standard error bars (N=3), log scale. Calculated IC50 values are displayed. P-value=0.3635 is depicted that compares IC50 values.

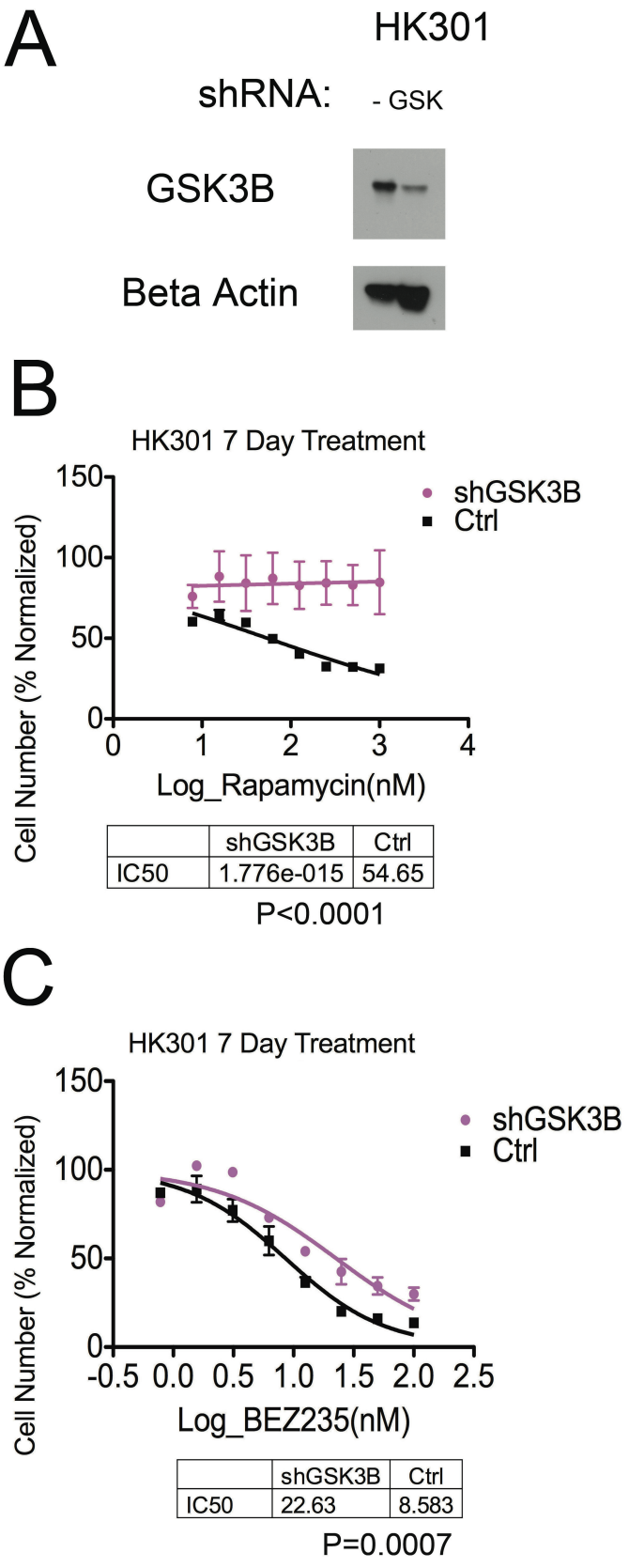
A
HK301
shRNA:
- GSK
GSK3B
Beta Actin
B
HK301 7 Day Treatment
shGSK3B
Ctrl
Cell Number (% Normalized)
150
100
50
0
0
1
2
3
4
Log_Rapamycin(nM)
shGSK3B
Ctrl
IC50
1.776e-015
54.65
P<0.0001
C
HK301 7 Day Treatment
shGSK3B
Ctrl
Cell Number (% Normalized)
150
100
50
0
-0.5
0.0
0.5
1.0
1.5
2.0
2.5
Log_BEZ235(nM)
shGSK3B
Ctrl
IC50
22.63
8.583
P=0.0007

Figure 28

Figure 28. shRNA knockdown of GSK3B confers resistance to mTOR inhibition while the constitutively active GSK3BCA may confer sensitivity. A. Western blot displays shGSK3B knockdown of GSK3B. B. Depletion of GSK3B confers resistance to mTOR pathway specific inhibition. Fitted curve of log transformed values for a titration of Rapamycin in HK301 GBM cells with calculated IC50 values below, with and without GSK3B knockdown (N=3). P-value<0.0001 is depicted that compares IC50 values. C. Fitted curve of log transformed values for a titration of BEZ235 in HK301 GBM cells with calculated IC50 values below, with and without GSK3B knockdown (N=3). P-value=0.0007 is depicted that compares IC50 values.

A

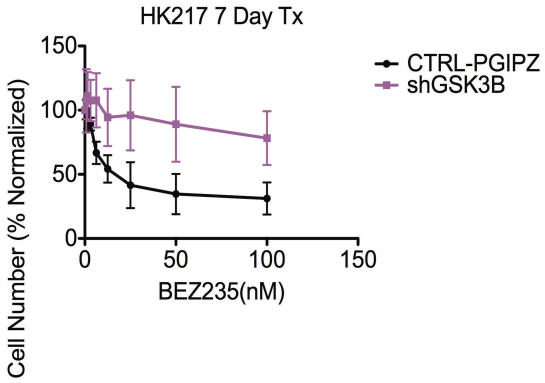

B

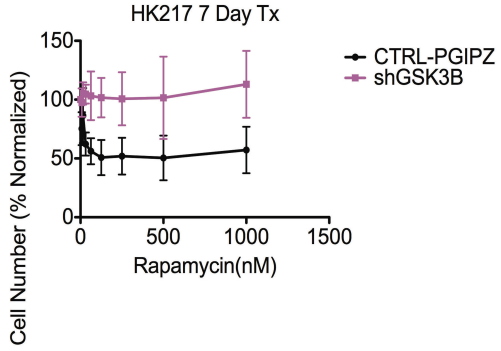

C

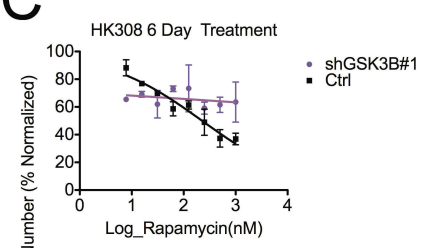

	shGSK3B#1	Ctrl
IC50	1.112e+008	226.6

P<0.0001

D

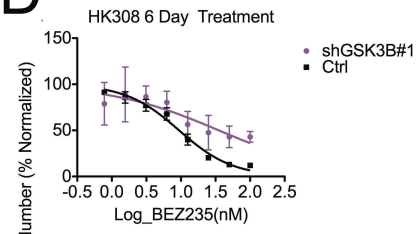

	shGSK3B#1	Ctrl
IC50	35.33	9.399

P<0.0001

Figure 29

Figure 29. Knockdown of GSK3B confers resistance to mTOR pathway specific inhibition. A. shRNA mediated GSK3B depletion confers resistance to Rapamycin. Dose response to a titration of Rapamycin in HK217 (Ctrl or shGSK3B), and standard error bars (N=3), fitted line and raw values. IC50 values could not be calculated because the line was not converged. B. shRNA mediated GSK3B depletion confers resistance to NVP-BEZ235. Dose response to a titration of BEZ235 in HK217, Ctrl or shGSK3B, fitted line for non-linear regression, and standard error bars (N=3), raw values. IC50 values could not be calculated because the line was ambiguous. C. shRNA mediated GSK3B depletion confers resistance to Rapamycin. Dose response to a titration of Rapamycin in HK308, Ctrl or shGSK3B, fitted line for non-linear regression, and standard error bars (N=2), log scale. Calculated IC50 values are displayed. The P-Value<0.0001 is depicted for the comparison between IC50 values. D. shRNA mediated GSK3B depletion confers resistance to NVP-BEZ235. Dose response to a titration of BEZ235 in HK308, Ctrl or shGSK3B, fitted line for non-linear regression, and standard error bars (N=2), log scale. Calculated IC50 values are displayed. The P-Value<0.0001 is depicted for the comparison between IC50 values.

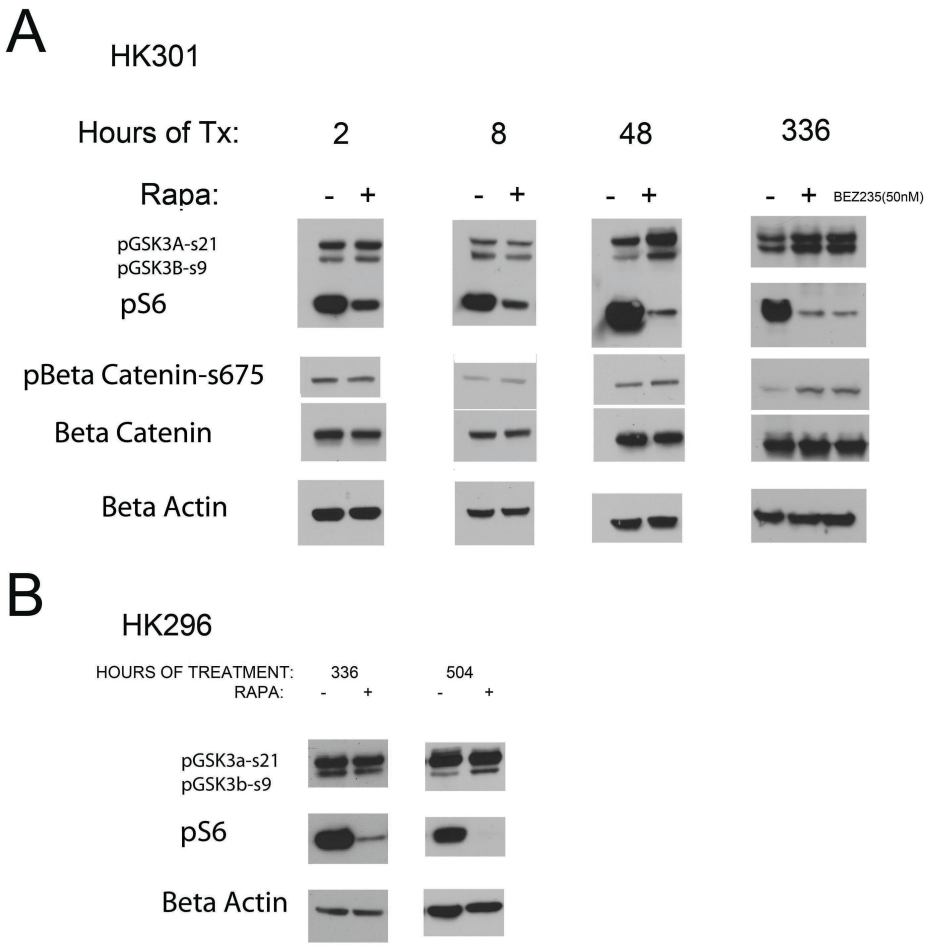
A
HK301
Hours of Tx: 2 8 48 336
Rapa: - + - + - + - + BEZ235(50nM)
pGSK3A-s21
pGSK3B-s9
pS6
pBeta Catenin-s675
Beta Catenin
Beta Actin
B
HK296
HOURS OF TREATMENT: 336 504
RAPA: - + - +
pGSK3a-s21
pGSK3b-s9
pS6
Beta Actin
C
Cell Growth Rapa Tx
% Fold Change -Cell Number (Normalized)
10000
5000
1000
900
800
700
600
500
400
300
200
100
0
0 5 10 15 20 25
Day
296 Rapamycin
296 DMSO

Figure 30

Figure 30. Inhibitory phosphorylation of GSK3B is an endogenous mechanism for adaptation and resistance to chronic mTOR inhibition. A. In HK301, GSK3B becomes phosphorylated at 48 hours of treatment with Rapamycin but not during acute treatment. Western blot of HK301 GBM cells under treatment with 100nM Rapamycin or DMSO for the indicated lengths of time. The last lane is the exception that was treated with BEZ235 (50nM) for 336 Hours, replenished every week. Beta Actin is the loading control, while GSK3B (un-phosphorylated) is the control for pGSK3B-s9). B. In, HK296, GSK3B becomes phosphorylation at 504 hours of treatment with Rapamycin but not at 336 hours. Western blot of HK296 GBM cells under treatment with 100nM Rapamycin or DMSO for the indicated lengths of time. Beta Actin is the loading control, while GSK3B (un-phosphorylated) is the control for pGSK3B-s9). C. Growth curves illustrate that GSK3B phosphorylation occurs at period of initiation of cell proliferation that signifies initiation of Rapamycin resistance. Graph illustrates the fold change of viable cells counted on the Countess automated cell counter for the indicated amount of time under 100nM Rapamycin or DMSO. The cell numbers are normalized to the original plating number that is set at 100% (dashed line).

Interestingly, HK296 only displays inhibitory phosphorylation of GSK3B after 21 days of chronic Rapamycin treatment and not after 14 days of treatment (Figure 30B). Significantly, this length of time is required for the HK296 cells to become resistant to Rapamycin treatment and to begin to proliferate (Figure 30C). Just as HK301 cells begin to proliferate at 48 hours after Rapamycin treatment (data not shown) when GSK3B becomes phosphorylated, HK296 cells become resistant when its GSK3B is phosphorylated at 21 days. These data indicate that inhibitory phosphorylation of GSK3B coincides with the moments when the cells become Rapamycin resistant and enter into a proliferative phase. Furthermore, as GSK3B phosphorylation precedes cellular proliferation, this indicates that phosphorylation of GSK3B is not the result of a selection process within a population of proliferating cells, but rather a cellular adaptive mechanism. Taken together, this data strongly suggests that inhibitory phosphorylation of GSK3B is an adaptive process that confers resistance to mTOR pathway specific inhibition.

Depletion of RICTOR or RAPTOR is capable of producing inhibitory phosphorylation of GSK3B. mTOR exists in two distinct complexes, mTORc1 and mTORc2(Zoncu et al., 2011). Each different complex possesses both shared and distinct proteins. For mTORc1 one distinct protein is RAPTOR, for mTORc2 one distinct protein is RICTOR. These distinct proteins are useful for targeting each complex. While Rapamycin is a known mTORc1 inhibitor, it has also been shown that chronic treatment with Rapamycin can inhibit mTORc2(Sarbassov et al., 2006). Therefore, we sought to determine which TOR complex was responsible for GSK3B phosphorylation. Western blots of 2 glioblastoma cultures, HK157 and HK301, display the phosphorylation of

GSK3B in response to RAPTOR and RICTOR knockdowns (Figure 31). Importantly, in HK157, both RAPTOR and RICTOR knockdowns result in inhibitory phosphorylation of GSK3B, with the RICTOR knockdown having a more dramatic effect on GSK3B phosphorylation. Both AKT (directly) and ERK (through p90-rsk1) are demonstrated to phosphorylate GSK3B(Cross et al., 1995; Saito et al., 1994; Stambolic and Woodgett, 1994). The fact that RICTOR knockdown results in GSK3B phosphorylation suggests that AKT is not the mediating kinase in this case as AKT is not activated by RICTOR knockdown mediated depletion of mTORc2 activity (Figure 31). Noteworthy is the activation of pERK in the RICTOR knockdown of GBM tumorsphere, HK157(Figure 31). These data indicate that ERK, presumably through p90-rsk1, may be the kinase mediating this interaction between depletion of mTORc2 and GSK3B phosphorylation. As ERK is not activated (via phosphorylation) in RAPTOR knockdown of HK301 (Figure 31), this suggests that ERK is not responsible for the GSK3B phosphorylation of these cells in response to RAPTOR knockdown mediated mTORc1 depletion. However, AKT is activated in the RAPTOR knockdown mediated depletion of mTORc1 in both HK301 and HK157 cells and therefore activated AKT (the phosphorylated form) could be the kinase mediating the phosphorylation of GSK3B after mTORc1 depletion. This data suggests that activated pERK mediates phosphorylation of GSK3B in certain cultures after inhibition of the mTORc2 pathway while activated pAKT mediates GSK3B phosphorylation after inhibition of the mTORc1 pathway. Moreover, the data indicate that inhibition of either mTORc1 or mTORc2 may result in inhibitory phosphorylation of GSK3B that confers resistance to mTOR pathway specific inhibition.

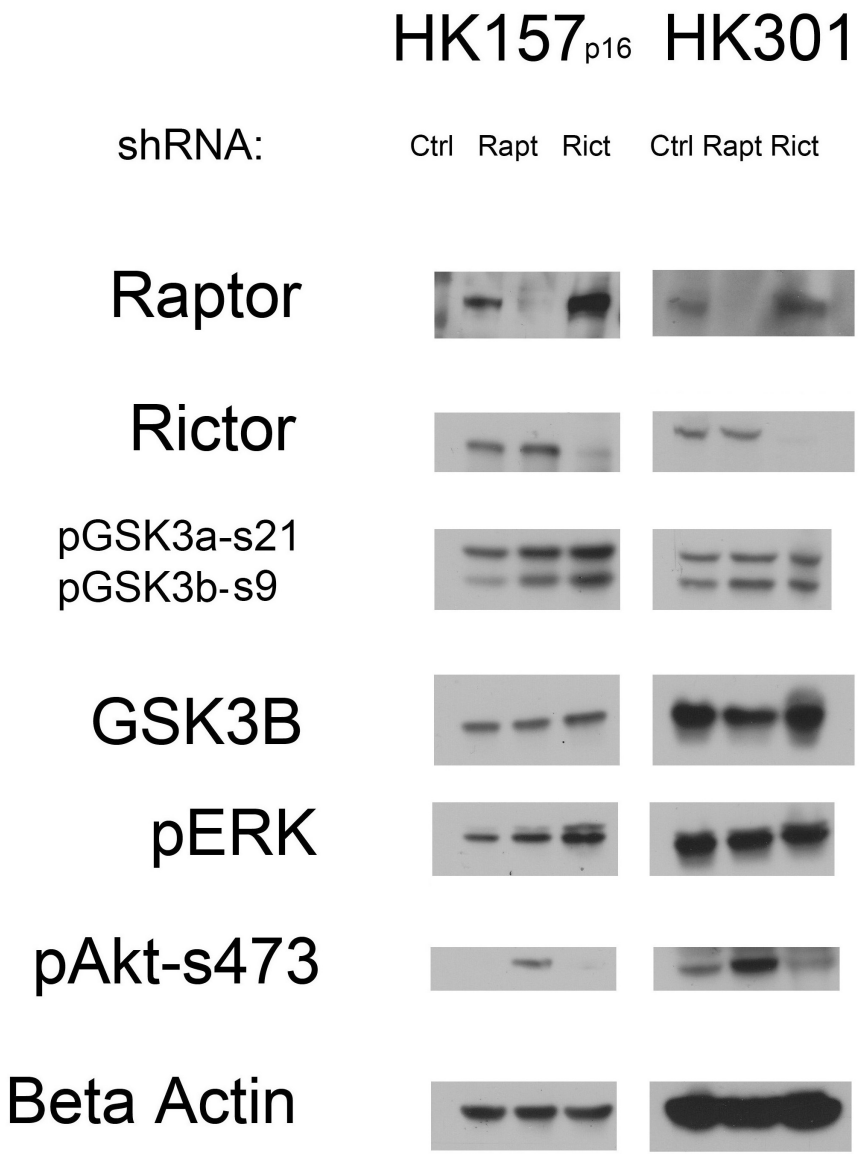
HK157p16
HK301
shRNA:
Ctrl
Rapt
Rict
Ctrl
Rapt
Rict
Raptor
Rictor
pGSK3a-s21
pGSK3b-s9
GSK3B
pERK
pAkt-s473
Beta Actin

Figure 31

Figure 31. Western blot of glioblastoma cultures HK157 and HK301 demonstrates that RICTOR and RAPTOR (associated with mTORc1 and mTORc2 respectively) both can play a role in the phosphorylation status of GSK3B.

Knockdown of RICTOR confers resistance to Rapamycin or NVP-BEZ235 in cultures where RICTOR depletion results in GSK3B inhibitory phosphorylation but not in cultures without that link. shRNA mediated knockdown of RICTOR (mTORc2) confers resistance to Rapamycin treatment in glioblastoma culture HK157 (Figure 32A) which undergoes inhibitory phosphorylation of GSK3B in response to Rapamycin treatment as shown by western blot (Figure 32E). In contrast, knockdown of RICTOR does not confer resistance to Rapamycin in glioblastoma culture HK301 (Figure 32C) that does not undergo inhibitory phosphorylation of GSK3B in response to Rapamycin treatment, as shown by western blot (Figure 32E). There is a more modest effect of RICTOR knockdown on HK157 resistance to NVP-BEZ235 (Figure 32B) and this is consistent with NVP-BEZ235 targeting of mTORc2 directly. In contrast, HK301 becomes modestly more sensitive to NVP-BEZ235 treatment after RICTOR knockdown (Figure 32D). This data supports the evidence that inhibition of RICTOR, and by association, depletion of mTORC2, results in a functional adaptation to further mTORc1 inhibition and the acquisition of resistance. This suggests that dual inhibition of mTORc1 and mTORc2 may not abrogate resistance to mTOR pathway specific inhibition in all glioblastoma cell cultures, but rather may contribute to the acquisition of resistance. This resistance is mediated through inhibitory phosphorylation of GSK3B.

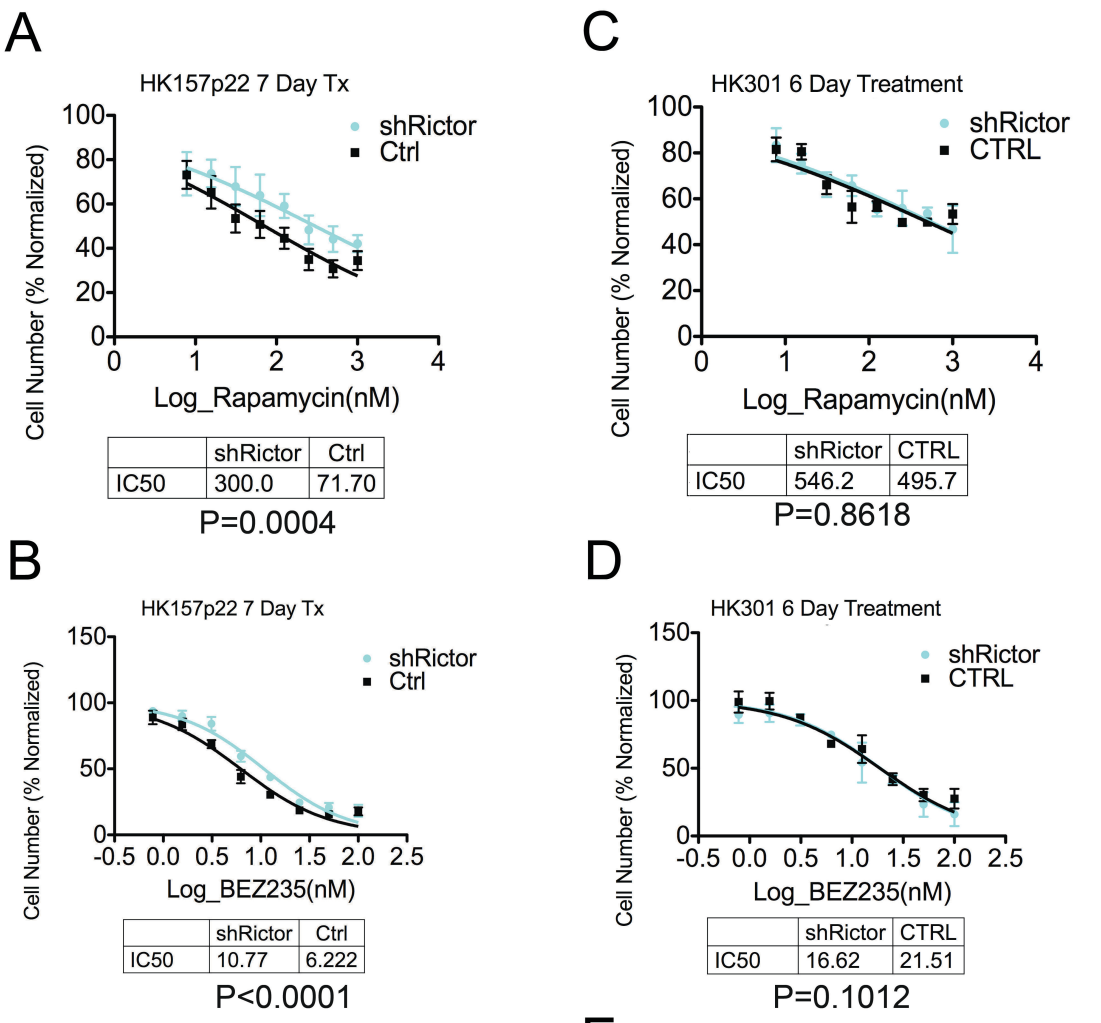
A
HK157p22 7 Day Tx
shRictor
Ctrl
Cell Number (% Normalized)
Log_Rapamycin(nM)
shRictor Ctrl
IC50 300.0 71.70
P=0.0004
C
HK301 6 Day Treatment
shRictor
CTRL
Cell Number (% Normalized)
Log_Rapamycin(nM)
shRictor CTRL
IC50 546.2 495.7
P=0.8618
B
HK157p22 7 Day Tx
shRictor
Ctrl
Cell Number (% Normalized)
Log_BEZ235(nM)
shRictor Ctrl
IC50 10.77 6.222
P<0.0001
D
HK301 6 Day Treatment
shRictor
CTRL
Cell Number (% Normalized)
Log_BEZ235(nM)
shRictor CTRL
IC50 16.62 21.51
P=0.1012
E
HK157p16 HK301
shRNA: Ctrl Rapt Rict Ctrl Rapt Rict
Raptor
Rictor
pGSK3a-s21
pGSK3b-s9

Figure 32

Figure 32. RICTOR depletion results in resistance to Rapamycin in HK157 where RICTOR knockdown results in GSK3B phosphorylation but not in HK301 where that association does not exist. A. Mean relative cell number and standard error bars as estimated by Dojindo Kit8 for a titration of Rapamycin treatments in HK157 demonstrates enhanced resistance in the RICTOR knockdown (N=3, Log scale). The calculated IC50 values are displayed. B. Mean relative cell number and standard error bars as estimated by Dojindo Kit8 for a titration of BEZ235 treatments in HK157 demonstrates very moderate enhanced resistance in the RICTOR knockdown (N=3, Log scale). The calculated IC50 values are displayed. C. Mean relative cell number and standard error bars as estimated by Dojindo Kit8 for a titration of Rapamycin treatments in HK301 demonstrates no change in resistance in the RICTOR knockdown (N=2, Log scale). P-value=0.8618 is depicted that compares the IC50 values. D. Mean relative cell number and standard error bars as estimated by Dojindo Kit8 for a titration of BEZ235 treatments in HK301 demonstrates slight enhanced sensitivity in the RICTOR knockdown (N=2, Log scale). The calculated IC50 values are displayed. E. Reiteration of Western Blot from Figure 31.

Resistance to mTOR inhibition by GSK3B is not mediated by an effect on CTNNB1 that we could detect. CTNNB1 is a known target of GSK3B. GSK3B phosphorylates CTNNB1 and marks it for degradation(Liu et al., 2002; Rubinfeld et al., 1996; Sakanaka et al., 1998). As GSK3B is inhibited after chronic Rapamycin treatment, we studied whether activated CTNNB1 mediated the observed resistance to Rapamycin. We generated cell cultures with knockdown of CTNNB1 via shRNA lentiviral infection to study whether this conferred sensitivity to Rapamycin. Depletion of CTNNB1 was demonstrated via western blot (Figure 33A). When HK301 was depleted of CTNNB1 by shRNA, there was only 26% of the cell number of Ctrl-shRNA cells after 7 days of proliferation and no sign of increased sensitivity to Rapamycin (data not shown). However, due to the low cell number in the shCTNNB1, which may obfuscate any effect of CTNNB1 depletion, we used HK157 cells that had a higher percentage, 86.5%, of the cell number of Ctrl-shRNA after 7 days of proliferation. Depletion of CTNNB1 did not confer sensitivity to either Rapamcyin (Figure 33B) or NVP-BEZ235 (Figure 33C). We also transfected HK301 cells with CTNNB1-delta90, a constitutively active, truncated form of CTNNB1, to test if overexpression of active CTNNB1 conferred resistance to chronic mTOR inhibition. Western blot confirmed the expression of the truncated, constitutively active CTNNB1-delta 90 (Figure 33D). However, overexpression of active CTNNB1 did not confer resistance to chronic mTOR inhibition by either Rapamycin or BEZ-235 (Figure 33E,F).

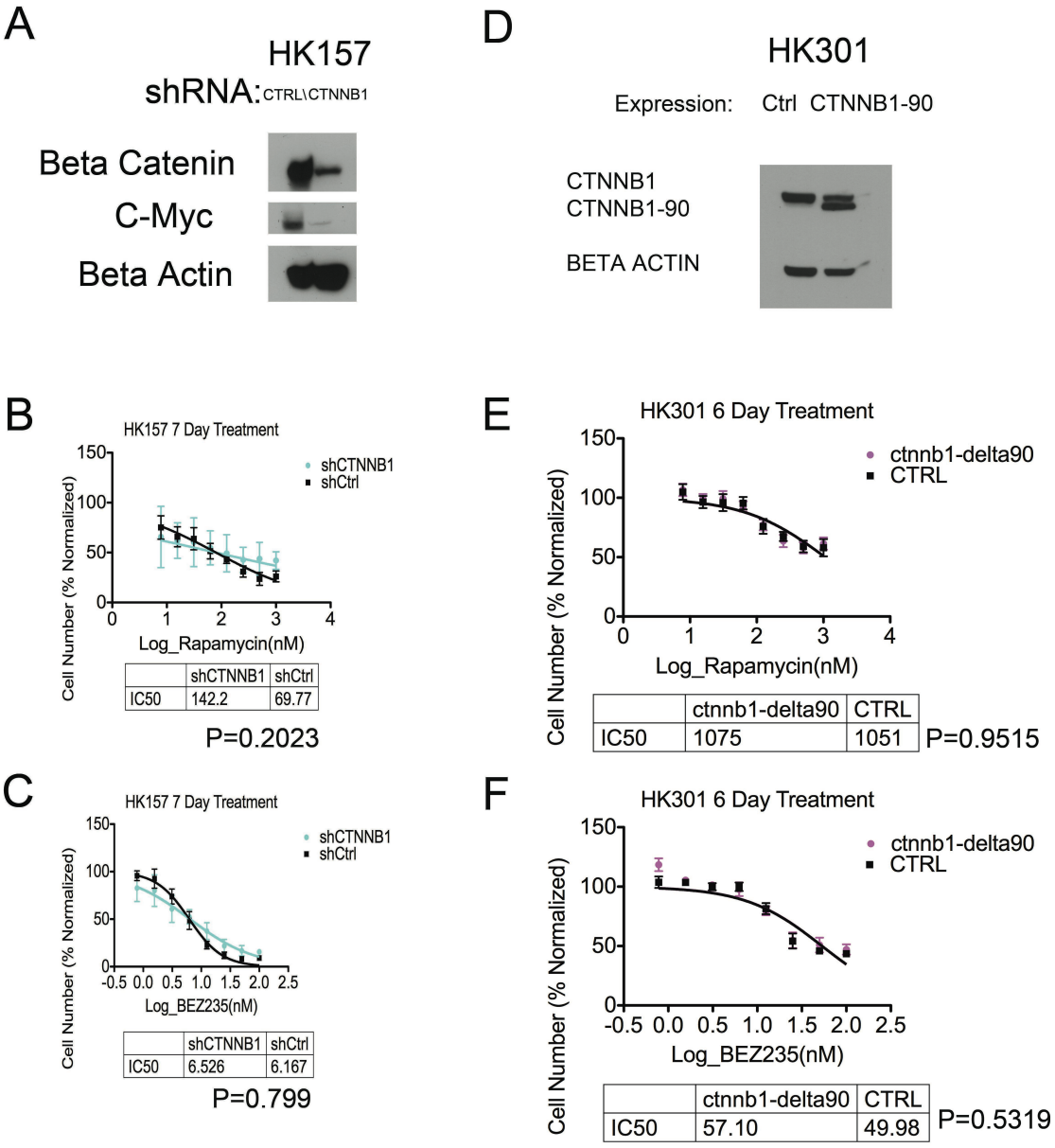
A
HK157
shRNA: CTRL\CTNNB1
Beta Catenin
C-Myc
Beta Actin
D
HK301
Expression: Ctrl CTNNB1-90
CTNNB1
CTNNB1-90
BETA ACTIN
B
HK157 7 Day Treatment
shCTNNB1
shCtrl
Cell Number (% Normalized)
Log_Rapamycin(nM)
shCTNNB1 shCtrl
IC50 142.2 69.77
P=0.2023
E
HK301 6 Day Treatment
ctnnb1-delta90
CTRL
Cell Number (% Normalized)
Log_Rapamycin(nM)
ctnnb1-delta90 CTRL
IC50 1075 1051
P=0.9515
C
HK157 7 Day Treatment
shCTNNB1
shCtrl
Cell Number (% Normalized)
Log_BEZ235(nM)
shCTNNB1 shCtrl
IC50 6.526 6.167
P=0.799
F
HK301 6 Day Treatment
ctnnb1-delta90
CTRL
Cell Number (% Normalized)
Log_BEZ235(nM)
ctnnb1-delta90 CTRL
IC50 57.10 49.98
P=0.5319

Figure 33

Figure 33. No detection of role for CTNNB1 in mediating resistance to mTOR pathway specific inhibition. A. Western blot displaying depletion of CTNNB1 in shRNA mediated knockdown of HK157 glioblastoma cell culture. B. shRNA mediated CTNNB1 depletion does not significantly change response to Rapamycin. Dose response to a titration of Rapamycin in HK157 (Ctrl or shCTNNB1), fitted line for non-linear regression, and standard error bars (N=3), log scale. Calculated IC50 values are displayed (nM). P-value=0.2023 is depicted for the comparison between IC50 values (extra sum of squares F-test). C. shRNA mediated CTNNB1 depletion does not change response to NVP-BEZ235. Dose response to a titration of BEZ235 in HK157, Ctrl or shCTNNB1, fitted line for non-linear regression, and standard error bars (N=3), log scale. Calculated IC50 values are displayed (nM). P-value=0.799 is depicted for the comparison between IC50 values (extra sum of squares F-test). D. Western blot of expression of CTNNB1-delta90 (constitutively active form) vs. Ctrl. E. Overexpression of the constitutively active form of CTNNB1 (CTNNB1-Delta 90) does not alter resistance to chronic mTOR inhibition. Dose response to a titration of Rapamycin in HK301 (Ctrl or CTNNB1-dleta90), fitted line for non-linear regression, and standard error bars (N=5), log scale. Calculated IC50 values are displayed (nM). The extra sum of squares F-test compared the calculated IC50 values, and the depicted P-value=0.9515 indicates the IC50 values are not significantly different. C. Overexpression of the constitutively active form of CTNNB1 (CTNNB1-Delta 90) does not alter resistance to NVP-BEZ235. Dose response to a titration of BEZ235 in HK301, Ctrl or CTNNB1-delta90, fitted line for non-linear regression, and standard error bars (N=5), log scale. Calculated IC50 values are displayed

(nM). The extra sum of squares F-test compared the calculated IC50 values, and the depicted P-value=0.5319 indicates the IC50 values are not significantly different.

A targeted shRNA screen predicts that MAP1B mediates GSK3B conferred resistance to mTOR pathway specific inhibition. We performed targeted shRNA screens to knockdown 50/52 of the proteins from our phosphoproteomics array that underwent phosphorylation changes under chronic Rapamycin and were associated with GSK3B from our KEA analysis. From this screen, 5 sensitizing candidates were chosen (Z Score <=-2): PRPF4B (Z-score=-2.12), MAP1B (Z-score=-2.29) (Figure 8A), LMO7 (Z-score=-2.24), PTK2 (Z-score -2.1), KHDRBS1 (Z-score=-2.36). MAPT (Z-score=2.88), AAK1 (Z-score=3.92), and 3 separate SNW1 clones (Z-scores= 2.57, 3.26, 4.07) (Figure 8A) conferred resistance upon knockdown (z score>=2) (Table 13).

Gene list and Z-scores

Gene	Z-Score
KHDRBS1	-2.36
MAP1B	-2.29
LMO7	-2.24
PRPF4B	-2.12
PTK2	-2.06
PRPF4B	-2.06
MAPT	-1.98
TERF2IP	-1.97
ZHX1	-1.90
SYNPO	-1.83
LMO7	-1.80
TCOF1	-1.78
DOCK7	-1.75
ANAPC1, LOC100134301	-1.71
HMGA1	-1.65
SRRM2	1.70
SNW1	1.73
SNW1	2.57
MAPT	2.88
SNW1	3.26
AAK1	3.92
SNW1	4.07

Table 13. Significant results from targeted shRNA screen under chronic Rapamycin.

Z scores >|1.65|, P<0.05, for cell titer glow (ATP levels/ cell number) after 7 days of proliferation under depletion of the gene indicated. The levels assessed were for chronic Rapamcyin treatment normalized to DMSO.

As we were primarily interested in sensitizing candidates from a therapeutic angle, we chose all 5 sensitizing candidates (Z-score<=-2) for validation. As SNW1 had 3 constructs that were associated with resistance, we chose SNW1 to validate from among our genes with + Z-scores. This procedural decision excluded our further study of MAPT and AAK1 (both had + Z-scores>=2) as we ignored these candidate genes in our validation study. Candidates' differential response to Rapamycin was validated using the shRNA's selected from the screen. For each candidate, cells were grown in a titration of Rapamycin, BEZ235, or DMSO for 7 days and then cell number was assessed. IC50 values were generated and compared using GraphPad Prism software. A P-value<0.01 was used to determine significance and adjust for multiple comparisons. It is important to note that we did not validate the knockdown of each presumed protein at this stage. Instead, we decided to first test for functional validation before validating the targeting of each shRNA. One exception was PTK2 whose knockdown we did validate using western blots (data not shown). Of the five candidate genes that showed sensitization upon knockdown in our targeted screen, knockdown of PRPF4B displayed no apparent effect on response, while knockdowns of three of the other candidate genes (KHDRBS1, PTK2, and LMO7) demonstrated non-significant trends towards sensitization for chronic Rapamycin treatment (Figure 34). As GSK3B targets numerous proteins, it is possible that each of these candidate genes contributes a partial effect that in sum amounts to resistance. However, the only candidate gene that alone exhibits a sensitization effect to chronic mTOR inhibition upon knockdown is MAP1B.

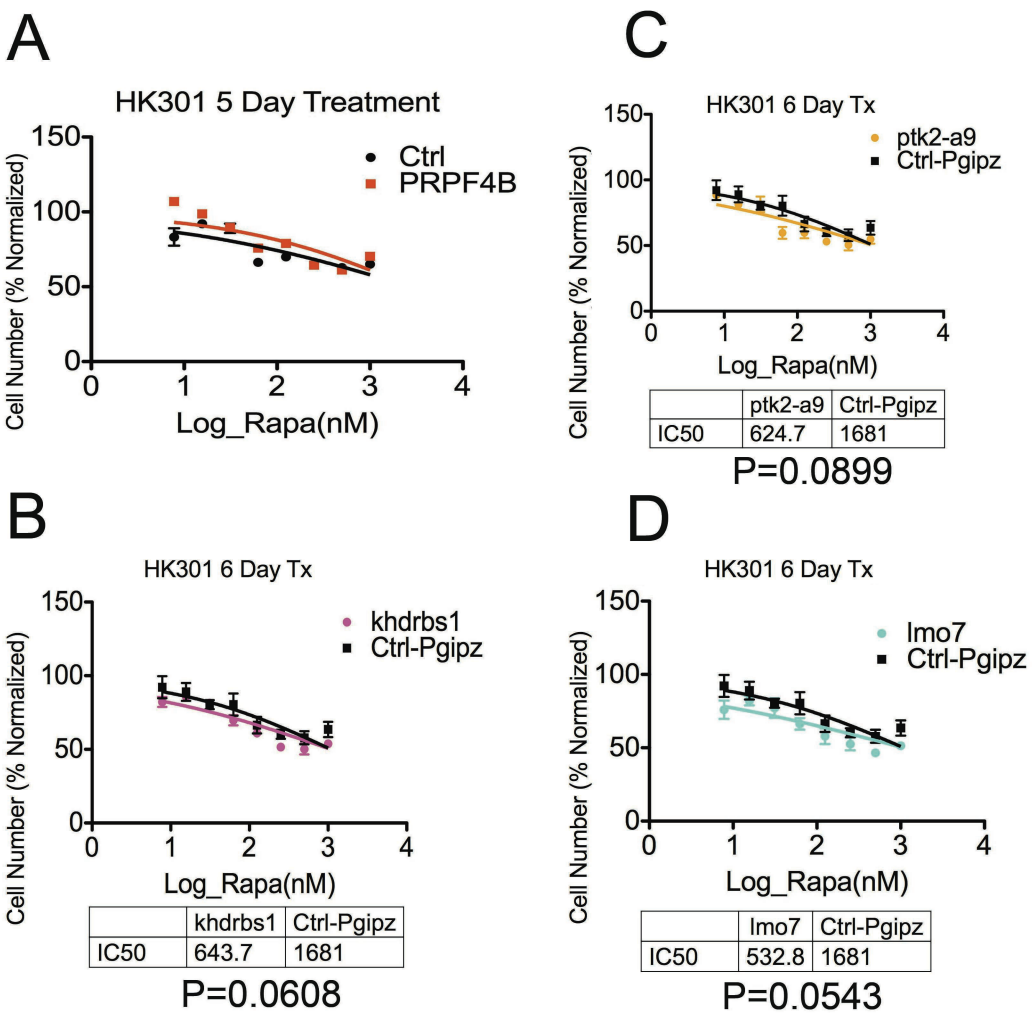
A
HK301 5 Day Treatment
Ctrl
PRPF4B
Cell Number (% Normalized)
Log_Rapa(nM)
C
HK301 6 Day Tx
ptk2-a9
Ctrl-Pgipz
Cell Number (% Normalized)
Log_Rapa(nM)
ptk2-a9 Ctrl-Pgipz
IC50 624.7 1681
P=0.0899
B
HK301 6 Day Tx
khdrbs1
Ctrl-Pgipz
Cell Number (% Normalized)
Log_Rapa(nM)
khdrbs1 Ctrl-Pgipz
IC50 643.7 1681
P=0.0608
D
HK301 6 Day Tx
Imo7
Ctrl-Pgipz
Cell Number (% Normalized)
Log_Rapa(nM)
Imo7 Ctrl-Pgipz
IC50 532.8 1681
P=0.0543

Figure 34

Figure 34. A trend towards Rapamycin sensitization is not significant in 4/5 candidates from the targeted shRNA screen. An important caveat is that these candidates were not confirmed to target the gene listed with these shRNA constructs, except shPTK2-A9 which was shown via western blot to target PTK2 (data not shown). Titrations of Rapamcyin were carried out in Ctrl cells as compared to shRNA mediated knockdown of each target gene listed. After 5-6 days, cell number was estimated, dose response curves generated, and IC50 values calculated and then compared. A. shPRPF4B did not seem to confer sensitivity to chronic Rapamycin. Measured values, fitted line, and IC50 values are depicted, (N=1), log scale. P-value and IC50 values could not be generated for these values. B. shKHDRBS1 trends towards sensitization but it is not significant. Measured values, fitted line, and IC50 values are depicted, (N=4), log scale. P-value=0.0608 is depicted for the comparison between IC50 values. C. shPTK2 trends towards sensitization but it is not significant. Measured values, fitted line, and IC50 values are depicted, (N=4), log scale. P-value=0.0899 is depicted for the comparison between IC50 values. D. shLMO7 trends towards sensitization but it is not significant. Measured values, fitted line, and IC50 values are depicted, (N=4), log scale. P-value=0.0543 is depicted for the comparison between IC50 values.

Depletion of MAP1B confers a significant sensitization effect to chronic mTOR inhibition (Figure 35B,C,D). In HK301, the PTEN null line in which the original target screen was carried out, the IC50 for shMAP1B under chronic Rapamycin conditions was significantly lower by over three fold from the IC50 of the shControl cells (P=0.0029) (Figure35B). Additionally, in another PTEN null GBM culture, HK217, the IC50 for shMAP1B under chronic Rapamycin conditions was significantly lower by over 25 fold from the IC50 of shControl cells (P=0.0002) (Figure35C).

In addition, in HK217, the IC50 for shMAP1B under chronic NVP-BEZ235 conditions was significantly lower by over 1.5 fold from the IC50 of shControl cells (P=0.0028) (Figure35D). This was not the case for HK301, where shMAP1B had no effect on the observed IC50 under chronic NVP-BEZ235 conditions as compared to shControl (data not shown). These data indicate that for some GBM cultures, particularly PTEN null cultures, MAP1B confers resistance to chronic mTOR inhibition. At least in one example, HK217, the sensitization effect imparted by knockdown of MAP1B was independent of resistance through mTORc2, as response to both the combined TOR inhibitor BEZ235 and to Rapamycin was significantly altered. These data indicate that MAP1B plays a functional role in resistance to chronic mTOR inhibition and, furthermore, this mechanism of resistance is not dependent on mTORc2.

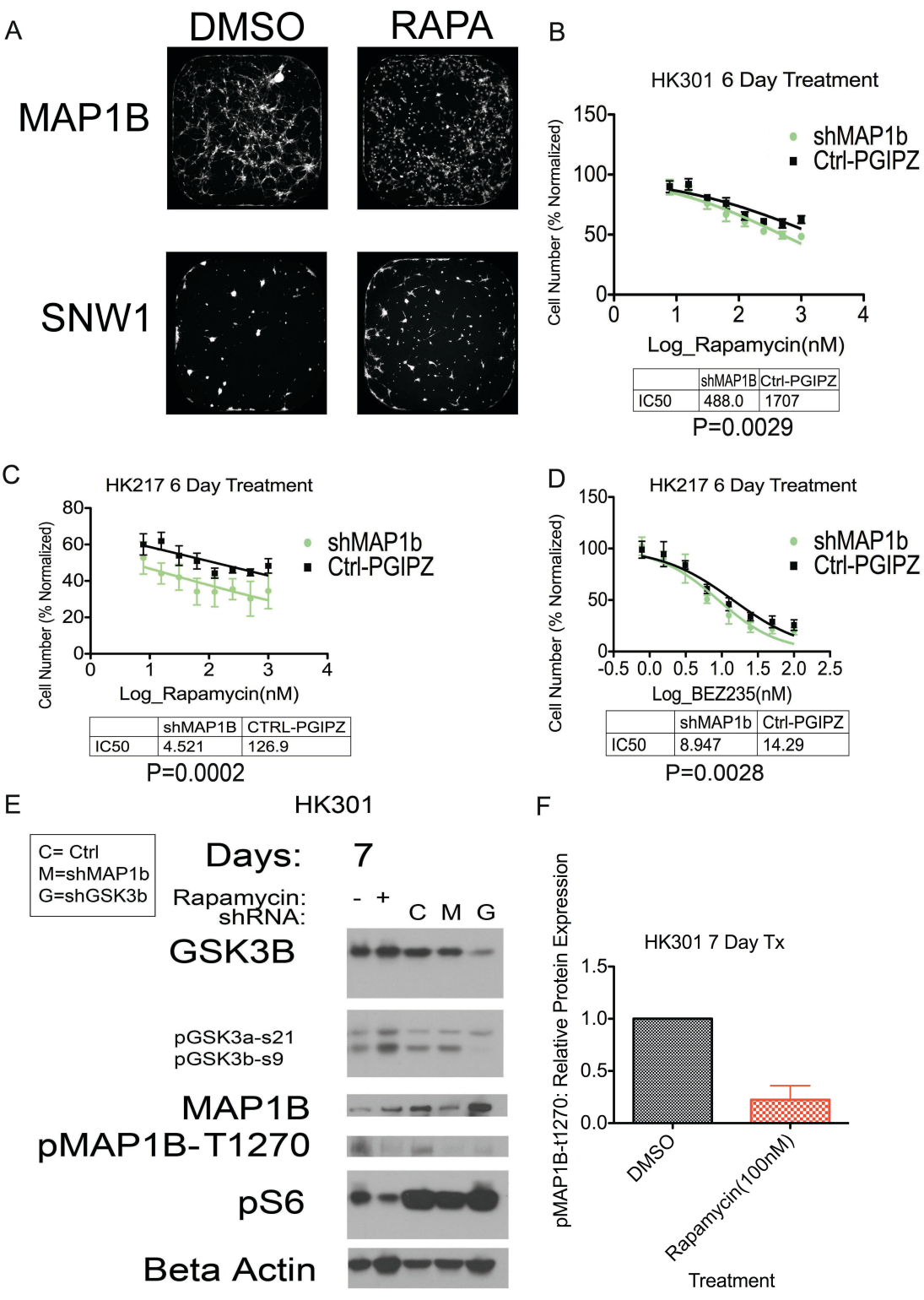
A
DMSO
RAPA
MAP1B
SNW1
B
HK301 6 Day Treatment
shMAP1b
Ctrl-PGIPZ
Cell Number (% Normalized)
Log_Rapamycin(nM)
shMAP1B Ctrl-PGIPZ
IC50 488.0 1707
P=0.0029
C
HK217 6 Day Treatment
shMAP1b
Ctrl-PGIPZ
Cell Number (% Normalized)
Log_Rapamycin(nM)
shMAP1B CTRL-PGIPZ
IC50 4.521 126.9
P=0.0002
D
HK217 6 Day Treatment
shMAP1b
Ctrl-PGIPZ
Cell Number (% Normalized)
Log_BEZ235(nM)
shMAP1b Ctrl-PGIPZ
IC50 8.947 14.29
P=0.0028
E
HK301
C= Ctrl
M=shMAP1b
G=shGSK3b
Days: 7
Rapamycin: - +
shRNA: C M G
GSK3B
pGSK3a-s21
pGSK3b-s9
MAP1B
pMAP1B-T1270
pS6
Beta Actin
F
HK301 7 Day Tx
pMAP1B-t1270: Relative Protein Expression
DMSO
Rapamycin(100nM)
Treatment

Figure 35

Figure 35. Knockdown of MAP1B confers sensitivity to chronic mTOR inhibition, while knockdown of SNW1 confers resistance. A. Images of wells from 384 well plates used in the targeted shRNA screen display GFP labeled cells in shMAP1B and shSNW1 conditions at 10 Days post treatment (DMSO-control or 100nM Rapamycin (RAPA)). Images of were taken by ImageExpress micro. Cell cultures grew as semi adherent/semi spheres. As the cultures are three dimensional, cell number is therefor difficult to assess by visual inspection. B. shMAP1B confers sensitivity to chronic Rapamycin in HK301 (PTEN null). Fitted curve of log transformed values for a titration of Rapamycin in HK301 GBM cells, with and without MAP1B knockdown, after 6 days of proliferation, with calculated IC50 values depicted below, (N=6). The P-Value (P=0.0029) is depicted for the comparison of the two IC50 values. C. shMAP1B confers sensitivity to chronic Rapamycin in HK217 (PTEN null). Fitted curve of log transformed values for a titration of Rapamycin in HK217 GBM cells, with and without MAP1B knockdown, after 6 days of proliferation, with calculated IC50 values depicted below, (N=3). The P-Value (P=0.0002) is depicted for the comparison of the two IC50 values. D. shMAP1B confers sensitivity to chronic NVP-BEZ235 in HK217 (PTEN null). Fitted curve of log transformed values for a titration of BEZ235 in HK217 GBM cells, with and without MAP1B knockdown, after 6 days of proliferation, with calculated IC50 values depicted below, (N=4). The P-Value (P=0.0028) is depicted for the comparison of the two IC50 values. E. Western blot supports the model wherein chronic mTOR inhibition regulates MAP1B levels via phosphorylation by GSK3B. Western blot columns are in order: 7day chronic DMSO-control, 7 day Rapamcyin, shRNA-control (C), shMAP1B (M), shGSK3B (G). F. Western blot quantification indicates that relative phosphorylation of

MAP1B at T-1270 is reduced in chronic rapamcyin (100nM, 7 Days). Western blot protein expression (from Figure 8E) and a biological replicate experiment (N=2) is quantified via ImageJ software. Relative expression of pMAP1B-t1270 is normalized to Beta Actin loading control and total MAP1B levels.

Knockdown of confers a significant resistance to chronic mTOR inhibition (Figure 36). Depletion of SNW1 is demonstrated via western blot (Figure 36A). The Western blot suggests that under chronic mTOR inhibition by Rapamycin, and under depletion of GSK3B, SNW1 protein levels are slightly decreased (Figure 36A). Knockdown of SNW1 confers resistance to Rapamycin and BEZ235 in HK301 GBM cells (Figure 36B,C). These trends are repeated in HK217 GBM cells as well (Figure 37). Indeed, in HK217, the reduction of SNW1 under chronic Rapamycin and depletion of GSK3B is more evident (Figure 37A). These data support the hypothesis that SNW1 confers sensitivity to Rapamycin, and it's depletion upon chronic Rapamycin exposure may be an adaptive response, contingent upon attenuated GSK3B, which confers resistance.

In our phosphoproteomics array, MAP1B had decreased phosphorylated serine 1265 after chronic Rapamycin treatment (0.435 ratio of phosphorylated MAP1B from chronic Rapamycin/DMSO treated controls) as would be expected if MAP1B were acted upon by GSK3B and GSK3B underwent an adaptive inhibitory phosphorylation due to chronic Rapamycin treatment. Likewise, SNW1 also demonstrated reduced phosphorylation at serine 224 after chronic Rapamycin treatment (0.47 ratio of phosphorylated SNW1 from chronic Rapamycin/DMSO treated controls). Thus, our data are consistent with a mechanism of resistance to chronic mTOR inhibition wherein phosphorylation dependent attenuation of GSK3B may abrogate the inhibitory phosphorylation of downstream target effectors, MAP1B and SNW1. In the case of MAP1B, diminished phosphorylation may lead to resistance to chronic mTOR inhibition. In the case of SNW1, we did not determine the role for diminished phosphorylation as we

did not generate the phospho-specific antibody towards SNW1-s224. Indeed, it is unknown whether SNW1 phosphorylation is reduced under chronic Rapamycin conditions as a result of the depletion of total SNW1 protein levels, as observed (Figure 37A).

A literature search indicates that GSK3B phosphorylates MAP1B at S1260 and T1265 in mice(Trivedi et al., 2005). These sites are homologous to S1265 and T1270 in humans. As S1265 was the site we discovered with reduced phosphorylation under chronic Rapamycin conditions in our phosphoproteomics array, we wanted to study whether GSK3B phosphorylated MAP1B in human GBM. To this end we utilized a commercially available antibody directed against MAP1B-T1270 in humans. As GSK3B is known to phosphorylate multiple consecutive sites in the same protein, we effectively used this T1270 antibody as a proximal proxy for the S1265 whose change we observed in our phosphoproteomics array.

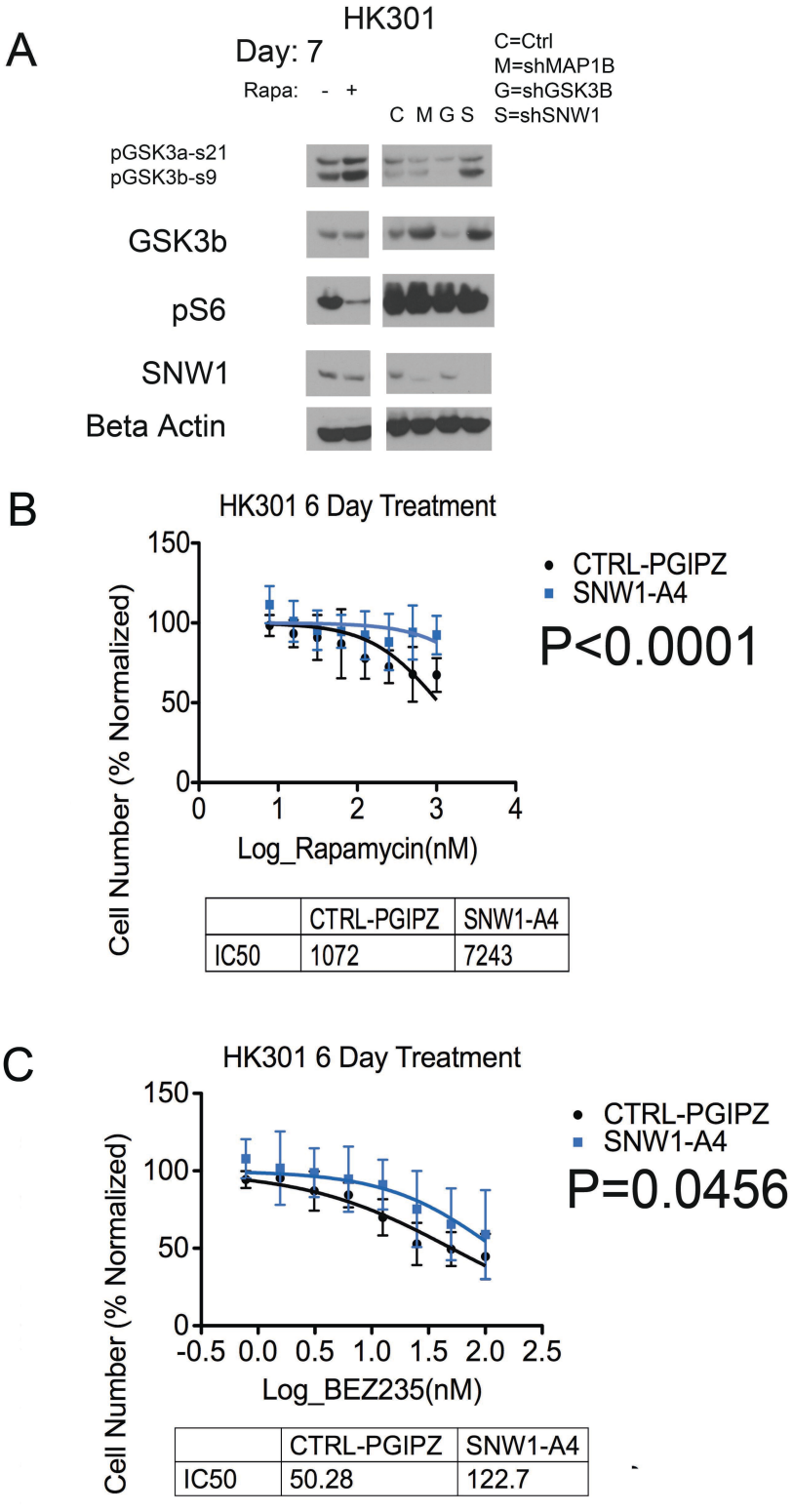
A
HK301
Day: 7
Rapa: - +
C M G S
C=Ctrl
M=shMAP1B
G=shGSK3B
S=shSNW1
pGSK3a-s21
pGSK3b-s9
GSK3b
pS6
SNW1
Beta Actin
B
HK301 6 Day Treatment
Cell Number (% Normalized)
Log_Rapamycin(nM)
CTRL-PGIPZ
SNW1-A4
P<0.0001
CTRL-PGIPZ SNW1-A4
IC50 1072 7243
C
HK301 6 Day Treatment
Cell Number (% Normalized)
Log_BEZ235(nM)
CTRL-PGIPZ
SNW1-A4
P=0.0456
CTRL-PGIPZ SNW1-A4
IC50 50.28 122.7

Figure 36

Figure 36. shSNW1 confers resistance to chronic Rapamycin and to BEZ235 in HK301. A. SNW1 is depleted by chronic Rapamycin and upon knockdown of GSK3B. Western blot shows depletion of SNW1 upon shRNA mediated knockdown of SNW1, SNW1 depletion upon 7 Days of chronic Rapamycin treatment, and SNW1 depletion upon knockdown of GSK3B. pS6 is reduced upon 7 day chronic Rapamcyin exposure as would be expected. GSK3B has increased phosphorylation upon 7 day exposure to Rapamcyin that may be responsible for the depletion of SNW1. B Curve of raw values for a titration of Rapamycin in HK301 GBM cells, with and without SNW1 knockdown, after 6 days of proliferation. IC50 values are calculated and displayed. (N=5 biological replicates). A comparison of the IC50 values indicates a significant difference in the observed values between shSNW1 and shCtrl ($P<0.0001$). C. Curve of raw values for a titration of BEZ235 in HK301 GBM cells, with and without SNW1 knockdown, after 6 days of proliferation. IC50 values are calculated and displayed. (N=4 biological replicates). A comparison of the IC50 values indicates a significant difference in the observed values between shSNW1 and shCtrl ($P<0.0456$).

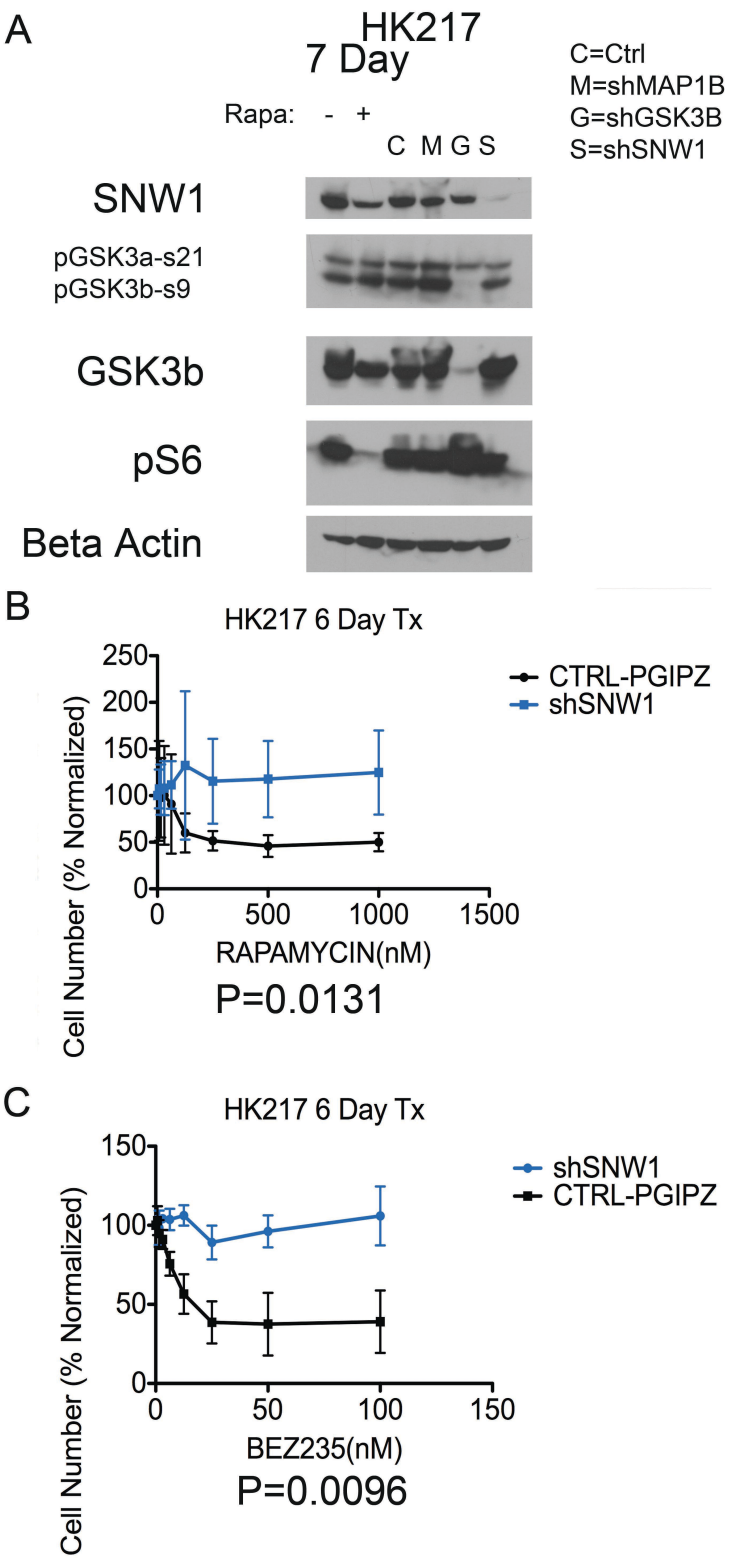
A
HK217
7 Day
C=Ctrl
M=shMAP1B
G=shGSK3B
S=shSNW1
Rapa: - +
C M G S
SNW1
pGSK3a-s21
pGSK3b-s9
GSK3b
pS6
Beta Actin
B
HK217 6 Day Tx
CTRL-PGIPZ
shSNW1
Cell Number (% Normalized)
250
200
150
100
50
0
0
500
1000
1500
RAPAMYCIN(nM)
P=0.0131
C
HK217 6 Day Tx
shSNW1
CTRL-PGIPZ
Cell Number (% Normalized)
150
100
50
0
0
50
100
150
BEZ235(nM)
P=0.0096

Figure 37

Figure 37. shSNW1 confers resistance to chronic Rapamycin and to BEZ235 in HK217 (PTEN null). A. Western blot shows depletion of SNW1 upon shRNA mediated knockdown. In addition, SNW1 is depleted after 7 days of chronic Rapamycin and after knockdown of GSK3B. B. shSNW1 confers resistance to chronic Rapamycin and to BEZ235 in HK217 (PTEN null). Curve of raw values for a titration of Rapamycin in HK217 GBM cells, with and without SNW1 knockdown, after 6 days of proliferation. IC50 values could not be calculated as the shSNW1 curve did not pass the IC50 value level (N=3). A pairwise T-test indicates a significant difference in the observed values between shSNW1 and shCtrl (P=0.0131). C. shSNW1 confers resistance to chronic NVP-BEZ235 in HK217 (PTEN null). Curve of raw values for a titration of BEZ235 in HK217 GBM cells, with and without SNW1 knockdown, after 6 days of proliferation. IC50 values could not be calculated as the shSNW1 curve did not pass the IC50 value level (N=3). A pairwise T-test indicates a significant difference in the observed values between shSNW1 and shCtrl (P=0.0096).

Evidence indicates that chronic Rapamycin, via GSK3B, Regulates MAP1B through Phosphorylation. Western blots indicate that chronic Rapamycin diminishes phosphorylation of MAP1B at T1270 and increases phosphorylation of GSK3B (Figure 35E,F). Moreover, depletion of GSK3B also diminishes phosphorylation of MAP1B (Figure 35E). This indicates that GSK3B is a kinase involved in the phosphorylation of MAP1B. Although we don't have evidence of a direct interaction, this data supports the model wherein chronic Rapamycin attenuates GSK3B via increased inhibitory phosphorylation and this results in reduced phosphorylation of MAP1B (Figure 35). These data support the hypothesis that a GSK3B mediated reduced phosphorylation of MAP1B is an adaptive response that confers resistance to chronic Rapamycin.

Activated ERK signaling may confer resistance to chronic Rapamycin through indirect phosphorylation of GSK3B. ERK phosphorylates RSK, which is known to phosphorylate GSK3B(Saito et al., 1994). We transplanted HK374 GBM cells as subcutaneous xenografts into mice, detectable tumors were allowed to form, and subsequently, after 9 days of treatment with either, Rapamycin, Selumetinib, or the combination of both, western blots were performed on the pooled samples. This is direct evidence that phosphorylated GSK3B is an adaptive response to chronic mTOR inhibition (Figure 38A). Furthermore, AKT is not activated by chronic mTOR inhibition, rather, the activating phosphorylation serine 473 on AKT is depleted in chronic Rapamycin (Figure 38A). This suggests that chronic Rapamycin may have targeted mTORc2 that is known to phosphorylate AKT at serine 473. Chronic Rapamycin has been demonstrated to target mTORc2 in certain cell cultures(Sarbassov et al., 2006). Interestingly, ERK is activated in the chronic Rapamycin conditions and, through RSK,

may be responsible for phosphorylation of GSK3B (Figure 38A). Further evidence for this is the depletion of phosphorylated GSK3B (pGSK3b-s9, Figure 38A) in the Selumetinib + Rapamycin conditions. Whereas chronic Rapamycin induces a phosphorylation of GSK3B, the addition of MEK/ERK inhibition by Selumetinib abrogates that effect. This data supports the hypothesis that ERK is involved in the inhibitory phosphorylation of GSK3B, in certain GBM cell cultures, as modeled in Figure 38B.

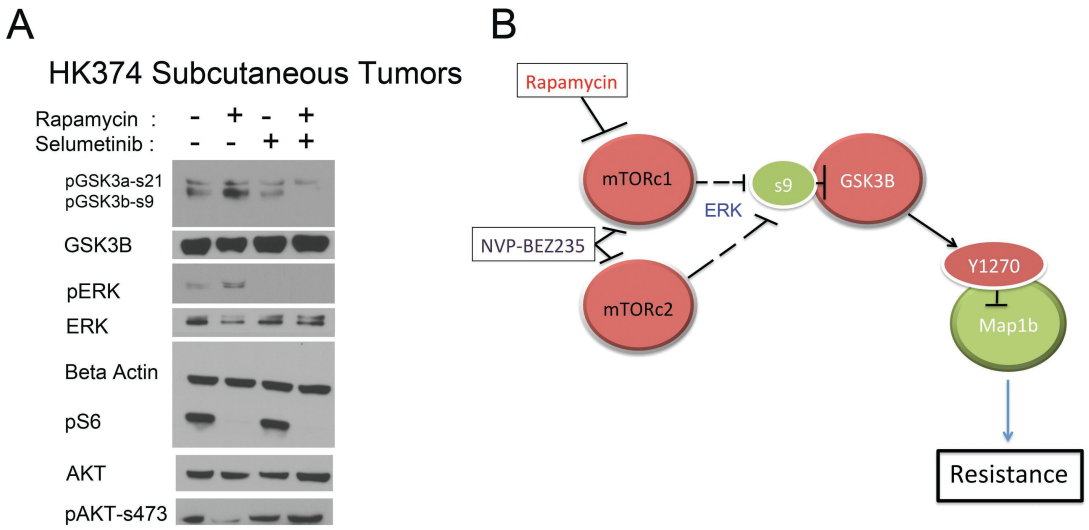
A
HK374 Subcutaneous Tumors
Rapamycin : - + - +
Selumetinib : - - + +
pGSK3a-s21
pGSK3b-s9
GSK3B
pERK
ERK
Beta Actin
pS6
AKT
pAKT-s473
B
Rapamycin
mTORc1
s9
GSK3B
ERK
NVP-BEZ235
mTORc2
Y1270
Map1b
Resistance

Figure 38

Figure 38. Activated ERK signaling may play a role in phosphorylation of GSK3B.

A. In vivo evidence of phosphorylation of GSK3B after chronic Rapamycin treatment. Western blots of pooled samples of in vivo, subcutaneous xenografts of HK374 GBM cells after 9 days of treatment. Activation of ERK may play a role in phosphorylation of GSK3B as pAKT is inhibited under chronic Rapamycin. B. Schematic of proposed model of resistance to chronic mTOR inhibition. Dotted line represents indirect association. Red color indicates inactivation under chronic treatment, green color indicates activation.

Discussion

This study is the first to demonstrate that phosphorylation dependent attenuation of GSK3B is a cellular adaptive mechanism that imparts resistance to chronic mTOR inhibition in GBM. During the course of our experiments, several other studies demonstrated in other cancer models that GSK3B was involved in resistance to mTOR inhibition(Koo et al., 2015; Koo et al., 2014; Sokolosky et al., 2014), but they did not show that GSK3B inhibition, through increased inhibitory phosphorylation, was an adaptive response to chronic mTOR inhibition that conferred resistance. Moreover, this study is the first to show that MAP1B partially mediates this resistance. In addition, we found that SNW1 also plays a role in sensitivity to chronic mTOR inhibition as knockdown of SNW1 dramatically confers resistance to chronic mTOR inhibition.

We did not detect a role for CTNNB1 in response to chronic mTOR inhibition despite the essential role for GSK3B. This discrepancy can be explained due to a sequestration of the GSK3B/CTNNB1 complex that prevents its interaction with the pool of GSK3B phosphorylated through the PI3Kinase cascade(Ng et al., 2009).

We discovered that both mTORc1 and mTORc2 mediate phosphorylation of GSK3B that confers resistance to mTOR pathway specific inhibition. In addition, as depletion of MAP1B conferred sensitivity to both Rapamycin and to the dual TOR kinase inhibitor NVP-BEZ235, we can deduce that mTORc2 is not a downstream mediator of MAP1B in its mode of resistance. Therefore, this data cautions against dual TOR inhibitors as a single approach at overcoming resistance to mTOR inhibition.

GSK3B targets numerous downstream effectors and we found 4 other candidates besides MAP1B that were associated with GSK3B and that, upon depletion, conferred

sensitivity to chronic Rapamycin in our targeted shRNA screen: LMO7, KHDRBS1, PRPF4B, and PTK2. We carried out a validation study on these candidate genes that was more rigorous than the initial targeted screen as it used a titration of Rapamycin, calculated IC50 values, and compared them. Although depletion of PRPF4B did not seem to confer sensitivity to chronic Rapamycin in our validation study, a non-significant trend towards sensitization was observed for KHDRBS1, PTK2, and LMO7. It is possible that by themselves these targets of GSK3B do not reach significance in sensitizing cells to Rapamycin but in sum they may. However, the fact that we observed a sensitization effect by depletion of MAP1B alone distinguishes MAP1B as an important mediator of resistance to chronic mTOR inhibition.

Due to the self-imposed limitations of our study, 2 proteins (AAK1, MAPT) with positive Z-scores, whose knockdowns conferred resistance to chronic Rapamycin treatment, were not validated. This leaves AAK1 and MAPT as interesting candidates for further study into their roles in conferring sensitivity to chronic mTOR inhibition. In addition, the relationship of SNW1 in relation to GSK3B remains to be elucidated. Although we discovered that SNW1 imparts sensitivity to chronic mTOR inhibition, as depletion imparts resistance, we did not develop phosphor-specific antibodies to further study how GSK3B may modulate SNW1 via phosphorylation at its observed phosphorylation site of S224. However, as this phosphorylation of SNW1 decreased under chronic Rapamycin treatment in our phosphoproteomics study, this is consistent with GSK3B involvement as GSK3B kinase activity is attenuated in chronic Rapamycin conditions. Generation of the phospho-antibody, SNW1-S224 would be a good starting

point to determine how this phosphorylation modulates SNW1 function and furthermore, how phosphorylation alters response to chronic mTOR inhibition.

Our biochemical study of MAP1B in response to chronic mTOR inhibition and GSK3B depletion demonstrates that phosphorylation of MAP1B is modulated by GSK3B. This interaction between GSK3B and MAP1B has been demonstrated previously(Garcia-Perez et al., 1998; Grimes and Jope, 2001; Lucas et al., 1998). In sum, our model of resistance to chronic mTOR inhibition describes a molecular adaptation where GSK3B is attenuated by inhibitory phosphorylation that results in increased MAP1B activity (among other downstream effectors) leading to an acquired resistance (Figure 9). Phosphorylated MAP1B has been demonstrated to destabilize microtubules(Trivedi et al., 2005). Furthermore, stabilized microtubules have recently been demonstrated to protect neurons from prion mediated toxicity(Zajkowski et al., 2015). Perhaps stabilized microtubules, or another function of de-phosphorylated MAP1B, serve to protect cells from chronic mTOR inhibition. Further study is necessary to determine how MAP1B confers resistance to chronic mTOR inhibition but this advancement in our understanding may lead to novel combinatorial therapies that overcome resistance and effectively target GBM cell proliferation and malignancy.

Our in vivo subcutaneous xeongraft model of tumor formation indicates that activated ERK could play a role in the phosphorylation of GSK3B under chronic Rapamycin in HK374 GBM cells. This reiterates our RICTOR/RAPTOR knockdown experiments that indicate either AKT or ERK could be responsible for phosphorylation of GSK3B and the subsequent adaptive resistance. The idea that ERK plays a central role in phosphorylation of GSK3B and adaptive resistance is supported by our data. When ERK

was inhibited with Selumetinib treatment and concomitant Rapamycin treatment, in our subcutaneous xenograft model, the phosphorylation of GSK3B was dramatically reduced. These data indicate that ERK may be a major effector of resistance to mTOR inhibition, through its role in inhibitory phosphorylation of GSK3B.

Methods

Tumor Collection. Human GBM (Who Grade 4) brain tumor samples were collected following surgical resection under institutional review board-approved protocols and graded by the neuropathologist in accordance with the World Health Organization established guidelines(Kleihues et al., 2002).

Neurosphere Cultures. Human GBM (WHO Grade 4) tumors were cultured as previously described (Galli, 2004;Hemmati, 2003; Laks, 2009) in Dulbecco's modified Eagle's medium (DMEM)/ F12 medium supplemented with B27 (Gibco, Grand Island, NY, http://www.invitrogen.com), 20 ng/ml basic fibroblast growth factor (bFGF) (Peprotech, Rocky Hill, NH, http://www.peprotech.com), 50ng/ml epidermal growth factor (EGF), penicillin/streptomycin (Invitrogen, Carlsbad, CA, http://www.invitrogen.com), l-glutamine (Invitrogen), and 5 ug/ml heparin (Sigma-Aldrich, St. Louis, http://www.sigmaaldrich.com). Neurosphere cultures were passaged every 7-10 days into fresh media following enzymatic dissociation with TryplE (Invitrogen). Heparin, bFGF, and EGF were added weekly.

Primary GBM Cell Cultures: HK157, HK217, HK296, HK301, HK308, HK390, HK374.

GBM Cell Culture	EGFr V3	EGFr Amplified	PTEN	Age	Gender
HK157	-	-	+	54	Female
HK217	-	-	-	81	Male
HK296	+	+	-	76	Male
HK301	+	+	-	65	Male
HK308	+		+	50	Female
HK390	-	-	+	73	Male
HK374	+	+	+	45	Male

Rapamycin treatment. To yield a Rapamycin resistant population, chronic Rapamycin (LC Laboratories, Woburn, MA, http://www.LCLabs.com) was administered twice weekly at 100 nano-molar for at least 7 days. These cultures were compared to DMSO treated control cell populations. Neurosphere formation assays under chronic Rapamycin treatment (to determine Rapamycin resistance or sensitivity) are presented as normalized sphere formation: sphere formation for the Rapamycin treated as a percent of sphere formation for the DMSO-controls. The Rapamycin was administered to a final concentration of 0.1% DMSO.

Exposure groups. Three exposure groups were devised for the purpose of the phosphoproteomics study. 1. DMSO-Control. 2. Chronic Rapamycin treatment (the Rapamycin resistant population after 42 days of 100 nM Rapamycin, twice weekly). 3. Acute Rapamycin (100nM Rapamycin for 4 hours). The latter 2 exposure groups were all compared to the DMSO-control to normalize changes and serve as a baseline.

iTRAQ: HK296 GBM cells were grown in acute or chronic conditions. For acute, cells were treated for 4 hours in 100nM Rapamycin or DMSO (Ctrl, vehicle). For chronic treatment, cells were grown in 100nM Rapamycin for 42 days (enough time to generate the amount of cells needed). Cells were pelleted and run through the protocol for iTRAQ. iTRAQ was used according to standard methods to determine changes in phosphorylation from Rapamycin to DMSO conditions(Jones and Nuhse, 2011).

The final list of phosphosites that were considered changed in chronic Rapamycin conditions as compared to DMSO (control) had to meet the following criteria:

1. Differentially occupied in chronic Rapamycin vs DMSO (relative levels difference beyond threshold value);

2) The relative quantitative value is median of several spectra corresponding to the same phosphopeptide, (or we have an overlapping peptide with the same site);

3) If we have several overlapping peptides that contain the same phosphosite, they do not disagree in their behavior (they all go up, or down);

4) The standard deviation of these readings is relatively small, compared to the change.

Cell lysis, reduction/alkylation and in-solution digestion: $1x10^8$ cell pellets were thawed and resuspended in 4 ml 25 mM ammonium bicarbonate buffer containing 8 M urea with phosphatase inhibitors (160 ul of Sigma Phosphatase Inhibitor Cocktail 1 and 3) . The amount of protein was checked by bicinchoninic acid (BCA) protein assay kit (Pierce, Rockford, IL); approximately 4 mg of protein was recovered per sample. DTT was added

to 2 mM, and samples were incubated for 10 min at 60 ºC. Iodoacetamide (IAA) was then added to the samples to 4.2 mM, and incubated 45 additional minutes in the dark at 21 ºC. The samples were then diluted 4-fold with 25 mM ammonium bicarbonate to reduce urea concentration to 2 M, and added 2% (W/W) modified trypsin (Promega, Madison, WI). The pH was adjusted to 8.0 with 250 mM ammonium bicarbonate, and the samples were incubated 12 h at 37 ºC. The digests were then desalted using a MAX-RP Sep Pak ® classic C18 cartridge (Waters) following the manufacturer's protocol. Briefly, the cartridges were conditioned with 70% acetonitrile (MeCN) and 0.1% trifluoroacetic acid (TFA), and then washed twice with 10 ml of 0.4% TFA in water. Next, samples previously acidified were loaded onto the column, and the adsorbed material was washed 10-20 times the volume of the resin with 0.4 % TFA in water. Peptides were eluted in 3 times with 0.5 ml of 70% MeCN, 0.1% TFA. The solvent was evaporated to dryness under vacuum and the peptides were resuspended in 35% MeCN, 200 mM NaCl, 0.4% TFA to perform phosphopeptide enrichment.

Enrichment of phosphorylated peptides using titanium dioxide: Phosphopeptide enrichment was performed using an AKTA Purifier (GE Healthcare, Piscataway, NJ) using 5 µm titanium dioxide (TiO_2) beads (GL Sciences, Tokyo, Japan) (18, 19) in-house packed into a 2.0 mm x 2 cm analytical guard column (Upchurch Scientific, Oak Harbor, WA). Tryptic digests (4 mg) were resuspended in 0.5 ml of 35% MeCN, 200 mM sodium chloride and 0.4% TFA, and divided into 2 aliquots of 250 µl, each containing 2 mg of material. Enrichment was performed separately in each of these aliquots. Aliquots were loaded onto the TiO_2 column at a flow rate of 2 ml/min. The column was then washed for 2 min with 35% MeCN, 200 mM NaCl, 0.4% TFA to remove non phosphorylated

peptides. Phosphopeptides were eluted from the column using 1 M Potassium Phosphate Monobasic (KH_2PO_4) pH 3.0 at a flow rate of 0.5 ml/min for 30 min directly onto an on-line coupled C18 macrotrap peptide column (Michrom Bioresources, Auburn, CA). This column was washed with 5% MeCN, 0.1% TFA for 14 min and the adsorbed material was eluted in 400 µl of 50% MeCN, 0.1% TFA at a flow rate of 0.25 ml/min. Small fractions (1/200) of the eluates were analyzed by LC-MS/MS. Data were searched (as described later) allowing phosphorylation in serine, threonine and tyrosine as variable modifications, to assess the enrichment in phosphopeptides on the eluates. 80% of all peptides identified were phosphorylated. Both eluates of the DMSO treated samples were pulled together, and the same was done for the acute and for the chronic rapamycin-treated samples. Peptide amounts in the eluates were estimated based on absorbance at 280 nm, using a nanodrop system (Thermo Scientific). The 3 samples (DMSO, acute, chronic) where then solvent evaporated in a speed vac system, and stored at -20 ºC until iTRAQ labelling.

Isobaric tagging for relative and absolute quantitation (i-TRAQ) labeling: iTRAQ® labeling (AB Sciex) was performed as follows: 80 µg of the TiO_2 eluate for each sample were resuspended in 20 µl of iTRAQ dissolution buffer (0.5M triethylammonium bicarbonate). iTRAQ labeling reagents were reconstituted in 70 µl of ethanol, and added to the samples. Labeling was as follows: 114, DMSO; 115, acute rapamycin; 116, chronic rapamycin. The labeling reaction was performed for 1 h at 21 °C. An aliquot of each labeling reaction was then examined by LC-MS/MS and searched allowing iTRAQ as a variable modification to confirm that at least 99% of all peptides identified showed iTRAQ labeling. Another aliquot containing a combination 1:1:1 of the three labeled

samples was analyzed by LC-MS/MS to confirm that total peptide levels were similar in the 3 labeling reactions. The 3 labeling reactions were then combined, solvent evaporated and desalted using a Sep Pak as described earlier, solvent evaporated in a speed vac system, and stored at -20C until fractionation of the peptide mixture by high pH RP chromatography was performed.

High pH Reverse Phase Chromatography: iTRAQ labelled phosphopeptides were further separated by high pH reverse phase chromatography on an AKTA purifier with a 1 x 100mm Gemini 3um C18 column (Phenomenex). Peptides were loaded onto the column in 20mM NH4OH, pH 10 and eluted off the column over a gradient from 2% to 70% 20mM NH4OH, pH 10 in 90% MeCN. 70 fractions were collected and pooled to a total of 40 samples. Aliquots of each phosphoenriched sample was analyzed by LC-MS/MS after resuspension in 0.1% formic acid.

Nano-LC-ESI-Qq-TOF tandem mass spectrometry analysis: Peptides were loaded onto a 75 μm x 150 mm reverse phase C18 PepMap column (Dionex, LC Packings, San Francisco, CA) to be separated using an Agilent 1100 series HPLC system equipped with an auto sampler (Agilent Technologies, Palo Alto, CA). A 3 hour MeCN gradient (3–32%) in 0.1% formic acid was used at a flow rate of 300 nl/min. The LC eluate was coupled to a nano-ion spray source attached to a QSTAR Elite mass spectrometer (Applied Biosystems/MDS Sciex). Peptides were analyzed in positive ion mode. MS spectra were acquired between 350 and 1500 m/z for 0.4 s. For each MS spectrum, the two most intense multiple charged peaks were selected for collision-induced dissociation

(CID). Per precursor ion selected, two MS/MS were taken; the first one was acquired between 180 and 1500 m/z for 2.5 s with resolution set to low and an automatically collision-induced dissociation energy based upon peptide charge and m/z ratio. The second MS/MS was acquired between 112 and 119 m/z for 2.5 s with a resolution set to unit and a constant voltage of 65v, in order to maximize generation of iTRAQ reporter ions. A dynamic exclusion window was applied which prevented the same m/z from being selected for 1 min after its acquisition. Typical performance characteristics were 12000 resolution with 30 ppm mass measurement accuracy in both MS and MSMS spectra.

Peptide and protein identification and iTRAQ quantitation: QSTAR Elite data was analyzed with Analyst QS software (Applied Biosystems/MDS Sciex, Foster City, CA, USA) and MS/MS centroid peak lists were generated using the Mascot.dll script. Peak lists were searched against the Swissprot Homo Sapiens database as of March 21st 2012 (containing 20255 entries), using Protein Prospector version 5.8 (http://prospector.ucsf.edu) with the following parameters: Enzyme specificity was set as Trypsin and up to 2 missed cleavages per peptide were allowed. Carbamidomethylation of cysteine residues, and iTRAQ labeling of lysine residues and N-terminus of the protein were allowed as fixed modifications. N-acetylation of the N-terminus of the protein, loss of protein N-terminal methionine, pyroglutamate formation from of peptide N-terminal glutamines, oxidation of methionine and phosphorylation of serine, threonine and tyrosine were allowed as variable modifications. Search was done using a peptide tolerance for QSTAR data in MS and MS/MS mode of 100 ppm and 0.2 Da, respectively. Proteins were considered positively identified when at least one peptide with a Protein

Prospector peptide expectation value lower than 0.1 was identified. The false positive rate was estimated by searching the data using a concatenated database which contains the original SwissProt database, as well as a version of each original entry where the sequence has been randomized. Only unique peptides were considered; peptides common to several proteins were not used for quantitative analysis. Sequence ID and phosphorylation sites were manually confirmed for all peptides that showed significant changes in levels compared to DMSO control.

Relative quantization of peptide abundance was performed via calculation of the raw area of reporter ions corresponding to the different iTRAQ labels, (114.1, 115.1, and 116.1 m/z) present in MS/MS spectra. Peak areas were determined by Protein Prospector, and used to calculate acute vs DMSO or chronic vs DMSO relative levels (115.1/114.1 and 116.1/114.1 ratios). Spectra representing replicate measurements of the same peptide were used to calculate the dispersion and the significance threshold for the analysis.

Drug treatment. Rapamycin was purchased from LC Laboratories. The GSK3B inhibitor Chir99021, the CDK4/6 inhibitor PD0332991, the PKA inhibitor H89, the MYC inhibitor JQ1, the CDC2 inhibitor Roscovitine, were purchased from Selleckchem. The CTNNB1 inhibitor, CCT031347 was purchased from Tocris Bioscience. The MEK inhibitor Selumetinib was purchased from Medchem Express. NVP-BEZ235 (Novartis) was administered at 10nM. In vitro drug titrations were performed in 96 well plates, 5 thousand cells/well, treated with a titration of drugs and then live cells were counted after 5-7 Days. The drugs were administered to a final concentration of 0.1% DMSO. Live cells were counted using Dojindo Cell Counting Kit8 (Dojindo, Rockville, Maryland,

http://www.dojindo.com). These values were normalized to DMSO treated controls and the IC50 was calculated. Dose dependent curves, IC50, and fitted lines were generated using Graphpad Prizm software (Graphpad). For confirmation purposes and for some cell growth curves, cells were counted from flasks using the Countess automated cell counter and trypan blue exclusion.

KEA analysis: Kinase Enrichment Analysis (KEA)(http://amp.pharm.mssm.edu/lib/kea.jsp) (Lachmann and Ma'ayan, 2009)was utilized to determine candidate kinases that were associated with our list proteins with phosphorylation changes under chronic Rapamycin conditions.

Western Blots: Western blots were performed using beta actin (Abcam) as an internal control. The primary antibodies used were rabbit anti GSK3B (Cell Signaling), rabbit anti phospho-GSK3A/B (ser 21/9) (Cell Signaling), rabbit anti phospho-Rb1(S249) (Abcam), rabbit anti Beta Catenin(Cell Signaling), rabbit anti phospho-B-Catenin (Ser675) (Cell Signaling), rabbit anti pS6 (Cell Signaling), rabbit anti pAKT-S473 (Cell Signaling), rabbit anti pAKT-T-308 (Cell Signaling), rabbit anti RICTOR (Cell Signaling), rabbit anti RAPTOR (Cell Signaling), rabbit anti pERK1/2 (Cell Signaling) and rabbit anti total ERK (Cell Signaling), rabbit anti phospho-4EBP1(Thr37/46) (Cell Signaling), rabbit anti 4EBP1 (Cell Signaling), rabbit anti Survivin (Cell Signaling), rabbit anti phospho-NF-kB p65(ser468) (Cell Signaling). The secondary antibody used was HRP conjugated anti rabbit (Cell Signaling).

shRNA Knockdown: Plasmids with shRICTOR (Addgene plasmid 1853, David Sabatini, (Sarbassov et al., 2005)), shRAPTOR (Addgene plasmid 1857, David Sabatini,(Sarbassov et al., 2005)), shGSK3B#1 (Addgene plasmid 32496 , Alex Toker,(Yoeli-Lerner et al., 2009)), and shCTNNB1 (Addgene plasmid 18803, Bob Weinberg,(Onder et al., 2008)) constructs, cloned into pLKO expression vectors, were purchased from Addgene. Clones against:

MAP1B (Full hairpin sequence:
TGCTGTTGACAGTGAGCGCGGACTCCAGTTTATCACATAATAGTGAAGCCAC
AGATGTATTATGTGATAAACTGGAGTCCTTGCCTACTGCCTCGGA),

LMO7 (Full hairpin sequence:
TGCTGTTGACAGTGAGCGCGGATGATGCTTGGAAGTATAATAGTGAAGCCAC
AGATGTATTATACTTCCAAGCATCATCCATGCCTACTGCCTCGGA),

KHDRBS1(Full hairpin sequence:
TGCTGTTGACAGTGAGCGATTGGTACGTGGTACACCAGTATAGTGAAGCCAC
AGATGTATACTGGTGTACCACGTACCAAATGCCTACTGCCTCGGA),

PTK2 (Full hairpin sequence:
TGCTGTTGACAGTGAGCGACGATTGGAAACCAACATATATTAGTGAAGCCAC
AGATGTAATATATGTTGGTTTCCAATCGGTGCCTACTGCCTCGGA),

PRPF4B (Full hairpin sequence:
TGCTGTTGACAGTGAGCGAATGGAAGATGCTAATTCTGAATAGTGA
AGCCACAGATGTATTCAGAATTAGCATCTTCCATCTGCCTACTGCCTCGGA),

SNW1 (Full hairpinsequence:
TGCTGTTGACAGTGAGCGACCCGATGAAGAAGCTATTAAATA

GTGAAGCCACAGATGTATTTAATAGCTTCTTCATCGGGCTGCCTACTGCCTCG GA) were all from Dharmacon-Harmon library (General Electric: http://dharmacon.gelifesciences.com/shrna/gipz-lentiviral-shrna/?Parent=12884902157).

Overexpression: pLV-CTNNB1-deltaN90 , the lenti-viral mediated overexpression of constitutively active CTNNB1 (Beta Catenin) was purchased from Addgene (Plasmid #36985), submitted as a gift from Dr. Bob Weinberg. Lentiviral TOP-dGFP reporter was used as a Control expression of the pLV backbone, and purchased from Addgene (Plasmid 14715), submitted by Dr. Reya. Ctrl-PGipz was also used as an alternative control.

FLUC-GFP: Fluc=Firefely luciferase, GFP=green fluorescent protein from Auquorea (jellyfish). Fluc-GFP (backbone= pRRL-sinCMV-iresGFP) was produced by UCLA Vectorcore and supported by Molecular Technologies Core (IMTC) CURE/P30 DK41301-26.

In Vivo Subcutaneous Transplant of HK374 GBM cells: This was done as previously described (Chapter 3).

Optical Imaging:

Optical imaging was performed at the Crump Institute for Molecular Imaging at UCLA. Mice were anesthetized by inhalation of isoflurane. Intraperitoneal injection of

100uL of luciferin (30mg/ml) was followed by 10 minutes of live uptake to interact with the luciferase expressing HK374 FLUC-GFP cells and produce bioluminescence. The IVIS Lumina 2 imaging system (Caliper life sciences) was utilized for in vivo bioluminescent imaging. A photograph of the mice is overlaid with a color scale of a region of interest representing total flux (photon/second) and quantified with the LivingImage software package (Xenogen Corporation, Alameda, Calif.).

Statistics. Summary statistics were performed using Anova followed by post-hoc Student T tests as implemented by Stata 8.0 software (StataCorp) or Prism5 (GraphPad Software). In certain cases, Welch's correction for unequal variances was utilized. In other cases, the non-parametric test, Mann-Whitney was employed. Synergy was determined by comparing the observed combinatorial dose to the theoretical combined calculation which is =100/(1+(100-Drug 1)/Drug 1 + (100-Drug 2)/Drug2 where Drug1 and Drug2 represent the observed survival for each dosage in the combinatorial treatment(Chou and Talalay, 1984).

Targeted shRNA screen: We performed targeted shRNA screens against 50/52 candidates that underwent phosphorylation changes in chronic Rapamycin and were associated with GSK3B. The remaining 2/52 genes were not in our shRNA library. HK301 glioblastoma cells were grown on 384 well plates (1000 cells/well) for 3 days with each shRNA. After 3 days. Cells were treated with and without 100nM Rapamycin. Cells were retreated with agent after another 3 days. After the initial treatment, cells were grown for 7 days. Cell number was determined using CellTiter-Glo 3D (Promega), which estimates cell number

based on measured ATP levels. Significant hits, or candidate genes were selected if their knockdowns significantly increased or decreased cell number in the presence of Rapamycin as compared to the DMSO treated controls. We chose a cutoff Z-score of >=2 or <=-2 to select candidates. Proteins that promote resistance to Rapamycin should show enhanced sensitivity to Rapamycin upon knockdown, those that promote sensitivity should show diminished sensitivity to Rapamicin upon knockdown. Candidates were validated by separate shRNA infection experiments wherein cell number was assessed after 7 days of proliferation in a titration of Rapamycin, BEZ-235, or DMSO controls. Cell number was assessed with Dojindo Kit-8 and absorbance at 450nM. IC50 values were compared using GraphPad Prism software that employed the extra sum of squares F-test to generate a P-value. A $P<0.01$ was chosen as a cutoff for significance to adjust for multiple comparisons.

We also utilized Image Express to image GFP expression of the tagged constructs. We imaged the proliferation of the cells after 0,3, 7, and 10 days post treatment.

In Vivo Orthotopic Xenotransplantation: 100 thousand HK301 FLUC-GFP cells (infected by lentivirus to constitutively express luciferase-green fluorescent protein) that were also either pLKO control infected or shGSK3B infected were each injected into the striatum of 8 male, 2 month old, nod scid gamma null mice. Injections were carried out as previously described(Laks et al., 2009). Mice were imaged for bioluminescent signals from the luciferase expressing GBM cells every two weeks in order to detect nascent tumor formation. After 4 weeks, when intracranial tumors were detected by optical

imaging, each of the two cell types, Ctrl-pLKO or shGSK3B were treated with daily intraperitoneal injections of either DMSO or 5mg/Kg Rapamycin (LC Laboratories # R-5000). Thus there were 4 distinct groups: Group 1 = Control + DMSO, Group 2= Control + Rapamycin, Group 3= shGSK3B + Rapamycin, Group 4= shGSK3B + DMSO. Every week of therapeutic treatment, tumors were imaged for bioluminescent intensity to determine tumor size.

Chapter 5

Summary and Perspectives

Informing Therapeutic Strategies

It is possible to use cancer cells as model purely to explore basic biology and signaling pathways. However, the research presented here is part of a broader effort to inform therapeutic strategies in the treatment of GBM. To this end, this study has achieved several important insights that coalesce into a combinatorial therapeutic strategy. This study has found that dual targeting of ERK and mTOR results in a sensitization effect in a vast majority of patient derived tumorsphere cultures. Therefore, this treatment strategy may widely applicable to the treatment of GBM tumors.

We discovered that phosphorylation dependent GSK3B inhibition is a mode of adaptive resistance to chronic mTOR inhibition. Therapeutic inhibition of GSK3B would be counter-productive as its attenuation confers resistance to Rapamycin. Although we found a role for MAP1B in mediating this resistance to mTOR inhibition, MAP1B may not be a suitable target for therapy as it is a necessary component of axons and other vital neuronal projections. However, the role of MAP1B outside of axons is very limited and our data provide compelling evidence that MAP1B may have crucial roles apart from their known functions in axonal remodeling. In contrast, preventing GSK3B phosphorylation may be an effective strategy to prevent Rapamycin resistance. GSK3B may be phosphorylated through ERK or AKT and our data suggest that either kinase may

be involved in the GBM response to chronic Rapamycin in different GBM cultures. These results present further evidence for the rational behind combinatorial targeting of mTOR and ERK as this approach may abrogate the inhibitory phosphorylation of GSK3B that leads to Rapamycin resistance. Indeed, in our in vivo subcutaneous model, our data suggest that ERK may be responsible for GSK3B phosphorylation while AKT, which is inhibited by chronic Rapamycin, is less likely to play a role.

Selumetinib has drawbacks in that it does not target ERK5, but only ERK1/2(Yeh et al., 2007). Other inhibitors of ERK1/2, such as PD98059 and UO126, inhibit both ERK1/2 and ERK5 and this may improve treatment as our analysis has shown that ERK5, along with ERK1/2, is associated with resistance to mTOR inhibition. For example, ERK5 can bind to RSK, which, in turn, can phosphorylate GSK3B(Ranganathan et al., 2006). Therefore, our study results suggest that a more universal MEK/ERK inhibitor, such as PD98059, or UO126, which target both ERK1/2 and ERK5, may be more efficacious than Selumetinib at overcoming resistance to Rapamycin.

Assessment of Tumorspheres

Our analysis of mRNA expression patterns in tumorsphere cultures indicates that this approach may be informative for discovering novel determinants of proliferation. However, classification of tumorspheres based on expression is less informative with regards to predicting survival, in vitro phenotypes, response to treatment, and even classification of the parent tumor. Bulk tumorsphere cultures are suitable in respect to

harboring a complex heterogeneity of different clonal BTSC that may represent a faithful model of how brain tumors respond to treatment and develop tumors in vivo. However, this heterogeneity may also impede proper classification of BTSC, accurate diagnosis of brain tumors, and design of personalized therapy.

A Reductionist Strategy to Dismantle a Complex Adaptive System

Studies have demonstrated that GBM tumors contain a heterogeneous population of tumor cells, both in terms of karyotype, mutation status, receptor kinases, and mRNA expression patterns (Little et al., 2012; Piccirillo et al., 2009; Shapiro et al., 1981; Snuderl et al., 2011; Sottoriva et al., 2013; Szerlip et al., 2012). While studies have consistently indicated that clonal heterogeneity derives from a common precursor cell, distinct BTSC clones evolve into distinct genetic subtypes that have been shown to have different tumorigenic properties and differential sensitivity to therapy(Meyer et al., 2015b; Piccirillo et al., 2015). Furthermore, tumor heterogeneity manifests itself in tumor recurrences that are distinct from the initial tumor and that adapt, clonally, to drug treatment(Johnson et al., 2014; Nickel et al., 2012). This suggests that there is clonal adaptation or clonal evolution to the initial treatment, and heterogeneity may thereby create a complex adaptive system, with inter-clone interactions, that is refractory to conventional treatments(Bonavia et al., 2011; Greaves and Maley, 2012; Laks et al., 2010). Treatment which targets one BTSC may be overcome by the proliferation of another, resistant BTSC within the same tumor or culture.

I propose a novel strategy for the diagnosis and treatment of brain tumors that dismantles each brain tumor from a complex adaptive system into its component parts for diagnosis, research, and treatment. For diagnosis, each brain tumor would be biopsied at multiple locations and each biopsy would be characterized for gene expression, preferably by single cell RNA-Seq. Major mutations would also be characterized. The resultant data would be compared to a database of clonal brain tumor samples. This procedure would determine how many BTSC exist within the tumor. Therapy would engage specific targeting of each distinct BTSC within the patient tumor.

In the research and development arm of this strategy, brain tumor derived tumorsphere cultures would be separated into multiple single cell, clonally derived subgroups. Each clonal subgroup of each different tumor derived culture would then be clustered based on gene expression. This clustering will define how many subgroups of BTSC exist. The problem with current methods for classification is that classification is performed on bulk cultures or bulk tumors which may mask the signatures of minority BTSC populations, conflate several signatures into one compiled signature that does not reflect any one BTSC, or may simply reflect the majority population of BTSC. An example of such error is in color perception. We may perceive the color orange when in reality the colors red and yellow are overlapped. In such a manner, characterizing bulk cultures or bulk tumors may cluster in one manner, when in reality that specific cluster is composed of two or three distinct clonal BTSC clusters. Once the clonal populations of tumorsphere cultures are characterized, their expression profiles and mutation status can be assessed in order to determine which pathways are activated. This will inform targeted therapeutic intervention for each subtype of clonal BTSC.

A screen of targeted therapy will be performed on these clonal populations of BTSC in order to determine which BTSC are most sensitive to which therapies. Once this is completed, there will be a procedure for how to target each specific BTSC. This information will be merged with the multiple tumor biopsy approach for clonal diagnosis. In this manner, each BTSC within the tumor will be targeted in a combinatorial therapeutic approach. This may require combinations of numerous drugs and these combinations can be tested on appropriate combinations of BTSC clonal cell cultures in order to determine dosages and efficacy.

This reductionist approach will deconstruct the complex adaptive system of glioblastoma into its component parts and serve to delineate a suitable course of treatment, tailored to each patient's needs. This approach may lead to a definitive classification of BTSC that is predictive of patient survival and response to treatment. In addition, it may clarify how many different BTSC commonly exist within a given tumor.

References.

Akhavan, D., Cloughesy, T.F., and Mischel, P.S. (2010). mTOR signaling in glioblastoma: lessons learned from bench to bedside. Neuro-oncology *12*, 882-889.

Albert, L., Karsy, M., Murali, R., and Jhanwar-Uniyal, M. (2009). Inhibition of mTOR Activates the MAPK Pathway in Glioblastoma Multiforme. Cancer Genomics Proteomics *6*, 255-261.

Alcantara Llaguno, S., Chen, J., Kwon, C.H., Jackson, E.L., Li, Y., Burns, D.K., Alvarez-Buylla, A., and Parada, L.F. (2009). Malignant astrocytomas originate from neural stem/progenitor cells in a somatic tumor suppressor mouse model. Cancer cell *15*, 45-56.

Androutsellis-Theotokis, A., Leker, R.R., Soldner, F., Hoeppner, D.J., Ravin, R., Poser, S.W., Rueger, M.A., Bae, S.K., Kittappa, R., and McKay, R.D. (2006). Notch signalling regulates stem cell numbers in vitro and in vivo. Nature *442*, 823-826.

Ashby, W. (1958). Requisite variety and its implications for the control of complex systems, Vol 1:2.

Axelrod, R., Axelrod, D.E., and Pienta, K.J. (2006). Evolution of cooperation among tumor cells. Proceedings of the National Academy of Sciences of the United States of America *103*, 13474-13479.

Benjamini, Y., and Hochberg, Y. (1995). Controlling the false discovery rate: a practical and powerful approach to multiple testing. Journal of the Royal Statistical Society Series B *57*, 289–300.

Benson, V.S., Pirie, K., Schuz, J., Reeves, G.K., Beral, V., Green, J., and Million Women Study, C. (2013). Mobile phone use and risk of brain neoplasms and other cancers: prospective study. Int J Epidemiol *42*, 792-802.

Bhat, K.P., Balasubramaniyan, V., Vaillant, B., Ezhilarasan, R., Hummelink, K., Hollingsworth, F., Wani, K., Heathcock, L., James, J.D., Goodman, L.D.*, et al.* (2013). Mesenchymal differentiation mediated by NF-kappaB promotes radiation resistance in glioblastoma. Cancer cell *24*, 331-346.

Binda, E., Visioli, A., Giani, F., Lamorte, G., Copetti, M., Pitter, K.L., Huse, J.T., Cajola, L., Zanetti, N., DiMeco, F.*, et al.* (2012). The EphA2 receptor drives self-renewal and tumorigenicity in stem-like tumor-propagating cells from human glioblastomas. Cancer cell *22*, 765-780.

Bjornsti, M.A., and Houghton, P.J. (2004). The TOR pathway: a target for cancer therapy. Nature reviews Cancer *4*, 335-348.

Bonavia, R., Inda, M.M., Cavenee, W.K., and Furnari, F.B. (2011). Heterogeneity maintenance in glioblastoma: a social network. Cancer research *71*, 4055-4060.

Brennan, C.W., Verhaak, R.G., McKenna, A., Campos, B., Noushmehr, H., Salama, S.R., Zheng, S., Chakravarty, D., Sanborn, J.Z., Berman, S.H.*, et al.* (2013). The somatic genomic landscape of glioblastoma. Cell *155*, 462-477.

Brown, E.J., Albers, M.W., Shin, T.B., Ichikawa, K., Keith, C.T., Lane, W.S., and Schreiber, S.L. (1994). A mammalian protein targeted by G1-arresting rapamycin-receptor complex. Nature *369*, 756-758.

Buckner, J.C., Brown, P.D., O'Neill, B.P., Meyer, F.B., Wetmore, C.J., and Uhm, J.H. (2007). Central nervous system tumors. Mayo Clin Proc *82*, 1271-1286.

Calabrese, C., Poppleton, H., Kocak, M., Hogg, T.L., Fuller, C., Hamner, B., Oh, E.Y., Gaber, M.W., Finklestein, D., Allen, M.*, et al.* (2007). A perivascular niche for brain tumor stem cells. Cancer cell *11*, 69-82.

Carracedo, A., Baselga, J., and Pandolfi, P.P. (2008). Deconstructing feedback-signaling networks to improve anticancer therapy with mTORC1 inhibitors. Cell Cycle *7*, 3805-3809.

Chabner, B.A., and Roberts, T.G., Jr. (2005). Timeline: Chemotherapy and the war on cancer. Nature reviews Cancer *5*, 65-72.

Chan, S.M., Weng, A.P., Tibshirani, R., Aster, J.C., and Utz, P.J. (2007). Notch signals positively regulate activity of the mTOR pathway in T-cell acute lymphoblastic leukemia. Blood *110*, 278-286.

Chen, J., Li, Y., Yu, T.S., McKay, R.M., Burns, D.K., Kernie, S.G., and Parada, L.F. (2012). A restricted cell population propagates glioblastoma growth after chemotherapy. Nature *488*, 522-526.

Chen, J.C., Alvarez, M.J., Talos, F., Dhruv, H., Rieckhof, G.E., Iyer, A., Diefes, K.L., Aldape, K., Berens, M., Shen, M.M.*, et al.* (2014). Identification of Causal Genetic Drivers of Human Disease through Systems-Level Analysis of Regulatory Networks. Cell *159*, 402-414.

Chiu, M.I., Katz, H., and Berlin, V. (1994). RAPT1, a mammalian homolog of yeast Tor, interacts with the FKBP12/rapamycin complex. Proceedings of the National Academy of Sciences of the United States of America *91*, 12574-12578.

Choe, G., Horvath, S., Cloughesy, T.F., Crosby, K., Seligson, D., Palotie, A., Inge, L., Smith, B.L., Sawyers, C.L., and Mischel, P.S. (2003). Analysis of the phosphatidylinositol 3'-kinase signaling pathway in glioblastoma patients in vivo. Cancer research *63*, 2742-2746.

Chou, T.C., and Talalay, P. (1984). Quantitative analysis of dose-effect relationships: the combined effects of multiple drugs or enzyme inhibitors. Adv Enzyme Regul *22*, 27-55.

Cloughesy, T.F., Yoshimoto, K., Nghiemphu, P., Brown, K., Dang, J., Zhu, S., Hsueh, T., Chen, Y., Wang, W., Youngkin, D.*, et al.* (2008). Antitumor activity of rapamycin in a Phase I trial for patients with recurrent PTEN-deficient glioblastoma. PLoS Med *5*, e8.

Coppola, G. (2011). Designing, performing, and interpreting a microarray-based gene expression study. Methods in molecular biology *793*, 417-439.

Cross, D.A., Alessi, D.R., Cohen, P., Andjelkovich, M., and Hemmings, B.A. (1995). Inhibition of glycogen synthase kinase-3 by insulin mediated by protein kinase B. Nature *378*, 785-789.

Cusulin, C., Chesnelong, C., Bose, P., Bilenky, M., Kopciuk, K., Chan, J.A., Cairncross, J.G., Jones, S.J., Marra, M.A., Luchman, H.A.*, et al.* (2015). Precursor States of Brain Tumor Initiating Cell Lines Are Predictive of Survival in Xenografts and Associated with Glioblastoma Subtypes. Stem cell reports.

Dabney, A.R. (2006). ClaNC: point-and-click software for classifying microarrays to nearest centroids. Bioinformatics *22*, 122-123.

Dahlstrand, J., Collins, V.P., and Lendahl, U. (1992). Expression of the class VI intermediate filament nestin in human central nervous system tumors. Cancer research *52*, 5334-5341.

Daumas-Duport, C., Scheithauer, B., O'Fallon, J., and Kelly, P. (1988). Grading of astrocytomas. A simple and reproducible method. Cancer *62*, 2152-2165.

Day, B.W., Stringer, B.W., Al-Ejeh, F., Ting, M.J., Wilson, J., Ensbey, K.S., Jamieson, P.R., Bruce, Z.C., Lim, Y.C., Offenhauser, C.*, et al.* (2013). EphA3 maintains tumorigenicity and is a therapeutic target in glioblastoma multiforme. Cancer cell *23*, 238-248.

Dean, M., Fojo, T., and Bates, S. (2005). Tumour stem cells and drug resistance. Nature reviews Cancer *5*, 275-284.

deCarvalho, A.C., Nelson, K., Lemke, N., Lehman, N.L., Arbab, A.S., Kalkanis, S., and Mikkelsen, T. (2010). Gliosarcoma stem cells undergo glial and mesenchymal differentiation in vivo. Stem cells *28*, 181-190.

Deltour, I., Johansen, C., Auvinen, A., Feychting, M., Klaeboe, L., and Schuz, J. (2009). Time trends in brain tumor incidence rates in Denmark, Finland, Norway, and Sweden, 1974-2003. J Natl Cancer Inst *101*, 1721-1724.

Deorah, S., Lynch, C.F., Sibenaller, Z.A., and Ryken, T.C. (2006). Trends in brain cancer incidence and survival in the United States: Surveillance, Epidemiology, and End Results Program, 1973 to 2001. Neurosurg Focus *20*, E1.

Dibble, C.C., and Manning, B.D. (2013). Signal integration by mTORC1 coordinates nutrient input with biosynthetic output. Nat Cell Biol *15*, 555-564.

Dolecek, T.A., Propp, J.M., Stroup, N.E., and Kruchko, C. (2012). CBTRUS statistical report: primary brain and central nervous system tumors diagnosed in the United States in 2005-2009. Neuro-oncology *14 Suppl 5*, v1-49.

Efeyan, A., and Sabatini, D.M. (2009). mTOR and cancer: many loops in one pathway. Curr Opin Cell Biol.

Ene, C.I., and Holland, E.C. (2015). Personalized medicine for gliomas. Surg Neurol Int *6*, S89-95.

Fan, X., Matsui, W., Khaki, L., Stearns, D., Chun, J., Li, Y.M., and Eberhart, C.G. (2006). Notch pathway inhibition depletes stem-like cells and blocks engraftment in embryonal brain tumors. Cancer research *66*, 7445-7452.

Feldman, M.E., Apsel, B., Uotila, A., Loewith, R., Knight, Z.A., Ruggero, D., and Shokat, K.M. (2009). Active-site inhibitors of mTOR target rapamycin-resistant outputs of mTORC1 and mTORC2. PLoS Biol *7*, e38.

Feng, H., Hu, B., Vuori, K., Sarkaria, J.N., Furnari, F.B., Cavenee, W.K., and Cheng, S.Y. (2014). EGFRvIII stimulates glioma growth and invasion through PKA-dependent serine phosphorylation of Dock180. Oncogene *33*, 2504-2512.

Fisher, J.L., Schwartzbaum, J.A., Wrensch, M., and Wiemels, J.L. (2007). Epidemiology of brain tumors. Neurol Clin *25*, 867-890, vii.

Furnari, F.B., Fenton, T., Bachoo, R.M., Mukasa, A., Stommel, J.M., Stegh, A., Hahn, W.C., Ligon, K.L., Louis, D.N., Brennan, C.*, et al.* (2007). Malignant astrocytic glioma: genetics, biology, and paths to treatment. Genes & development *21*, 2683-2710.

Gaiano, N., and Fishell, G. (2002). The role of notch in promoting glial and neural stem cell fates. Annu Rev Neurosci *25*, 471-490.

Gallagher, W.M., Argentini, M., Sierra, V., Bracco, L., Debussche, L., and Conseiller, E. (1999). MBP1: a novel mutant p53-specific protein partner with oncogenic properties. Oncogene *18*, 3608-3616.

Galli, R., Binda, E., Orfanelli, U., Cipelletti, B., Gritti, A., De Vitis, S., Fiocco, R., Foroni, C., Dimeco, F., and Vescovi, A. (2004). Isolation and characterization of tumorigenic, stem-like neural precursors from human glioblastoma. Cancer research *64*, 7011-7021.

Gallia, G.L., Tyler, B.M., Hann, C.L., Siu, I.M., Giranda, V.L., Vescovi, A.L., Brem, H., and Riggins, G.J. (2009). Inhibition of Akt inhibits growth of glioblastoma and glioblastoma stem-like cells. Molecular cancer therapeutics *8*, 386-393.

Garcia-Perez, J., Avila, J., and Diaz-Nido, J. (1998). Implication of cyclin-dependent kinases and glycogen synthase kinase 3 in the phosphorylation of microtubule-associated protein 1B in developing neuronal cells. Journal of neuroscience research *52*, 445-452.

Gilbertson, R.J., and Rich, J.N. (2007). Making a tumour's bed: glioblastoma stem cells and the vascular niche. Nature reviews Cancer *7*, 733-736.

Greaves, M., and Maley, C.C. (2012). Clonal evolution in cancer. Nature *481*, 306-313.

Grimes, C.A., and Jope, R.S. (2001). The multifaceted roles of glycogen synthase kinase 3beta in cellular signaling. Progress in neurobiology *65*, 391-426.

Grizzi, F., and Chiriva-Internati, M. (2005). The complexity of anatomical systems. Theor Biol Med Model *2*, 26.

Grizzi, F., and Chiriva-Internati, M. (2006). Cancer: looking for simplicity and finding complexity. Cancer Cell Int *6*, 4.

Gunther, H.S., Schmidt, N.O., Phillips, H.S., Kemming, D., Kharbanda, S., Soriano, R., Modrusan, Z., Meissner, H., Westphal, M., and Lamszus, K. (2008). Glioblastoma-derived stem cell-enriched cultures form distinct subgroups according to molecular and phenotypic criteria. Oncogene *27*, 2897-2909.

Hadjipanayis, C.G., and Van Meir, E.G. (2009). Brain cancer propagating cells: biology, genetics and targeted therapies. Trends Mol Med *15*, 519-530.

Hambardzumyan, D., Becher, O.J., and Holland, E.C. (2008). Cancer stem cells and survival pathways. Cell Cycle *7*, 1371-1378.

Harrington, D.P., and Fleming, T. R. (1982). A class of rank test procedures for censored survival data. Biometrika *69*, 553-566.

Hecht, A., Vleminckx, K., Stemmler, M.P., van Roy, F., and Kemler, R. (2000). The p300/CBP acetyltransferases function as transcriptional coactivators of beta-catenin in vertebrates. The EMBO journal *19*, 1839-1850.

Hecht, B.K., Turc-Carel, C., Chatel, M., Grellier, P., Gioanni, J., Attias, R., Gaudray, P., and Hecht, F. (1995). Cytogenetics of malignant gliomas: I. The autosomes with reference to rearrangements. Cancer genetics and cytogenetics *84*, 1-8.

Hegi, M.E., Diserens, A.C., Gorlia, T., Hamou, M.F., de Tribolet, N., Weller, M., Kros, J.M., Hainfellner, J.A., Mason, W., Mariani, L.*, et al.* (2005). MGMT gene silencing and benefit from temozolomide in glioblastoma. N Engl J Med *352*, 997-1003.

Hemmati, H.D., Nakano, I., Lazareff, J.A., Masterman-Smith, M., Geschwind, D.H., Bronner-Fraser, M., and Kornblum, H.I. (2003). Cancerous stem cells can arise from pediatric brain tumors. Proceedings of the National Academy of Sciences of the United States of America *100*, 15178-15183.

Heppner, G.H. (1984). Tumor heterogeneity. Cancer research *44*, 2259-2265.

Hess, K.R., Broglio, K.R., and Bondy, M.L. (2004). Adult glioma incidence trends in the United States, 1977-2000. Cancer *101*, 2293-2299.

Hirschmann-Jax, C., Foster, A.E., Wulf, G.G., Nuchtern, J.G., Jax, T.W., Gobel, U., Goodell, M.A., and Brenner, M.K. (2004). A distinct "side population" of cells with high drug efflux capacity in human tumor cells. Proceedings of the National Academy of Sciences of the United States of America *101*, 14228-14233.

Hoang, B., Benavides, A., Shi, Y., Yang, Y., Frost, P., Gera, J., and Lichtenstein, A. (2012). The pp242 mammalian target of rapamycin (mTOR) inhibitor activates extracellular signal-regulated kinase (ERK) in multiple myeloma cells via a target of rapamycin complex 1 (TORC1)/eukaryotic translation initiation factor 4E (eIF-4E)/RAF pathway and activation is a mechanism of resistance. J Biol Chem.

Hoelzinger, D.B., Demuth, T., and Berens, M.E. (2007). Autocrine factors that sustain glioma invasion and paracrine biology in the brain microenvironment. J Natl Cancer Inst *99*, 1583-1593.

Horvath, S., Zhang, B., Carlson, M., Lu, K.V., Zhu, S., Felciano, R.M., Laurance, M.F., Freije, W., Qi, S., Lee, Y.*, et al.* (2006). Analysis of Oncogenic Signaling Networks in Glioblastoma Identifies ASPM as a Novel Molecular Target. Proceedings of the National Academy of Sciences of the United States of America *in Press*.

Hosoi, H., Dilling, M.B., Liu, L.N., Danks, M.K., Shikata, T., Sekulic, A., Abraham, R.T., Lawrence, J.C., Jr., and Houghton, P.J. (1998). Studies on the mechanism of resistance to rapamycin in human cancer cells. Mol Pharmacol *54*, 815-824.

Hosokawa, N., Hara, T., Kaizuka, T., Kishi, C., Takamura, A., Miura, Y., Iemura, S., Natsume, T., Takehana, K., Yamada, N.*, et al.* (2009). Nutrient-dependent mTORC1 association with the ULK1-Atg13-FIP200 complex required for autophagy. Mol Biol Cell *20*, 1981-1991.

Hsieh, A.C., Costa, M., Zollo, O., Davis, C., Feldman, M.E., Testa, J.R., Meyuhas, O., Shokat, K.M., and Ruggero, D. (2010). Genetic dissection of the oncogenic mTOR pathway reveals druggable addiction to translational control via 4EBP-eIF4E. Cancer cell *17*, 249-261.

Ignatova, T.N., Kukekov, V.G., Laywell, E.D., Suslov, O.N., Vrionis, F.D., and Steindler, D.A. (2002). Human cortical glial tumors contain neural stem-like cells expressing astroglial and neuronal markers in vitro. Glia *39*, 193-206.

Irizarry, R.A., Bolstad, B.M., Collin, F., Cope, L.M., Hobbs, B., and Speed, T.P. (2003). Summaries of Affymetrix GeneChip probe level data. Nucleic acids research *31*, e15.

Ivanova, N.B., Dimos, J.T., Schaniel, C., Hackney, J.A., Moore, K.A., and Lemischka, I.R. (2002). A stem cell molecular signature. Science *298*, 601-604.

Johnson, B.E., Mazor, T., Hong, C., Barnes, M., Aihara, K., McLean, C.Y., Fouse, S.D., Yamamoto, S., Ueda, H., Tatsuno, K.*, et al.* (2014). Mutational analysis reveals the origin and therapy-driven evolution of recurrent glioma. Science *343*, 189-193.

Johnson, W.E., Li, C., and Rabinovic, A. (2007). Adjusting batch effects in microarray expression data using empirical Bayes methods. Biostatistics *8*, 118-127.

Jones, A.M., and Nuhse, T.S. (2011). Phosphoproteomics using iTRAQ. Methods in molecular biology *779*, 287-302.

Jordan, C.T., Guzman, M.L., and Noble, M. (2006). Cancer stem cells. N Engl J Med *355*, 1253-1261.

Juengel, E., Vogt, A., Makarevic, J., Wiesner, C., Tsaur, I., Bartsch, G., Haferkamp, A., and Blaheta, R.A. (2012). Acetylation of histone H3 prevents resistance development caused by chronic mTOR inhibition in renal cell carcinoma cells. Cancer Lett.

Jukich, P.J., McCarthy, B.J., Surawicz, T.S., Freels, S., and Davis, F.G. (2001). Trends in incidence of primary brain tumors in the United States, 1985-1994. Neuro-oncology *3*, 141-151.

Khalil, A.A., Jameson, M.J., Broaddus, W.C., Lin, P.S., Dever, S.M., Golding, S.E., Rosenberg, E., Valerie, K., and Chung, T.D. (2013). The Influence of Hypoxia and pH on Bioluminescence Imaging of Luciferase-Transfected Tumor Cells and Xenografts. International journal of molecular imaging *2013*, 287697.

Kitano, H. (2004). Cancer as a robust system: implications for anticancer therapy. Nature reviews Cancer *4*, 227-235.

Kitano, H. (2007). A robustness-based approach to systems-oriented drug design. Nat Rev Drug Discov *6*, 202-210.

Kleihues, P., Louis, D.N., Scheithauer, B.W., Rorke, L.B., Reifenberger, G., Burger, P.C., and Cavenee, W.K. (2002). The WHO classification of tumors of the nervous system. Journal of neuropathology and experimental neurology *61*, 215-225; discussion 226-219.

Koo, J., Wang, X., Owonikoko, T.K., Ramalingam, S.S., Khuri, F.R., and Sun, S.Y. (2015). GSK3 is required for rapalogs to induce degradation of some oncogenic proteins and to suppress cancer cell growth. Oncotarget.

Koo, J., Yue, P., Gal, A.A., Khuri, F.R., and Sun, S.Y. (2014). Maintaining glycogen synthase kinase-3 activity is critical for mTOR kinase inhibitors to inhibit cancer cell growth. Cancer research *74*, 2555-2568.

Lachmann, A., and Ma'ayan, A. (2009). KEA: kinase enrichment analysis. Bioinformatics *25*, 684-686.

Laks, D.R., Masterman-Smith, M., Visnyei, K., Angenieux, B., Orozco, N.M., Foran, I., Yong, W.H., Vinters, H.V., Liau, L.M., Lazareff, J.A*., et al.* (2009). Neurosphere formation is an independent predictor of clinical outcome in malignant glioma. Stem cells *27*, 980-987.

Laks, D.R., Visnyei, K., and Kornblum, H.I. (2010). Brain tumor stem cells as therapeutic targets in models of glioma. Yonsei medical journal *51*, 633-640.

Langfelder, P., Zhang, B., and Horvath, S. (2008). Defining clusters from a hierarchical cluster tree: the Dynamic Tree Cut package for R. Bioinformatics *24*, 719-720.

Lathia, J.D., Mack, S.C., Mulkearns-Hubert, E.E., Valentim, C.L., and Rich, J.N. (2015). Cancer stem cells in glioblastoma. Genes & development *29*, 1203-1217.

Lee, J., Kotliarova, S., Kotliarov, Y., Li, A., Su, Q., Donin, N.M., Pastorino, S., Purow, B.W., Christopher, N., Zhang, W*., et al.* (2006). Tumor stem cells derived from glioblastomas cultured in bFGF and EGF more closely mirror the phenotype and genotype of primary tumors than do serum-cultured cell lines. Cancer cell *9*, 391-403.

Li, Z., Wang, H., Eyler, C.E., Hjelmeland, A.B., and Rich, J.N. (2009). Turning cancer stem cells inside out: an exploration of glioma stem cell signaling pathways. J Biol Chem *284*, 16705-16709.

Little, S.E., Popov, S., Jury, A., Bax, D.A., Doey, L., Al-Sarraj, S., Jurgensmeier, J.M., and Jones, C. (2012). Receptor tyrosine kinase genes amplified in glioblastoma exhibit a mutual exclusivity in variable proportions reflective of individual tumor heterogeneity. Cancer research *72*, 1614-1620.

Liu, C., Li, Y., Semenov, M., Han, C., Baeg, G.H., Tan, Y., Zhang, Z., Lin, X., and He, X. (2002). Control of beta-catenin phosphorylation/degradation by a dual-kinase mechanism. Cell *108*, 837-847.

Liu, Y., Sun, S.Y., Owonikoko, T.K., Sica, G., Curran, W.J., Khuri, F.R., and Deng, X. (2011). Rapamycin Induces Bad Phosphorylation in Association with Its Resistance to Human Lung Cancer Cells. Molecular cancer therapeutics.

Loeb, L.A. (2001). A mutator phenotype in cancer. Cancer research *61*, 3230-3239.

Louis, D.N., Ohgaki, H., Wiestler, O.D., Cavenee, W.K., Burger, P.C., Jouvet, A., Scheithauer, B.W., and Kleihues, P. (2007). The 2007 WHO classification of tumours of the central nervous system. Acta Neuropathol *114*, 97-109.

Lu, C., and Shervington, A. (2008). Chemoresistance in gliomas. Mol Cell Biochem *312*, 71-80.

Lucas, F.R., Goold, R.G., Gordon-Weeks, P.R., and Salinas, P.C. (1998). Inhibition of GSK-3beta leading to the loss of phosphorylated MAP-1B is an early event in axonal remodelling induced by WNT-7a or lithium. Journal of cell science *111 (Pt 10)*, 1351-1361.

Luo, J., Wang, X., Xia, Z., Yang, L., Ding, Z., Chen, S., Lai, B., and Zhang, N. (2015). Transcriptional factor specificity protein 1 (SP1) promotes the proliferation of glioma cells by up-regulating midkine (MDK). Mol Biol Cell *26*, 430-439.

Luwor, R.B., Stylli, S.S., and Kaye, A.H. (2013). The role of Stat3 in glioblastoma multiforme. Journal of clinical neuroscience : official journal of the Neurosurgical Society of Australasia *20*, 907-911.

Ma, J., Meng, Y., Kwiatkowski, D.J., Chen, X., Peng, H., Sun, Q., Zha, X., Wang, F., Wang, Y., Jing, Y.*, et al.* (2010). Mammalian target of rapamycin regulates murine and human cell differentiation through STAT3/p63/Jagged/Notch cascade. J Clin Invest *120*, 103-114.

Maira, S.M., Stauffer, F., Schnell, C., and Garcia-Echeverria, C. (2009). PI3K inhibitors for cancer treatment: where do we stand? Biochem Soc Trans *37*, 265-272.

Meyer, M., Reimand, J., Lan, X., Head, R., Zhu, X., Kushida, M., Bayani, J., Pressey, J.C., Lionel, A.C., Clarke, I.D.*, et al.* (2015a). Single cell-derived clonal analysis of human glioblastoma links functional and genomic heterogeneity. Proc Natl Acad Sci U S A.

Meyer, M., Reimand, J., Lan, X., Head, R., Zhu, X., Kushida, M., Bayani, J., Pressey, J.C., Lionel, A.C., Clarke, I.D.*, et al.* (2015b). Single cell-derived clonal analysis of human glioblastoma links functional and genomic heterogeneity. Proceedings of the National Academy of Sciences of the United States of America *112*, 851-856.

Miller, C.R., and Perry, A. (2007). Glioblastoma. Arch Pathol Lab Med *131*, 397-406.

Miller, D.G. (1980). On the nature of susceptibility to cancer. The presidential address. Cancer *46*, 1307-1318.

Mischel, P.S., and Cloughesy, T.F. (2003). Targeted molecular therapy of GBM. Brain Pathol *13*, 52-61.

Monje, P., Hernandez-Losa, J., Lyons, R.J., Castellone, M.D., and Gutkind, J.S. (2005). Regulation of the transcriptional activity of c-Fos by ERK. A novel role for the prolyl isomerase PIN1. The Journal of biological chemistry *280*, 35081-35084.

Mullighan, C.G., Phillips, L.A., Su, X., Ma, J., Miller, C.B., Shurtleff, S.A., and Downing, J.R. (2008). Genomic analysis of the clonal origins of relapsed acute lymphoblastic leukemia. Science *322*, 1377-1380.

Mungamuri, S.K., Yang, X., Thor, A.D., and Somasundaram, K. (2006). Survival signaling by Notch1: mammalian target of rapamycin (mTOR)-dependent inhibition of p53. Cancer research *66*, 4715-4724.

Nakada, M., Nambu, E., Furuyama, N., Yoshida, Y., Takino, T., Hayashi, Y., Sato, H., Sai, Y., Tsuji, T., Miyamoto, K.I.*, et al.* (2013). Integrin alpha3 is overexpressed in glioma stem-like cells and promotes invasion. British journal of cancer *108*, 2516-2524.

Nakano, I., and Kornblum, H.I. (2006). Brain tumor stem cells. Pediatr Res *59*, 54R-58R.

Nakano, I., Masterman-Smith, M., Saigusa, K., Paucar, A.A., Horvath, S., Shoemaker, L., Watanabe, M., Negro, A., Bajpai, R., Howes, A.*, et al.* (2007). Maternal embryonic leucine zipper kinase is a key regulator of the proliferation of malignant brain tumors, including brain tumor stem cells. Journal of neuroscience research.

Nakano, I., Paucar, A.A., Bajpai, R., Dougherty, J.D., Zewail, A., Kelly, T.K., Kim, K.J., Ou, J., Groszer, M., Imura, T.*, et al.* (2005). Maternal embryonic leucine zipper kinase (MELK) regulates multipotent neural progenitor proliferation. J Cell Biol *170*, 413-427.

Nathanson, D.A., Gini, B., Mottahedeh, J., Visnyei, K., Koga, T., Gomez, G., Eskin, A., Hwang, K., Wang, J., Masui, K.*, et al.* (2014). Targeted therapy resistance mediated by dynamic regulation of extrachromosomal mutant EGFR DNA. Science *343*, 72-76.

Ng, J.M., and Curran, T. (2011). The Hedgehog's tale: developing strategies for targeting cancer. Nature reviews Cancer *11*, 493-501.

Ng, S.S., Mahmoudi, T., Danenberg, E., Bejaoui, I., de Lau, W., Korswagen, H.C., Schutte, M., and Clevers, H. (2009). Phosphatidylinositol 3-kinase signaling does not activate the wnt cascade. J Biol Chem *284*, 35308-35313.

Nickel, G.C., Barnholtz-Sloan, J., Gould, M.P., McMahon, S., Cohen, A., Adams, M.D., Guda, K., Cohen, M., Sloan, A.E., and LaFramboise, T. (2012). Characterizing mutational heterogeneity in a glioblastoma patient with double recurrence. PloS one *7*, e35262.

Noushmehr, H., Weisenberger, D.J., Diefes, K., Phillips, H.S., Pujara, K., Berman, B.P., Pan, F., Pelloski, C.E., Sulman, E.P., Bhat, K.P.*, et al.* (2010). Identification of a CpG island methylator phenotype that defines a distinct subgroup of glioma. Cancer cell *17*, 510-522.

Nowell, P.C. (1976). The clonal evolution of tumor cell populations. Science *194*, 23-28.

O'Reilly, K.E., Rojo, F., She, Q.B., Solit, D., Mills, G.B., Smith, D., Lane, H., Hofmann, F., Hicklin, D.J., Ludwig, D.L.*, et al.* (2006). mTOR inhibition induces upstream receptor tyrosine kinase signaling and activates Akt. Cancer research *66*, 1500-1508.

Ohgaki, H., and Kleihues, P. (2005). Epidemiology and etiology of gliomas. Acta Neuropathol *109*, 93-108.

Ohgaki, H., and Kleihues, P. (2009). Genetic alterations and signaling pathways in the evolution of gliomas. Cancer Sci *100*, 2235-2241.

Olar, A., and Aldape, K.D. (2014). Using the molecular classification of glioblastoma to inform personalized treatment. J Pathol *232*, 165-177.

Omuro, A., and DeAngelis, L.M. (2013). Glioblastoma and other malignant gliomas: a clinical review. JAMA *310*, 1842-1850.

Onder, T.T., Gupta, P.B., Mani, S.A., Yang, J., Lander, E.S., and Weinberg, R.A. (2008). Loss of E-cadherin promotes metastasis via multiple downstream transcriptional pathways. Cancer research *68*, 3645-3654.

Pallini, R., Ricci-Vitiani, L., Banna, G.L., Signore, M., Lombardi, D., Todaro, M., Stassi, G., Martini, M., Maira, G., Larocca, L.M.*, et al.* (2008). Cancer stem cell analysis and

clinical outcome in patients with glioblastoma multiforme. Clinical cancer research : an official journal of the American Association for Cancer Research *14*, 8205-8212.

Pardal, R., Clarke, M.F., and Morrison, S.J. (2003). Applying the principles of stem-cell biology to cancer. Nature reviews Cancer *3*, 895-902.

Patel, A.P., Tirosh, I., Trombetta, J.J., Shalek, A.K., Gillespie, S.M., Wakimoto, H., Cahill, D.P., Nahed, B.V., Curry, W.T., Martuza, R.L.*, et al.* (2014). Single-cell RNA-seq highlights intratumoral heterogeneity in primary glioblastoma. Science *344*, 1396-1401.

Paternot, S., and Roger, P.P. (2009). Combined inhibition of MEK and mammalian target of rapamycin abolishes phosphorylation of cyclin-dependent kinase 4 in glioblastoma cell lines and prevents their proliferation. Cancer research *69*, 4577-4581.

Paul, I., Bhattacharya, S., Chatterjee, A., and Ghosh, M.K. (2013). Current Understanding on EGFR and Wnt/beta-Catenin Signaling in Glioma and Their Possible Crosstalk. Genes & cancer *4*, 427-446.

Perumalsamy, L.R., Nagala, M., Banerjee, P., and Sarin, A. (2009). A hierarchical cascade activated by non-canonical Notch signaling and the mTOR-Rictor complex regulates neglect-induced death in mammalian cells. Cell Death Differ *16*, 879-889.

Phillips, H.S., Kharbanda, S., Chen, R., Forrest, W.F., Soriano, R.H., Wu, T.D., Misra, A., Nigro, J.M., Colman, H., Soroceanu, L.*, et al.* (2006). Molecular subclasses of high-grade glioma predict prognosis, delineate a pattern of disease progression, and resemble stages in neurogenesis. Cancer cell *9*, 157-173.

Piccirillo, S.G., Colman, S., Potter, N.E., van Delft, F.W., Lillis, S., Carnicer, M.J., Kearney, L., Watts, C., and Greaves, M. (2015). Genetic and functional diversity of propagating cells in glioblastoma. Stem cell reports *4*, 7-15.

Piccirillo, S.G., Combi, R., Cajola, L., Patrizi, A., Redaelli, S., Bentivegna, A., Baronchelli, S., Maira, G., Pollo, B., Mangiola, A.*, et al.* (2009). Distinct pools of cancer stem-like cells coexist within human glioblastomas and display different tumorigenicity and independent genomic evolution. Oncogene *28*, 1807-1811.

Piccirillo, S.G., Reynolds, B.A., Zanetti, N., Lamorte, G., Binda, E., Broggi, G., Brem, H., Olivi, A., Dimeco, F., and Vescovi, A.L. (2006). Bone morphogenetic proteins inhibit the tumorigenic potential of human brain tumour-initiating cells. Nature *444*, 761-765.

Pierfelice, T.J., Schreck, K.C., Eberhart, C.G., and Gaiano, N. (2008). Notch, neural stem cells, and brain tumors. Cold Spring Harb Symp Quant Biol *73*, 367-375.

Pirouzmand, F., and Sadanand, V. (2007). The incidence trends of primary brain tumors in Saskatchewan from 1970 to 2001. Can J Neurol Sci *34*, 181-186.

Purow, B.W., Haque, R.M., Noel, M.W., Su, Q., Burdick, M.J., Lee, J., Sundaresan, T., Pastorino, S., Park, J.K., Mikolaenko, I.*, et al.* (2005). Expression of Notch-1 and its ligands, Delta-like-1 and Jagged-1, is critical for glioma cell survival and proliferation. Cancer research *65*, 2353-2363.

Ranganathan, A., Pearson, G.W., Chrestensen, C.A., Sturgill, T.W., and Cobb, M.H. (2006). The MAP kinase ERK5 binds to and phosphorylates p90 RSK. Archives of biochemistry and biophysics *449*, 8-16.

Rehen, S.K., McConnell, M.J., Kaushal, D., Kingsbury, M.A., Yang, A.H., and Chun, J. (2001). Chromosomal variation in neurons of the developing and adult mammalian nervous system. Proceedings of the National Academy of Sciences of the United States of America *98*, 13361-13366.

Reya, T., Morrison, S.J., Clarke, M.F., and Weissman, I.L. (2001). Stem cells, cancer, and cancer stem cells. Nature *414*, 105-111.

Reynolds, B.A., Tetzlaff, W., and Weiss, S. (1992). A multipotent EGF-responsive striatal embryonic progenitor cell produces neurons and astrocytes. J Neurosci *12*, 4565-4574.

Reynolds, B.A., and Weiss, S. (1992). Generation of neurons and astrocytes from isolated cells of the adult mammalian central nervous system. Science *255*, 1707-1710.

Rickman, D.S., Bobek, M.P., Misek, D.E., Kuick, R., Blaivas, M., Kurnit, D.M., Taylor, J., and Hanash, S.M. (2001). Distinctive molecular profiles of high-grade and low-grade

gliomas based on oligonucleotide microarray analysis. Cancer research *61*, 6885-6891.

Rubinfeld, B., Albert, I., Porfiri, E., Fiol, C., Munemitsu, S., and Polakis, P. (1996). Binding of GSK3beta to the APC-beta-catenin complex and regulation of complex assembly. Science *272*, 1023-1026.

Sabatini, D.M., Erdjument-Bromage, H., Lui, M., Tempst, P., and Snyder, S.H. (1994). RAFT1: a mammalian protein that binds to FKBP12 in a rapamycin-dependent fashion and is homologous to yeast TORs. Cell *78*, 35-43.

Saito, Y., Vandenheede, J.R., and Cohen, P. (1994). The mechanism by which epidermal growth factor inhibits glycogen synthase kinase 3 in A431 cells. The Biochemical journal *303 (Pt 1)*, 27-31.

Sakanaka, C., Weiss, J.B., and Williams, L.T. (1998). Bridging of beta-catenin and glycogen synthase kinase-3beta by axin and inhibition of beta-catenin-mediated transcription. Proceedings of the National Academy of Sciences of the United States of America *95*, 3020-3023.

Sami, A., and Karsy, M. (2013). Targeting the PI3K/AKT/mTOR signaling pathway in glioblastoma: novel therapeutic agents and advances in understanding. Tumour Biol *34*, 1991-2002.

Sanai, N., Alvarez-Buylla, A., and Berger, M.S. (2005). Neural stem cells and the origin of gliomas. N Engl J Med *353*, 811-822.

Sarbassov, D.D., Ali, S.M., Sengupta, S., Sheen, J.H., Hsu, P.P., Bagley, A.F., Markhard, A.L., and Sabatini, D.M. (2006). Prolonged rapamycin treatment inhibits mTORC2 assembly and Akt/PKB. Molecular cell *22*, 159-168.

Sarbassov, D.D., Guertin, D.A., Ali, S.M., and Sabatini, D.M. (2005). Phosphorylation and regulation of Akt/PKB by the rictor-mTOR complex. Science *307*, 1098-1101.

Sareen, D., McMillan, E., Ebert, A.D., Shelley, B.C., Johnson, J.A., Meisner, L.F., and Svendsen, C.N. (2009). Chromosome 7 and 19 trisomy in cultured human neural progenitor cells. PloS one *4*, e7630.

Sarkaria, J.N., Yang, L., Grogan, P.T., Kitange, G.J., Carlson, B.L., Schroeder, M.A., Galanis, E., Giannini, C., Wu, W., Dinca, E.B.*, et al.* (2007). Identification of molecular characteristics correlated with glioblastoma sensitivity to EGFR kinase inhibition through use of an intracranial xenograft test panel. Molecular cancer therapeutics *6*, 1167-1174.

Sassone-Corsi, P., Ransone, L.J., Lamph, W.W., and Verma, I.M. (1988). Direct interaction between fos and jun nuclear oncoproteins: role of the 'leucine zipper' domain. Nature *336*, 692-695.

Schwab, E.D., and Pienta, K.J. (1996). Cancer as a complex adaptive system. Medical hypotheses *47*, 235-241.

Schwartzbaum, J.A., Fisher, J.L., Aldape, K.D., and Wrensch, M. (2006). Epidemiology and molecular pathology of glioma. Nat Clin Pract Neurol *2*, 494-503; quiz 491 p following 516.

Shackleton, M., Quintana, E., Fearon, E.R., and Morrison, S.J. (2009). Heterogeneity in cancer: cancer stem cells versus clonal evolution. Cell *138*, 822-829.

Shah, S.P., Morin, R.D., Khattra, J., Prentice, L., Pugh, T., Burleigh, A., Delaney, A., Gelmon, K., Guliany, R., Senz, J.*, et al.* (2009). Mutational evolution in a lobular breast tumour profiled at single nucleotide resolution. Nature *461*, 809-813.

Shapiro, J.R., Yung, W.K., and Shapiro, W.R. (1981). Isolation, karyotype, and clonal growth of heterogeneous subpopulations of human malignant gliomas. Cancer research *41*, 2349-2359.

Shaw, R.J., and Cantley, L.C. (2006). Ras, PI(3)K and mTOR signalling controls tumour cell growth. Nature *441*, 424-430.

Singh, S.K., Clarke, I.D., Hide, T., and Dirks, P.B. (2004a). Cancer stem cells in nervous system tumors. Oncogene *23*, 7267-7273.

Singh, S.K., Clarke, I.D., Terasaki, M., Bonn, V.E., Hawkins, C., Squire, J., and Dirks, P.B. (2003). Identification of a cancer stem cell in human brain tumors. Cancer research *63*, 5821-5828.

Singh, S.K., Hawkins, C., Clarke, I.D., Squire, J.A., Bayani, J., Hide, T., Henkelman, R.M., Cusimano, M.D., and Dirks, P.B. (2004b). Identification of human brain tumour initiating cells. Nature *432*, 396-401.

Smith, M.A., Freidlin, B., Ries, L.A., and Simon, R. (1998). Trends in reported incidence of primary malignant brain tumors in children in the United States. J Natl Cancer Inst *90*, 1269-1277.

Smyth, G. (2005). Limma: linear models for microarray data. In: Bioinformatics and Computational Biology Solutions using R and Bioconductor (New York: Springer).

Snuderl, M., Fazlollahi, L., Le, L.P., Nitta, M., Zhelyazkova, B.H., Davidson, C.J., Akhavanfard, S., Cahill, D.P., Aldape, K.D., Betensky, R.A*., et al.* (2011). Mosaic amplification of multiple receptor tyrosine kinase genes in glioblastoma. Cancer cell *20*, 810-817.

Sokolosky, M., Chappell, W.H., Stadelman, K., Abrams, S.L., Davis, N.M., Steelman, L.S., and McCubrey, J.A. (2014). Inhibition of GSK-3beta activity can result in drug and hormonal resistance and alter sensitivity to targeted therapy in MCF-7 breast cancer cells. Cell Cycle *13*, 820-833.

Solecki, D.J., Liu, X.L., Tomoda, T., Fang, Y., and Hatten, M.E. (2001). Activated Notch2 signaling inhibits differentiation of cerebellar granule neuron precursors by maintaining proliferation. Neuron *31*, 557-568.

Sottoriva, A., Spiteri, I., Piccirillo, S.G., Touloumis, A., Collins, V.P., Marioni, J.C., Curtis, C., Watts, C., and Tavare, S. (2013). Intratumor heterogeneity in human glioblastoma reflects cancer evolutionary dynamics. Proceedings of the National Academy of Sciences of the United States of America *110*, 4009-4014.

Stambolic, V., and Woodgett, J.R. (1994). Mitogen inactivation of glycogen synthase kinase-3 beta in intact cells via serine 9 phosphorylation. The Biochemical journal *303 (Pt 3)*, 701-704.

Stommel, J.M., Kimmelman, A.C., Ying, H., Nabioullin, R., Ponugoti, A.H., Wiedemeyer, R., Stegh, A.H., Bradner, J.E., Ligon, K.L., Brennan, C*., et al.* (2007). Coactivation of receptor tyrosine kinases affects the response of tumor cells to targeted therapies. Science *318*, 287-290.

Stupp, R., Mason, W.P., van den Bent, M.J., Weller, M., Fisher, B., Taphoorn, M.J., Belanger, K., Brandes, A.A., Marosi, C., Bogdahn, U.*, et al.* (2005). Radiotherapy plus concomitant and adjuvant temozolomide for glioblastoma. N Engl J Med *352*, 987-996.

Sunayama, J., Matsuda, K., Sato, A., Tachibana, K., Suzuki, K., Narita, Y., Shibui, S., Sakurada, K., Kayama, T., Tomiyama, A.*, et al.* (2010). Crosstalk between the PI3K/mTOR and MEK/ERK pathways involved in the maintenance of self-renewal and tumorigenicity of glioblastoma stem-like cells. Stem cells *28*, 1930-1939.

Szerlip, N.J., Pedraza, A., Chakravarty, D., Azim, M., McGuire, J., Fang, Y., Ozawa, T., Holland, E.C., Huse, J.T., Jhanwar, S.*, et al.* (2012). Intratumoral heterogeneity of receptor tyrosine kinases EGFR and PDGFRA amplification in glioblastoma defines subpopulations with distinct growth factor response. Proceedings of the National Academy of Sciences of the United States of America *109*, 3041-3046.

Taipale, J., and Beachy, P.A. (2001). The Hedgehog and Wnt signalling pathways in cancer. Nature *411*, 349-354.

Takemaru, K.I., and Moon, R.T. (2000). The transcriptional coactivator CBP interacts with beta-catenin to activate gene expression. The Journal of cell biology *149*, 249-254.

TCGA (2008). Comprehensive genomic characterization defines human glioblastoma genes and core pathways. Nature *455*, 1061-1068.

Team, R.C. (2013). A language and environment for statistical computing. R Foundation for Statistical Computing, Vienna, Austria. http://wwwR-projectorg/.

Therneau, T. (2014). A Package for Survival Analysis in S. R package version 2.37-7. http://CRANR-projectorg/package=survival.

Thoreen, C.C., Kang, S.A., Chang, J.W., Liu, Q., Zhang, J., Gao, Y., Reichling, L.J., Sim, T., Sabatini, D.M., and Gray, N.S. (2009). An ATP-competitive mammalian target of rapamycin inhibitor reveals rapamycin-resistant functions of mTORC1. J Biol Chem *284*, 8023-8032.

Thoreen, C.C., and Sabatini, D.M. (2009). Rapamycin inhibits mTORC1, but not completely. Autophagy *5*, 725-726.

Tohyama, T., Lee, V.M., Rorke, L.B., Marvin, M., McKay, R.D., and Trojanowski, J.Q. (1992). Nestin expression in embryonic human neuroepithelium and in human neuroepithelial tumor cells. Lab Invest *66*, 303-313.

Totary-Jain, H., Sanoudou, D., Dautriche, C.N., Schneller, H., Zambrana, L., and Marks, A.R. (2012). Rapamycin resistance is linked to defective regulation of Skp2. Cancer research *72*, 1836-1843.

Trivedi, N., Marsh, P., Goold, R.G., Wood-Kaczmar, A., and Gordon-Weeks, P.R. (2005). Glycogen synthase kinase-3beta phosphorylation of MAP1B at Ser1260 and Thr1265 is spatially restricted to growing axons. Journal of cell science *118*, 993-1005.

Tso, C.L., Freije, W.A., Day, A., Chen, Z., Merriman, B., Perlina, A., Lee, Y., Dia, E.Q., Yoshimoto, K., Mischel, P.S.*, et al.* (2006). Distinct transcription profiles of primary and secondary glioblastoma subgroups. Cancer research *66*, 159-167.

Uhm, J.H., Gladson, C.L., and Rao, J.S. (1999). The role of integrins in the malignant phenotype of gliomas. Frontiers in bioscience : a journal and virtual library *4*, D188-199.

Verhaak, R.G., Hoadley, K.A., Purdom, E., Wang, V., Qi, Y., Wilkerson, M.D., Miller, C.R., Ding, L., Golub, T., Mesirov, J.P.*, et al.* (2010). Integrated genomic analysis identifies clinically relevant subtypes of glioblastoma characterized by abnormalities in PDGFRA, IDH1, EGFR, and NF1. Cancer cell *17*, 98-110.

Vivanco, I., and Sawyers, C.L. (2002). The phosphatidylinositol 3-Kinase AKT pathway in human cancer. Nature reviews Cancer *2*, 489-501.

Wang, B.T., Ducker, G.S., Barczak, A.J., Barbeau, R., Erle, D.J., and Shokat, K.M. (2011). The mammalian target of rapamycin regulates cholesterol biosynthetic gene expression and exhibits a rapamycin-resistant transcriptional profile. Proceedings of the National Academy of Sciences of the United States of America *108*, 15201-15206.

Wang, G., Kang, C., and Pu, P. Increased expression of Akt2 and activity of PI3K and cell proliferation with the ascending of tumor grade of human gliomas. Clinical neurology and neurosurgery.

Wang, G., Kang, C., and Pu, P. (2010a). Increased expression of Akt2 and activity of PI3K and cell proliferation with the ascending of tumor grade of human gliomas. Clin Neurol Neurosurg *112*, 324-327.

Wang, Z., Li, Y., Banerjee, S., Kong, D., Ahmad, A., Nogueira, V., Hay, N., and Sarkar, F.H. (2010b). Down-regulation of Notch-1 and Jagged-1 inhibits prostate cancer cell growth, migration and invasion, and induces apoptosis via inactivation of Akt, mTOR, and NF-kappaB signaling pathways. J Cell Biochem.

Wechsler-Reya, R., and Scott, M.P. (2001). The developmental biology of brain tumors. Annu Rev Neurosci *24*, 385-428.

Wen, P.Y., Lee, E.Q., Reardon, D.A., Ligon, K.L., and Alfred Yung, W.K. (2012). Current clinical development of PI3K pathway inhibitors in glioblastoma. Neuro-oncology *14*, 819-829.

Westra, J.W., Peterson, S.E., Yung, Y.C., Mutoh, T., Barral, S., and Chun, J. (2008). Aneuploid mosaicism in the developing and adult cerebellar cortex. J Comp Neurol *507*, 1944-1951.

Wick, W., Weller, M., van den Bent, M., Sanson, M., Weiler, M., von Deimling, A., Plass, C., Hegi, M., Platten, M., and Reifenberger, G. (2014). MGMT testing--the challenges for biomarker-based glioma treatment. Nat Rev Neurol *10*, 372-385.

Wiese, C., Rolletschek, A., Kania, G., Blyszczuk, P., Tarasov, K.V., Tarasova, Y., Wersto, R.P., Boheler, K.R., and Wobus, A.M. (2004). Nestin expression--a property of multi-lineage progenitor cells? Cell Mol Life Sci *61*, 2510-2522.

Wrensch, M., Minn, Y., Chew, T., Bondy, M., and Berger, M.S. (2002). Epidemiology of primary brain tumors: current concepts and review of the literature. Neuro Oncol *4*, 278-299.

Wu, M., Pastor-Pareja, J.C., and Xu, T. Interaction between Ras(V12) and scribbled clones induces tumour growth and invasion. Nature.

Wullschleger, S., Loewith, R., and Hall, M.N. (2006). TOR signaling in growth and metabolism. Cell *124*, 471-484.

Yamashita, D., Kondo, T., Ohue, S., Takahashi, H., Ishikawa, M., Matoba, R., Suehiro, S., Kohno, S., Harada, H., Tanaka, J.*, et al.* (2015). miR340 Suppresses the Stem-like Cell Function of Glioma-Initiating Cells by Targeting Tissue Plasminogen Activator. Cancer research *75*, 1123-1133.

Yeh, T.C., Marsh, V., Bernat, B.A., Ballard, J., Colwell, H., Evans, R.J., Parry, J., Smith, D., Brandhuber, B.J., Gross, S.*, et al.* (2007). Biological characterization of ARRY-142886 (AZD6244), a potent, highly selective mitogen-activated protein kinase kinase 1/2 inhibitor. Clinical cancer research : an official journal of the American Association for Cancer Research *13*, 1576-1583.

Yoeli-Lerner, M., Chin, Y.R., Hansen, C.K., and Toker, A. (2009). Akt/protein kinase b and glycogen synthase kinase-3beta signaling pathway regulates cell migration through the NFAT1 transcription factor. Molecular cancer research : MCR *7*, 425-432.

Yokogami, K., Wakisaka, S., Avruch, J., and Reeves, S.A. (2000). Serine phosphorylation and maximal activation of STAT3 during CNTF signaling is mediated by the rapamycin target mTOR. Curr Biol *10*, 47-50.

Yung, W.K., Shapiro, J.R., and Shapiro, W.R. (1982). Heterogeneous chemosensitivities of subpopulations of human glioma cells in culture. Cancer research *42*, 992-998.

Zajkowski, T., Nieznanska, H., and Nieznanski, K. (2015). Stabilization of microtubular cytoskeleton protects neurons from toxicity of N-terminal fragment of cytosolic prion protein. Biochimica et biophysica acta.

Zhang, B., and Horvath, S. (2005). A general framework for weighted gene co-expression network analysis. Statistical applications in genetics and molecular biology *4*, Article17.

Zhu, Z., Khan, M.A., Weiler, M., Blaes, J., Jestaedt, L., Geibert, M., Zou, P., Gronych, J., Bernhardt, O., Korshunov, A.*, et al.* (2014). Targeting Self-Renewal in High-Grade Brain Tumors Leads to Loss of Brain Tumor Stem Cells and Prolonged Survival. Cell stem cell.

Zoncu, R., Efeyan, A., and Sabatini, D.M. (2011). mTOR: from growth signal integration to cancer, diabetes and ageing. Nature reviews Molecular cell biology *12*, 21-35.

Zong, H., Parada, L.F., and Baker, S.J. (2015). Cell of Origin for Malignant Gliomas and Its Implication in Therapeutic Development. Cold Spring Harb Perspect Biol.